

Fluorinated boranes in dehydrocoupling and hydroboration

Elizabeth Anne Jacobs

Thesis submitted for the degree of PhD

University of East Anglia
School of Chemistry

April 2014

© This copy of the thesis has been supplied on the condition that anyone who consults it is understood to recognize that its copyright rests with the author and that use of any information derived there from must be in accordance with current UK Copyright Law. In addition, any quotation or extract must include full attribution.

Declaration

This thesis is submitted to the University of East Anglia for the degree of PhD and has not been previously submitted for any other degree at this or any other university or institution. Except where stated, and reference and acknowledgement is provided, this work is original and has been carried out by the author alone.

Abstract

This thesis describes the chemistry of the Lewis adducts of mono- and bis-(pentafluorophenyl)borane ($\text{LB}\cdot\text{BH}_n(\text{C}_6\text{F}_5)_{3-n}$; $n = 1, 2$; $\text{LB} = \text{SMe}_2, \text{NH}_3$) as it applies to the development of novel perfluoroarylboranes. **Chapter 2** details the use of $\text{Me}_2\text{S}\cdot\text{BH}_n(\text{C}_6\text{F}_5)_{3-n}$ in the preparation of the pentafluorophenyl substituted amine borane adducts, $\text{LB}\cdot\text{BH}_n(\text{C}_6\text{F}_5)_{3-n}$ ($\text{LB} = \text{NR}_3, \text{NHR}_2, \text{NH}_2\text{R}, \text{py}$). Their solid state structures feature $\text{N}\cdots\text{H}\cdots\text{B}$ and $\text{N}\cdots\text{H}\cdots\text{F}\cdots\text{C}$ hydrogen bonding interactions, important structural motifs for further application of these materials. The related pentafluorophenyl substituted amine boranes $\text{H}_3\text{N}\cdot\text{BH}_n(\text{C}_6\text{F}_5)_{3-n}$ may be used as ligand precursors for the synthesis of group 4 metallocene amidoborane complexes. **Chapter 3** describes the divergent chemistry observed for each of the group 4 metals in the presence of the pentafluorophenyl substituted amidoborane ligands, including $\text{N}\cdots\text{H}$ activation with hafnium, $\text{B}\cdots\text{H}$ activation in the case of zirconium and single electron reduction of titanium. In all but one instance, the crystal structures of isolated group 4 metallocene amidoboranes display a β -B-agostic interaction. This structural feature is proposed to play a significant role in catalytic dehydrocoupling of amine boranes by early transition metal catalysts. **Chapter 4** describes the preparation of novel pentafluorophenyl substituted organoboranes $\text{R}_n\text{B}(\text{C}_6\text{F}_5)_{3-n}$ ($n = 1, 2$) through facile hydroboration of alkenes using $\text{Me}_2\text{S}\cdot\text{BH}_n(\text{C}_6\text{F}_5)_{3-n}$. In particular, the double hydroboration of 1,5-cyclooctadiene with $\text{Me}_2\text{S}\cdot\text{BH}_2(\text{C}_6\text{F}_5)$ resulted in isolation and crystallographic characterization of pentafluorophenyl-9-borobicyclo[3.3.1]nonane dimethylsulfide adduct, the $-\text{C}_6\text{F}_5$ substituted analog of the popular hydroboration reagent 9-BBN (9-borabicyclo[3.3.1]nonane).

Table of Contents

Declaration	2
Abstract	3
List of Figures	7
List of Schemes	11
List of Tables.....	13
Abbreviations	14
Acknowledgements	15
Chapter 1 Introduction to boranes	16
1.1 Overview	16
1.2 Properties of boranes	16
1.3 Development of perfluoroaryl boranes	20
1.4 Borane adducts for use in hydrogen activation	22
1.5 Borane adducts for use in hydrogen storage	24
1.6 Adducts of other pentafluorophenyl substituted boranes.....	26
Chapter 2 Amine and nitrogen donor adducts of mono- and bis- (pentafluorophenyl)borane	29
2.1 Introduction.....	29
2.1.1 Ammonia borane	29
2.1.2 N-substituted amine boranes	32
2.1.3 Pentafluorophenyl substituted amine boranes	34
2.2 Results	38
2.2.1 Crystallography.....	40
2.2.1.1 Amine and nitrogen donor adducts of $H_2B(C_6F_5)$	41
2.2.1.2 Amine and nitrogen donor adducts of $HB(C_6F_5)_2$	49

2.3	Discussion	56
2.3.1	Structural analysis	56
2.3.2	Adduct stability	59
2.3.2.1	Triethylamine adducts of $H_2B(C_6F_5)$ and $HB(C_6F_5)_2$	60
2.3.2.2	Aniline adducts of $H_2B(C_6F_5)$ and $HB(C_6F_5)_2$	62
2.4	Conclusions	63
Chapter 3 Pentafluorophenyl stabilized models for dehydrocoupling		
intermediates		65
3.1	Introduction.....	65
3.1.1	Amine borane dehydrocoupling using late transition metal catalysts.....	66
3.1.2	Amine borane dehydrocoupling using group 4 metal catalysts.....	68
3.1.3	Aminoborane versus alkene bonding to transition metal centers	70
3.1.4	$-C_6F_5$ stabilized amidoborane complexes of the group 4 metals.....	77
3.2	Results	79
3.2.1	$[Cp_2Zr]$ complexes bearing $-C_6F_5$ substituted amidoborane ligands.....	79
3.2.2	$[Cp_2Hf]$ complexes bearing $-C_6F_5$ substituted amidoborane ligands	92
3.2.3	$[Cp_2Ti]$ complexes bearing $-C_6F_5$ substituted amidoborane ligands.....	99
3.2.4	Group 4 metallocene complexes bearing the $-NPhBH_2(C_6F_5)$ ligand	105
3.3	Discussion	110
3.4	Conclusions.....	121
Chapter 4 Hydroboration using $Me_2S \cdot BH_n(C_6F_5)_{3-n}$ (n = 1, 2)		124
4.1	Introduction.....	124
4.1.1	Use of perfluoroaryl boranes as hydroboration reagents.....	126
4.2	Results and discussion	131
4.2.1	Hydroboration using $Me_2S \cdot BH(C_6F_5)_2$	132
4.2.2	Hydroboration using $Me_2S \cdot BH_2(C_6F_5)$	135
4.2.3	Double hydroboration of 1,5-cyclooctadiene with $Me_2S \cdot BH_2(C_6F_5)$	140

4.3	Conclusions.....	143
Chapter 5	Experimental.....	145
Chapter 6	Crystallography	166
Chapter 7	References	167
Chapter 8	Appendix	182

List of Figures

- Figure 1.1:** Molecular structure of diborane (left), pentaborane (middle) and decaborane (right) featuring a B—H—B bridging hydride structural motif.....17
- Figure 1.2:** Efficiency of the π -bonding character for the boron trihalides (top) and contributing resonance structures as a result of π -donation from occupied halide p-orbitals into the unoccupied p-orbital on boron (bottom).....18
- Figure 2.1:** Crystal packing and dihydrogen bonding network of ammonia borane (top), methylamine borane (bottom, left) and dimethylamine borane (bottom, right), with displacement ellipsoids displayed at the 50% probability level.⁹³ Boron (pink), nitrogen (blue), carbon (dark grey), hydrogen (light grey). Hydrogen atoms of the methyl groups of methylamine borane and dimethylamine borane have been omitted for clarity.33
- Figure 2.2:** Molecular structure of $\text{H}_3\text{N}\cdot\text{B}(\text{C}_6\text{F}_5)_3$ showing intramolecular (blue) and intermolecular (red) N—H...F—C interactions.35
- Figure 2.3:** Nitrogen donor adducts of tris(pentafluorophenyl)borane.....36
- Figure 2.4:** Crystal structure of dimeric $\text{H}_3\text{N}\cdot\text{BH}_2(\text{C}_6\text{F}_5)$ with displacement ellipsoids displayed at the 50% probability level.¹⁰² The N—H...H—B dihydrogen bonding interactions are indicated in red, with the H(1A)...H(2A) distance measuring 2.121 Å.37
- Figure 2.5:** Crystal structure of $\text{Me}_2\text{HN}\cdot\text{BH}_2(\text{C}_6\text{F}_5)$ (**1a**) with displacement ellipsoids displayed at the 50% probability level. The dihydrogen contacts formed by bifurcated $\text{BH}_2\cdots\text{HN}$ interactions are indicated in red. Hydrogen atoms of the methyl groups have been omitted for clarity.....42
- Figure 2.6:** Crystal packing of $\text{Me}_2\text{HN}\cdot\text{BH}_2(\text{C}_6\text{F}_5)$ (**1a**) with displacement ellipsoids displayed at the 50% probability level. The dihydrogen bonding network formed from bifurcated $\text{BH}_2\cdots\text{HN}$ interactions is indicated in red. Hydrogen atoms of the methyl groups have been omitted for clarity.42
- Figure 2.7:** Crystal packing of ${}^t\text{BuH}_2\text{N}\cdot\text{BH}_2(\text{C}_6\text{F}_5)$ (**1b**) with displacement ellipsoids displayed at the 50% probability level. The crystal packing consists of alternating short and long H...H contacts indicated in red. Hydrogen atoms of the tert-butyl groups have been omitted for clarity.....43
- Figure 2.8:** Crystal packing of $\text{PhH}_2\text{N}\cdot\text{BH}_2(\text{C}_6\text{F}_5)$ (**1c**) with displacement ellipsoids displayed at the 50% probability level. Stacking diagrams show (a) chains formed through dihydrogen bonding (indicated in red) and (b) intermolecular N—H...F—C interactions (indicated in blue).45
- Figure 2.9:** Crystal structure of dimeric $\text{BnH}_2\text{N}\cdot\text{BH}_2(\text{C}_6\text{F}_5)$ (**1d**) with displacement ellipsoids displayed at the 50% probability level. Dimerization occurs through intermolecular bifurcated $\text{BH}_2\cdots\text{HN}$ contacts indicated in red.....46
- Figure 2.10:** Crystal packing of $\text{BnH}_2\text{N}\cdot\text{BH}_2(\text{C}_6\text{F}_5)$ (**1d**) with displacement ellipsoids displayed at the 50% probability level. The intermolecular N—H...F—C interactions and weak H...H contacts which link dimeric pairs of **1d** are indicated in blue and red, respectively. Hydrogen atoms of the benzyl groups have been omitted for clarity.....47

Figure 2.11: Crystal packing of py·BH ₂ (C ₆ F ₅) (1f) with displacement ellipsoids displayed at the 50% probability level. The crystal packing is dominated by alternating –C ₆ F ₅ pairing interactions and van der Waals interactions.....	48
Figure 2.12: Crystal packing of Me ₂ HN·BH(C ₆ F ₅) ₂ (2a) with displacement ellipsoids displayed at the 50% probability level. The packing is dominated by N—H···F—C contacts (indicated in blue) and off-set face-to-face –C ₆ F ₅ stacking interactions.....	50
Figure 2.13: Crystal structure of ^t BuH ₂ N·BH(C ₆ F ₅) ₂ (2b) with displacement ellipsoids displayed at the 50% probability level. Molecular pairing occurs through bifurcated inter- and intra-molecular N—H···F—C interactions, indicated in blue. Hydrogen atoms of the tert-butyl groups have been omitted for clarity.	51
Figure 2.14: Crystal structure of PhH ₂ N·BH(C ₆ F ₅) ₂ (2c) with displacement ellipsoids displayed at the 50% probability level. Molecular pairing occurs through one intermolecular N—H···F—C interaction, indicated in blue, and a –C ₆ F ₅ stacking interaction.....	52
Figure 2.15: Crystal structure of BnH ₂ N·BH(C ₆ F ₅) ₂ (2d) with displacement ellipsoids displayed at the 50% probability level. Molecular pairing occurs through one intermolecular N—H···F—C interaction, indicated in blue, and a –C ₆ F ₅ stacking interaction.....	53
Figure 2.16: Crystal structure of Et ₃ N·BH(C ₆ F ₅) ₂ (2e) with displacement ellipsoids displayed at the 50% probability level. Hydrogen atoms of the ethyl groups have been omitted for clarity.	54
Figure 2.17: Molecular packing of py·BH(C ₆ F ₅) ₂ (2f) with displacement ellipsoids displayed at the 50% probability level. Molecular pairing occurs through intermolecular H···F contacts, indicated in green.	55
Figure 2.18: Dihydrogen bonding and H···H contacts observed in the amine adducts of mono(pentafluorophenyl)borane.....	57
Figure 2.19: N—H···F—C contacts observed in the amine adducts of bis(pentafluorophenyl)borane.	58
Figure 3.1: Crystallographically characterized transition metal complexes featuring end-on coordination of amine boranes ^{138,139,143,144,204,209–211,214} and linear diborazines. ^{139,212,215}	71
Figure 3.2: Crystallographically characterized transition metal complexes featuring end-on coordination of aminoboranes. ^{138,143,197,217}	73
Figure 3.3: Crystallographically characterized transition metal complexes featuring side-on coordination of alkenes.	73
Figure 3.4: Resonance forms of metal amidoborane complexes (x ≠ H).	74
Figure 3.5: Crystallographically characterized transition metal alkyl and alkene complexes which feature a C—H agostic interaction.	75
Figure 3.6: Crystallographically characterized early transition metal amidoborane complexes.	77

- Figure 3.7:** Crystallographically characterized tris(pentafluorophenyl)borane substituted amido- and nitrido-borane complexes of the group 4 metals.78
- Figure 3.8:** Crystal structure of $\text{Cp}_2\text{Zr}(\text{NH}_2\text{BH}(\text{C}_6\text{F}_5)_2)_2$ (**3**) with displacement ellipsoids displayed at the 50% probability level. The cyclopentadienyl hydrogen atoms and toluene solvate molecule have been omitted for clarity. Intramolecular $\text{N}-\text{H}\cdots\text{F}-\text{C}$ interactions are indicated in red and the β -B-agostic interaction is indicated in blue.81
- Figure 3.9:** ^1H NMR spectrum of **4** recorded in CD_2Cl_2 at 25 °C.84
- Figure 3.10:** Crystal structure of $\{\text{H}_2\text{NB}(\text{C}_6\text{F}_5)_2\}_3$ (**6**) with displacement ellipsoids displayed at the 50% probability level. The pentafluorophenyl rings have been omitted for clarity (right).85
- Figure 3.11:** Crystal structure of $\{\text{HNB}(\text{C}_6\text{F}_5)\}_3$ (**7**) with displacement ellipsoids displayed at the 50% probability level. The short $\text{N}-\text{H}\cdots\text{F}-\text{C}$ contacts (red) measure 2.119 Å ($\text{H}(2)\cdots\text{F}(3)$), 2.130 Å ($\text{H}(2)\cdots\text{F}(6)$) and 2.113 Å ($\text{H}(1)\cdots\text{F}(10)$).86
- Figure 3.12:** Crystal structure of $\text{Cp}''_2(\text{CH}_3)(\text{NH}_2\text{BH}_2(\text{C}_6\text{F}_5))$ (**8**) with displacement ellipsoids displayed at the 50% probability level. The cyclopentadienyl hydrogen atoms, silicon-bound methyl groups and zirconium-bound methyl hydrogen atoms have been omitted for clarity. The intramolecular $\text{N}-\text{H}\cdots\text{F}-\text{C}$ interaction is indicated in red and the β -B-agostic interaction is indicated in blue.88
- Figure 3.13:** Crystal structure of $\text{Cp}''_2(\text{CH}_3)(\text{NH}_2\text{BH}(\text{C}_6\text{F}_5)_2)$ (**9**) with displacement ellipsoids displayed at the 50% probability level. The cyclopentadienyl hydrogen atoms, silicon-bound methyl groups and zirconium-bound methyl hydrogen atoms have been omitted for clarity. Intramolecular $\text{N}-\text{H}\cdots\text{F}-\text{C}$ interactions are indicated in red and the β -B-agostic interaction is indicated in blue.89
- Figure 3.14:** Crystal structure of $\text{Cp}_2\text{Zr}(\text{CH}_3)(\text{NH}_2\text{BH}(\text{C}_6\text{F}_5)_2)$ (**10**) with displacement ellipsoids displayed at the 50% probability level. Cyclopentadienyl and methyl hydrogen atoms have been omitted for clarity. The intramolecular $\text{N}-\text{H}\cdots\text{F}-\text{C}$ interaction is indicated in red and the β -B-agostic interaction is indicated in blue.91
- Figure 3.15:** Crystal structure of $\text{Cp}_2\text{Hf}(\text{NHBH}(\text{C}_6\text{F}_5)_2)$ (**12**) with displacement ellipsoids displayed at the 50% probability level. Cyclopentadienyl hydrogen atoms and the toluene solvate molecule have been omitted for clarity. The β -B-agostic interaction is indicated in blue.93
- Figure 3.16:** Resonance forms of compound **12**.94
- Figure 3.17:** Crystal structure of $\text{Cp}_2\text{Hf}(\text{NH}_2\text{BH}(\text{C}_6\text{F}_5)_2)_2 \cdot 4\text{thf}$ (**13-4thf**) with displacement ellipsoids displayed at the 50% probability level. Two of the four thf solvate molecules, the hydrogen atoms of the remaining thf molecules and the cyclopentadienyl hydrogen atoms have been omitted for clarity. Intramolecular $\text{N}-\text{H}\cdots\text{F}-\text{C}$ interactions are indicated in red, hydrogen bonded $\text{thf}\cdots\text{H}_2\text{N}$ contacts are indicated in green and the β -B-agostic interaction is indicated in blue.95
- Figure 3.18:** Crystal structure of $\text{Cp}_2\text{Hf}(\text{NH}_2\text{BH}(\text{C}_6\text{F}_5)_2)_2$ (**13**) with displacement ellipsoids displayed at the 50% probability level. The toluene solvate molecule and cyclopentadienyl hydrogen atoms have been omitted for clarity. Intramolecular $\text{N}-\text{H}\cdots\text{F}-\text{C}$ interactions are indicated in red.96

- Figure 3.19:** Crystal structure of $\text{Cp}_2\text{Ti}(\text{NH}_2\text{BH}_2(\text{C}_6\text{F}_5))$ (**16**) with displacement ellipsoids displayed at the 50% probability level. The cyclopentadienyl hydrogen atoms have been omitted for clarity. The intramolecular $\text{N—H}\cdots\text{F—C}$ interaction is indicated in red and the β -B-agostic interaction is indicated in blue. 100
- Figure 3.20:** One of two crystallographically independent molecules in the unit cell of $\text{Cp}_2\text{Ti}(\text{NH}_2\text{BH}(\text{C}_6\text{F}_5)_2)$ (**17**) with displacement ellipsoids displayed at the 50% probability level. The cyclopentadienyl hydrogen atoms have been omitted for clarity. The intramolecular $\text{N—H}\cdots\text{F—C}$ interaction is indicated in red and the β -B-agostic interaction is indicated in blue. 102
- Figure 3.21:** Crystal structure of $[\text{Cp}_2\text{Ti}(\text{NHB}(\text{C}_6\text{F}_5)_3)(\text{NH}_2\text{B}(\text{C}_6\text{F}_5)_3)]^-$ ion (**18**) with displacement ellipsoids displayed at the 50% probability level. The $[\text{Li}\{\text{thf}\}_4]$ cation, toluene solvate molecule and cyclopentadienyl hydrogen atoms have been omitted for clarity. The intramolecular $\text{N—H}\cdots\text{F—C}$ interactions are indicated in red. 104
- Figure 3.22:** Crystal structure of $[\text{Li}\{12\text{-crown-4}\}_2][\text{NHPPhBH}(\text{C}_6\text{F}_5)_2]$ (**19a**) with displacement ellipsoids displayed at the 50% probability level. The crown ether hydrogen atoms have been omitted for clarity. The intramolecular $\text{N—H}\cdots\text{F—C}$ interaction is indicated in red. 106
- Figure 3.23:** Crystal structure of $\text{Cp}_2\text{Hf}(\text{CH}_3)(\text{NHPPhBH}_2(\text{C}_6\text{F}_5))$ (**22**) with displacement ellipsoids displayed at the 50% probability level. Cyclopentadienyl and methyl hydrogen atoms have been omitted for clarity. The intramolecular $\text{N—H}\cdots\text{F—C}$ interaction is indicated in red and the β -B-agostic interaction is indicated in blue. 108
- Figure 3.24:** Crystal structure of $\text{Cp}_2\text{Ti}(\text{NHPPhBH}_2(\text{C}_6\text{F}_5))$ (**23**) with displacement ellipsoids displayed at the 50% probability level. The cyclopentadienyl hydrogen atoms have been omitted for clarity. The β -B-agostic interaction is indicated in blue. 109
- Figure 3.25:** The first structurally characterized transition metal amidoborane complexes.¹¹⁰ 112
- Figure 4.1:** Molecular structure of diborane (left), 9-BBN (middle) and Piers' borane, $[\text{HB}(\text{C}_6\text{F}_5)_2]_2$ (right). 128
- Figure 4.2:** ^{19}F NMR spectrum showing three sets of ortho-fluorine resonances. The symbol \diamond indicates resonances associated with the starting material, $\text{Me}_2\text{S}\cdot\text{BH}_2(\text{C}_6\text{F}_5)$. . 138
- Figure 4.3:** ^{19}F NMR spectrum showing three sets of para-fluorine resonances. The symbol \diamond indicates resonances associated with the starting material, $\text{Me}_2\text{S}\cdot\text{BH}_2(\text{C}_6\text{F}_5)$. . 138
- Figure 4.4:** ^{19}F NMR spectrum showing three sets of meta-fluorine resonances (two overlapping). The symbol \diamond indicates resonances associated with the starting material, $\text{Me}_2\text{S}\cdot\text{BH}_2(\text{C}_6\text{F}_5)$ 139
- Figure 4.5:** Crystal structure of pentafluorophenyl-9-borobicyclo[3.3.1]nonane dimethylsulfide adduct (**32**) with displacement ellipsoids displayed at the 50% probability level. Hydrogen atoms have been omitted for clarity. 142

List of Schemes

Scheme 1.1: Borane geometry change upon Lewis base coordination.	19
Scheme 1.2: Generic hydrolysis reaction of boranes.	19
Scheme 1.3: Preparation methods for tris(pentafluorophenyl)boron.....	21
Scheme 1.4: Methyl abstraction by $B(C_6F_5)_3$ used for the generation of catalytically active electrophilic group 4 metal centers.	22
Scheme 1.5: Reactivity between tris(pentafluorophenyl)boron and small phosphine Lewis bases PR_3 to produce a zwitterion ($R = Cy$), frustrated Lewis pair ($R = tBu$) and Lewis adduct ($R = H, Me, Ph$).	23
Scheme 1.6: Reversible dihydrogen activation by the frustrated Lewis pair $(C_6H_2Me_3)_2P(C_6F_4)B(C_6F_5)_2$	23
Scheme 1.7: Dehydrogenation of an amine borane by a frustrated Lewis pair.	24
Scheme 1.8: Reactivity of bis(pentafluorophenyl)borane and its chloride analog.	26
Scheme 2.1: Preparation of ammonia borane through decomposition of ammonium borohydride.....	30
Scheme 2.2: Thermal decomposition of solid ammonia borane.	31
Scheme 2.3: Preparation of the dimethylsulfide and ammonia adducts of mono- and bis-(pentafluorophenyl)borane.	37
Scheme 2.4: Preparation of nitrogen donor Lewis adducts of $H_nB(C_6F_5)_{3-n}$ ($n = 1, 2$).	39
Scheme 2.5: Treatment of perfluoroaryl boranes with NR_3 ($R = Me, Et$).	61
Scheme 2.6: Spontaneous dehydrocoupling of aniline borane.	62
Scheme 3.1: Simplified partial reaction pathways for the catalytic dehydrocoupling of dimethylamine borane with the $[Rh(PCy_3)_2]^+$ fragment.	67
Scheme 3.2: Preparation of crystallographically characterized aminoborane coordination compounds. ^{138,143,197}	68
Scheme 3.3: Proposed catalytic cycle for the dehydrocoupling of amine boranes by $[Cp_2Ti]$, generated in situ.....	69
Scheme 3.4: C—H bond activation pathway.	72
Scheme 3.5: Charge redistribution at the metal center in the presence of an agostically-bound amidoborane ligand.	76
Scheme 3.6: Reactivity of Cp_2ZrCl_2 with the lithium salt $Li[NH_2BH(C_6F_5)_2]$	80
Scheme 3.7: Solution equilibrium of 3 in CD_2Cl_2	83

Scheme 3.8: Generation of highly electrophilic metal centers using $B(C_6F_5)_3$	87
Scheme 3.9: Possible dynamic exchange of 13 in solution.	97
Scheme 3.10: Observed difference of the reactivity of zirconocenes and hafnocenes in the presence of the methyl abstraction reagent, $B(C_6F_5)_3$	98
Scheme 3.11: Preparation of pentafluorophenyl stabilized hafnocene complexes.....	115
Scheme 3.12: Proposed routes to compound 12	116
Scheme 3.13: Possible routes to compound 18	120
Scheme 4.1: Generic description of the hydroboration reaction.	124
Scheme 4.2: Markovnikov (a) and anti-Markovnikov (b) addition products using $H-X / H_3O^+$ and $B-H / H_2O_2$ to produce primary alcohols.	126
Scheme 4.3: Synthetic methods reported for the preparation of Piers' borane.	127
Scheme 4.4: Equilibrium between the monomeric and dimeric forms of Piers' borane in solution.	129
Scheme 4.5: Catalytic hydroboration of alkynes using $Me_2S \cdot BH(C_6F_5)$ generated in situ.	130
Scheme 4.6: Solution equilibrium of the hydroboration product from the reaction between $Me_2S \cdot BH(C_6F_5)_2$ and an alkenic substrate. The same equilibrium is observed for the analogous reactions with $Me_2S \cdot BH_2(C_6F_5)$	132
Scheme 4.8: Room temperature double hydroboration of 1,5-cyclooctadiene.....	140
Scheme 4.9: Double hydroboration of 1,5-cyclooctadiene using $Me_2S \cdot BH_2(C_6F_5)$	141

List of Tables

Table 2.1: $\delta(\text{N—H})$ for the amines and amine adducts of $\text{BH}_n(\text{C}_6\text{F}_5)_{3-n}$ ($n = 1, 2$). ^{a,b}	39
Table 3.1: Selected bond and $\text{N—H}\cdots\text{F—C}$ contact lengths for $\text{Cp}_2\text{Zr}(\text{NH}_2\text{BH}(\text{C}_6\text{F}_5)_2)_2$...	81
Table 3.2: ^{11}B NMR chemical shifts and $^1J_{\text{B,H}}$ coupling constants for the amine boranes $\text{H}_3\text{N}\cdot\text{BH}_n(\text{C}_6\text{F}_5)_{3-n}$, their lithium salts $[\text{Li}\{\text{thf}\}_x][\text{NH}_2\text{BH}_n(\text{C}_6\text{F}_5)_{3-n}]$ and the zirconocene complexes $\text{Cp}''_2(\text{CH}_3)(\text{NH}_2\text{BH}_n(\text{C}_6\text{F}_5)_{3-n})$ for $n = 1, 2$	90
Table 3.3: Comparison between the B—N / C—C bond lengths between the neutral free small molecule and bound anionic ligand ($-\text{NH}_2\text{BH}_3$ / $-\text{CH}_2\text{CH}_3$).	110
Table 3.4: Structural parameters of group 4 metallocene amidoborane complexes.	114
Table 3.5: Ti—N bond lengths for selected titanocene amides.	119
Table 4.1: Hydroboration of selected alkene and alkyne substrates with $\text{Me}_2\text{S}\cdot\text{BH}(\text{C}_6\text{F}_5)_2$	133
Table 4.2: Hydroboration of selected alkene and alkyne substrates with $\text{Me}_2\text{S}\cdot\text{BH}_2(\text{C}_6\text{F}_5)$	136

Abbreviations

ⁱ Bu	<i>iso</i> -Butyl
ⁿ Bu	<i>n</i> -Butyl
^t Bu	<i>tert</i> -Butyl
Bn	Benzyl
Cp	Cyclopentadienyl
Cp ^{''}	1,3-bis(trimethylsilyl)cyclopentadienyl
Cp [*]	Pentamethylcyclopentadienyl
Cy	Cyclohexyl
Et	Ethyl
<i>m</i> -F	<i>meta</i> -fluorine atom
Me	Methyl
Mes	Mesityl
NMR	Nuclear Magnetic Resonance
<i>p</i> -F	<i>para</i> -fluorine atom
Ph	Phenyl
ⁱ Pr	<i>iso</i> -Propyl
py	Pyridine
thf	Tetrahydrofuran
<i>o</i> -F	<i>ortho</i> -fluorine atom
OTf	Triflate

Acknowledgements

I would like to begin with an expression of immense gratitude for my supervisor Dr Simon Lancaster and for the support, encouragement and countless opportunities that he has provided during my time at UEA. I am especially thankful for the incredible team of crystallographers who contributed to this work, including Dr Graham Tizzard, Dr Dan Smith, Dr David Hughes, Dr Joseph Wright and Dr Simon Coles, without whom I would not have been able to complete my research. I would like to thank the University of East Anglia and the School of Chemistry for the gifts of the Dean's Studentship and A. R. Katritzky Scholarship, both of which greatly relieved the cost of tuition and fees. I am additionally grateful for the useful discussions and lab facilities provided by my secondary supervisor, Prof. Manfred Bochmann.

I would like to thank Dr Anna Fuller for establishing the foundation chemistry on which my project relied (especially compound **13-4thf**) and for her help and encouragement during the final writing process. I have been fortunate enough to work with several project students who have contributed directly to this thesis, and my deepest thanks go to Jenni Harris and Mark Wright for the preparation and characterization of the adducts presented in **Chapter 2** and the $\text{Li}[\text{NHPPhBH}_n(\text{C}_6\text{F}_5)_{3-n}]$ salts discussed in **Chapter 3**. My time in lab 1.34b was incredibly enjoyable thanks to members of the Lancaster, Bochmann and Wildgoose groups, for their suggestions, encouragement and friendly lab banter.

My family and friends have been a constant source of encouragement and support during my PhD research, and for this I will be forever grateful. I would like pay special thanks Dr John Turner for inspiring me to pursue a degree in chemistry and for always reminding me to focus on and believe in the fundamental beauty of science. I am eternally grateful for and constantly humbled by the incredible love and support that I have received from Richard, most especially in sharing this experience together. Now, on to the next adventure!

Chapter 1 Introduction to boranes

1.1 Overview

The chemistry of boron has frustrated and surprised chemists since before borane research began in the mid-1800s,¹ and has progressed into a well understood and highly active area of synthetic research. Of considerable importance, the established chemistry of perfluoroaryl boranes has found application in both organic and inorganic chemistry, along with recent advances in organometallic chemistry and catalysis.²⁻⁴ The following overview provides a general introduction to the preparation, properties and uses of boranes, specifically as they apply to small molecule transformations and functionalizations in hydroboration and dehydrocoupling.

1.2 Properties of boranes

Boranes are small, neutral molecules formed from a central boron atom surrounded by three covalently bound groups such as hydrogen, halides or alkyl / aryl groups. Boron has only three valence electrons and therefore boranes bear an empty p-orbital⁵ which, in general, contributes significantly to their observed chemistry. The simplest borane, BH_3 , exists as the B_2H_6 dimer, featuring bridging hydrides that share electron density with the empty p-orbital of the neighboring boron atom. As a result of this electron sharing, the B—H—B bridging hydride forms a 3 center, 2 electron (3c2e) unit.^{5,6} In general, small boranes containing at least one B—H bond tend to form dinuclear or multinuclear compounds through 3c2e bridging hydrides. This structural precedence is even observed in multinuclear boron hydride clusters, such as pentaborane (B_5H_9)⁷ and decaborane ($\text{B}_{10}\text{H}_{14}$) (**Figure 1.1**),⁸ and may be described in electron counting terms using Wade's rules.⁹

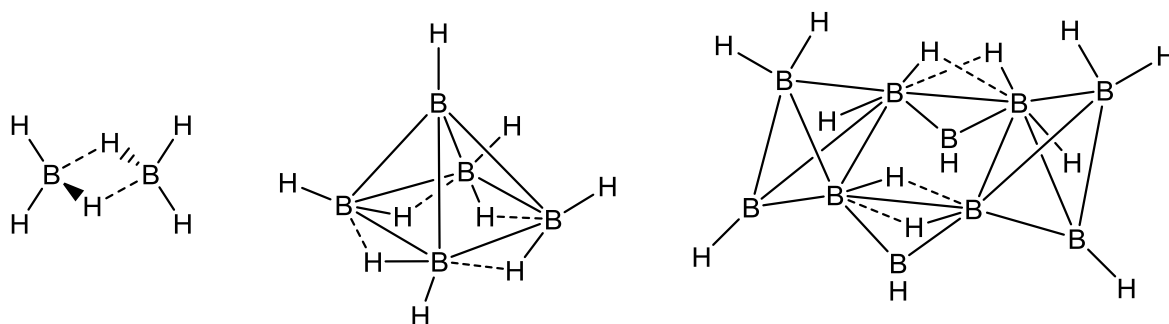


Figure 1.1: Molecular structure of diborane (left), pentaborane (middle) and decaborane (right) featuring a B—H—B bridging hydride structural motif.

Due to the dimeric nature of borane (B_2H_6), application of its electron deficiency for synthetic use requires retrodimerization to precede reactivity. For this reason, the closely related monomeric boron trihalides BX_3 ($X = F, Cl, Br$) are often preferred for use in both catalytic and stoichiometric chemical reactions. In a similar fashion to borane, the boron trihalides are classified as strong Lewis acids. The Lewis acid strength of the boron trihalides is governed, in large part, by the degree of π -bonding from the halide ligand to the empty p-orbital of boron (**Figure 1.2**).¹⁰ For the boron trihalides, efficient π -donation occurs in instances where the electron donating orbital of the halide and the electron deficient orbital of the boron are of similar size (**Figure 1.2**). This restricts localization of the electron pair from the occupied halide p-orbital to a space which may participate in maximum orbital overlap with the empty boron p-orbital. More efficient overlap results in a higher percentage of electron occupancy of the empty p-orbital on boron, reducing the overall Lewis acidic nature of the borane. For this reason, the order of Lewis acidity for the boron trihalides is found to be $BF_3 < BCl_3 < BBr_3$.^{11–13}

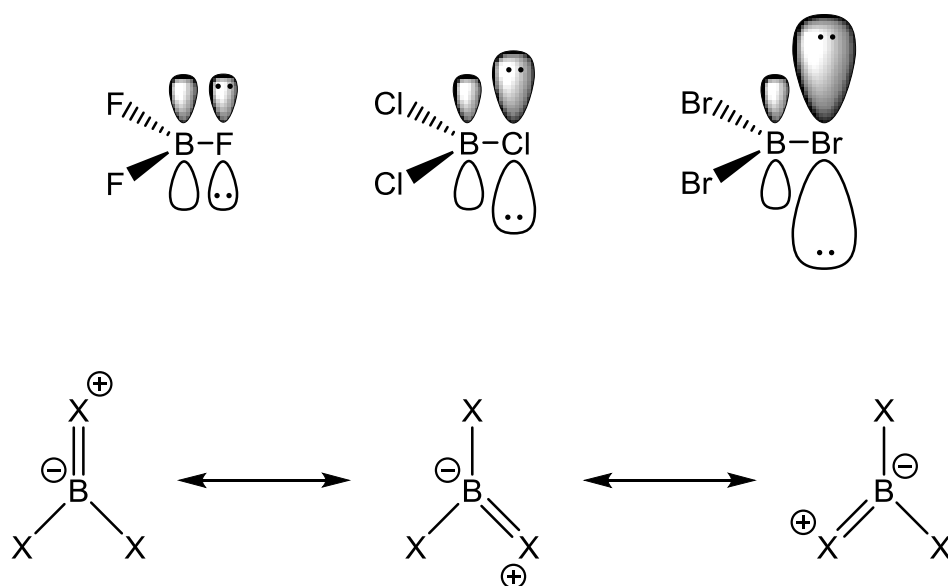
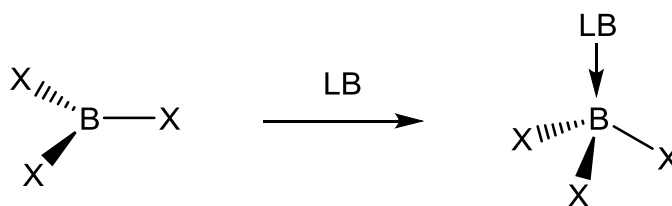


Figure 1.2: Efficiency of the π -bonding character for the boron trihalides (top) and contributing resonance structures as a result of π -donation from occupied halide p-orbitals into the unoccupied p-orbital on boron (bottom).

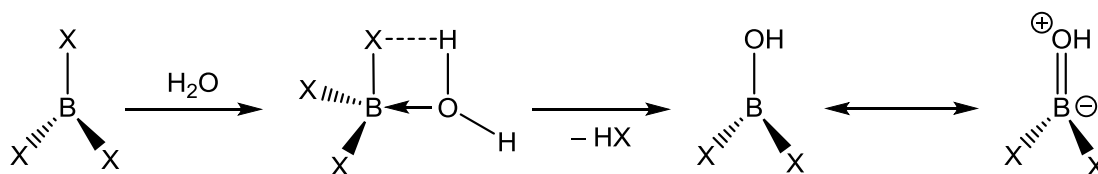
Borane and the boron trihalides demonstrate facile and often undesirable reaction with water, especially when handled in their neat form as gases (B_2H_6 , BF_3) or volatile liquids (BCl_3 , BBr_3). Initial contact between the borane and a water molecule results in adduct formation through donation of an electron pair from the oxygen atom of the water molecule into the empty p-orbital on boron. Upon coordination of water or another donor molecule, the essentially planar borane will adopt a nearly tetrahedral geometry (**Scheme 1.1**). Ease of this geometry change is affected by the π -donation strength of the covalently bound halide group, such that strong π -donation inhibits facile geometry change and thus competing hydrolysis.¹³

Scheme 1.1: Borane geometry change upon Lewis base coordination.



In the case of water coordination, the resulting water adduct ($\text{H}_2\text{O}\cdot\text{BX}_3$; $\text{X} = \text{H}, \text{F}, \text{Cl}, \text{Br}$) may then undergo further intramolecular activation to produce a strong boron—oxygen bond,¹⁴ concomitant with release of an acid by-product (**Scheme 1.2**).

Scheme 1.2: Generic hydrolysis reaction of boranes.



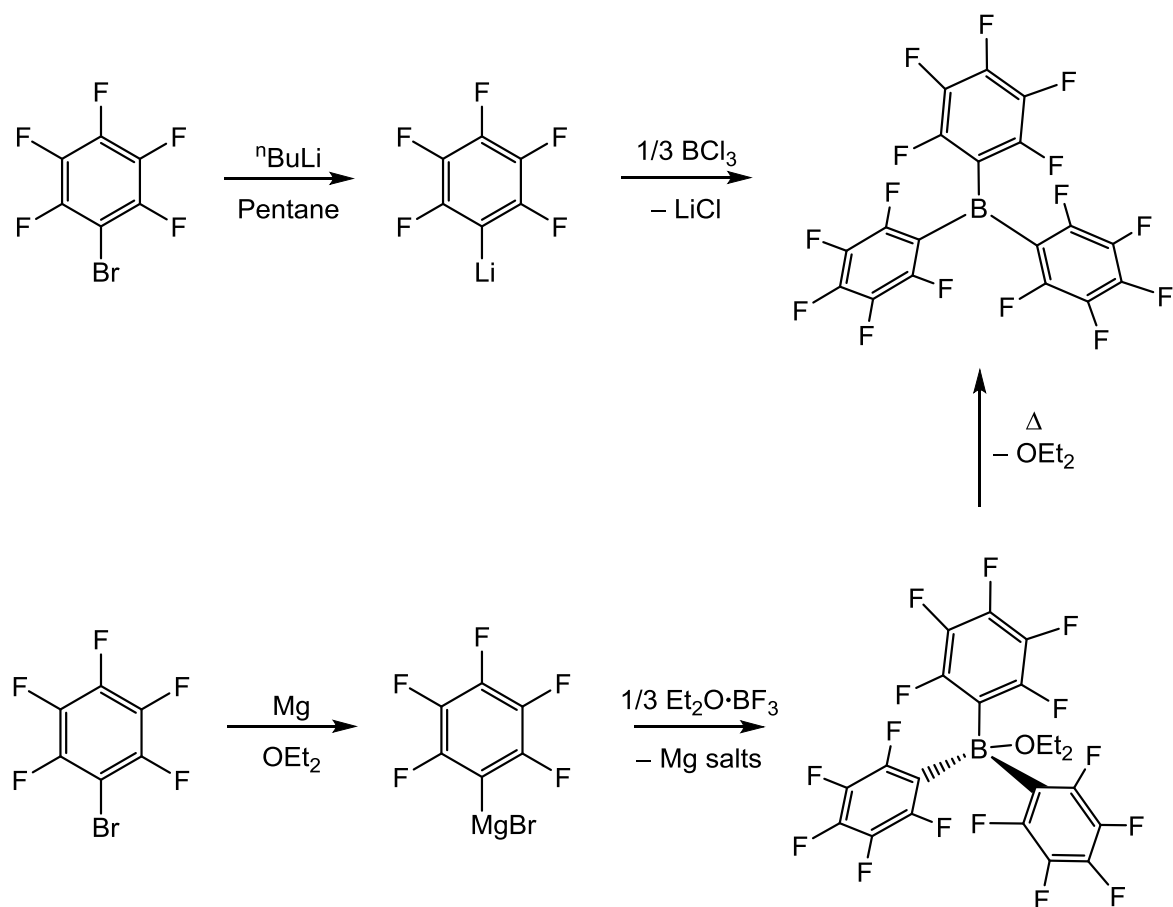
Complete hydrolysis produces the corresponding boric acids,¹⁵ rendering the severely reduced Lewis acidity at the boron insufficient for many applications. For this reason, boranes are often handled in their Lewis adduct form, in which a small, unreactive donor molecule occupies the empty coordination site on boron until the desired chemistry may occur. Borane and the boron trihalides are known to form stable Lewis adducts with donor molecules^{14,16,17} such as amines,^{18,19} ethers,^{17,20} nitriles,^{12,17} pyridines,^{11,17} sulfides²¹ and phosphines.¹⁹

1.3 Development of perfluoroaryl boranes

In response to the synthetic versatility of the Lewis acidic boron trihalides, research efforts turned toward the development of more thermally robust and water tolerant alternatives. Boranes bearing alkyl and aryl groups have increased resistance to hydrolysis due to the larger steric size of the groups and the increased strength of the B—C bond towards hydrolysis in comparison with the B—X bond in the boron trihalides.²² The organoboranes, however, have markedly decreased Lewis acidity compared to the boron trihalides due to the electron donating nature of the covalently bound alkyl or aryl group. As a result, research efforts turned towards the organofluorine group, which features increased electron withdrawing strength in comparison with its alkyl analogs, while still maintaining the robust B—C bond.²² Preparations of small boranes containing at least one organofluorine group date back to the 1960s with reports of the mixed organoboron halides $(F_3C)BF_2$ ²³ and $(CF_2CF)BX_2$ ($X = F, Cl$)²⁴ in addition to the organoborane $(CF_2CF)_3B$.²⁴ Those boranes featuring small organofluorine groups, such as the $-CF_3$ group, suffered from facile decomposition through halide abstraction and the irreversible formation of B—F bonds.²⁵ It was therefore important to consider the choice of covalently bound organofluorine group in terms of this side reactivity.

Tris(pentafluorophenyl)borane may, in many instances, be regarded as a quintessential Lewis acid. Its ease of preparation and handling, combined with its robust stability towards hydrolysis^{26–28} and high Lewis acidity,^{29–31} have resulted in a multitude of chemical applications.^{2–4} The perfluoroaryl borane was first prepared by Stone and Massey in 1963 by treatment of BCl_3 with pentafluorophenyl lithium (**Scheme 1.3**).²⁵ In part due to the highly reactive nature of the chemical intermediate C_6F_5Li ,³² an additional preparation method was reported^{33,34} using the $-C_6F_5$ transfer reagent C_6F_5MgBr to afford $Et_2O \cdot B(C_6F_5)_3$ in high yield.

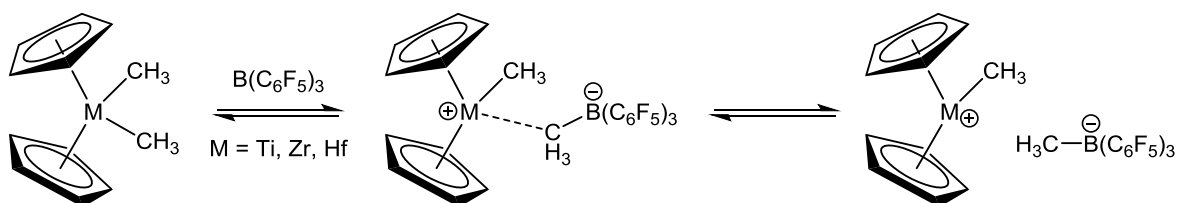
Scheme 1.3: Preparation methods for tris(pentafluorophenyl)boron.



The base free alternative may be isolated from the Lewis adduct by sublimation at $120\text{ }^\circ\text{C}$. The Lewis acidity of $\text{B}(\text{C}_6\text{F}_5)_3$ has been measured with the Childs³⁵ and Gutmann³⁶ methods and is found to fall between that of BF_3 and BCl_3 .²⁹⁻³¹

Despite its initial appearance in the 1960s, the utilization of $\text{B}(\text{C}_6\text{F}_5)_3$ for chemical transformations has only recently gained popularity. In a seminal report published in the early 1990s, $\text{B}(\text{C}_6\text{F}_5)_3$ was shown to activate group 4 metallocenes through methyl abstraction to generate electrophilic metal centers^{37,38} (**Scheme 1.4**), effective for the catalytic polymerization of alkenes.³⁹⁻⁴¹

Scheme 1.4: Methyl abstraction by $B(C_6F_5)_3$ used for the generation of catalytically active electrophilic group 4 metal centers.

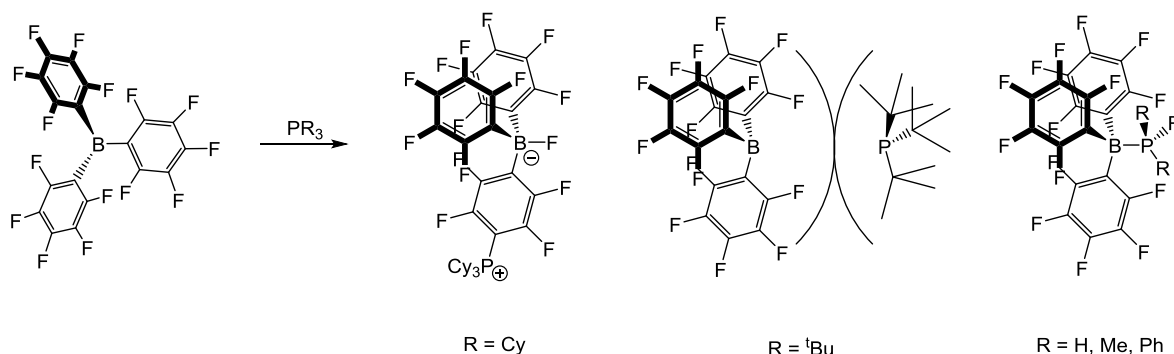


Since then, the chemistry of $B(\text{C}_6\text{F}_5)_3$ has grown to include applications in catalysis,^{3,42} the preparation of weakly coordinating anions^{43,44} and the preparation of novel perfluoroaryl boranes and their Lewis adducts.^{45–47} It is also commonly used as a $-\text{C}_6\text{F}_5$ transfer reagent in organometallic synthesis.^{3,48–54} Tris(pentafluorophenyl)borane forms Lewis adducts with small donor molecules³ such as water,^{26–28} pyridines,^{55,56} sulfides,²¹ phosphines,^{25,55} nitriles,³⁰ isonitriles,³⁰ imines⁵⁷ and amines.^{25,55,56,58} To demonstrate the continued interest in and use of these Lewis adducts, two currently prosperous research areas which involve Lewis adducts of borane and tris(pentafluorophenyl)boron are described below.

1.4 Borane adducts for use in hydrogen activation

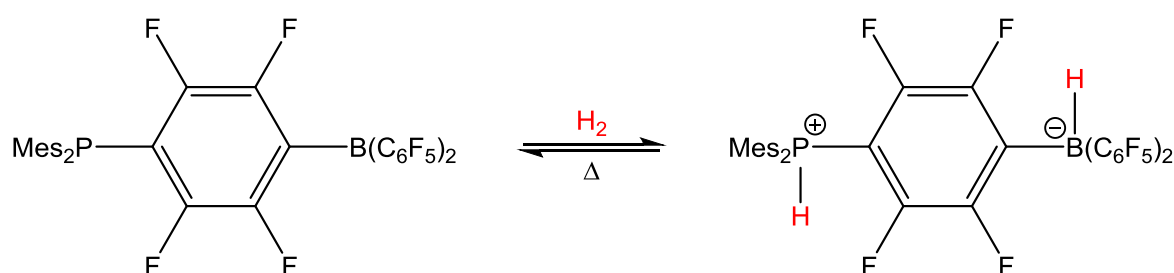
Perfluoroarylboranes (and alanes) in combination with sterically inaccessible phosphine moieties have recently found application in metal-free small molecule activation. The reaction of $B(\text{C}_6\text{F}_5)_3$ with tertiary organophosphines (PR_3) generally proceeds in one of three ways, depending on the steric and electronic features of R: adduct formation,^{19,25,30,55,59,60} zwitterion formation⁶¹ or an unquenched Lewis acid / base pair⁶² (Scheme 1.5).

Scheme 1.5: Reactivity between tris(pentafluorophenyl)boron and small phosphine Lewis bases PR_3 to produce a zwitterion ($R = \text{Cy}$), frustrated Lewis pair ($R = \text{}^t\text{Bu}$) and Lewis adduct ($R = \text{H, Me, Ph}$).



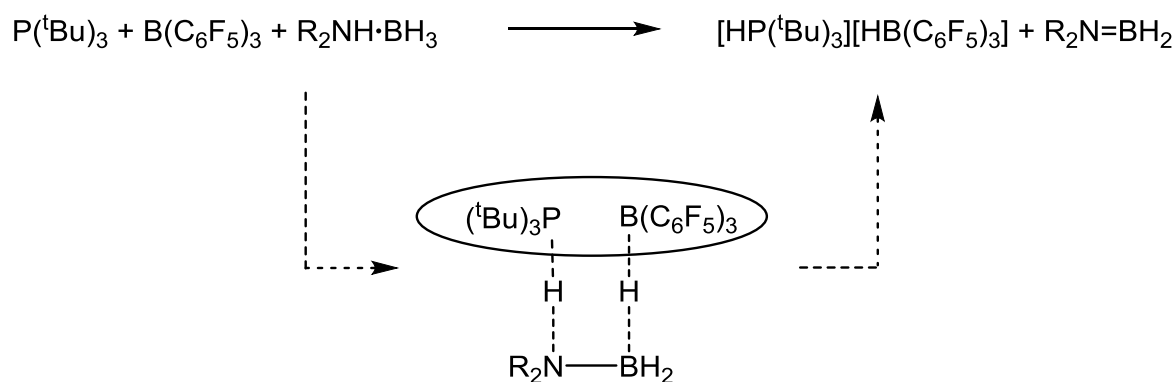
These and similar systems which contain a Lewis acid and Lewis base which are unable to react due to steric congestion⁶³ (either forming a zwitterion or an unquenched Lewis acid / base pair) have recently been termed 'frustrated Lewis pairs'.⁶⁴ In 2006, the first example of reversible, metal-free dihydrogen activation was reported by Stephan and coworkers using the intramolecular frustrated Lewis pair $(\text{C}_6\text{H}_2\text{Me}_3)_2\text{P}(\text{C}_6\text{F}_4)\text{B}(\text{C}_6\text{F}_5)_2$ (**Scheme 1.6**).^{65,66} This work has led to numerous examples of stoichiometric metal-free activation of other small molecules^{64,67–69} such as CO_2 ,⁷⁰ N_2O ,⁷¹ alkenes,⁷² CO ⁷³ and alkynes.⁶⁸

Scheme 1.6: Reversible dihydrogen activation by the frustrated Lewis pair $(\text{C}_6\text{H}_2\text{Me}_3)_2\text{P}(\text{C}_6\text{F}_4)\text{B}(\text{C}_6\text{F}_5)_2$.



Frustrated Lewis pairs have also been shown to react with amine borane Lewis adducts under both stoichiometric and catalytic conditions.⁷⁴⁻⁷⁷ For example, when treated with a secondary amine borane, the frustrated Lewis pair $(^t\text{Bu})_3\text{P} / \text{B}(\text{C}_6\text{F}_5)_3$ reacts to produce the phosphonium borohydride $[\text{HP}(^t\text{Bu})_3][\text{HB}(\text{C}_6\text{F}_5)_3]$ and equimolar amounts of amidoborane $\text{R}_2\text{N}=\text{BH}_2$ (**Scheme 1.7**).⁷⁴

Scheme 1.7: Dehydrogenation of an amine borane by a frustrated Lewis pair.



In contrast to the chemistry of the boron trihalides, which form 1:1 Lewis adducts with bulky tertiary phosphines, the exceptional properties of tris(pentafluorophenyl)borane, along with steric bulk provided by the $-\text{C}_6\text{F}_5$ rings, has offered an extension to the currently accepted chemistry of Lewis acidic boranes. Frustrated Lewis pairs have developed into a unique and highly valuable class of molecules which continue to provide chemical information directly applicable to industrially important processes.

1.5 Borane adducts for use in hydrogen storage

The fuel reserves with which local and global economies function are becoming rapidly depleted, prompting concern regarding the viability of alternative forms of energy. Current

research efforts focus on the development of renewable systems, which are required to meet strict energy goals and specifications for industrial-scale applications.⁷⁸ Among the proposed solutions to the current energy crisis is the introduction of chemical hydrogen storage materials to transport systems such as cars and buses.⁷⁹ Such hydrogen storage systems are expected to facilitate facile uptake, storage and release of molecular hydrogen to be used as fuel. Among other proposed chemical hydrogen storage media, such as metal hydrides,^{80,81} carbon nanotubes⁸² and metal organic frameworks (MOFs),^{83,84} metal amidoboranes^{85–88} and amine borane Lewis adducts^{89,90} have been nominated as suitable classes of molecules for storage purposes.

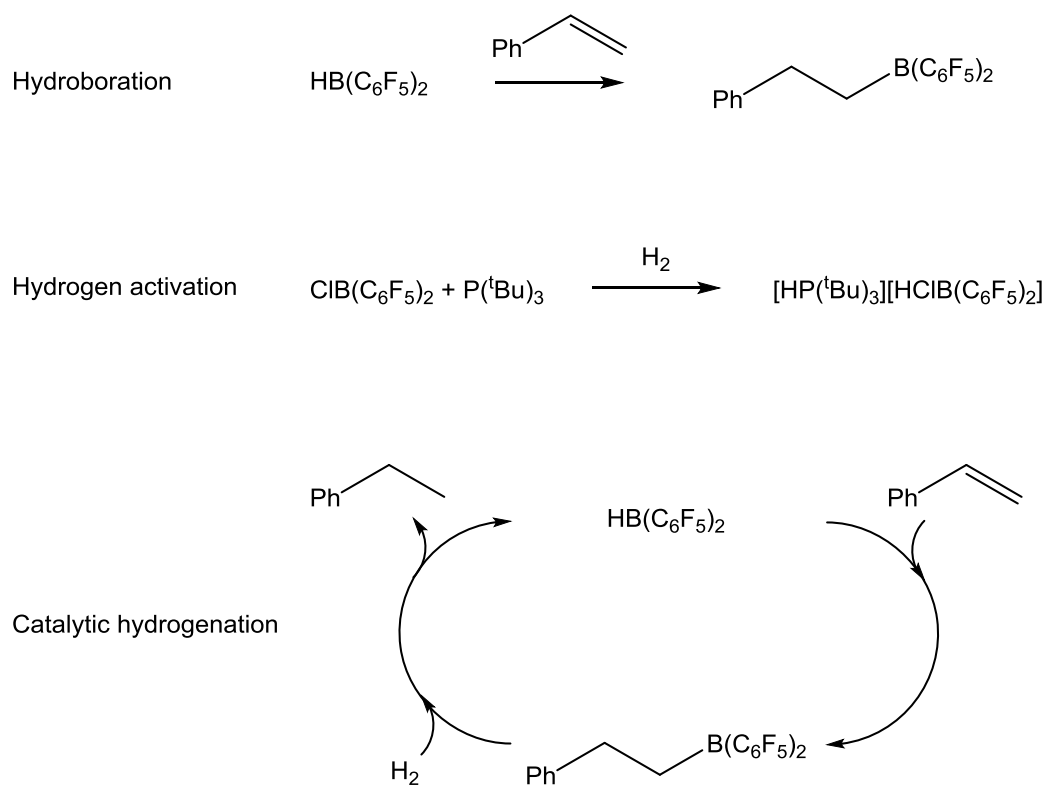
A large variety of amine boranes have been developed for use as structural models to the parent compound, ammonia borane ($\text{H}_3\text{N}\cdot\text{BH}_3$), attractive as a storage medium due to its high weight percentage of hydrogen (19.6%).^{89,90} For this reason, amine boranes and related adducts (such as phosphine boranes) serve as the foundation of several active areas of academic and industrial research.⁹¹ Current interest lies in the development of catalytic dehydrocoupling pathways for a variety of amine adducts of BH_3 , such as $\text{MeH}_2\text{N}\cdot\text{BH}_3$ and $\text{Me}_2\text{HN}\cdot\text{BH}_3$.⁹² Dihydrogen bonding between the protic N—H and hydridic B—H groups in these Lewis adducts is thought to play an integral part in the dehydrocoupling mechanism.⁹³ For this reason, research efforts focus, in part, on the understanding of the solid state structures of these Lewis adducts and development of novel adducts to enhance structure / function relationships.

In addition to the utilization of molecular dihydrogen released from the various storage media, the isolation and characterization of the resulting B/N containing materials has drawn considerable attention in the literature.^{94–97} Boron nitride materials, which result from complete dehydrogenation of ammonia borane, are highly researched due to their isoelectronic relationship with industrially important graphenes and carbon nanotubes.

1.6 Adducts of other pentafluorophenyl substituted boranes

In response to the tremendous array of chemistry demonstrated by tris(pentafluorophenyl)borane,²⁻⁴ derivatives with only one or two $-\text{C}_6\text{F}_5$ rings have become an intriguing area of research. Chemistry of bis(pentafluorophenyl)borane, $\text{HB}(\text{C}_6\text{F}_5)_2$ and its halogenated analogue, $\text{ClB}(\text{C}_6\text{F}_5)_2$, includes functionalization of unsaturated bonds by hydroboration,⁴⁶ hydrogen activation as part of a frustrated Lewis pair⁹⁸ and most recently in catalytic metal-free hydrogenation of unfunctionalized olefins (Scheme 1.8).⁹⁹

Scheme 1.8: Reactivity of bis(pentafluorophenyl)borane and its chloride analog.



In a similar fashion to borane (B_2H_6), base free $HB(C_6F_5)_2$ is dimeric in nature and therefore suffers from the same retrodimerization requirement for reactivity. However, both $HB(C_6F_5)_2$ and the mono(pentafluorophenyl)borane analog $H_2B(C_6F_5)$ are easily isolated as Lewis adducts with dimethylsulfide.⁴⁷ These highly crystalline compounds exhibit similar reactivity to the dimeric boranes without the need for dimer dissociation. This is exemplified in a comparison between the hydroboration chemistry of Piers' borane $[HB(C_6F_5)_2]_2$ and the more readily prepared dimethylsulfide adducts of mono- and bis-(pentafluorophenyl)borane, presented in **Chapter 4**.

Facile ligand exchange between $LB \cdot B(C_6F_5)_3$ ($LB = SMe_2, OEt_2$) and other Lewis bases has led to the isolation of a number of amine and other nitrogen donor adducts of tris(pentafluorophenyl)borane.^{58,100} In an analogous fashion, the dimethylsulfide adducts $Me_2S \cdot BH_n(C_6F_5)_{3-n}$ ($n = 0, 1, 2$) have been used as precursors to the more chemically intriguing amine borane adducts $H_3N \cdot BH_n(C_6F_5)_{3-n}$ ($n = 1, 2$).^{101,102} These adducts, bearing protic N—H and hydridic B—H bonds, similar to those observed in $H_3N \cdot BH_3$ and $Me_2HN \cdot BH_3$, may be used as model substrates for the dehydrocoupling of amine boranes. A selection of amine and nitrogen donor ligands were used to prepare new Lewis adducts of mono- and bis-(pentafluorophenyl)borane. Synthetic procedures, characterization data and comparisons between the structure and bonding trends of the mono- and bis-(pentafluorophenyl)borane adducts are presented in **Chapter 2**.

Facile deprotonation of amine boranes produces the corresponding amidoborane anions in quantitative yields. Metal amidoboranes such as MNH_2BH_3 ($M = Li$,^{86,103} Na ,⁸⁶ K ⁸⁷), $M(NH_2BH_3)_2$ ($M = Ca$,^{88,103} Sr ¹⁰⁴) and the recently reported mixed metal amidoboranes $Na[Li(NH_2BH_3)_2]$ ¹⁰⁵ and $Na_2Mg(NH_2BH_3)_4$ ¹⁰⁶ contain a high weight percentage of dihydrogen and have been investigated for their dehydrogenation properties.^{85,107} Dehydrogenation of the metal amidoboranes occurs at lower temperatures and with less borazine release⁸⁶ than dehydrogenation of ammonia borane as a result of the difference in their bonding relative to the parent compound.^{108,109} Metal amidoboranes have also

been used in the preparation of early transition metal complexes bearing the $-\text{NH}_2\text{BH}_3$ ligand,¹¹⁰⁻¹¹² thought to play a significant role in catalytic dehydrocoupling by early transition metals.

In a similar fashion to the generation of the described $\text{M}(\text{NH}_2\text{BH}_3)$ ($\text{M} = \text{Na}, \text{K}, \text{Li}$) species, facile deprotonation of the ammonia adduct of tris(pentafluorophenyl)borane and its mono(pentafluorophenyl)borane and bis(pentafluorophenyl)borane analogs results in quantitative conversion to the corresponding lithium salts $\text{Li}[\text{NH}_2\text{BH}_n(\text{C}_6\text{F}_5)_{3-n}]$ ($n = 0, 1, 2$).^{101,102,113} These salts have been used to stabilize transition metal amidoborane complexes, analogous to those of the $-\text{NH}_2\text{BH}_3$ ligand, which exhibit structure and bonding motifs which have been imposed as possible intermediate states in catalytic dehydrocoupling cycles.^{101,102} A collection of group 4 metallocene complexes of the ligands $-\text{NH}_2\text{B}(\text{C}_6\text{F}_5)_3$, $-\text{NH}_2\text{BH}(\text{C}_6\text{F}_5)_2$ and $-\text{NH}_2\text{BH}_2(\text{C}_6\text{F}_5)$ are presented in **Chapter 3**, along with application of the resulting structure and bonding to currently accepted mechanisms for early transition metal catalyzed dehydrocoupling.

Chapter 2 Amine and nitrogen donor adducts of mono- and bis-(pentafluorophenyl)borane

2.1 Introduction

Lewis adducts featuring the combination of Lewis acidic boranes and amine lone pair donors constitute a class of molecules known as amine boranes. Despite the isoelectronic relationship between these Lewis adducts and closely related alkanes, amine boranes exhibit molecular polarity, a characteristic responsible for significant variation in bonding and chemistry relative to their C—C congeners.^{90,111,114–116} In addition, amine boranes have acidic N—H and hydridic B—H groups present within the adduct, an attractive feature which supports their use as hydrogen storage materials.^{89,90,117} The chemistry of these Lewis adducts and related compounds has been extensively reviewed,^{90,118–120} with fundamental research into the structure of ammonia borane ($\text{H}_3\text{N}\cdot\text{BH}_3$) and isomeric diammoniate of diborane ($[(\text{NH}_3)_2\text{BH}_2][\text{BH}_4]$) dating back to the 1920s.^{121–124}

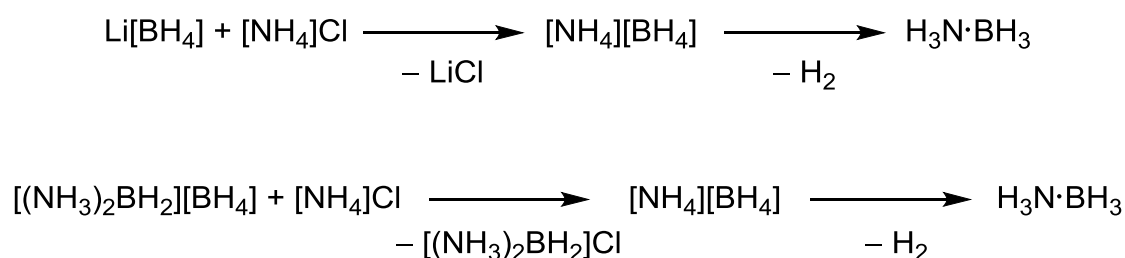
Renewed interest in these compounds has resulted from their suggested function as hydrogen storage materials. Current efforts are largely concerned with amine borane dehydrocoupling to yield dihydrogen along with amino- and imino-boranes as polyalkene and polyalkyne analogues, or quantitative dihydrogen elimination to give boron nitride materials. This potentially reversible process is under investigation as a means to store and use hydrogen to meet increasing energy demands.^{89,95,125–128}

2.1.1 Ammonia borane

A high yielding and high purity preparation of ammonia borane was first reported in 1955 from salt metathesis between lithium borohydride and ammonium chloride

(**Scheme 2.1**).¹²⁹ The Lewis adduct was isolated as a colorless, air-stable solid. The authors also report preparation through the reaction of diammoniate of diborane, $[(\text{NH}_3)_2\text{BH}_2][\text{BH}_4]$ with ammonium chloride. Both reactions proceed through formation, and subsequent decomposition, of ammonium borohydride to make ammonia borane and one equivalent of dihydrogen gas.

Scheme 2.1: *Preparation of ammonia borane through decomposition of ammonium borohydride.*



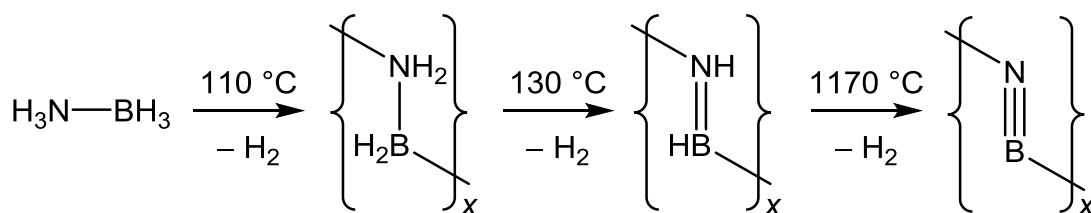
Today, ammonia borane is most commonly prepared through either the metathesis reactions described above or by the direct addition of ammonia to diborane or a borane adduct such as $\text{thf}\cdot\text{BH}_3$.^{90,128,130} The ease of handling, resistance to hydrolysis, low molecular weight and high weight percentage of dihydrogen (19.6%) contribute to the proposed use of ammonia borane as a hydrogen storage medium.

Discussion of the solid state structure of ammonia borane has a lengthy history in the literature, beginning in 1956 with the use of powder X-ray diffraction methods.^{131,132} However, the structure was unequivocally refined by Crabtree and co-workers in 1999 using neutron diffraction.¹¹⁵ Ammonia borane adopts a low energy staggered conformation, with a B—N bond length of 1.58(2) Å. In the solid state, ammonia borane exhibits dihydrogen bonding, a distinct bonding type described as a short H...H interaction between an acidic N—H and a hydridic B—H group measuring between 1.7 and 2.2 Å.¹¹⁵

A dihydrogen bond is therefore significantly shorter than the sum of the van der Waals radii for two hydrogen atoms, measuring 2.4 Å. Dihydrogen bonding in ammonia borane strongly influences the crystal packing and as a result, ammonia borane has a very dense stacking arrangement in the solid state. This is in contrast to the isoelectronic C—C congener, ethane, in which the loose packing exhibits no H···H inter- or intra-molecular distances shorter than the sum of the van der Waals radii.¹³³ As a result, ammonia borane exhibits very low solubility in common organic solvents,⁸⁹ a characteristic which reduces efficient use in homogeneous catalytic dehydrocoupling.

As a solid, ammonia borane is stable towards thermal decomposition up to 110 °C, whereupon the first equivalent of dihydrogen is released, producing the aminoborane {H₂N=BH₂}_x polymer. Further dihydrogen release requires temperatures up to 130 °C to produce the iminoborane {HN=BH}_x, and the final equivalent of dihydrogen is released only above 1170 °C (**Scheme 2.2**).¹³⁴ Due to the high temperatures required for thermal degradation of ammonia borane, its use as a hydrogen storage medium requires careful consideration of catalyst efficiency, reaction solvent, reaction duration and temperature.

Scheme 2.2: Thermal decomposition of solid ammonia borane.



In response to the robust stability of ammonia borane, synthetic strategies focus on the modification of ammonia borane to make a material with more readily accessible dihydrogen. Synthetic considerations include not only ease of dihydrogen loss, but also

increased solubility of the starting adducts and resulting aminoborane polymers in organic solvents. One popular approach is use of N-substituted amine boranes, which feature small R groups bound to nitrogen in place of the N—H groups which encourage dihydrogen bonding in the parent molecules. The resulting decrease in the density of the dihydrogen bonding network has been proposed to alleviate the high temperatures and pressures required for efficient dihydrogen loss in addition to increasing substrate solubility.⁹⁰

2.1.2 *N*-substituted amine boranes

Alkyl substituted amine boranes have been employed as suitable models for ammonia borane due to their similar size and reported dehydrocoupling chemistry in comparison with the parent amine borane. In a similar fashion to ammonia borane, alkyl substituted amine boranes are most commonly prepared through either salt metathesis between an ammonium chloride and a metal borohydride or through Lewis acid / Lewis base exchange between the amine and either diborane or a borane adduct (such as thf·BH₃).⁹⁰ The most frequently used substituted amine boranes are the N-methylated amine boranes H_{3-n}R_nN·BH₃ (n = 1, 2; R = CH₃), however one can envisage the depth of this class of compounds when considering larger R groups or the possibility of mixed R groups on the nitrogen atom. Of the two mentioned N-methylamine boranes, dimethylamine borane (DMAB) is the most popular choice for several reasons, including its commercial availability, low cost, single dehydrocoupling product ({Me₂N=BH₂}₂) and increased solubility in organic solvents.¹³⁵ In addition, the relatively small size of the methyl groups allow for meaningful comparisons between the dehydrocoupling chemistry of dimethylamine borane and ammonia borane.

The solid state structure of DMAB (and that of methylamine borane)⁹³ exhibits a similar dihydrogen bonding network to that observed for ammonia borane,¹¹⁵ but due to the

presence of the methyl groups, this arrangement is less densely packed in the crystal lattice (**Figure 2.1**).⁹³ This decrease in dihydrogen bonding is reflected in the improved solubility of the methylated amine boranes in comparison with ammonia borane.

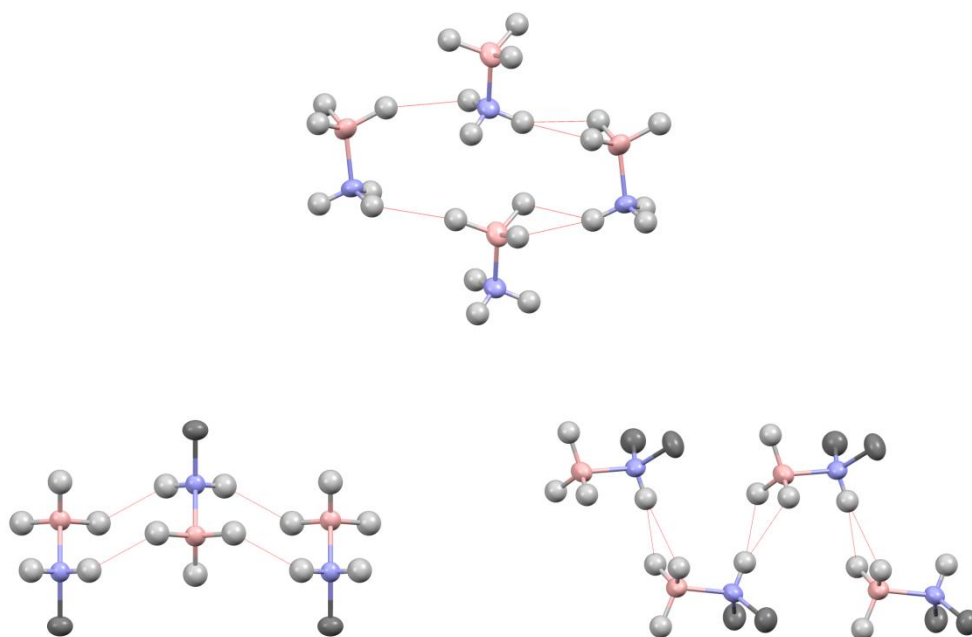


Figure 2.1: Crystal packing and dihydrogen bonding network of ammonia borane (top), methylamine borane (bottom, left) and dimethylamine borane (bottom, right), with displacement ellipsoids displayed at the 50% probability level.⁹³ Boron (pink), nitrogen (blue), carbon (dark grey), hydrogen (light grey). Hydrogen atoms of the methyl groups of methylamine borane and dimethylamine borane have been omitted for clarity.

In addition to general mechanistic considerations, identification of the resulting oligomeric and polymeric polyamino- and polyimino-boranes is required for the application of a reversible dehydrocoupling process. Increased interest in the aminoborane oligomerization or polymerization is evident in the literature, with these steps proposed to occur either as metal-assisted^{136–139} or off-metal cyclization / oligomerization processes.^{137,138,140} While dehydrocoupling of dimethylamine borane leads to isolation of

the aminoborane dimer $\{\text{Me}_2\text{N}=\text{BH}_2\}_2$,^{135,141} use of methylamine borane produces a mixture of oligomeric and polymeric materials.¹⁴² Other substituted amine boranes such as $^i\text{Pr}_2\text{HN}\cdot\text{BH}_3$ and $\text{Cy}_2\text{HN}\cdot\text{BH}_3$ feature in dehydrocoupling studies^{141,143–145} because of the known monomeric and isolable nature of the dehydrogenated aminoboranes, $^i\text{Pr}_2\text{N}=\text{BH}_2$ ^{140,141,146} and $\text{Cy}_2\text{N}=\text{BH}_2$.¹⁴⁶

Dehydrocoupling of N-methyl substituted amine boranes has been accomplished under relatively mild conditions and with low catalyst loadings. Whilst early and mid transition metal based catalysts have been used to dehydrocouple ammonia borane, dimethylamino borane, and other substituted amine boranes,^{140,147–150} the late transition metal catalysts offer the most desirable dehydrocoupling conditions to date.^{91,143,144,151–153}

2.1.3 Pentafluorophenyl substituted amine boranes

Interest in pentafluorophenyl substituted boranes has focused primarily on their role in polymerization catalysis^{37,38,40,154} and as weakly coordinating anions.^{2,43,44,155} Due to their unique chemistry, it seems fitting to extend applications of perfluoroarylboranes to include pentafluorophenyl substituted amine boranes as models for dehydrocoupling substrates. Among the first Lewis base adducts of tris(pentafluorophenyl)borane was the ammonia adduct, $\text{H}_3\text{N}\cdot\text{B}(\text{C}_6\text{F}_5)_3$.^{25,55} The solid state structure of $\text{H}_3\text{N}\cdot\text{B}(\text{C}_6\text{F}_5)_3$, determined over 40 years after the initial preparation in 1963, exhibits $\text{N}-\text{H}\cdots\text{F}-\text{C}$ intramolecular hydrogen bonding between the $\text{N}-\text{H}$ groups of ammonia and the *ortho*-fluorine atoms of each pentafluorophenyl ring.⁵⁸ Two ammonia $\text{N}-\text{H}$ groups participate in an additional intermolecular $\text{N}-\text{H}\cdots\text{F}-\text{C}$ hydrogen bond with a pentafluorophenyl ring of a neighboring molecule, forming a bifurcated hydrogen bonding interaction (**Figure 2.2**).

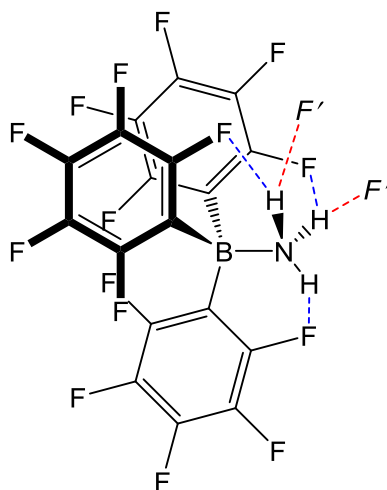
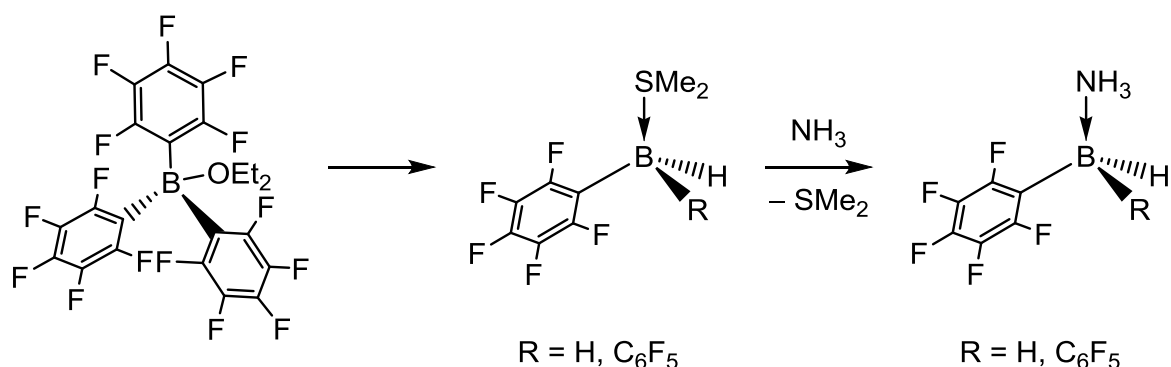


Figure 2.2: Molecular structure of $H_3N \cdot B(C_6F_5)_3$ showing intramolecular (blue) and intermolecular (red) $N-H \cdots F-C$ interactions.

The $N-H \cdots F-C$ interaction is a significant structural feature observed in pentafluorophenyl substituted amine boranes, noteworthy because the organofluorine group is, in general, considered to be a poor hydrogen bond acceptor.¹⁵⁶ Short $H \cdots F$ contacts have been defined by Dunitz as those measuring less than 2.2 Å.¹⁵⁶ As an extension to the classification of $H \cdots F$ contacts between protic amines and organofluorine bonds, Lancaster and co-workers have considered a medium $H \cdots F$ contact to measure between 2.2 Å and 2.35 Å and a long contact described as being between 2.35 Å and 2.55 Å.⁵⁸ These criteria have been used to describe the inter- and intramolecular hydrogen bonding of several amine adducts of tris(pentafluorophenyl)borane (**Figure 2.3, I**) and alane⁵⁸ along with Lewis base adducts of tris(pentafluorophenyl)borane with heterocyclic nitrogen bases¹⁰⁰ (**Figure 2.3, III**) and nitrogen-centered anions¹⁵⁷ (**Figure 2.3, II**).

Scheme 2.3: Preparation of the dimethylsulfide and ammonia adducts of mono- and bis-(pentafluorophenyl)borane.



Both $\text{H}_3\text{N}\cdot\text{BH}(\text{C}_6\text{F}_5)_2$ and $\text{H}_3\text{N}\cdot\text{BH}_2(\text{C}_6\text{F}_5)$ show boron and nitrogen atoms in a tetrahedral geometry, with a B—N bond distance of 1.603(2) Å and 1.615(1) Å, respectively, consistent with that reported for $\text{H}_3\text{N}\cdot\text{B}(\text{C}_6\text{F}_5)_3$ at 1.623(2) Å. While the crystal structure of $\text{H}_3\text{N}\cdot\text{BH}(\text{C}_6\text{F}_5)_2$ is unremarkable, that of $\text{H}_3\text{N}\cdot\text{BH}_2(\text{C}_6\text{F}_5)$ exists as a dimer through dihydrogen bonding between the hydridic B—H groups and the acidic N—H groups with an H(1A)⋯H(2A) distance of 2.121 Å (**Figure 2.4**).¹⁰²

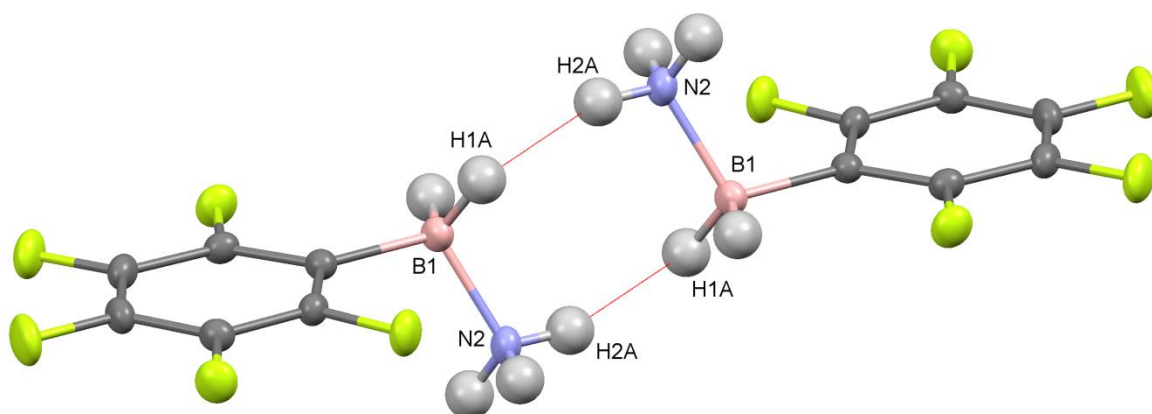


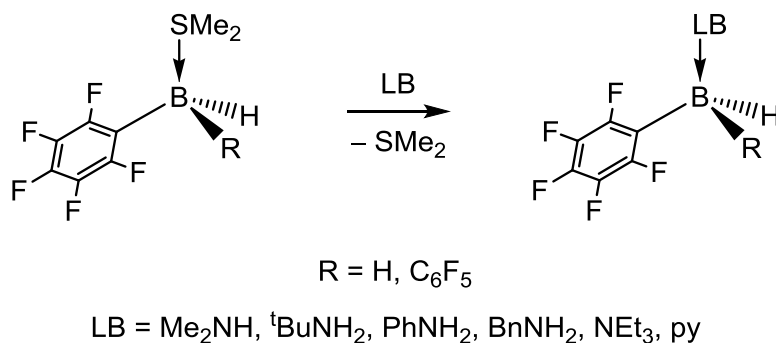
Figure 2.4: Crystal structure of dimeric $\text{H}_3\text{N}\cdot\text{BH}_2(\text{C}_6\text{F}_5)$ with displacement ellipsoids displayed at the 50% probability level.¹⁰² The N—H⋯H—B dihydrogen bonding interactions are indicated in red, with the H(1A)⋯H(2A) distance measuring 2.121 Å.

The amine and nitrogen donor adducts of tris(pentafluorophenyl)borane show a variety of inter- and intra-molecular interactions. These include N—H...F—C contacts, which are noteworthy due to the poor hydrogen bond acceptor properties of the organofluorine group,¹⁵⁶ which form six-membered rings predicted by Etter's rules.¹⁵⁸ Nitrogen donor adducts of mono- and bis-(pentafluorophenyl)borane would be expected to display similar inter- and intra-molecular N—H...F—C contacts, with the addition of the possibility for N—H...H—B dihydrogen bonding interactions and off-set face-to-face $-C_6F_5$ stacking. In order to investigate the supramolecular chemistry of the Lewis adducts of mono- and bis-(pentafluorophenyl)borane, amine and nitrogen donor adducts of both boranes have been prepared and crystallographically characterized. Their significant structure and bonding motifs are discussed and the resulting supramolecular features compared with those of similar adducts.

2.2 Results

The ammonia adduct of tris(pentafluorophenyl)borane is prepared through facile Lewis base displacement from $Et_2O \cdot B(C_6F_5)_3$ or $Me_2S \cdot B(C_6F_5)_3$ with ammonia at room temperature. Following this procedure, a variety of other amine and nitrogen donor adducts of tris(pentafluorophenyl)borane have been reported.⁵⁸ In a similar fashion, treatment of the dimethylsulfide adducts of mono- and bis-(pentafluorophenyl)borane with Lewis bases such as ammonia,^{101,102} amines and other nitrogen donors produces the corresponding Lewis adducts $LB \cdot BH_n(C_6F_5)_{3-n}$ ($n = 1, 2$) (**Scheme 2.4**).

Scheme 2.4: Preparation of nitrogen donor Lewis adducts of $H_nB(C_6F_5)_{3-n}$ ($n = 1, 2$).



As a result of adduct formation with protic amines, the relative Brønsted acidity of the N—H group increases, which is reflected in the downfield shift for the N—H ¹H resonance relative to that of the free amine (**Table 2.1**). This result is also observed in the case of protic amine adducts of tris(pentafluorophenyl)borane.^{58,100}

Table 2.1: $\delta(N-H)$ for the amines and amine adducts of $BH_n(C_6F_5)_{3-n}$ ($n = 1, 2$).^{a,b}

Amine	N—H	Amine·BH ₂ (C ₆ F ₅)		Amine·BH(C ₆ F ₅) ₂		Amine·B(C ₆ F ₅) ₃	
		N—H	$\delta(N-H)$	N—H	$\delta(N-H)$	N—H	$\delta(N-H)$
PhNH ₂	2.49	3.94	1.45	4.69	2.20	6.79	4.30
^t BuNH ₂	0.79	2.46	1.67	3.48	2.69	4.29	3.50
BnNH ₂	0.72	2.65	1.93	3.63	2.91	4.42	3.70
Me ₂ NH	0.23	2.47	2.24	3.79	3.56	6.23	6.00

^a All δ values reported in ppm and referenced to C₆D₆ with the exception of PhH₂N·B(C₆F₅)₃ which is reported relative to CDCl₃.

^b Values for N—H resonances for amine adducts of B(C₆F₅)₃ are from references 62 and 156.

Adduct formation may also be confirmed by comparing the resulting ¹¹B NMR spectrum with that of the Lewis base-free borane. For example, the ¹¹B NMR spectrum for base-free B(C₆F₅)₃ displays a broad resonance near 60 ppm, indicative of a three coordinate neutral boron atom. Upon adduct formation with NH₃, this broad resonance is

replaced by a sharp singlet around -10 ppm, indicating the formation of a four coordinate neutral boron atom. Therefore, direct comparison between the ^{11}B NMR spectrum of the free borane with that of its amine adduct is a quantitative and reliable method for assessment of reaction completion.

Base free $\text{HB}(\text{C}_6\text{F}_5)_2$ exists as a dimer in the solid state.^{45,46} Dissolution of the $[\text{HB}(\text{C}_6\text{F}_5)_2]_2$ dimer in deuterated benzene results in a ^{11}B NMR spectrum consisting of resonances attributed to the dimeric (around 18 ppm) and dissociated monomeric borane (near 60 ppm). Therefore, an analogous assessment of Lewis adduct formation, relative to that described for $\text{B}(\text{C}_6\text{F}_5)_3$ and its amine adducts, may be made with respect to the ^{11}B resonance of $\text{HB}(\text{C}_6\text{F}_5)_2$ near to 60 ppm. The reported nitrogen base adducts of $\text{HB}(\text{C}_6\text{F}_5)_2$ have signals in the ^{11}B NMR spectra between -8 and -20 ppm, consistent with adduct formation and a four coordinate neutral boron atom. For mono(pentafluorophenyl)borane and its Lewis adducts, a shift in the ^{11}B NMR spectra upon adduct formation cannot be directly analyzed as NMR spectroscopic data for base-free $\text{H}_2\text{B}(\text{C}_6\text{F}_5)$ has not been reported to date.

2.2.1 Crystallography

In addition to multinuclear NMR spectroscopic characterization, all but one of the adducts have been characterized by single crystal X-ray diffraction methods. For the reported adducts with amine donors, all boron and nitrogen atoms adopt a nearly tetrahedral geometry, with very little variation in the B—N bond lengths. The boron atoms for $\text{py}\cdot\text{BH}_n(\text{C}_6\text{F}_5)_{3-n}$ ($n = 1, 2$) adopt a nearly tetrahedral geometry, with slightly shorter B—N bond lengths than those observed for the amine adducts.

2.2.1.1 *Amine and nitrogen donor adducts of H₂B(C₆F₅)*

The dimethylamine adduct of mono(pentafluorophenyl)borane, Me₂HN·BH₂(C₆F₅) (**1a**) is prepared through treatment of a toluene solution of Me₂S·BH₂(C₆F₅) with dimethylamine. X-ray quality crystals of **1a** were isolated after addition of light petroleum to the crude reaction mixture and subsequent cooling to -25 °C. Both the boron and nitrogen atoms are in a slightly distorted tetrahedral geometry, with a B—N bond length of 1.609(5) Å. The supramolecular structure of **1a** (**Figure 2.5**) exhibits weak H···H contacts between acidic N—H and hydridic B—H groups in a bifurcated BH₂···HN fashion. Whilst this arrangement is reminiscent of the bonding in the pentafluorophenyl-free analog Me₂HN·BH₃,⁹³ the presence of one pentafluorophenyl ring in the new adduct results in lengthening of one of the B—H···H—N contacts to just outside the accepted range for a dihydrogen bond (contact H(1A)···H(2) is 2.088 Å while contact H(1B)···H(2) is 2.273 Å). Molecular chains of **1a** are linked together through off-set face-to-face -C₆F₅ pairing interactions, with an interplanar distance of 3.269 Å (**Figure 2.6**).

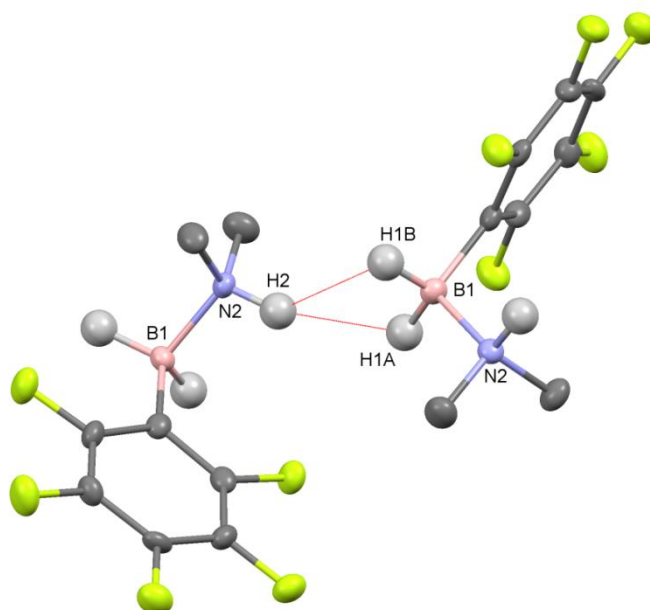


Figure 2.5: Crystal structure of $\text{Me}_2\text{HN}\cdot\text{BH}_2(\text{C}_6\text{F}_5)$ (**1a**) with displacement ellipsoids displayed at the 50% probability level. The dihydrogen contacts formed by bifurcated $\text{BH}_2\cdots\text{HN}$ interactions are indicated in red. Hydrogen atoms of the methyl groups have been omitted for clarity.

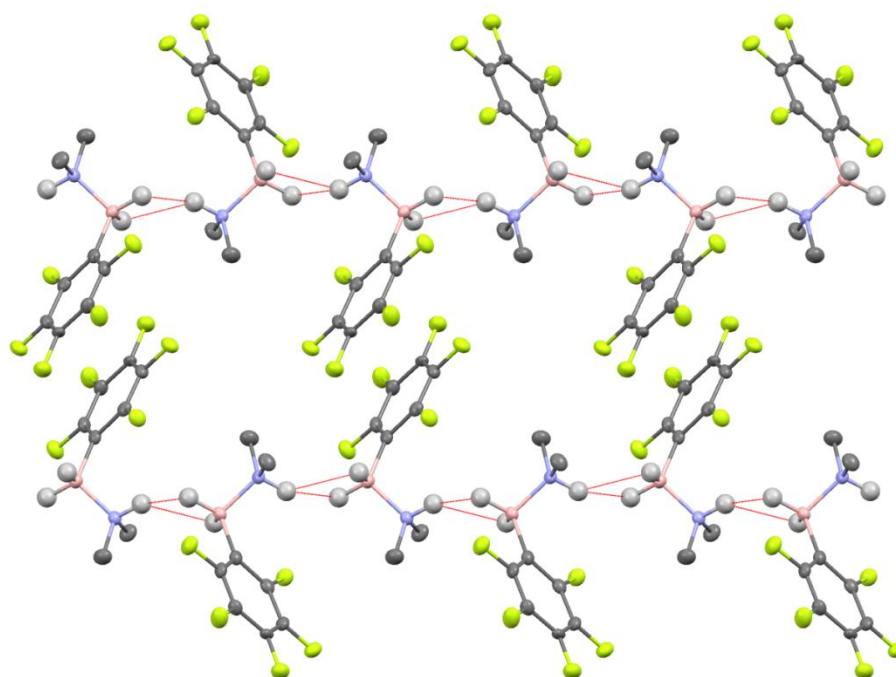


Figure 2.6: Crystal packing of $\text{Me}_2\text{HN}\cdot\text{BH}_2(\text{C}_6\text{F}_5)$ (**1a**) with displacement ellipsoids displayed at the 50% probability level. The dihydrogen bonding network formed from bifurcated $\text{BH}_2\cdots\text{HN}$ interactions is indicated in red. Hydrogen atoms of the methyl groups have been omitted for clarity.

Treatment of a toluene solution of $\text{Me}_2\text{S}\cdot\text{BH}_2(\text{C}_6\text{F}_5)$ with ${}^t\text{BuNH}_2$ and crystallization from a toluene / light petroleum mixture at $-25\text{ }^\circ\text{C}$ yields colorless crystals of ${}^t\text{BuH}_2\text{N}\cdot\text{BH}_2(\text{C}_6\text{F}_5)$ (**1b**). Two crystallographically independent molecules of **1b** are found in the crystal lattice, with B—N bond lengths of $1.618(8)\text{ \AA}$ (B(1)—N(2)) and $1.622(9)\text{ \AA}$ (B(101)—N(102)). In the solid state, molecules of **1b** form chains through alternating short and long dihydrogen bonds (**Figure 2.7**). Pairs of ${}^t\text{BuH}_2\text{N}\cdot\text{BH}_2(\text{C}_6\text{F}_5)$ molecules form through short N(102)—H(10E)⋯H(1A)—B(1) dihydrogen bonding interactions which measure 2.07 \AA while the H(2B)⋯H(10M) contacts which link these molecular pairs together throughout the crystal lattice measure 2.197 \AA .

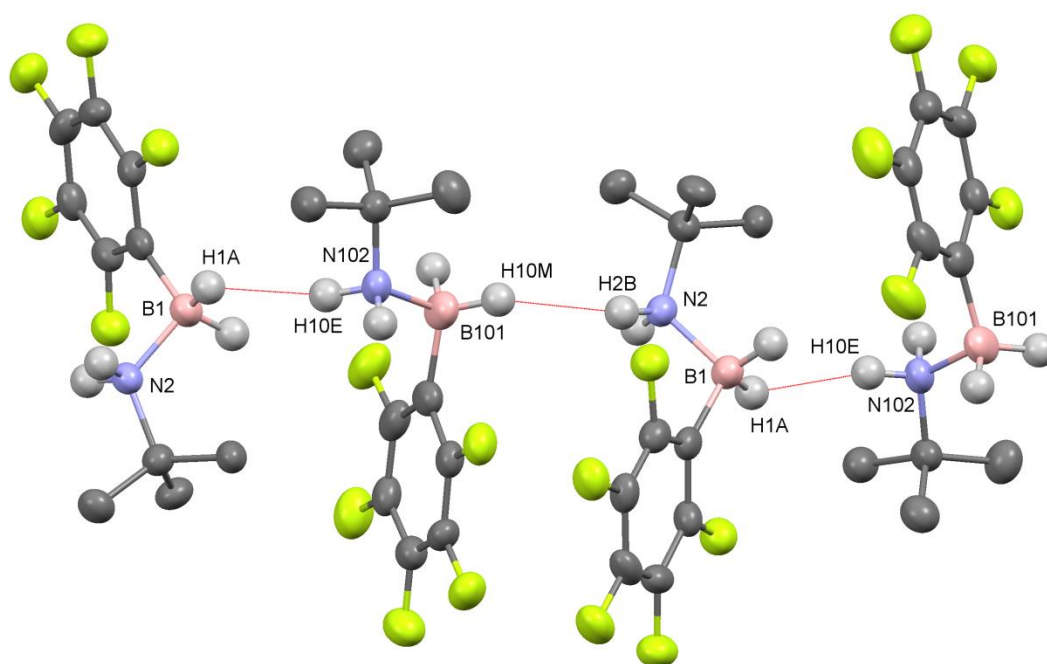
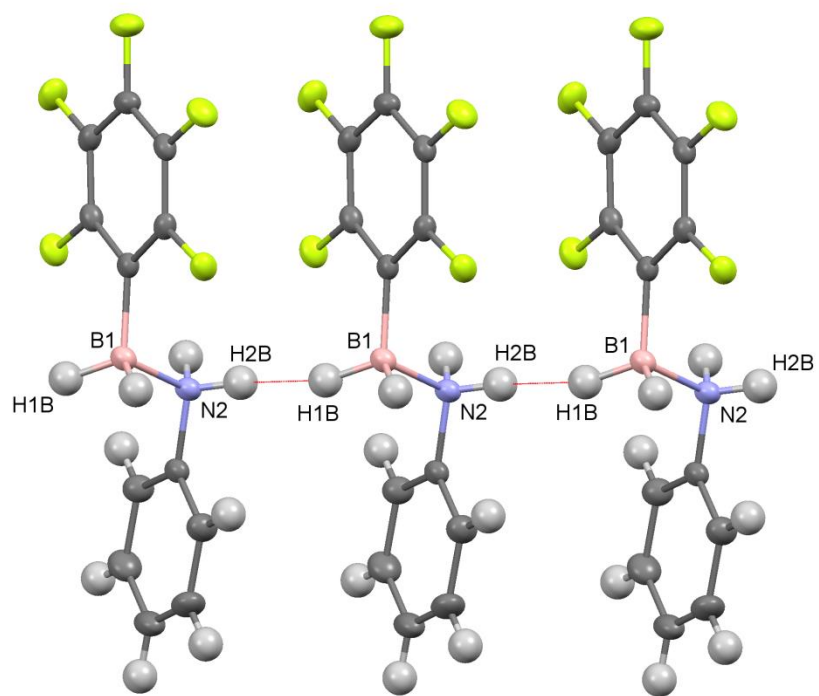


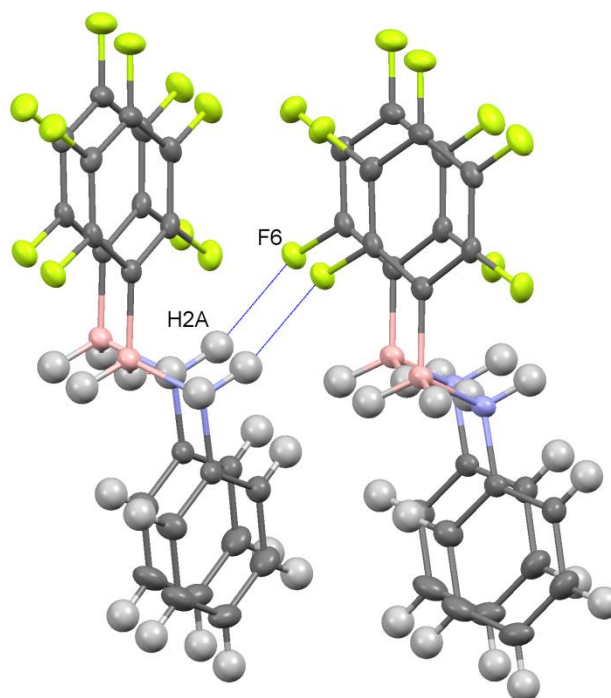
Figure 2.7: Crystal packing of ${}^t\text{BuH}_2\text{N}\cdot\text{BH}_2(\text{C}_6\text{F}_5)$ (**1b**) with displacement ellipsoids displayed at the 50% probability level. The crystal packing consists of alternating short and long $\text{H}\cdots\text{H}$ contacts indicated in red. Hydrogen atoms of the tert-butyl groups have been omitted for clarity.

In a similar fashion, displacement of dimethylsulfide from $\text{Me}_2\text{S}\cdot\text{BH}_2(\text{C}_6\text{F}_5)$ with aniline at ambient temperature results in the formation of $\text{PhH}_2\text{N}\cdot\text{BH}_2(\text{C}_6\text{F}_5)$ (**1c**). The product was

isolated in 43% yield from a toluene / light petroleum solution cooled to 2 °C. In the solid state, both the boron and nitrogen atoms of **1c** assume a distorted tetrahedral geometry, and the hydridic and protic hydrogen atoms are mutually *trans* about the B—N bond (1.627(3) Å). Intermolecular dihydrogen bonding interactions result from this *trans* configuration (**Figure 2.8**) and aid in the arrangement of the molecules into a chain-like structure. The H(1B)⋯H(2B) dihydrogen bond distance measures 1.966 Å. In addition, the chain arrangement is facilitated by stacking of $-\text{C}_6\text{F}_5$ and $-\text{C}_6\text{H}_5$ rings of neighboring molecules of **1c**, with interplanar distances of 3.185 Å and 3.396 Å, respectively (**Figure 2.8a**). Neighboring chains of **1c** molecules pack together in the solid state in part by interactions between the remaining N—H group and the *ortho*-fluorine of a $-\text{C}_6\text{F}_5$ ring from a molecule of **1c** in the neighboring chain, with the H(2A)⋯F(6) contact measuring 2.176 Å (**Figure 2.8b**).



(a)



(b)

Figure 2.8: Crystal packing of $\text{PhH}_2\text{N}\cdot\text{BH}_2(\text{C}_6\text{F}_5)$ (**1c**) with displacement ellipsoids displayed at the 50% probability level. Stacking diagrams show (a) chains formed through dihydrogen bonding (indicated in red) and (b) intermolecular $\text{N}-\text{H}\cdots\text{F}-\text{C}$ interactions (indicated in blue).

The benzylamine adduct of mono(pentafluorophenyl)borane, $\text{BnH}_2\text{N}\cdot\text{BH}_2(\text{C}_6\text{F}_5)$ (**1d**) was prepared through treatment of a toluene solution of $\text{Me}_2\text{S}\cdot\text{BH}_2(\text{C}_6\text{F}_5)$ with benzylamine at ambient temperature. Compound **1d** exhibits both boron and nitrogen in a distorted tetrahedral geometry, with a B—N bond length of 1.627(3) Å. In contrast to the previously discussed adducts of mono(pentafluorophenyl)borane, **1d** exists as a dimer in the solid state, with dimerization occurring through short H···H contacts (**Figure 2.9**). This is reminiscent of the structure of the previously reported ammonia adduct of the same borane, $\text{H}_3\text{N}\cdot\text{BH}_2(\text{C}_6\text{F}_5)$.¹⁰²

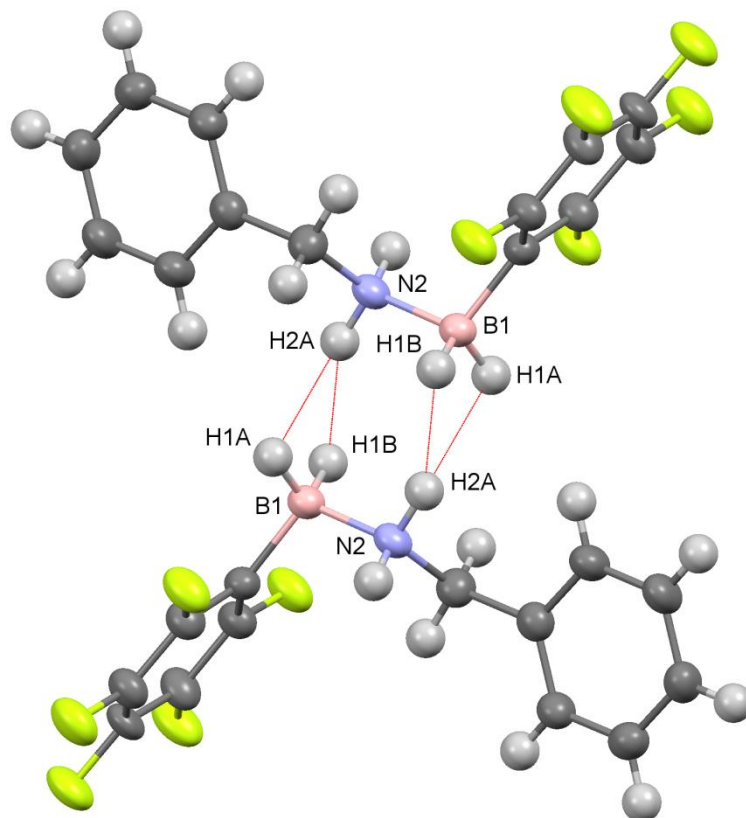


Figure 2.9: Crystal structure of dimeric $\text{BnH}_2\text{N}\cdot\text{BH}_2(\text{C}_6\text{F}_5)$ (**1d**) with displacement ellipsoids displayed at the 50% probability level. Dimerization occurs through intermolecular bifurcated $\text{BH}_2\cdots\text{HN}$ contacts indicated in red.

Supramolecular dimerization through H...H contacts facilitates an arrangement where the N—H and B—H groups are closer to a *cis* arrangement than a *trans* arrangement about the B—N bond. This contrasts with the adducts **1b** and **1c** in which a chain-like arrangement of H...H contacts facilitates a *trans* configuration between the N—H and B—H groups. For **1d**, the H...H contacts arrange in a bifurcated BH₂...HN fashion, similar to the dimethylamine adducts of BH₃⁹³ and HB(C₆F₅)₂.¹⁰² The bifurcated interaction is formed from dihydrogen bonding contacts measuring 2.161 Å (H(1A)...H(2A)) and 2.024 Å (H(1B)...H(2A)). The crystal packing of the dimeric units is dominated by a weak H(1B)...H(2B) contact (2.218 Å) and the intermolecular N—H(2B)...F(2)—C interaction (2.493 Å) and —C₆F₅ and —C₆H₅ stacking interactions with interplanar distances of 3.092 Å and 3.626 Å, respectively (**Figure 2.10**).

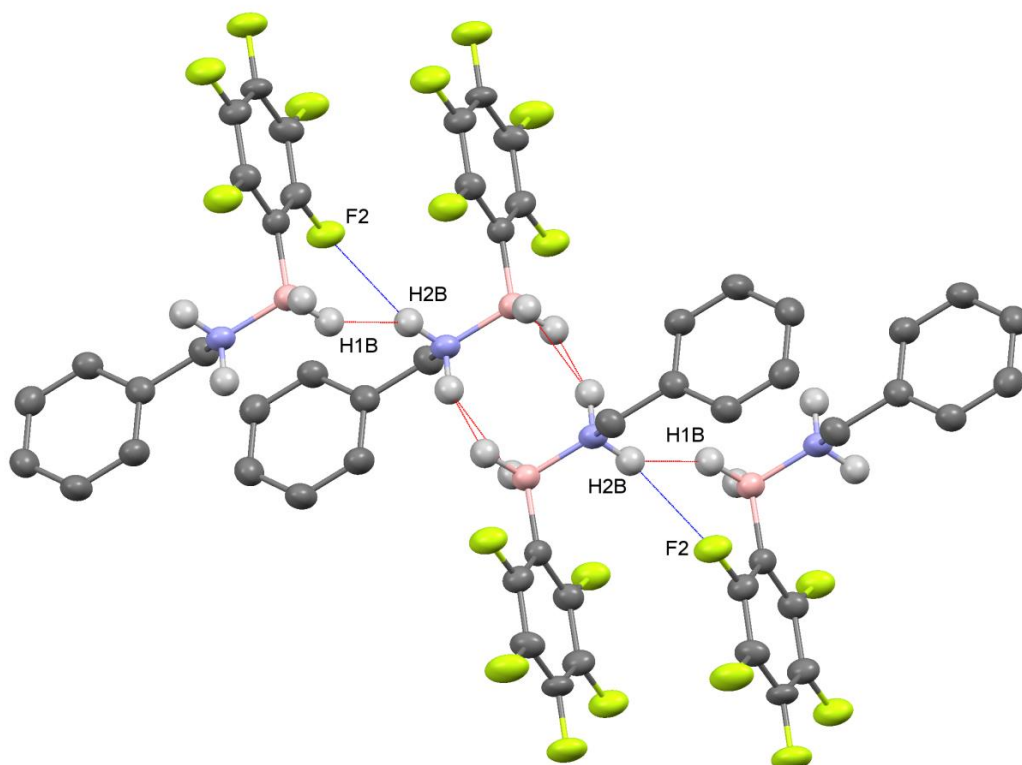


Figure 2.10: Crystal packing of BnH₂N·BH₂(C₆F₅) (**1d**) with displacement ellipsoids displayed at the 50% probability level. The intermolecular N—H...F—C interactions and weak H...H contacts which link dimeric pairs of **1d** are indicated in blue and red, respectively. Hydrogen atoms of the benzyl groups have been omitted for clarity.

The triethylamine adduct of mono(pentafluorophenyl)borane, $\text{Et}_3\text{N}\cdot\text{BH}_2(\text{C}_6\text{F}_5)$ (**1e**) is prepared through treatment of a toluene solution of $\text{Me}_2\text{S}\cdot\text{BH}_2(\text{C}_6\text{F}_5)$ with triethylamine at ambient temperature. Adduct formation was confirmed by multinuclear NMR spectroscopy, with specific attention being paid to the shift of the ^{11}B NMR signal from -17 ppm (t , $^1J_{\text{B,H}} = 105$ Hz) in the starting material to -14 ppm (t , $^1J_{\text{B,H}} = 92$ Hz) for the final product, as well as the replacement of the SMe_2 peak in the ^1H NMR spectrum of the starting borane (1.20 ppm in C_6D_6) with peaks corresponding to adducted NEt_3 . This adduct exists as an oil at ambient temperature which has prevented structural characterization by elemental analysis and X-ray diffraction methods.

The pyridine adduct of mono(pentafluorophenyl)borane, $\text{py}\cdot\text{BH}_2(\text{C}_6\text{F}_5)$ (**1f**) was isolated in 40% yield from a dichloromethane / light petroleum mixture at -25 °C after treatment of a toluene solution of $\text{Me}_2\text{S}\cdot\text{BH}_2(\text{C}_6\text{F}_5)$ with pyridine. In a similar fashion to the other reported adducts, the boron adopts a tetrahedral geometry, with a B—N bond length of $1.605(2)$ Å. The crystal structure shows the main packing feature to be off-set face-to-face $-\text{C}_6\text{F}_5$ pairing interactions, with an interplanar distance of 3.336 Å (**Figure 2.11**).

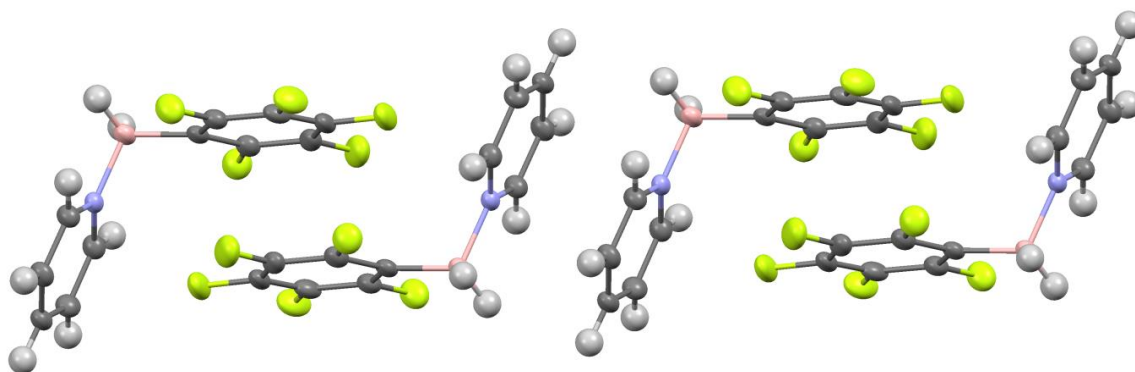


Figure 2.11: *Crystal packing of $\text{py}\cdot\text{BH}_2(\text{C}_6\text{F}_5)$ (**1f**) with displacement ellipsoids displayed at the 50% probability level. The crystal packing is dominated by alternating $-\text{C}_6\text{F}_5$ pairing interactions and van der Waals interactions.*

In addition to the $-\text{C}_6\text{F}_5$ stacking interactions between the pentafluorophenyl rings, van der Waals interactions between the pyridine rings facilitate further packing in the crystal structure. The interplanar distance between the pyridine rings is comparable to, but slightly longer than any reported $-\text{C}_6\text{F}_5$ stacking or pairing interactions, at 3.488 Å (**Figure 2.11**).

2.2.1.2 Amine and nitrogen donor adducts of $\text{HB}(\text{C}_6\text{F}_5)_2$

In a comparable fashion to the preparation of $\text{Me}_2\text{HN}\cdot\text{BH}_2(\text{C}_6\text{F}_5)$, a toluene solution of $\text{Me}_2\text{S}\cdot\text{BH}(\text{C}_6\text{F}_5)_2$ was treated with dimethylamine to form the new adduct $\text{Me}_2\text{HN}\cdot\text{BH}(\text{C}_6\text{F}_5)_2$ (**2a**) in quantitative yield. Crystals of the product were isolated by slow cooling of a concentrated toluene / light petroleum mixture from 50 °C to ambient temperature. The boron and nitrogen atoms adopt a nearly tetrahedral geometry, with a B—N bond length of 1.612(3) Å. In contrast to the structure of compound **1a**, the crystal structure of **2a** exhibits no intermolecular dihydrogen bonding or weak H...H contacts (**Figure 2.12**). Instead, the acidic N—H proton participates in a bifurcated N—H...F—C interaction with an *ortho*-fluorine from each pentafluorophenyl ring, resulting in the N—H and B—H groups featuring a *trans* conformation about the B—N bond. These N—H...F—C contacts measure 2.353 Å and 2.369 Å for H(2)...F(6) and H(2)...F(8), respectively. Molecules of **2a** form a chain-like arrangement throughout the crystal lattice directed by off-set face-to-face $-\text{C}_6\text{F}_5$ stacking interactions, with an alternating interplanar distance of 3.189 Å and 3.263 Å.

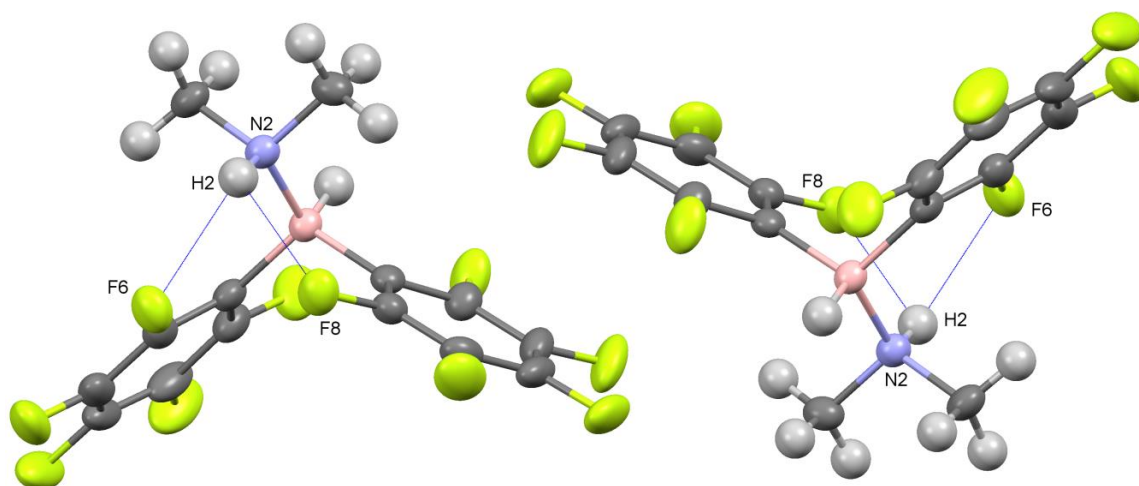


Figure 2.12: *Crystal packing of $\text{Me}_2\text{HN}\cdot\text{BH}(\text{C}_6\text{F}_5)_2$ (**2a**) with displacement ellipsoids displayed at the 50% probability level. The packing is dominated by $\text{N—H}\cdots\text{F—C}$ contacts (indicated in blue) and off-set face-to-face $-\text{C}_6\text{F}_5$ stacking interactions.*

The bifurcated $\text{N—H}\cdots\text{F—C}$ interactions exhibited in **2a** are reminiscent of the dimethylamine adduct of tris(pentafluorophenyl)borane, $\text{Me}_2\text{HN}\cdot\text{B}(\text{C}_6\text{F}_5)_3$, in which the same bonding pattern is observed.⁵⁸ However, the $\text{N—H}\cdots\text{F—C}$ interactions in $\text{Me}_2\text{HN}\cdot\text{B}(\text{C}_6\text{F}_5)_3$ are markedly shorter than those of **2a**, measuring around 2.1 Å.

The $^t\text{BuNH}_2$ adduct of bis(pentafluorophenyl)borane is accessible through displacement of the dimethylsulfide of $\text{Me}_2\text{S}\cdot\text{BH}(\text{C}_6\text{F}_5)_2$ for $^t\text{BuNH}_2$ in toluene to produce $^t\text{BuH}_2\text{N}\cdot\text{BH}(\text{C}_6\text{F}_5)_2$ (**2b**). A 19% yield of crystalline material was isolated from a toluene / light petroleum mixture of the crude material cooled to 2 °C. Both the boron and nitrogen atoms adopt a nearly tetrahedral geometry in the solid state, with a B—N bond length of 1.619(1) Å. In contrast to the crystal structure of $^t\text{BuH}_2\text{N}\cdot\text{BH}_2(\text{C}_6\text{F}_5)$ (**1b**), which exhibits no short $\text{H}\cdots\text{F}$ contacts molecules of **2b** exhibit both intra- and inter-molecular $\text{N—H}\cdots\text{F—C}$ interactions (**Figure 2.13**).

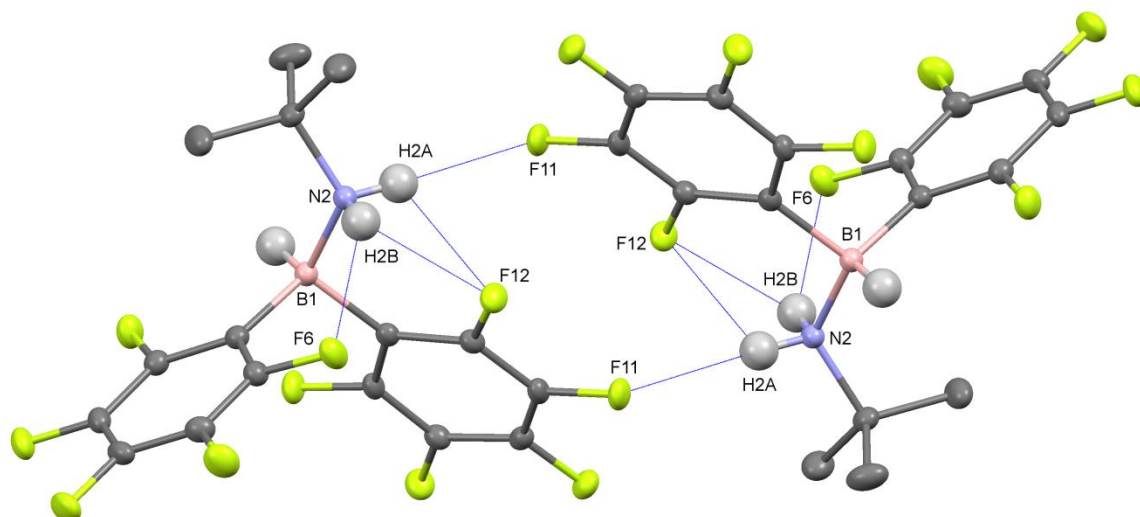


Figure 2.13: Crystal structure of ${}^t\text{BuH}_2\text{N}\cdot\text{BH}(\text{C}_6\text{F}_5)_2$ (**2b**) with displacement ellipsoids displayed at the 50% probability level. Molecular pairing occurs through bifurcated inter- and intra-molecular $\text{N—H}\cdots\text{F—C}$ interactions, indicated in blue. Hydrogen atoms of the tert-butyl groups have been omitted for clarity.

Each N—H proton in **2b** participates in a bifurcated $\text{H}\cdots\text{F}$ interaction, with one set of interactions being solely intramolecular, similar to the ${}^t\text{BuNH}_2$ amine adduct of $\text{B}(\text{C}_6\text{F}_5)_3$,⁵⁸ and one consisting of one intra- and one inter-molecular interaction. Proton H(2B) is involved in two intramolecular $\text{N—H}\cdots\text{F—C}$ interactions, measuring 2.229 Å and 2.425 Å for $\text{H}(2\text{B})\cdots\text{F}(6)$ and $\text{H}(2\text{B})\cdots\text{F}(12)$, respectively. The remaining N—H participates in one intramolecular interaction, $\text{H}(2\text{A})\cdots\text{F}(12)$ at 2.297 Å and one intermolecular interaction, $\text{H}(2\text{A})\cdots\text{F}(11)$ measuring 2.432 Å. The intermolecular $\text{N—H}\cdots\text{F—C}$ interaction is not a feature which is shared with the related adduct ${}^t\text{BuH}_2\text{N}\cdot\text{B}(\text{C}_6\text{F}_5)_3$. The $\text{N—H}\cdots\text{F—C}$ interactions facilitate dimerization of **2b** in the solid state, with neighboring dimers packing through off-set face-to-face $-\text{C}_6\text{F}_5$ stacking interactions with an interplanar distance of 3.088 Å.

The adduct $\text{PhH}_2\text{N}\cdot\text{BH}(\text{C}_6\text{F}_5)_2$ (**2c**) is prepared through an analogous method to that of $\text{PhH}_2\text{N}\cdot\text{BH}_2(\text{C}_6\text{F}_5)$ (**1c**), with treatment of the dimethylsulfide adduct with aniline in toluene at ambient temperature. X-ray quality crystals of **2c** were grown from a toluene / light petroleum solution at -25 °C. The boron and nitrogen atoms adopt a distorted tetrahedral

geometry, with a B—N bond length of 1.632(2) Å. In a similar fashion to **2b**, several intra- and inter-molecular N—H...F—C interactions facilitate pairing of PhH₂N·BH(C₆F₅)₂ molecules in the solid state (**Figure 2.14**).

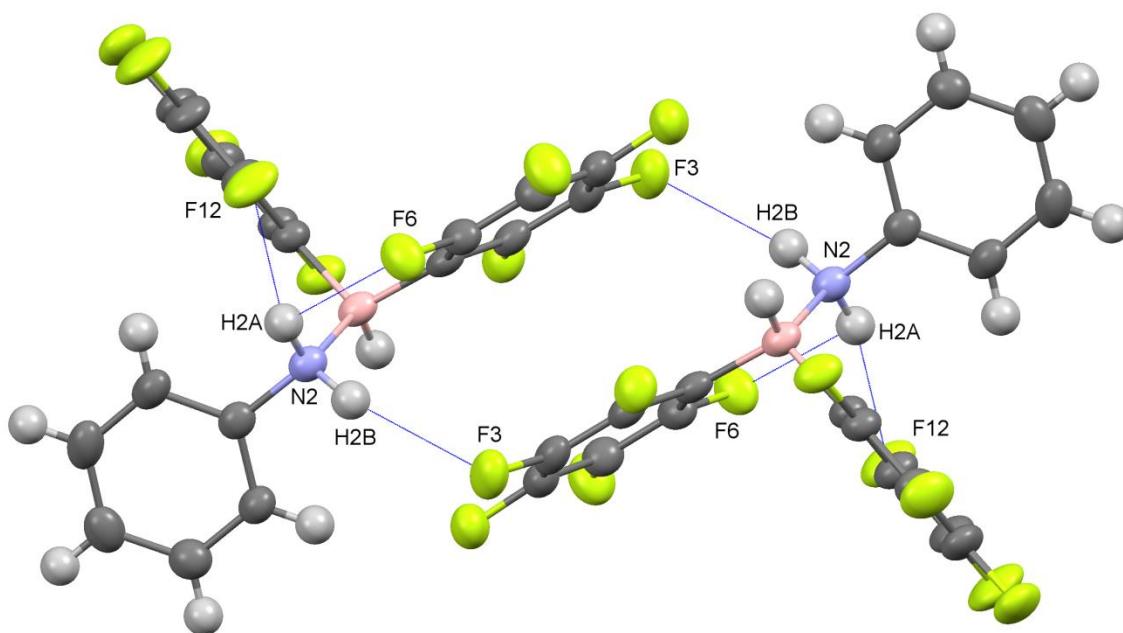


Figure 2.14: Crystal structure of PhH₂N·BH(C₆F₅)₂ (**2c**) with displacement ellipsoids displayed at the 50% probability level. Molecular pairing occurs through one intermolecular N—H...F—C interaction, indicated in blue, and a —C₆F₅ stacking interaction.

One N—H group participates in a bifurcated intramolecular N—H...F—C interaction, with H...F contacts measuring 2.181 Å and 2.323 Å for H(2A)...F(12) and H(2A)...F(6), respectively. The remaining N—H group engages in an intermolecular H(2B)...F(3) interaction, slightly longer than the two intramolecular interactions, at 2.408 Å. The resulting off-set face-to-face —C₆F₅ stacking interaction has an interplanar distance of 3.391 Å, consistent with the previously discussed adducts which exhibit this type of packing.

The benzylamine adduct of mono(pentafluorophenyl)borane (**2d**) is prepared through treatment of $\text{Me}_2\text{S}\cdot\text{BH}(\text{C}_6\text{F}_5)_2$ with a stoichiometric amount of benzylamine at ambient temperature. In a similar fashion to **2b** and **2c**, compound **2d** exhibits molecular pairing in the solid state, with dimerization resulting from an intermolecular $\text{N—H}\cdots\text{F—C}$ interaction. Both the boron and nitrogen atoms adopt a tetrahedral geometry, and the B—N bond length measures 1.616(1) Å. One N—H group participates in an intramolecular bifurcated interaction with an *ortho*-fluorine of each $-\text{C}_6\text{F}_5$ ring. The $\text{H}(2\text{A})\cdots\text{F}(6)$ interaction measures 2.255 Å, while the $\text{H}(2\text{A})\cdots\text{F}(12)$ distance is slightly shorter at 2.236 Å. The remaining N—H group participates in an intermolecular $\text{N—H}(2\text{B})\cdots\text{F}(4)—\text{C}$ interaction measuring 2.442 Å (**Figure 2.15**). The resulting off-set face-to-face $-\text{C}_6\text{F}_5$ stacking interaction in $\text{BnH}_2\text{N}\cdot\text{BH}(\text{C}_6\text{F}_5)_2$ has an interplanar distance of 3.238 Å.

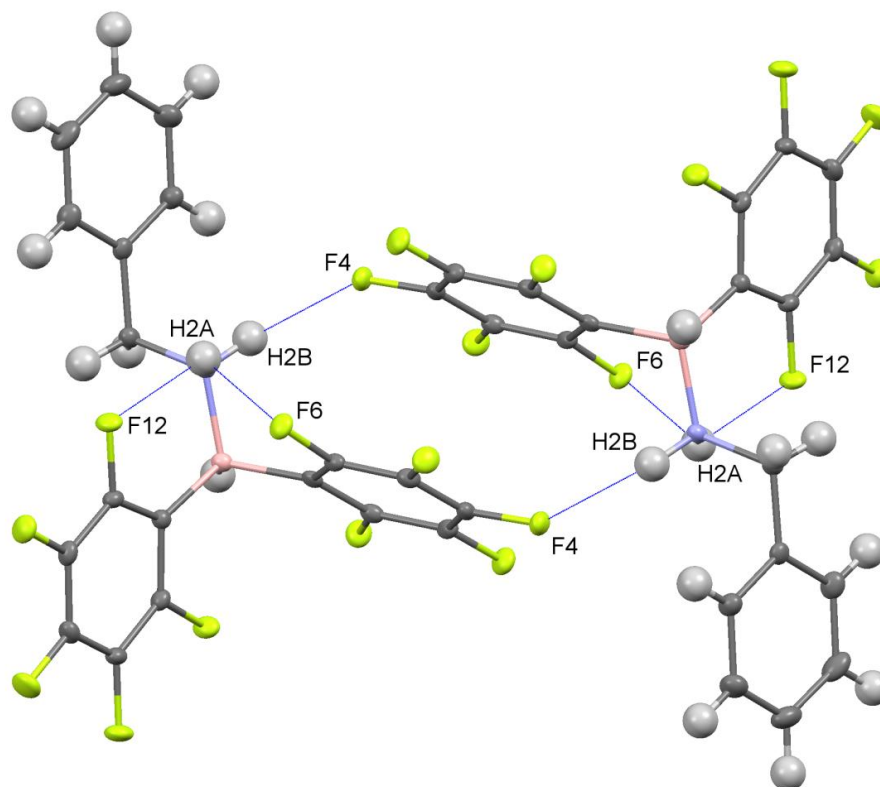


Figure 2.15: Crystal structure of $\text{BnH}_2\text{N}\cdot\text{BH}(\text{C}_6\text{F}_5)_2$ (**2d**) with displacement ellipsoids displayed at the 50% probability level. Molecular pairing occurs through one intermolecular $\text{N—H}\cdots\text{F—C}$ interaction, indicated in blue, and a $-\text{C}_6\text{F}_5$ stacking interaction.

Treatment of a toluene solution of $\text{Me}_2\text{S}\cdot\text{BH}(\text{C}_6\text{F}_5)_2$ with triethylamine at ambient temperature produces the triethylamine adduct of bis(pentafluorophenyl)borane, $\text{Et}_3\text{N}\cdot\text{BH}(\text{C}_6\text{F}_5)_2$ (**2e**). This triethylamine adduct, in contrast to that of mono(pentafluorophenyl)borane, is easily isolated as a colorless solid in 68% yield from a toluene / light petroleum solution at $-25\text{ }^\circ\text{C}$. Both the boron and nitrogen atoms adopt a nearly tetrahedral geometry, and the B—N bond measures $1.664(3)\text{ \AA}$ (**Figure 2.16**).

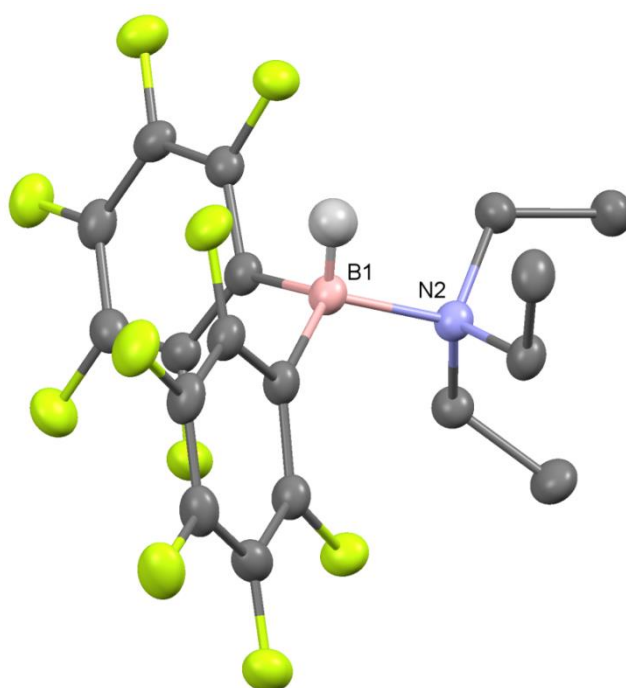


Figure 2.16: *Crystal structure of $\text{Et}_3\text{N}\cdot\text{BH}(\text{C}_6\text{F}_5)_2$ (**2e**) with displacement ellipsoids displayed at the 50% probability level. Hydrogen atoms of the ethyl groups have been omitted for clarity.*

Due to the lack of an acidic N—H functionality, no dihydrogen bonding or N—H...F—C interactions are present in the crystal structure. The formation of compound **2e** and stability of its structure, in contrast with the analogous chemistry of tris(pentafluorophenyl)borane,⁵⁶ may be related to the relative Lewis acidity of the boron

center, which is decreased due to the presence of only one or two two, rather than three, $-\text{C}_6\text{F}_5$ groups.

The pyridine adduct of bis(pentafluorophenyl)borane, $\text{py}\cdot\text{BH}(\text{C}_6\text{F}_5)_2$, (**2f**), was isolated in 27% yield from a toluene / light petroleum mixture at $-25\text{ }^\circ\text{C}$ following treatment of a toluene solution of $\text{Me}_2\text{S}\cdot\text{BH}(\text{C}_6\text{F}_5)_2$ with pyridine at ambient temperature. The crystal structure of $\text{py}\cdot\text{BH}(\text{C}_6\text{F}_5)_2$ (**2f**) displays the shortest B—N bond length of any of the reported adducts, measuring $1.597(7)\text{ \AA}$. The two $-\text{C}_6\text{F}_5$ rings and the pyridine ring arrange about the boron atom in a propeller-like fashion, with the B—H group directed away from the center of the propeller, reminiscent of the $[\text{HB}(\text{C}_6\text{F}_5)_3]^-$ ion.^{62,160–162}

Molecules of **2f** pair in the solid state through long intermolecular $\text{H}\cdots\text{F}$ contacts between an *ortho*-hydrogen of the pyridine ring and the *para*-fluorine from the $-\text{C}_6\text{F}_5$ ring on a neighboring molecule, with the $\text{F}(10)\cdots\text{H}(13)$ distance measuring 2.356 \AA . Within the dimer, the $-\text{C}_6\text{F}_5$ rings stack in an off-set face-to-face arrangement, with an interplanar distance of 3.308 \AA . Molecular pairs of **2f** interact in the solid state through slightly shorter $-\text{C}_6\text{F}_5$ stacking interactions, with an interplanar distance measuring 3.280 \AA (**Figure 2.17**).

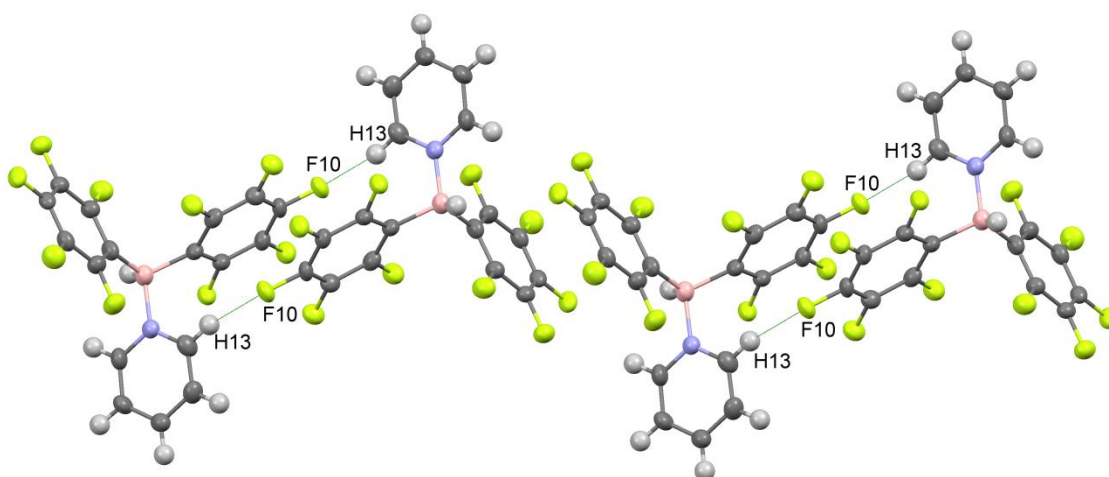


Figure 2.17: Molecular packing of $\text{py}\cdot\text{BH}(\text{C}_6\text{F}_5)_2$ (**2f**) with displacement ellipsoids displayed at the 50% probability level. Molecular pairing occurs through intermolecular $\text{H}\cdots\text{F}$ contacts, indicated in green.

2.3 Discussion

2.3.1 Structural analysis

The amine and pyridine adducts of mono- and bis-(pentafluorophenyl)borane exhibit inter- and intra-molecular interactions which have relevance to several areas of chemistry, including bioorganic chemistry,^{163,164} organic crystal engineering^{165–167} and inorganic materials for hydrogen storage purposes.⁹⁰ While those adducts of $\text{H}_2\text{B}(\text{C}_6\text{F}_5)$ exhibit primarily dihydrogen bonding interactions in the solid state, it is inter- and intra-molecular $\text{N—H}\cdots\text{F—C}$ interactions which dictate the supramolecular architectures for adducts of $\text{HB}(\text{C}_6\text{F}_5)_2$.

The adducts **1a** and **1d** both exhibit a bifurcated intermolecular $\text{BH}_2\cdots\text{HN}$ contacts, which have been observed for the related amine boranes $\text{H}_3\text{N}\cdot\text{BH}_3$,¹¹⁵ $\text{Me}_2\text{HN}\cdot\text{BH}_3$,⁹³ and the recently published linear triborazanes.¹⁶⁸ Such interactions are reported to play a significant role in the dehydrocoupling chemistry of $\text{H}_3\text{N}\cdot\text{BH}_3$ and $\text{Me}_2\text{HN}\cdot\text{BH}_3$, with the close $\text{H}\cdots\text{H}$ contact proposed to precede dihydrogen loss.^{90,93} However, whereas the solid state structure of **1a** displays these contacts as facilitating the occurrence of chains (**Figure 2.18, I**), the $\text{BH}_2\cdots\text{HN}$ bonding in **1d** serves as a bridging contact (**Figure 2.18, II**), pairing molecules into supramolecular dimers in the solid state. The remaining adducts **1b** and **1c** display a dihydrogen bonding motif as a single $\text{N—H}\cdots\text{H—B}$ chain which links molecules together into molecular chains (**Figure 2.18, III**).

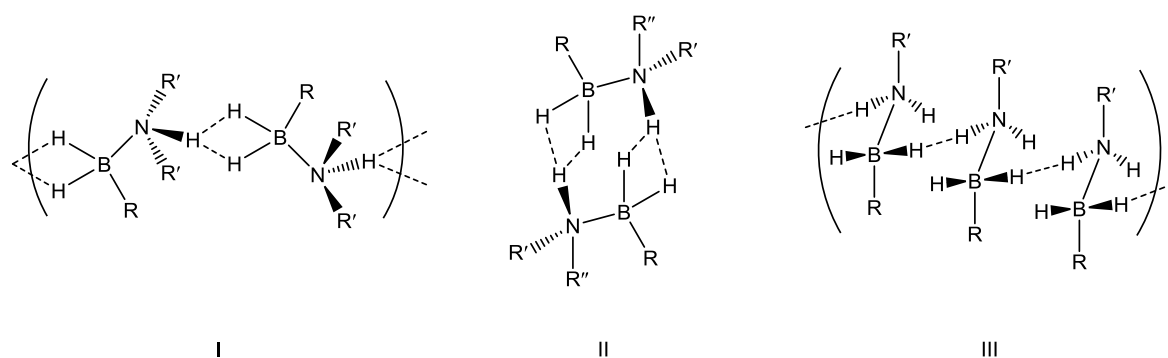


Figure 2.18: Dihydrogen bonding and H...H contacts observed in the amine adducts of mono(pentafluorophenyl)borane.

Both **1a** and **1d** exhibit the bifurcated $\text{BH}_2\cdots\text{HN}$, featuring $\text{H}\cdots\text{H}$ contact lengths within the defined range of a dihydrogen bond, with the exception of the $\text{H}(1\text{B})\cdots\text{H}(2)$ contact in **1a** which lies just outside of the 2.2 Å maximum. Because this dimethylamine adduct contains only one N—H group, and that bond is engaged in a dihydrogen bonding network, no $\text{N—H}\cdots\text{F—C}$ interactions are observed. Instead, supramolecular $-\text{C}_6\text{F}_5$ pairing facilitates arrangement of molecular chains in a parallel fashion. In comparison, the pentafluorophenyl-free analog $\text{Me}_2\text{HN}\cdot\text{BH}_3$ exhibits interchain interactions through van der Waals forces.⁹³ The benzylamine adduct (**1d**), on the other hand, has two N—H groups which may potentially engage in dihydrogen bonding. While one N—H is involved in the bridging $\text{BH}_2\cdots\text{HN}$ interactions, the remaining N—H instead participates in an $\text{N—H}\cdots\text{F—C}$ interaction with an *ortho*-fluorine of the $-\text{C}_6\text{F}_5$ ring of a neighboring molecule, which aids in the packing of dimeric **1d** in the crystal lattice.

The protic amine adducts of bis(pentafluorophenyl)borane all exhibit an intramolecular bifurcated $\text{N—H}\cdots\text{F—C}$ interaction between one protic N—H group and one *ortho*-fluorine from each $-\text{C}_6\text{F}_5$ ring. This type of interaction is distinctive among the amine adducts of pentafluorophenyl-substituted boranes, as the organofluorine group is considered to be a weak hydrogen bond acceptor.¹⁵⁶ However, the prevalence of this type of interaction in the primary and secondary amine adducts of tris(pentafluorophenyl)borane and

bis(pentafluorophenyl)borane appears to play a significant role in the crystal packing of these adducts. In most cases, the N—H...F—C interactions complete the formation of an intramolecular six-membered ring, as would be expected by Etter's rules for predicting the occurrence of hydrogen bonds.¹⁵⁸ The remaining N—H bond (if one is present) either participates in one intramolecular and one intermolecular N—H...F—C interaction, as is the case for **2b**, or participates solely in one intermolecular N—H...F—C interaction which can be seen in **2c** and **2d**.

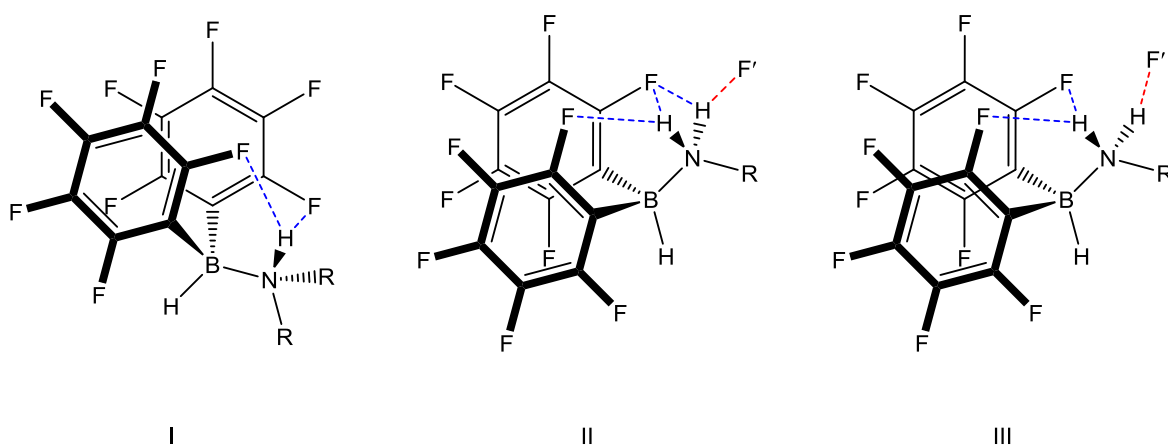


Figure 2.19: *N—H...F—C* contacts observed in the amine adducts of bis(pentafluorophenyl)borane.

Because of the single N—H proton present in **2a**, and due to the steric bulk of the $-\text{C}_6\text{F}_5$ groups, only intramolecular N—H...F—C contacts exist in the solid state structure of this adduct (**Figure 2.19, I**). However, the primary amine adducts, with two N—H hydrogen bond donors present, display a more complex system of both intra- and inter-molecular hydrogen bonding. In contrast to the molecular structures of **2c** and **2d**, in which only one N—H proton participates in a bifurcated interaction, both N—H protons of **2b** participate in bifurcated N—H...F—C contacts (**Figure 2.19, II**). Where the R group contains a phenyl ring, however, the N—H group which participates in the intermolecular N—H...F—C

interaction is sterically hindered from participating in an additional intramolecular N—H...F—C interaction. Instead, the intermolecular interaction with a *meta*-fluorine (in the case of **2c**) or a *para*-fluorine (in the case of **2d**) of the neighboring molecule is the sole N—H...F—C interaction in which the N—H hydrogen bond donor participates.

With the absence of any hydrogen donor N—H group, the molecular packing of the pyridine adducts **1f** and **2f** significantly simplifies in nature. The lack of dihydrogen bonding and intra- and inter-molecular N—H...F—C interactions results in the crystallization of **1f** with no remarkable supramolecular features to the structure. However, the formation of a stable adduct with triethyl amine is in stark contrast to the related chemistry of tris(pentafluorophenyl)borane (**Section 2.3.2**).⁵⁶

2.3.2 Adduct stability

The application of ammonia borane as a hydrogen storage material is supported, in part, by its robust chemical stability. In addition to its long shelf life and resistance to hydrolysis and oxidation, undesirable spontaneous dehydrocoupling and rearrangement is not observed. In general, amine borane Lewis adducts exhibit great stability, especially in comparison with the closely related phosphine boranes, which readily oxidize to produce phosphine oxides and the free borane. However, due to the variety of chemistry in which B(C₆F₅)₃ participates,^{2,3} the stability of Lewis adducts of B(C₆F₅)₃ may at times be surprisingly difficult to predict.

In particular, careful consideration must be applied to the steric properties of the chosen Lewis base. The phosphine Lewis adducts of tris(pentafluorophenyl)boron of the general formula R₃P·B(C₆F₅)₃ (R = H, Me, ^tBu) are an illustrative example of the effect of prohibitive steric size on adduct formation. While H₃P·B(C₆F₅)₃ and Me₃P·B(C₆F₅)₃ are stable and isolable Lewis adducts of tris(pentafluorophenyl)borane at ambient

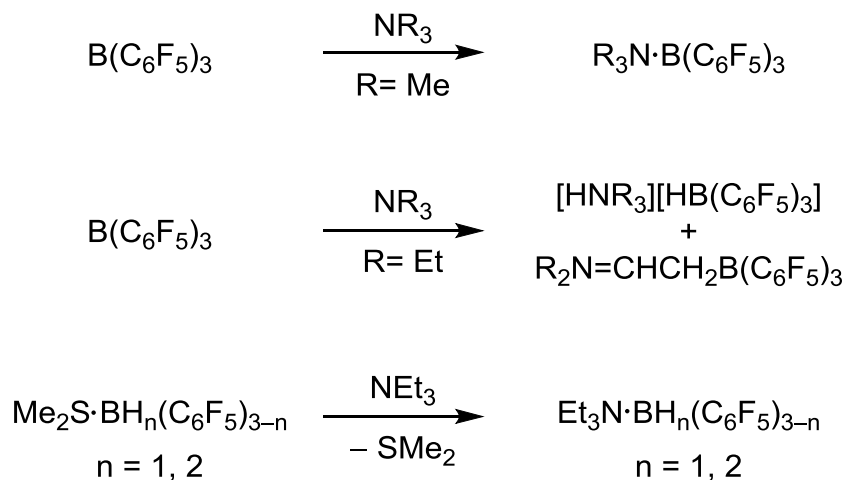
temperature,^{59,60} the intended formation of a Lewis adduct between $P(tBu)_3$ and tris(pentafluorophenyl)borane is prevented by the steric repulsion between the tBu groups and pentafluorophenyl rings. Such Lewis acid / Lewis base systems which are unable to neutralize due to steric bulk requirements have been termed 'frustrated Lewis pairs' and find application as reagents for the activation of dihydrogen and other small molecules (**Section 1.2.1**).^{68,169} Frustrated Lewis pairs formed from the reaction between $B(C_6F_5)_3$ and sterically encumbered amines has also been reported.¹⁷⁰ Other considerations regarding the stability of Lewis adducts of tris(pentafluorophenyl)borane involve further adduct reactivity, such as competing abstraction or intermolecular rearrangements.

2.3.2.1 *Triethylamine adducts of $H_2B(C_6F_5)$ and $HB(C_6F_5)_2$*

The Lewis acidity of $B(C_6F_5)_3$ is responsible for much of its chemistry, including its popular use as a hydride, halide and alkyl abstraction reagent.^{2,3} While these abstraction reactions are significant steps in polymerization chemistry,^{39,171} the favorability of abstraction reactions has been shown to interfere with Lewis adduct formation between $B(C_6F_5)_3$ and some tertiary amines.⁵⁶

For example, treatment of $B(C_6F_5)_3$ with NEt_3 results in hydride abstraction to generate $[HNEt_3][HB(C_6F_5)_3]$ and $Et_2N=CHCH_2B(C_6F_5)_3$ rather than formation of the adduct $Et_3N \cdot B(C_6F_5)_3$. Similar reactivity is observed in the treatment of a $B(C_6F_5)_3$ solution with other amines, such as dimethyl- and diethyl-aniline.^{56,172} However, the reaction between $B(C_6F_5)_3$ and the methyl-substituted tertiary amine NMe_3 proceeds with the favourable formation of the Lewis adduct $Me_3N \cdot B(C_6F_5)_3$ (**Scheme 2.5**).⁵⁵

Scheme 2.5: Treatment of perfluoroaryl boranes with NR_3 ($R = \text{Me}, \text{Et}$).

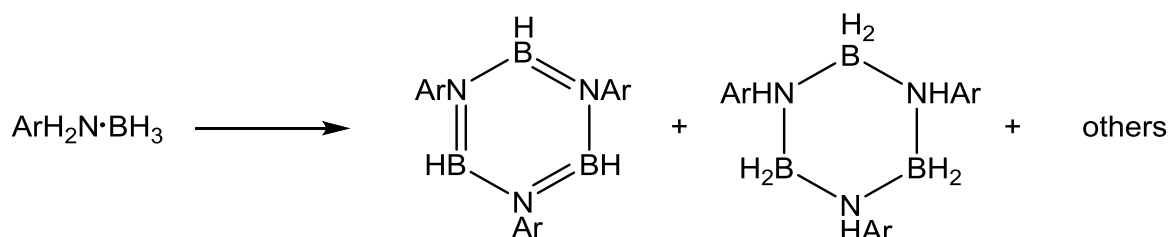


While the use of $\text{B}(\text{C}_6\text{F}_5)_3$ as a hydride abstraction reagent in organic^{2,42,173–175} and organometallic chemistry^{176–179} is often reported in the literature, the favorability of hydride abstraction rather than adduct formation in the presence of certain substituted amines, such as triethylamine and diethylaniline, is an interesting addition to the rich chemistry of $\text{B}(\text{C}_6\text{F}_5)_3$ and its Lewis adducts. It is therefore somewhat surprising that similar reactivity is not observed for the combination of NEt_3 with $\text{H}_n\text{B}(\text{C}_6\text{F}_5)_{3-n}$ ($n = 1, 2$) to produce stable Lewis adducts. This difference in reactivity may be attributed to the slightly decreased Lewis acidity of mono- and bis-(pentafluorophenyl)borane in comparison with that of tris(pentafluorophenyl)borane, hindering the potential for further reactivity with the tertiary amine NEt_3 , and serves to stabilize adduct formation. Both borane adducts were left in toluene solution at ambient temperature and were monitored by multinuclear NMR spectroscopy over the course of several weeks with only slow evidence of hydride abstraction.

2.3.2.2 Aniline adducts of $H_2B(C_6F_5)$ and $HB(C_6F_5)_2$

Recently, the spontaneous dehydrocoupling of aromatic amine boranes (including aniline borane, $PhH_2N \cdot BH_3$) at ambient temperature was demonstrated in a variety of organic solvents. Whilst the authors were able to grow single crystals of the starting adducts for X-ray diffraction studies, prolonged dissolution resulted in loss of dihydrogen and the formation of dehydrocoupling products $\{ArNBH\}_3$, and $\{(Ar)(H)NBH_2\}_3$ (**Scheme 2.6**).¹⁸⁰ This highly favourable decomposition pathway is attributed to the reduced lone pair donor strength of the aromatic amine, and therefore weak B—N bond of the adduct,^{180–184} in addition to the increased N—H Brønsted acidity upon adduct formation.^{58,180,182}

Scheme 2.6: Spontaneous dehydrocoupling of aniline borane.



In contrast to these observations, the aniline adduct $PhH_2N \cdot BH_2(C_6F_5)$ demonstrates robust solution stability at ambient temperature. Thermal decomposition of $PhH_2N \cdot BH_2(C_6F_5)$ may be initiated by warming a toluene solution of the adduct to 80 °C. The resulting crude ^{11}B NMR spectrum displays a broad resonance around 34 ppm as the major product. This is consistent with the reported signal shift from ambient temperature dehydrocoupling of aniline borane to produce the cyclic trimer $\{PhNBH\}_3$.¹⁸⁰ The properties of aromatic amine boranes which facilitate favourable spontaneous decomposition, such as the highly Brønsted acidic N—H group and relatively weak N—B interaction, alter with the presence of at least one electron withdrawing pentafluorophenyl

ring at the boron center. In a similar fashion to the pentafluorophenyl-free aromatic amine borane adducts, the Brønsted acidity of the N—H group increases upon adduct formation with $B(C_6F_5)_3$,⁵⁸ a feature expected to be maintained, in part, for adducts with mono- and bis-(pentafluorophenyl)borane. However, the resulting decrease in hydridic character of the remaining B—H groups may help to prevent spontaneous degradation. The increased Lewis acidity at the perfluoroaryl substituted boron allows for increased donor strength from the nitrogen atom of the aromatic amine, resulting in a potentially stronger B—N bond in the adducts $PhH_2N \cdot BH_n(C_6F_5)_{3-n}$ ($n = 1, 2$) than in $PhH_2N \cdot BH_3$. Therefore, the solution stability of the adducts $PhH_2N \cdot BH_n(C_6F_5)_{3-n}$ ($n = 1, 2$) may be attributed, in part, to the effect of the electron withdrawing of the $-C_6F_5$ ring on the B—N bond strength.

2.4 Conclusions

Starting from the easily prepared and handled dimethylsulfide adducts, various amine and nitrogen-donor adducts of mono- and bis-(pentafluorophenyl)borane have been prepared and crystallographically characterized. Treatment of a toluene solution of $Me_2S \cdot BH_n(C_6F_5)_{3-n}$ ($n = 1, 2$) with the desired amine or nitrogen donor at ambient temperature yields quantitative conversion to the corresponding Lewis adduct. Initial adduct formation is easily confirmed through multinuclear NMR spectroscopy, and in most cases the materials are easily isolated as crystalline solids in reasonable yields.

The solid state structures of the adducts display a variety of bonding interactions which are similar to those observed in the pentafluorophenyl-free analogs.⁵⁸ The presence of inter- and intra-molecular N—H...F—C interactions is a characteristic feature of the Lewis adducts between protic amines and pentafluorophenyl substituted boranes. Although considered to be a poor hydrogen bond acceptor,¹⁵⁶ the C—F functionality plays a very important role in the solid state structures of the amine adducts of mono- and bis-(pentafluorophenyl)borane. Perhaps a more promising advance towards the functionality

of these materials as hydrogen sources is the presence of N—H...H—B and BH₂...HN bifurcated dihydrogen bonding. These interactions are observed in the solid state structures of **1a-d** and are thought to precede dihydrogen release from similar materials.^{93,124,128} The bifurcated dihydrogen bonding in **1a** and **1d** specifically is reminiscent of that observed in the solid state structures of Me₂HN·BH₃ and H₃N·BH₃⁹³ which have been used as chemical hydrogen storage systems.⁹⁰

The related ammonia adducts H₃N·BH_n(C₆F₅)_{3-n} (n = 0, 1, 2) have been used as precursors to the corresponding amidoborane ligands, facilitating the preparation of isolable organometallic complexes which have relevance to the catalytic dehydrocoupling of ammonia borane.^{102,113} In addition, the N-substituted amine borane PhH₂N·B(C₆F₅)₃ will readily react with ⁿBuLi to afford Li[NHPhB(C₆F₅)₃] as a stable and isolable salt,¹⁵⁹ providing an entry way to reactivity with transition metal complexes. It seems fitting to conclude, then, that the reported protic amine and nitrogen donor adducts of mono- and bis-(pentafluorophenyl)borane have the potential to provide valuable information to contribute to the understanding of catalytic dehydrocoupling of amine boranes at transition metal centers.

Chapter 3 Pentafluorophenyl stabilized models for dehydrocoupling intermediates

3.1 Introduction

The bonding of ethyl and ethylene ligands to transition metals, and the relationship between the resulting structures and their role in catalytic cycles, has been a popular research area since the 1950s.^{39,154,171,185,186} Amine boranes, which are isoelectronic with alkanes, have moved into the spotlight of current research endeavours due to their potential role as hydrogen storage materials.^{89,90,187} However, despite their isoelectronic relationship, alkyl / alkene and amine borane / aminoborane moieties display considerable variation in their coordination and bonding to transition metal centers.

Reports of transition metal catalysts which are active towards the dehydrocoupling of amine boranes first appeared in the early 2000s^{141,188} and the arsenal of both heterogeneous and homogeneous catalyst systems include metals from across the d-block.^{89,90,187} To date, use of catalysts based on the late transition metals has provided the most significant insights into individual steps of the catalytic dehydrocoupling cycles.^{138,139,143,144}

Early transition metal catalysts facilitate the dehydrocoupling of amine boranes under conditions similar to those of the late transition metals.^{75,148–150,189–191} However, considerably less mechanistic information has been identified for the early transition metal catalysed processes, which has prompted active research in this area. Of significant interest to the study of any catalytic cycle is the isolation of chemical intermediates, which provide details about the active reaction pathways. As a consequence of the challenging research surrounding group 4 metal catalyzed dehydrocoupling, only a handful of the corresponding metal amidoborane complexes have been reported.^{110–112} The use of pentafluorophenyl stabilized boranes has facilitated the isolation of titanium, zirconium

and hafnium species containing metal—nitrogen multiple bonds,^{101,102,113,192–195} functionalities which are proposed to play a significant role in catalytic and industrial processes such as the formation of metal-nitride thin films. It therefore seems fitting to use the pentafluorophenyl group as a synthetic strategy for stabilizing intermediates and characterizing bonding interactions of the group 4 transition metals related to the dehydrocoupling of amine boranes.

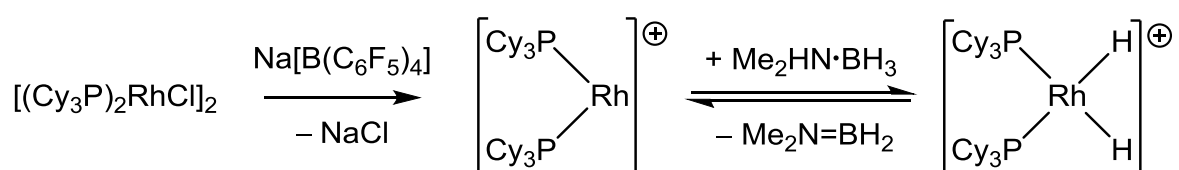
3.1.1 Amine borane dehydrocoupling using late transition metal catalysts

The first example of catalytic dehydrocoupling of amine boranes was reported by Manners and coworkers, using the group 9 transition metal catalyst precursor $[\text{Rh}(1,5\text{-cod})\text{-}\mu\text{-Cl}]_2$.^{141,188} This premier report was shortly followed by similar catalytic activity observed for another group 9 transition metal catalyst, $(\text{POCOP})\text{Ir}(\text{H})_2$ ($\text{POCOP} = \mu^3\text{-}1,3\text{-(OP}^t\text{Bu}_2\text{C}_6\text{H}_3)$),⁹¹ initially developed by Brookhart for catalytic transfer dehydrogenation of alkanes.¹⁹⁶ Brookhart's catalyst is still one of the most efficient for catalytic dehydrocoupling, with addition of as little as 0.25 mol% allowing for quantitative conversion of amine boranes to polyaminoboranes at ambient temperature.⁹¹ Since these initial reports, a large number of group 9 and other late transition metal catalysts have been developed which effectively dehydrocouple ammonia borane and its N-substituted analogs at low catalyst loadings and under mild conditions.^{90,139,144,153,197–199}

The high activity of catalysts based on the late transition metals may be attributed, in part, to the availability of multiple stable metal oxidation states, and great attention must be paid to the oxidation state changes of the transition metal, or lack thereof, during catalysis. In at least one reported instance, two simultaneous mechanistic pathways participate in the dehydrocoupling of amine boranes using a group 9 transition metal. The sterically and electronically unsaturated $[\text{Rh}(\text{PCy}_3)_2]^+$ fragment facilitates dehydrocoupling through both redox and non-redox reaction pathways.¹³⁵ The former pathway includes a Rh(I) / Rh(III)

redox cycle, which includes initial B—H bond activation at the Rh(I) center to ultimately generate the Rh(III) dihydride $[(PCy_3)_2Rh(H)_2]^+$ (**Scheme 3.1**). The generated Rh(III) dihydride is itself effective as a catalyst for amine borane dehydrocoupling through a constant oxidation state Rh(III) process.¹³⁵

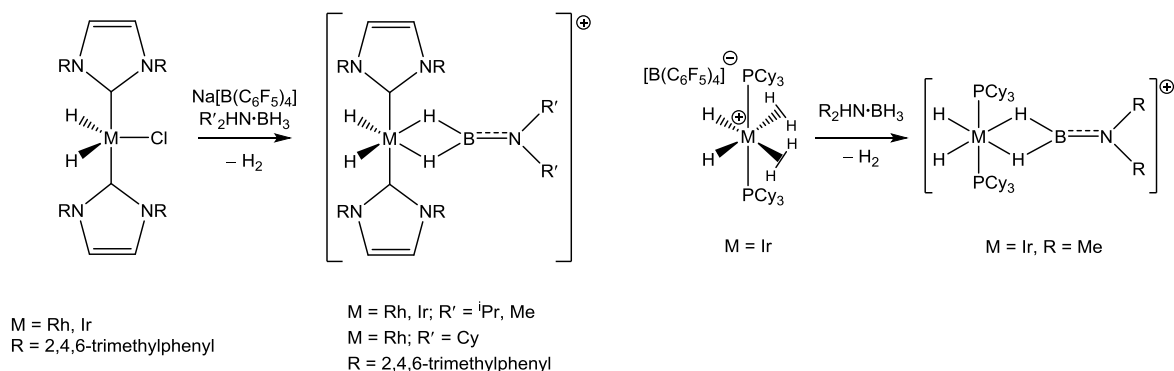
Scheme 3.1: Simplified partial reaction pathways for the catalytic dehydrocoupling of dimethylamine borane with the $[Rh(PCy_3)_2]^+$ fragment.



Mechanistic cycles are generally corroborated either through computational methods or trapping of intermediate species and inferring those steps preceding their formation. For example, group 9 complexes bearing an N-heterocyclic carbene ligand, of the formula $(L)_2MCl(H)_2$ ($M = Rh, Ir$; $L = IMes$ (N,N'-bis(2,4,6-trimethylphenyl)imidazol-2-ylidene)) have been reported as effective pre-catalysts for the dehydrocoupling of N-substituted amine boranes.^{143,144,197} Treatment of the substrates $R_2HN \cdot BH_3$ ($R = iPr, Cy, Me$) with catalytic amounts of $(L)_2MCl(H)_2$ ($M = Ir, Rh$) has resulted in the isolation of the metal aminoborane coordination compounds of $R_2N=BH_2$ ($R = iPr, Cy, Me$).^{143,144} Similar complexes have been isolated from reaction of the iridium catalyst $[(H)_2Ir(PCy_3)_2]^+$ with $Me_2HN \cdot BH_3$ (**Scheme 3.2**).¹³⁸ Because of the often unavoidable rapid and spontaneous cyclization of unhindered aminoboranes (for example, $H_2N=BH_2$),¹¹⁸ details surrounding their oligomerization events are, in general, poorly understood. However, isolation of these late transition metal σ -borane coordination complexes has resulted in strong evidence for the suggestion that aminoborane cyclization, or further substrate activation,²⁰⁰ occurs rapidly at, or at least very near to, the metal center through an off-metal dimerization process also

postulated for mid transition metal carbonyl catalysts such as $[\text{CpFe}(\text{CO})_2]_2$ ¹⁴⁰ and $\text{M}(\text{CO})_6$ ($\text{M} = \text{Cr}, \text{Mo}, \text{W}$).¹⁸⁹

Scheme 3.2: Preparation of crystallographically characterized aminoborane coordination compounds.^{138,143,197}



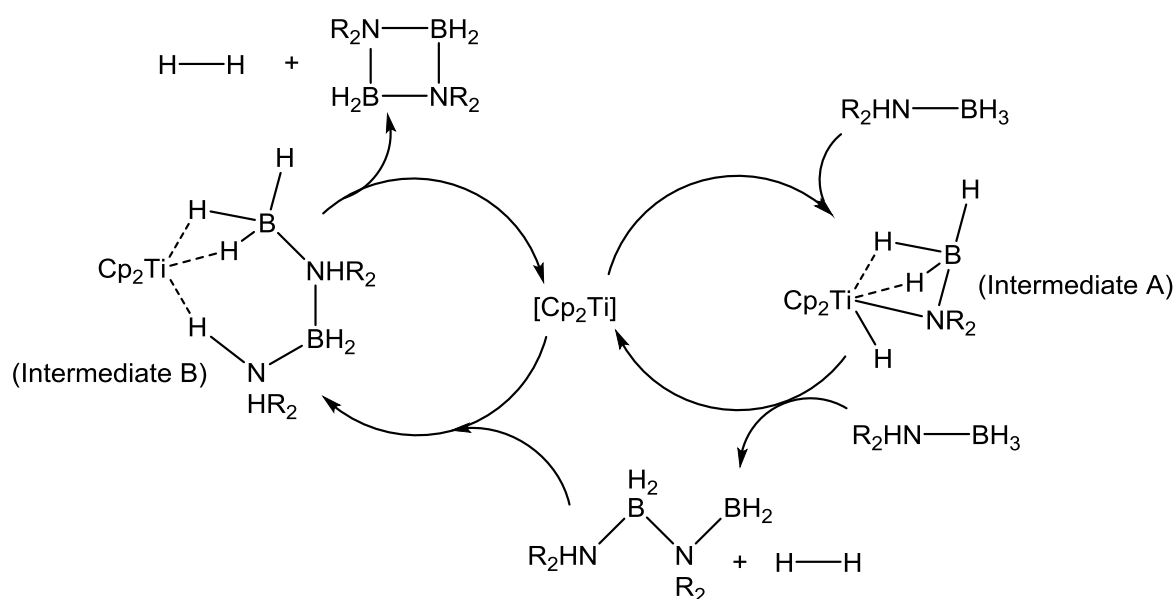
The use of N-heterocyclic carbene ligands has facilitated the development of more robust catalysts than the phosphine analogs,^{201–203} which have the potential to participate in side reactions to produce phosphine boranes or decomposition resulting in insoluble metals and metal salts. The combination of equimolar quantities of an N-heterocyclic carbene with $\text{Ni}(\text{COD})_2$ has provided a cheaper alternative to the later transition metals.¹⁴⁷ This Ni based catalyst demonstrates amine borane dehydrocoupling at comparable or better rates than the rhodium or iridium analogs.

3.1.2 Amine borane dehydrocoupling using group 4 metal catalysts

Early^{75,76,148–150,189–191} and mid^{137,140,151,152,191,204} transition metal catalysts have been developed as more economically viable alternatives to the late transition metal systems. For example, the in situ generation of $[\text{Cp}_2\text{Ti}]$ from $\text{Cp}_2\text{TiCl}_2 / 2 \text{ } ^n\text{BuLi}$ presents an attractive option for catalytic dehydrocoupling due to the low commercial price and robust stability of

the catalyst precursor. $[\text{Cp}_2\text{Ti}]$ has been reported as a highly active catalyst for the dehydrocoupling of ammonia borane and its N-methylated analogs at low catalyst loading and with rapid dihydrogen evolution.^{148,150} While individual mechanistic steps have been postulated,^{150,205} the intermediate species are short-lived and therefore evade isolation and examination by NMR spectroscopy and X-ray crystallography. In a similar fashion to one of the parallel proposed mechanisms for dehydrocoupling using the rhodium catalyst $[(\text{C}_3\text{P})_2\text{Rh}]^+$,¹³⁵ that for $[\text{Cp}_2\text{Ti}]$ is reported to occur through a Ti(II) / Ti(IV) redox cycle (**Scheme 3.3**).¹⁵⁰

Scheme 3.3: Proposed catalytic cycle for the dehydrocoupling of amine boranes by $[\text{Cp}_2\text{Ti}]$, generated in situ.



The proposed dehydrocoupling mechanism proceeds through a step-wise procedure beginning with N—H bond activation.^{150,205} This is in contrast to the initial B—H bond activation step proposed, in general, for the late-transition metal systems.^{135,147,206–208} Therefore, particular interest in the $[\text{Cp}_2\text{Ti}]$ cycle focuses on the presence and possible

isolation of Intermediate A (**Scheme 3.3**), which is the product of formal N—H bond activation and oxidative addition to the Ti(II) center. Intermediate A may be described as a titanium(IV) amidoborane hydride, with the amidoborane ligand proposed to exhibit an additional interaction with the metal center through one or more hydridic B—H groups. The result of such an interaction is a Ti—H bond and Ti...H—B interaction at the metal center, a combination which may facilitate dihydrogen elimination through H...H coupling at titanium. Interest in the isolation of Intermediates A and B is driven by the implications that such a species would have on the current understanding of this catalytic cycle. Due to the rapid reactivity observed in [Cp₂Ti] mediated dehydrocoupling, the isolation of model species currently requires the use of ancillary ligands which inhibit further turnover at the titanium center. Amidoborane ligands containing no B—H bonds¹¹³ and / or bulky aryl groups^{101,102,113} on boron have facilitated the isolation of metallocene complexes bearing the 'M—N—B' unit which has been postulated in intermediate stages of dehydrocoupling mechanisms (**Figure 3.7**).¹⁵⁰

3.1.3 Aminoborane versus alkene bonding to transition metal centers

The first step for amine borane dehydrocoupling, as with any catalytic process, is approach of the substrate to the active transition metal center. As a result of the molecular polarity of ammonia borane, end-on coordination through one^{204,209} or two^{138,139,143,144,209–212} of the B—H hydrogen atoms with the electrophilic metal center is observed for adducted amine boranes (and linear diborazines) with the late transition metals (**Figure 3.1**). This end-on coordination mode facilitates B—H activation at the metal center as the next step in the catalytic dehydrocoupling cycle.²¹³

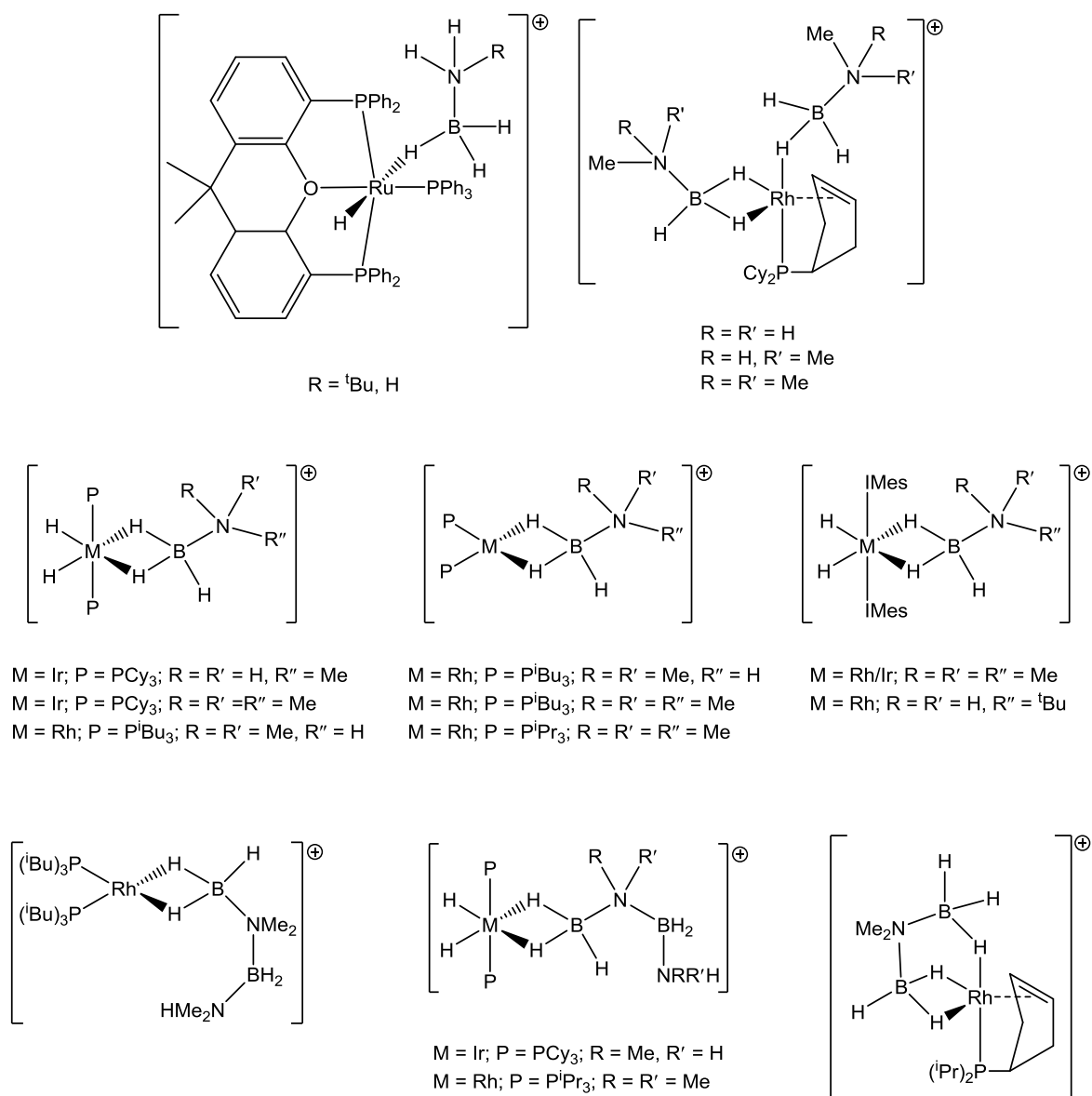
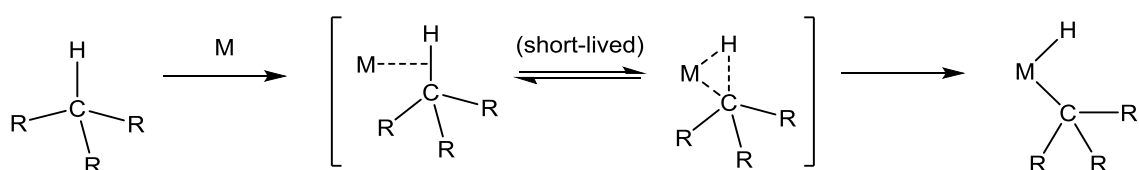


Figure 3.1: Crystallographically characterized transition metal complexes featuring end-on coordination of amine boranes^{138,139,143,144,204,209–211,214} and linear diborazines.^{139,212,215}

In contrast, the proposed bonding mode for the relatively non-polar alkane σ -complexes differs to that observed for amine borane σ -complexes. Alkane σ -complexes are believed to be key intermediates in the activation of C—H bonds with transition metals.^{186,216} For this activation to occur, the alkane substrate is proposed to coordinate with the metal in a side-on fashion through donation of the electron density of the relatively non-polar C—H bond to the electrophilic transition metal center (**Scheme 3.4**).²¹⁶ Structural

characterization of alkane σ -complexes is very limited due to the weak bonding and rapid reactivity of the coordination compound towards formal C—H bond activation at the metal center.^{185,216}

Scheme 3.4: C—H bond activation pathway.



Monomeric aminoboranes ($\text{R}_2\text{N}=\text{BH}_2$) favor interaction with transition metals in an end on arrangement, through coordination from both B—H groups in a bridging fashion. The stability of most monomeric aminoboranes towards spontaneous cyclization is quite poor, limiting the number of examples of such species coordinated to transition metals. However, the use of N-heterocyclic carbene^{143,144,197} and phosphine¹³⁸ ligands on group 9 transition metals has provided a synthetic strategy for stabilizing coordinated monomeric aminoboranes (**Figure 3.2**). These species provide valuable insight into the mechanism of amine borane dehydrocoupling, specifically regarding the on-metal or off-metal nature of amidoborane dimerization.

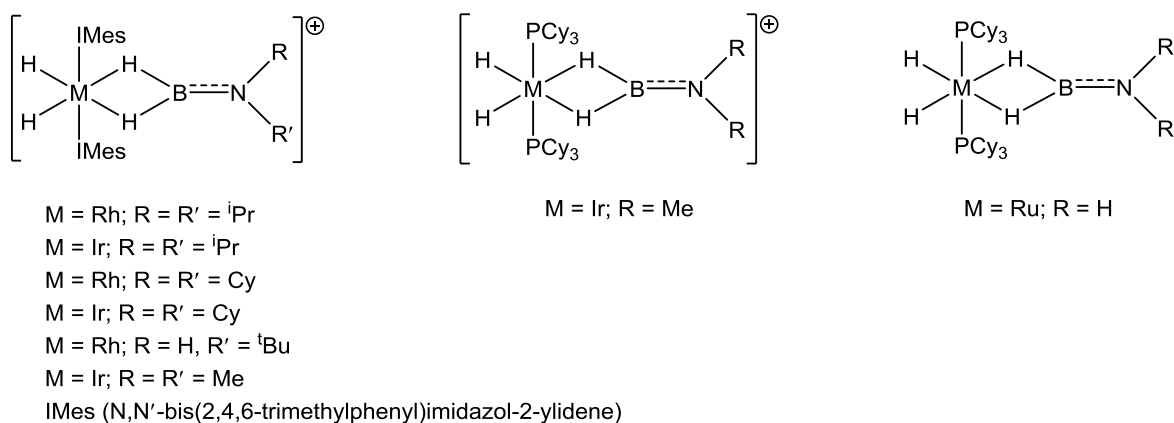


Figure 3.2: Crystallographically characterized transition metal complexes featuring end-on coordination of aminoboranes.^{138,143,197,217}

This bonding pattern is in contrast to the isoelectronic C=C complexes which, in general, interact with the metal center through π -donation from the double bond to the metal center in a side-on fashion.²¹⁸ Transition metal alkene complexes appear quite frequently in the literature, with the first crystallographically characterized transition metal alkene complex prepared in the 1800s,²¹⁹ and structural characterization following in the 1950s.²²⁰ A few examples of transition metal ethylene complexes are reported in **Figure 3.3**.^{221–224}

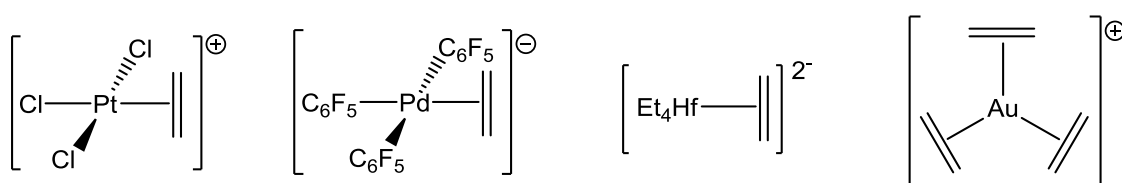


Figure 3.3: Crystallographically characterized transition metal complexes featuring side-on coordination of alkenes.

Despite differences in coordination mode between amine boranes / alkenes and aminoboranes / alkenes with transition metal centers, some structural similarities are observed in metal amidoborane ($M\text{—NH}_2\text{BX}_3$) and metal alkyl ($M\text{—CH}_2\text{CX}_3$) complexes. Due to the molecular polarity of amine boranes, complexes bearing an amidoborane

ligand (in the absence of an additional chelate interaction) feature a metal—nitrogen bond which may be described through two resonance forms (**Figure 3.4**).¹¹³ The first defines the metal—nitrogen bond as being formed by donation of the nitrogen lone pair into an empty d-orbital on the metal, with the ligand acting as a neutral two electron donor (L-type). This implies an N—B sigma bond in which the boron and nitrogen each contribute one electron, and one hydride ligand on the boron occupies the formerly empty p-orbital. The second resonance form assumes that lone pair donation from the nitrogen is directed towards the empty p-orbital on boron rather than an empty d-orbital of the metal, resulting in the amidoborane ligand acting as an anionic single electron donor towards the metal center (X-type) and the borane fragment as a Lewis acid stabilizing the Lewis basic metal—amide bond. Careful assessment of the metal-nitrogen bond length allows for distinction between the two resonance types. Structures which show bonding similar to resonance form A^{225,226} would be expected to have longer M—N bonds than those which are best described through resonance form B.¹¹³ In contrast, transition metal alkyls are not commonly considered in light of any resonance structures because the C—C bond is essentially non-polar.

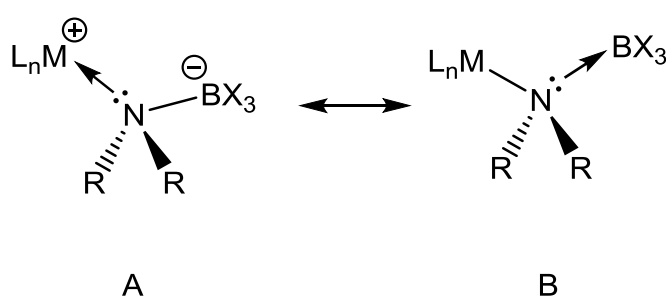


Figure 3.4: Resonance forms of metal amidoborane complexes ($x \neq H$).

However, both amidoborane and alkyl ligands may participate in a β -agostic interaction when the appropriate metal d-orbitals and B—H or C—H functionalities are available. An agostic interaction is described as the additional ligation of a hydrogen atom from the

ligand to an empty orbital of the metal, producing a significantly decreased M—N—B or M—C—C bond angle.^{227,228} The term ‘agostic’ was originally coined²²⁷ for transition metal alkyl complexes and to avoid confusion, analogous interactions from amidoborane ligands have been referred to as ‘ β -B-agostic’.¹¹⁰ In crystallographically characterized instances of agostic interactions, the hydrogen atom is generally from the β -boron or carbon atom,^{229,230} but α -agostic^{231,232} and even γ -agostic²³³ interactions are known for select transition metal complexes (**Figure 3.5**).^{231,233–236}

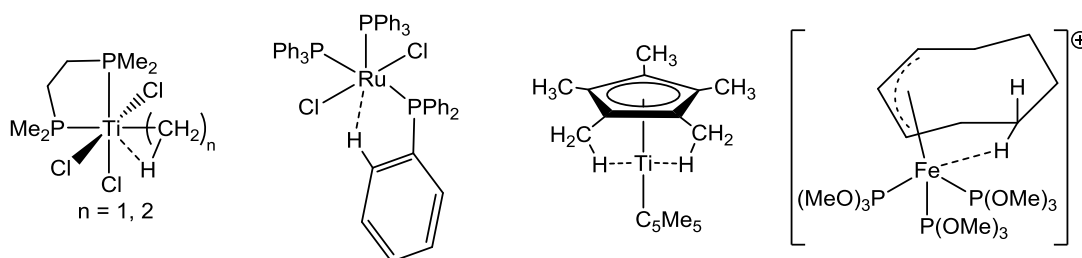
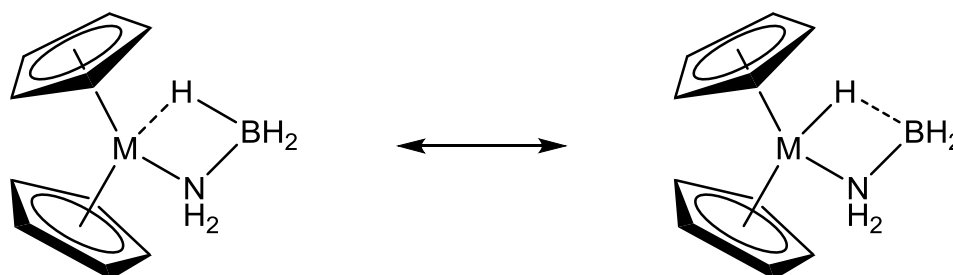


Figure 3.5: Crystallographically characterized transition metal alkyl and alkene complexes which feature a C—H agostic interaction.

The hydridic nature and high polarization of the B—H bond of amidoborane ligands has facilitated a large number of examples of complexes which exhibit a β -B-agostic interaction. The B—H agostic interaction has been described as a charge re-distribution at the metal center, resulting in the agostically bound hydride adopting partial metal—hydride character (**Scheme 3.5**).

Scheme 3.5: Charge redistribution at the metal center in the presence of an agostically-bound amidoborane ligand.



This results in a less hydridic B—H bond than that of the parent amine borane. The opposite effect is observed for alkyl agostic interactions in which the polarization of the C—H bond increases relative to that of the free non-polar alkane.¹¹¹ However, a shortening of both the alkane C—C and amidoborane B—N bonds is observed as a result of the agostic interaction. There are several structurally characterized examples of metal alkyl complexes which display β -agostic interactions (**Figure 3.5**), with the first example being reported in 1982.²³¹ Unsurprisingly, several early transition metal amidoborane complexes exhibit the analogous β -B-agostic interaction (**Figure 3.6**).^{110–112,190}

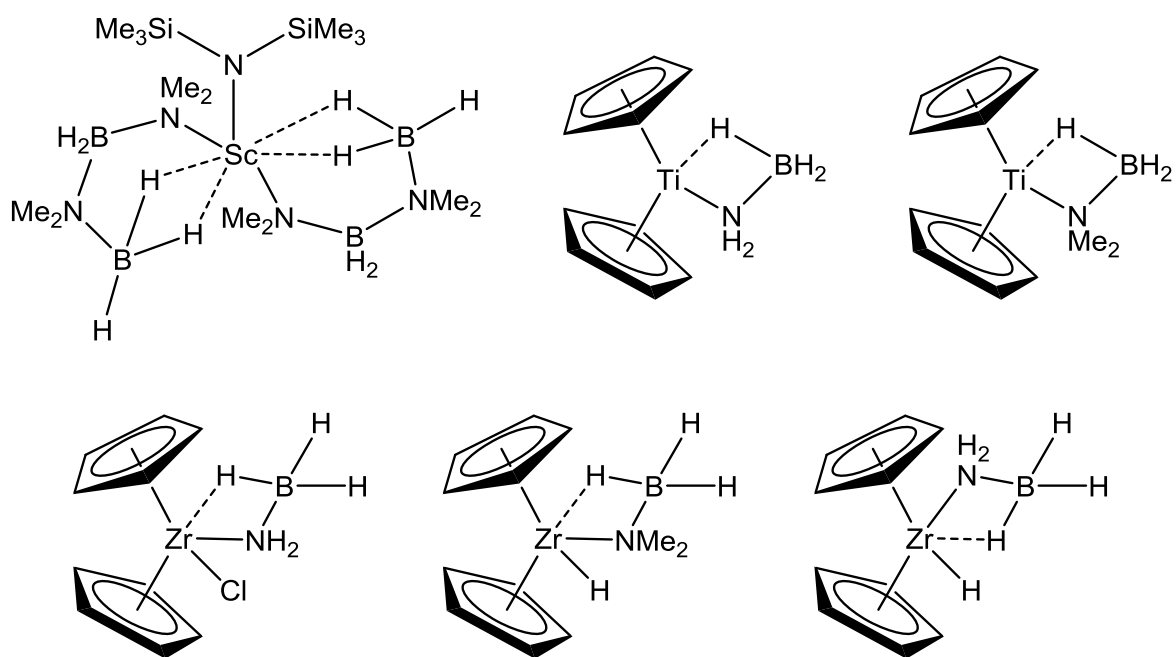


Figure 3.6: Crystallographically characterized early transition metal amidoborane complexes.

3.1.4 $-C_6F_5$ stabilized amidoborane complexes of the group 4 metals

In order to further investigate the structure and bonding which occurs during catalytic dehydrocoupling, synthetic strategies are employed which act to hinder reaction turnover and aid isolation of proposed intermediates. The bulky Lewis acid tris(pentafluorophenyl)borane has been used to stabilize metal–nitrogen bonds between group 4 metals and amido^{113,192,194} and nitrido^{193,195,237} fragments resulting from facile deprotonation of $H_3N \cdot B(C_6F_5)_3$ (**Figure 3.7**). These structures provide information relevant to several important processes, including amine borane dehydrocoupling and the production of TiN thin films. Increased research interest in the isolation of group 4 metallocene amidoborane complexes has resulted from several reports of catalytic dehydrocoupling with group 4 sandwich complexes.^{148–150}

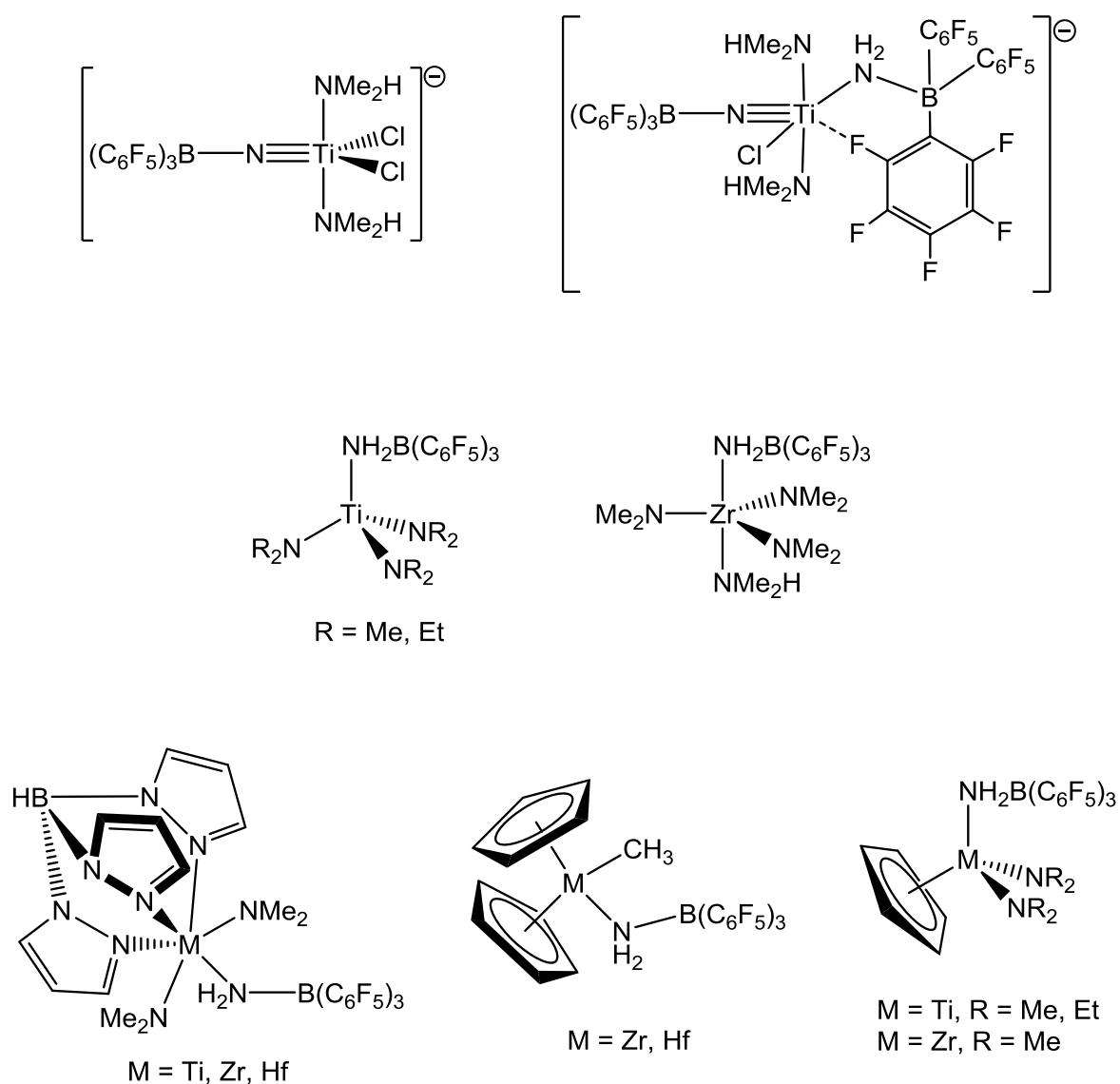


Figure 3.7: Crystallographically characterized tris(pentafluorophenyl)borane substituted amido- and nitrido-borane complexes of the group 4 metals.

The tendency towards the formation of agostic interactions in other reported group 4 amidoborane complexes,^{110–112} and the consequences such an interaction may have in the overall dehydrocoupling process, has informed the development of pentafluorophenyl substituted amidoborane ligands containing at least one β -hydrogen, $-\text{NH}_2\text{BH}_2(\text{C}_6\text{F}_5)$ and $-\text{NH}_2\text{BH}(\text{C}_6\text{F}_5)_2$. The availability of a B—H group which may coordinate in an agostic fashion towards the metal center provides more detailed information regarding potential

intermediate species in catalytic dehydrocoupling. Group 4 metallocene complexes of $\text{-NH}_2\text{BH}_2(\text{C}_6\text{F}_5)$, $\text{-NH}_2\text{BH}(\text{C}_6\text{F}_5)_2$ and related ligands have been prepared and crystallographically characterized. The presence of a β -B-agostic interaction plays a prominent role in the solid and solution state structure of these complexes and supports features of proposed intermediates in the catalytic dehydrocoupling by $[\text{Cp}_2\text{Ti}]$ and other early transition metals.

3.2 Results

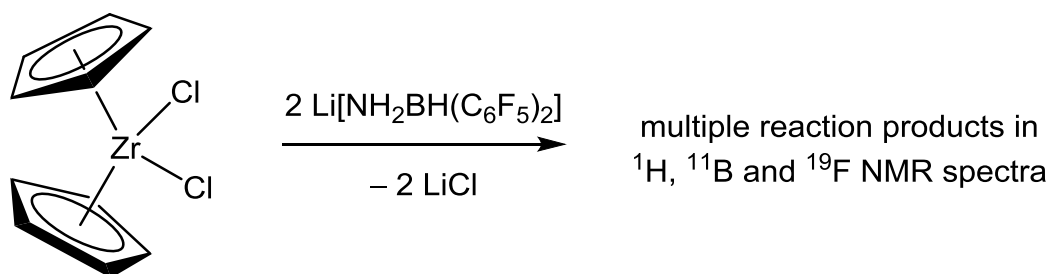
The ammonia adducts $\text{H}_3\text{N}\cdot\text{BH}(\text{C}_6\text{F}_5)_2$ and $\text{H}_3\text{N}\cdot\text{BH}_2(\text{C}_6\text{F}_5)$ were used as ligand precursors in an analogous fashion to the related chemistry of $\text{H}_3\text{N}\cdot\text{B}(\text{C}_6\text{F}_5)_3$.¹¹³ Facile deprotonation with $^n\text{BuLi}$ in thf produces the lithium salts $[\text{Li}\{\text{thf}\}_x][\text{NH}_2\text{BH}_n(\text{C}_6\text{F}_5)_{3-n}]$ for $n = 1, 2$ in quantitative yield. Complete conversion to the lithium salts was confirmed through multinuclear NMR spectroscopy. In the case of $\text{Li}[\text{NH}_2\text{BH}(\text{C}_6\text{F}_5)_2]$, the addition of one equivalent of 12-crown-4 afforded X-ray quality crystals of $[\text{Li}\{12\text{-crown-4}\}][\text{NH}_2\text{BH}(\text{C}_6\text{F}_5)_2]$, isolated from a dichloromethane / light petroleum solution at $-25\text{ }^\circ\text{C}$.¹⁰¹ Analogous treatment of $\text{Li}[\text{NH}_2\text{BH}_2(\text{C}_6\text{F}_5)]$ and attempted crystallization from a dichloromethane / light petroleum solution at $-25\text{ }^\circ\text{C}$ resulted in the formation of $[\text{Li}\{12\text{-crown-4}\}]\text{Cl}$, the product of halide abstraction from the dichloromethane solvent. X-ray quality crystals of the desired lithium salt could not be isolated from any other solvent mixtures despite numerous attempts. However, during reaction screening with group 4 metallocene starting materials, the lithium salts were prepared *in situ* and used without isolation.

3.2.1 $[\text{Cp}_2\text{Zr}]$ complexes bearing $-\text{C}_6\text{F}_5$ substituted amidoborane ligands

Treatment of a toluene solution of Cp_2ZrCl_2 with two equivalents of base-free $\text{Li}[\text{NH}_2\text{BH}(\text{C}_6\text{F}_5)_2]$ at $-78\text{ }^\circ\text{C}$ and slow warming of the reaction mixture to ambient

temperature produced a set of crude NMR spectra which indicated a complex mixture of compounds (**Scheme 3.6**).

Scheme 3.6: Reactivity of Cp_2ZrCl_2 with the lithium salt $\text{Li}[\text{NH}_2\text{BH}(\text{C}_6\text{F}_5)_2]$.



The ^1H NMR spectrum in C_6D_6 consisted of several major cyclopentadienyl containing species between 5.19 and 5.56 ppm, of which the major product by integration was at 5.34 ppm. The corresponding ^{19}F and ^{11}B NMR spectra also displayed numerous reaction products. Filtration of the crude reaction mixture and subsequent cooling of the toluene solution to $-25\text{ }^\circ\text{C}$ overnight afforded, on one occasion, X-ray quality crystals of $\text{Cp}_2\text{Zr}(\text{NH}_2\text{BH}(\text{C}_6\text{F}_5)_2)_2$ (**3**) as the toluene solvate. In the solid state, the zirconium atom of **3** is in a distorted tetrahedral geometry, resulting from coordination to the two cyclopentadienyl rings and two $-\text{NH}_2\text{BH}(\text{C}_6\text{F}_5)_2$ amidoborane ligands (**Figure 3.8**). Additional coordination to the zirconium occurs from one of the $-\text{NH}_2\text{BH}(\text{C}_6\text{F}_5)_2$ ligands which participates in a β -B-agostic interaction, resulting in a $\text{Zr}(1)\text{—N}(1)\text{—B}(1)$ bond angle of $92.2(6)^\circ$. The remaining amidoborane ligand does not participate in any additional metal—ligand interactions and displays a $\text{Zr}(1)\text{—N}(2)\text{—B}(2)$ bond angle of $120.0(6)^\circ$. Both ligands exhibit intramolecular $\text{N—H}\cdots\text{F—C}$ interactions between the protic N—H group and an *ortho*-fluorine of the pentafluorophenyl rings (**Table 3.1**).

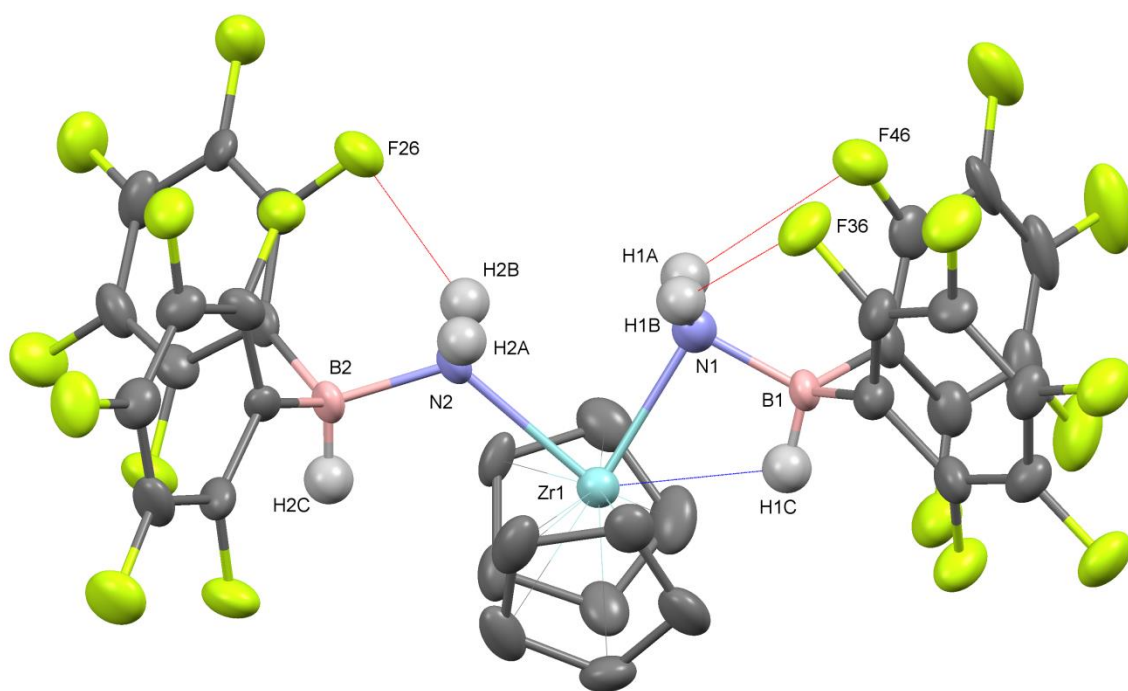


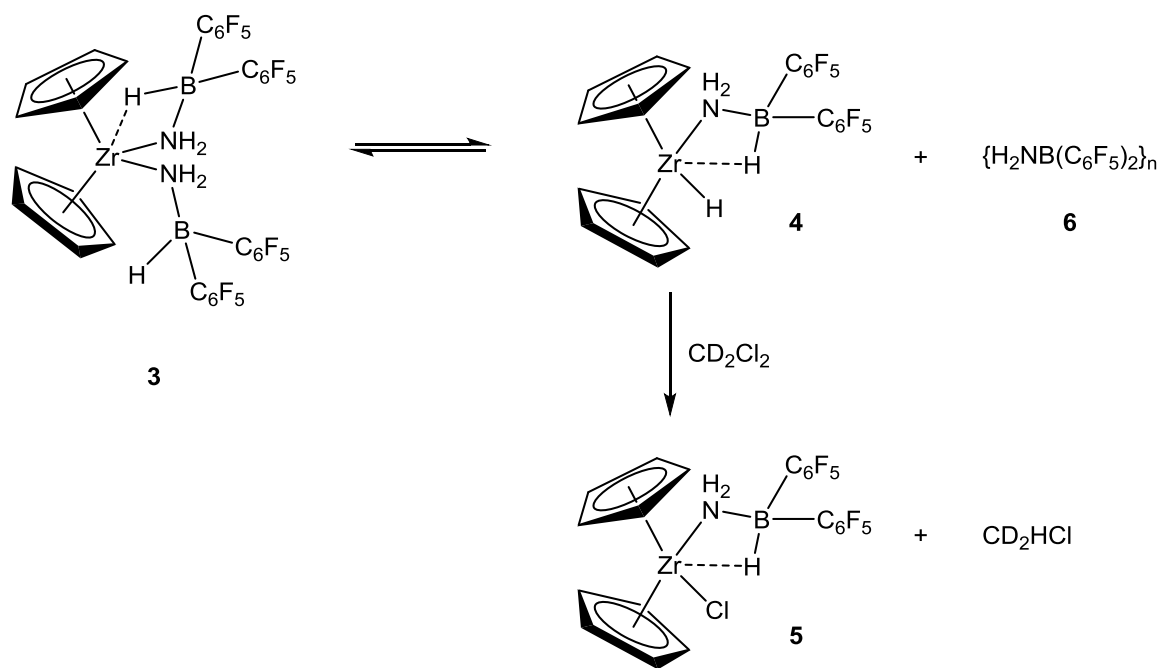
Figure 3.8: Crystal structure of $\text{Cp}_2\text{Zr}(\text{NH}_2\text{BH}(\text{C}_6\text{F}_5)_2)_2$ (**3**) with displacement ellipsoids displayed at the 50% probability level. The cyclopentadienyl hydrogen atoms and toluene solvate molecule have been omitted for clarity. Intramolecular $\text{N}-\text{H}\cdots\text{F}-\text{C}$ interactions are indicated in red and the β -B-agostic interaction is indicated in blue.

Table 3.1: Selected bond and $\text{N}-\text{H}\cdots\text{F}-\text{C}$ contact lengths for $\text{Cp}_2\text{Zr}(\text{NH}_2\text{BH}(\text{C}_6\text{F}_5)_2)_2$.

Bond/contact	Length (Å)
Zr(1)—N(1)	2.263(8)
Zr(1)—N(2)	2.335(8)
B(1)—N(1)	1.52(2)
B(2)—N(2)	1.60(1)
Zr(1) \cdots H(1C)	2.294
N(1)—H(1B) \cdots F(36)—C(36)	2.187
N(1)—H(1A) \cdots F(46)—C(46)	2.539
N(2)—H(2B) \cdots F(26)—C(36)	2.226

One cyclopentadienyl resonance in the C_6D_6 1H NMR spectrum of the crude reaction mixture appeared broadened, a feature which was tentatively attributed to solution exchange, similar to that observed for related zirconocene amidoborane complexes.¹¹⁰ Changing the NMR solvent to CD_2Cl_2 resulted in sharpening of the cyclopentadienyl signals and preliminary identification of the resonances associated with $Cp_2Zr(NH_2BH(C_6F_5)_2)_2$ by relative integration between the Cp and NH_2 peaks at 5.18 and 2.23 ppm, respectively. The presence of additional cyclopentadienyl resonances indicated formation of a second major cyclopentadienyl-containing species. Ambient temperature aging of the CD_2Cl_2 NMR sample resulted in the formation of a single species different to that of **3**. Integration of the new major cyclopentadienyl resonance in comparison with that of the new NH_2 resonance (10:2) indicated the loss of one amidoborane ligand. This has been proposed to occur through B—H activation of the agostically bound $-NH_2BH(C_6F_5)_2$ ligand to produce $Cp_2Zr(H)(NH_2BH(C_6F_5)_2)$ (**4**). Further confirmation of the presence of a Zr—H moiety was demonstrated through treatment of **4** with a halogenated solvent to produce $Cp_2Zr(Cl)(NH_2BH(C_6F_5)_2)$ (**5**) as the final product (**Scheme 3.7**).

Scheme 3.7: Solution equilibrium of **3** in CD_2Cl_2 .



Compound **4** was fully characterized using multinuclear NMR spectroscopy (^1H NMR spectrum shown in **Figure 3.9**) and elemental analysis in the absence of suitable crystals for X-ray diffraction methods. The Zr—H resonance was identified in the ^1H NMR spectrum as a doublet at 3.85 ppm with an integration of one proton relative to the new cyclopentadienyl resonance at 5.75 ppm in CD_2Cl_2 . The peak position of the Zr—H resonance is consistent with the recently reported zirconocene amidoborane hydride.¹¹⁰ Signal splitting ($^2J_{\text{H,H}} = 5$ Hz) was observed and has been attributed to the Zr—H resonance coupling with the agostic B—H interaction exhibited by the remaining amidoborane ligand.

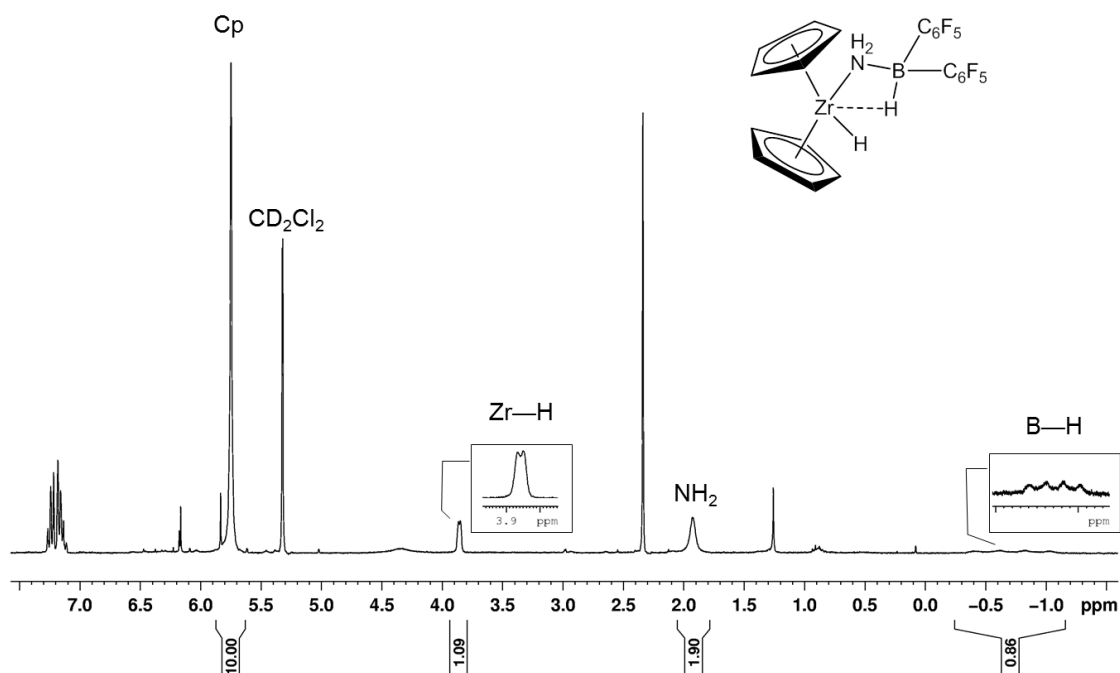


Figure 3.9: ^1H NMR spectrum of **4** recorded in CD_2Cl_2 at $25\text{ }^\circ\text{C}$.

The observed splitting of the Zr—H resonance is a spectral feature specific to the bis(pentafluorophenyl) substituted borane, in which the B—H agostic interaction does not participate in a solution equilibrium with a second B—H group. This relatively static interaction on the NMR time scale prevents free rotation about the B—N bond of $\text{Cp}_2\text{Zr}(\text{H})(\text{NH}_2\text{BH}(\text{C}_6\text{F}_5)_2)$ in solution, allowing for coupling between the Zr—H and agostic B—H hydrogen atom. In the other reported zirconocene amidoborane hydrides, which do not have substitution at the boron center,¹¹⁰ the Zr—H resonance appears as a broad singlet, the result of averaging of the three individual B—H environments which are in dynamic exchange, with only one participating in the agostic interaction at any one time.

In addition to formation of $\text{Cp}_2\text{Zr}(\text{H})(\text{NH}_2\text{BH}(\text{C}_6\text{F}_5)_2)$, the pentafluorophenyl substituted polyaminoborane $\{\text{H}_2\text{NB}(\text{C}_6\text{F}_5)_2\}_3$ (**6**) was identified as the major B/N containing product. This cyclic aminoborane trimer was isolated as a colorless crystalline solid and has been characterized by multinuclear NMR spectroscopy, elemental analysis and X-ray diffraction methods (**Figure 3.10**). The molecule adopts a twisted boat conformation with B—N bond

lengths ranging between 1.592(7) to 1.610(8) Å. Each N—H engages in anywhere between one and three N—H...F—C interactions ranging in length from 2.104 Å to 2.667 Å

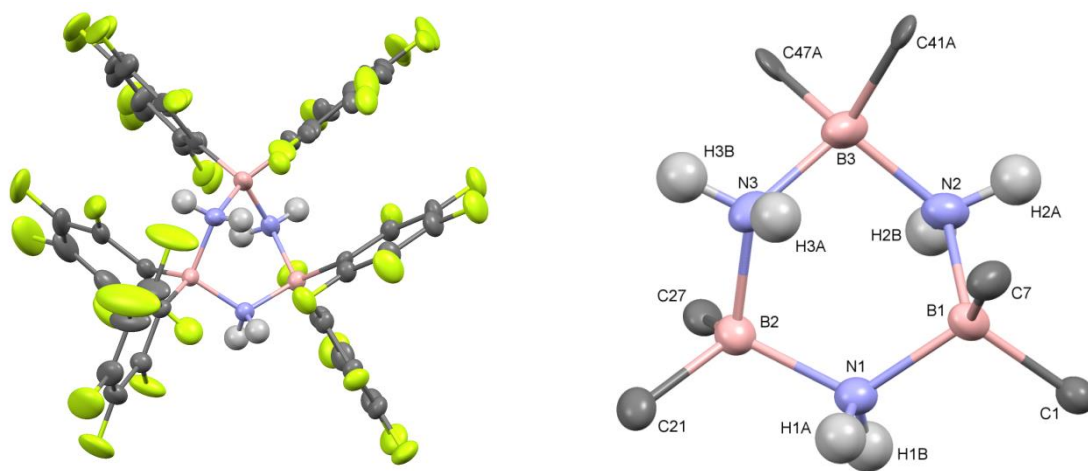


Figure 3.10: Crystal structure of $\{H_2NB(C_6F_5)_2\}_3$ (**6**) with displacement ellipsoids displayed at the 50% probability level. The pentafluorophenyl rings have been omitted for clarity (right).

In light of the successes with stable and isolable zirconocene species bearing the $-NH_2BH(C_6F_5)_2$ ligand, analogous chemistry was attempted with the related ligand precursor $Li[NH_2BH_2(C_6F_5)]$. Treatment of a toluene solution of Cp_2ZrCl_2 with two equivalents of base free $Li[NH_2BH_2(C_6F_5)]$ produced a crude 1H NMR spectrum with four major cyclopentadienyl containing products and several candidate $-NH_2$ resonances. On one occasion, X-ray quality crystals were isolated from the reaction mixture and the material was identified as $\{HNB(C_6F_5)_3\}_3$ (**7**), the cyclic trimer of the iminoborane dehydrocoupling product. This pentafluorophenyl substituted borazine has B—N bond lengths ranging between 1.413(4) and 1.432(4) Å, in close agreement to the B—N bond length in unsubstituted borazine (1.435 Å).²³⁸ The solid state structure of $\{HNB(C_6F_5)_3\}_3$ exhibits short N—H...F—C interactions between the protic N—H groups and the *ortho*-fluorine atoms of the neighboring pentafluorophenyl rings. Each N—H...F—C

interaction completes the formation of a six membered intramolecular ring, complying with Etter's rules for the occurrence and formation of hydrogen bonds.¹⁵⁸ These interactions help to inhibit rotation about the B—C bonds and result in a nearly planar molecule (Figure 3.11).

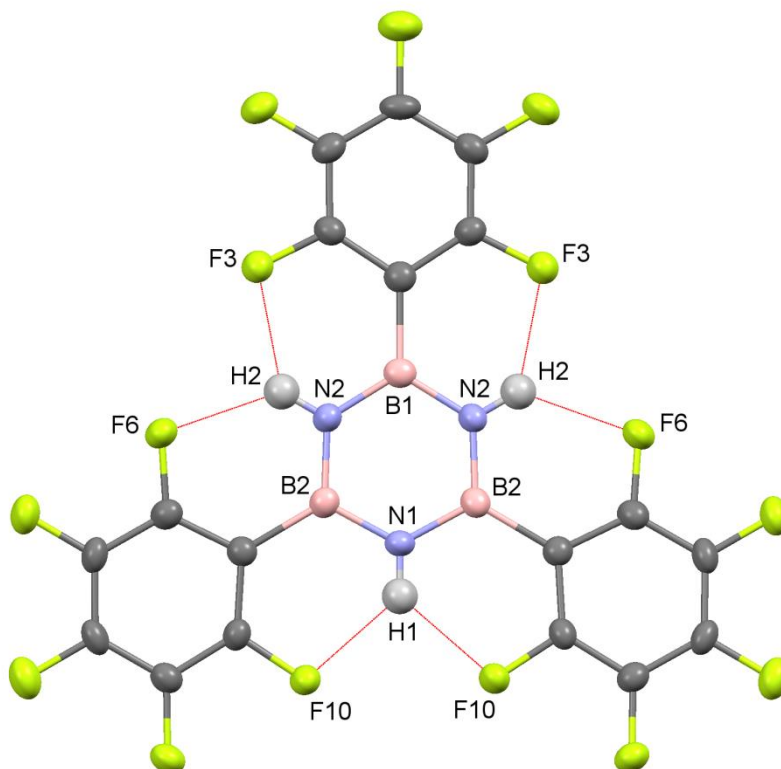
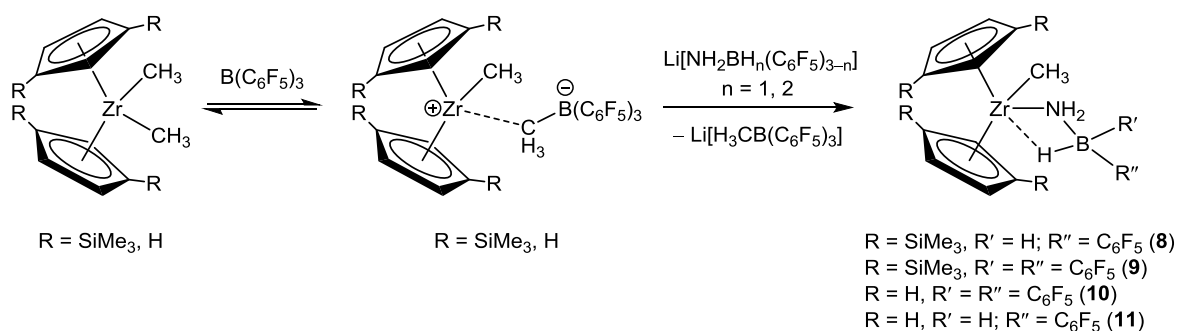


Figure 3.11: Crystal structure of $\{HNB(C_6F_5)\}_3$ (**7**) with displacement ellipsoids displayed at the 50% probability level. The short N—H...F—C contacts (red) measure 2.119 Å ($H(2)\cdots F(3)$), 2.130 Å ($H(2)\cdots F(6)$) and 2.113 Å ($H(1)\cdots F(10)$).

Isolation of the $-NH_2BH_2(C_6F_5)$ ligand on zirconocene through metathesis between the metallocene dichloride and the lithium salt proved to be unsuccessful. However, in the presence of a more electrophilic metal center, such as $Cp_2Zr(CH_3)(\mu-H_3CB(C_6F_5)_3)$ or $Cp''_2Zr(CH_3)(\mu-H_3CB(C_6F_5)_3)$, reaction with the lithium amidoborane salts led to isolable zirconocene complexes. Treatment of group 4 metallocene dimethyl complexes with $B(C_6F_5)_3$ is a widely used synthetic method for the generation of highly electrophilic metal

centers.^{37,38} This synthetic strategy has been extensively applied since the early 1990s as a method for the generation of active catalytic centers for alkene polymerization.^{39,40,154,171}

Scheme 3.8: Generation of highly electrophilic metal centers using $B(C_6F_5)_3$.



Treatment of $\text{Cp}^*{}_{2}\text{Zr}(\text{CH}_3)_2$ with one equivalent of freshly sublimed $\text{B}(\text{C}_6\text{F}_5)_3$ at $-78\text{ }^\circ\text{C}$ in toluene generates the metallocenium zwitterion $\text{Cp}^*{}_{2}\text{Zr}(\text{CH}_3)(\mu\text{-H}_3\text{CB}(\text{C}_6\text{F}_5)_3)$. The addition of one equivalent of $\text{Li}[\text{NH}_2\text{BH}_2(\text{C}_6\text{F}_5)]$ and subsequent warming of the crude reaction mixture to ambient temperature produced $\text{Cp}^*{}_{2}\text{Zr}(\text{CH}_3)(\text{NH}_2\text{BH}_2(\text{C}_6\text{F}_5))$ (**8**) as the major zirconium species, concomitant with the formation of $\text{Li}[\text{H}_3\text{CB}(\text{C}_6\text{F}_5)_3]$. Extraction of the product in light petroleum, dissolution of the crude material in a minimum of toluene and cooling of the toluene solution to $-25\text{ }^\circ\text{C}$ afforded X-ray quality crystals of compound **8** (Figure 3.12).

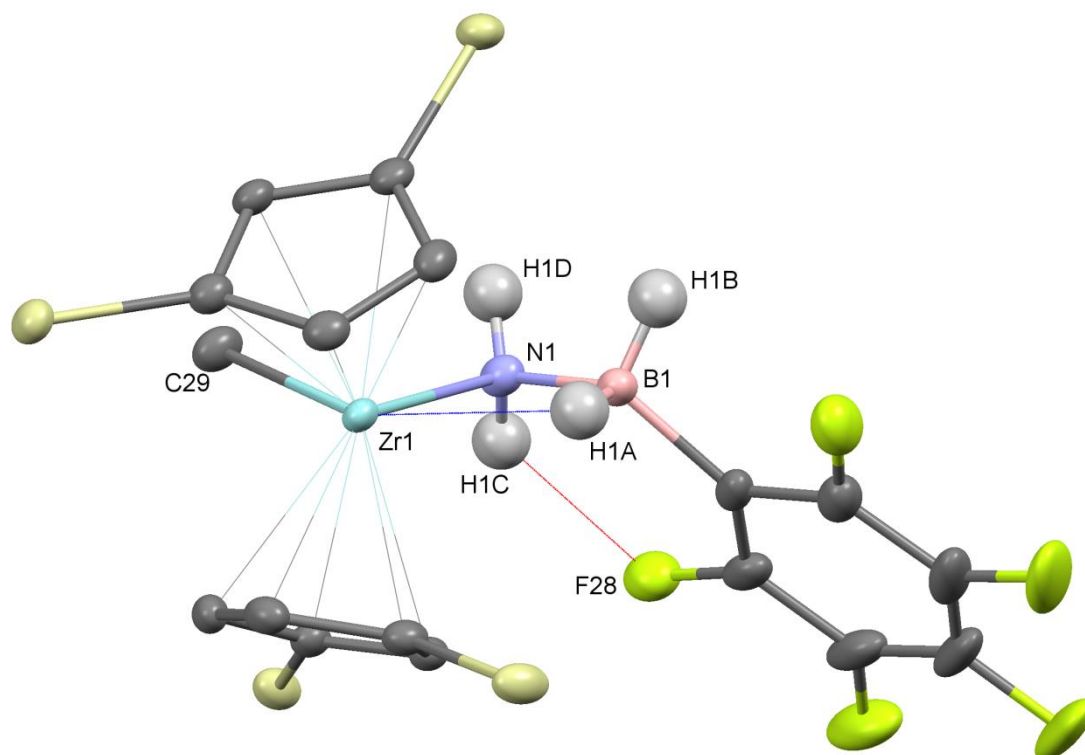


Figure 3.12: Crystal structure of $\text{Cp}''_2(\text{CH}_3)(\text{NH}_2\text{BH}_2(\text{C}_6\text{F}_5))$ (**8**) with displacement ellipsoids displayed at the 50% probability level. The cyclopentadienyl hydrogen atoms, silicon-bound methyl groups and zirconium-bound methyl hydrogen atoms have been omitted for clarity. The intramolecular $\text{N—H}\cdots\text{F—C}$ interaction is indicated in red and the β -B-agostic interaction is indicated in blue.

In the solid state, $\text{Cp}''_2\text{Zr}(\text{CH}_3)(\text{NH}_2\text{BH}_2(\text{C}_6\text{F}_5))$ exhibits a zirconium atom coordinated by two Cp'' ligands, one methyl group and the amidoborane ligand. The $\text{Zr}(1)\text{—N}(1)\text{—B}(1)$ bond angle measures $88.6(2)^\circ$, consistent with the presence of a β -B-agostic interaction. The agostic interaction causes the amidoborane ligand to face away from the methyl ligand, placing the agostic $\text{B—H}\cdots\text{Zr}$ and —CH_3 moieties in a *trans* relationship which serves to minimize steric crowding. One protic N—H group engages in a short contact with an *ortho*-fluorine of the pentafluorophenyl ring, measuring 2.182 \AA .

The related compound $\text{Cp}''_2\text{Zr}(\text{CH}_3)(\text{NH}_2\text{BH}(\text{C}_6\text{F}_5)_2)$ was prepared in an analogous fashion and its structure determined using single crystal X-ray diffraction methods. Treatment of a toluene solution of $\text{Cp}''_2\text{Zr}(\text{CH}_3)(\mu\text{-H}_3\text{CB}(\text{C}_6\text{F}_5)_3)$ with freshly prepared $\text{Li}[\text{NH}_2\text{BH}(\text{C}_6\text{F}_5)_2]$

affords $\text{Cp}^*_2\text{Zr}(\text{CH}_3)(\text{NH}_2\text{BH}(\text{C}_6\text{F}_5)_2)$ (**9**), which after extraction with light petroleum was crystallized from toluene at $-25\text{ }^\circ\text{C}$ (**Figure 3.13**).

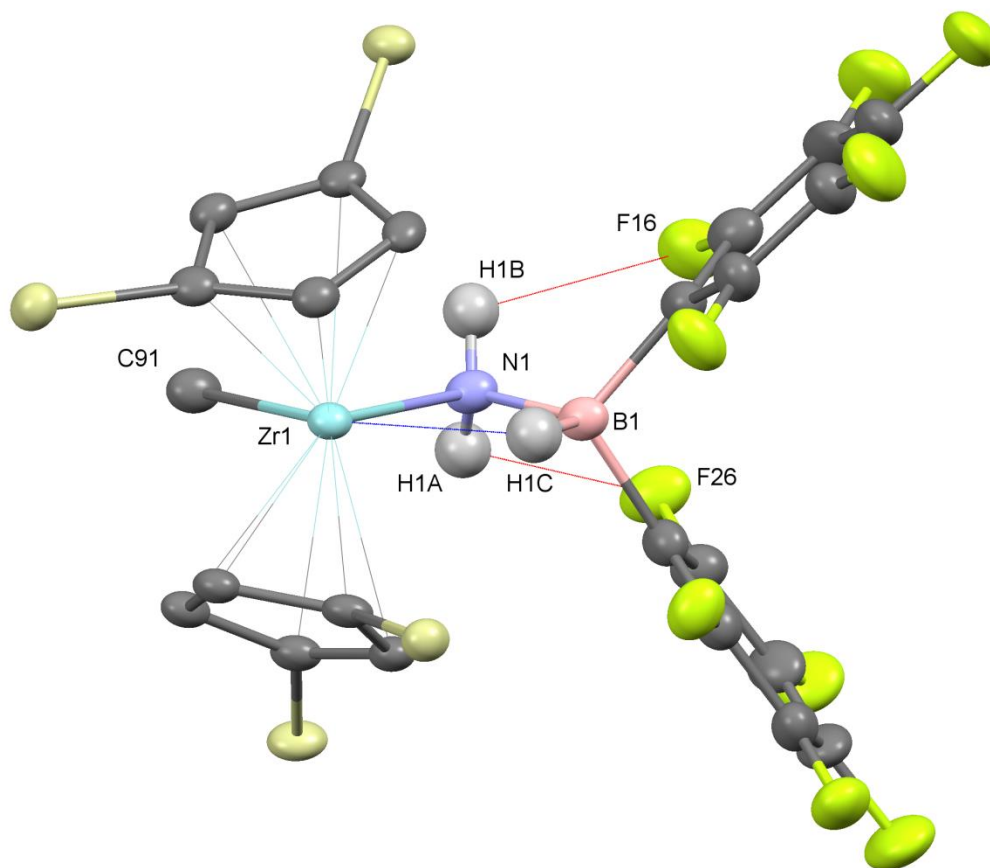


Figure 3.13: Crystal structure of $\text{Cp}^*_2(\text{CH}_3)(\text{NH}_2\text{BH}(\text{C}_6\text{F}_5)_2)$ (**9**) with displacement ellipsoids displayed at the 50% probability level. The cyclopentadienyl hydrogen atoms, silicon-bound methyl groups and zirconium-bound methyl hydrogen atoms have been omitted for clarity. Intramolecular $\text{N}-\text{H}\cdots\text{F}-\text{C}$ interactions are indicated in red and the β -B-agostic interaction is indicated in blue.

The crystal structure of $\text{Cp}^*_2(\text{CH}_3)(\text{NH}_2\text{BH}(\text{C}_6\text{F}_5)_2)$ is very similar to that of $\text{Cp}^*_2\text{Zr}(\text{CH}_3)(\text{NH}_2\text{BH}_2(\text{C}_6\text{F}_5))$ in that both contain an amidoborane ligand which engages in a β -B-agostic interaction with the metal center. This results in a small $\text{M}-\text{N}-\text{B}$ bond angle in both complexes, with that of $\text{Cp}^*_2(\text{CH}_3)(\text{NH}_2\text{BH}(\text{C}_6\text{F}_5)_2)$ being slightly larger at $92.0(1)^\circ$. In addition, the amidoborane ligands in both compounds point away from the

methyl group, so as to separate the $-\text{CH}_3$ ligand from the $\text{B}-\text{H}\cdots\text{Zr}$ moiety and reduce steric crowding. Spectroscopically, the two compounds show a $^1J_{\text{B,H}}$ coupling constant significantly lower than that of the parent amine borane and the ligand precursors, $\text{Li}[\text{NH}_2\text{BH}_n(\text{C}_6\text{F}_5)_{3-n}]$ ($n = 1, 2$), reflecting the contribution of the β -B-agostic interaction in weakening the $\text{B}-\text{H}$ bond (**Table 3.2**).

Table 3.2: ^{11}B NMR chemical shifts and $^1J_{\text{B,H}}$ coupling constants for the amine boranes $\text{H}_3\text{N}\cdot\text{BH}_n(\text{C}_6\text{F}_5)_{3-n}$, their lithium salts $[\text{Li}\{\text{thf}\}_x][\text{NH}_2\text{BH}_n(\text{C}_6\text{F}_5)_{3-n}]$ and the zirconocene complexes $\text{Cp}''_2\text{Zr}(\text{CH}_3)(\text{NH}_2\text{BH}_n(\text{C}_6\text{F}_5)_{3-n})$ for $n = 1, 2$.

Compound	^{11}B chemical shift (ppm) ^a	$^1J_{\text{B,H}}$ (Hz)
$\text{H}_3\text{N}\cdot\text{BH}_2(\text{C}_6\text{F}_5)$	-19.2, t	102
$\text{Li}[\text{NH}_2\text{BH}_2(\text{C}_6\text{F}_5)]$	-19.3, t	82
$\text{Cp}''_2\text{Zr}(\text{CH}_3)(\text{NH}_2\text{BH}_2(\text{C}_6\text{F}_5))$	-25.6, t	76
$\text{H}_3\text{N}\cdot\text{BH}(\text{C}_6\text{F}_5)_2$	-15.8, d	102
$\text{Li}[\text{NH}_2\text{BH}(\text{C}_6\text{F}_5)_2]$	-15.0, d	94
$\text{Cp}''_2\text{Zr}(\text{CH}_3)(\text{NH}_2\text{BH}(\text{C}_6\text{F}_5)_2)$	-21.8, d	74

^a Spectra recorded in C_6D_6 at ambient temperature.

The unsubstituted zirconocene $\text{Cp}_2\text{Zr}(\text{CH}_3)_2$ was also used as a starting material for the preparation of amidoborane complexes. Treatment of a toluene solution of $\text{Cp}_2\text{Zr}(\text{CH}_3)_2$ with $\text{B}(\text{C}_6\text{F}_5)_3$ generated the highly colored metallocenium zwitterion $\text{Cp}_2\text{Zr}(\text{CH}_3)(\mu\text{-H}_3\text{CB}(\text{C}_6\text{F}_5)_3)$, which is reactive towards the lithium salts $\text{Li}[\text{NH}_2\text{BH}_n(\text{C}_6\text{F}_5)_{3-n}]$ ($n = 1, 2$) to produce $\text{Cp}_2\text{Zr}(\text{CH}_3)(\text{NH}_2\text{BH}_n(\text{C}_6\text{F}_5)_{3-n})$. In the case where $n = 1$, X-ray quality crystals were isolated from toluene after extraction of the crude reaction mixture with light petroleum. The solid state structure of $\text{Cp}_2\text{Zr}(\text{CH}_3)(\text{NH}_2\text{BH}(\text{C}_6\text{F}_5)_2)$ (**10**) shows a distorted tetrahedral zirconium atom bound by two cyclopentadienyl ligands and an agostically bound amidoborane ligand in addition to the methyl group (**Figure 3.14**). In contrast to

the structures of **8** and **9**, the agostically bound B—H...Zr contact is in a *cis* arrangement relative to the methyl group.

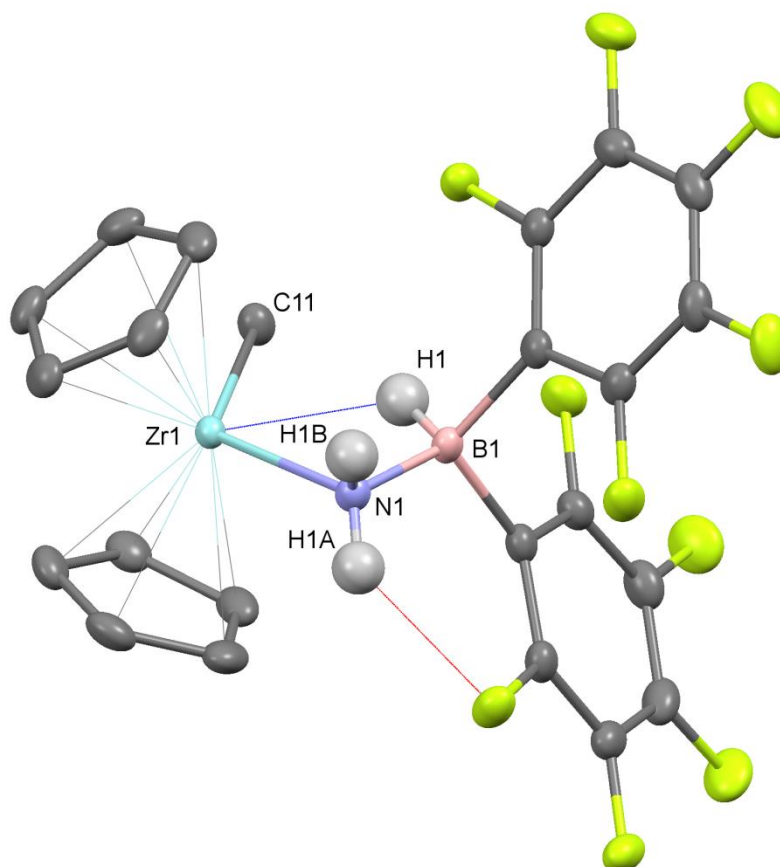


Figure 3.14: Crystal structure of $\text{Cp}_2\text{Zr}(\text{CH}_3)(\text{NH}_2\text{BH}(\text{C}_6\text{F}_5)_2)$ (**10**) with displacement ellipsoids displayed at the 50% probability level. Cyclopentadienyl and methyl hydrogen atoms have been omitted for clarity. The intramolecular N—H...F—C interaction is indicated in red and the β-B-agostic interaction is indicated in blue.

Analogous chemistry is observed for the $n = 2$ complex, $\text{Cp}_2\text{Zr}(\text{CH}_3)(\text{NH}_2\text{BH}_2(\text{C}_6\text{F}_5))$ (**11**), although isolation of crystalline material proved impossible, preventing characterization using elemental analysis and X-ray diffraction methods. The ¹H NMR spectrum of the crude reaction mixture between $\text{Cp}_2\text{Zr}(\text{CH}_3)(\mu\text{-H}_3\text{CB}(\text{C}_6\text{F}_5)_3)$ and $\text{Li}[\text{NH}_2\text{BH}_2(\text{C}_6\text{F}_5)]$ shows a major cyclopentadienyl resonance at 5.32 ppm, which integrates to 10 protons relative to the NH₂ resonance at 0.90 ppm (2 protons) and the methyl resonance at -0.13 ppm

(3 protons). The ^{19}F NMR spectrum consists of two sets of pentafluorophenyl resonances, attributable to the desired product and the reaction by-product $\text{Li}[\text{H}_3\text{CB}(\text{C}_6\text{F}_5)_3]$. The ^{11}B resonance of the major product appears as a triplet at -26 ppm with a coupling constant of $^1J_{\text{B,H}} = 84$ Hz. The chemical shift and coupling constant value indicate that the amidoborane is coordinated to the zirconium center and that the B—H group interacts in an agostic fashion.

3.2.2 $[\text{Cp}_2\text{Hf}]$ complexes bearing $-\text{C}_6\text{F}_5$ substituted amidoborane ligands

Despite the observed reduction in catalytic activity descending the group 4 metals,^{149,150} the isolation of hafnocene amidoborane complexes allows for further comparison between the dehydrocoupling activities of the group 4 metals. In contrast to the preparation of zirconocene amidoboranes from Cp_2ZrCl_2 bearing the $-\text{NH}_2\text{BH}(\text{C}_6\text{F}_5)_2$ ligand, the analogous chemistry with Cp_2HfCl_2 resulted in a crude NMR spectrum indicating only three major cyclopentadienyl containing complexes, with resonances at 5.29, 5.28 and 5.16 ppm. The consistently isolated crystalline product was assigned to the resonance at 5.16 ppm, but was not the expected bis(amidoborane) complex. Instead, the hafnocene imidoborane $\text{Cp}_2\text{Hf}(\text{NHBH}(\text{C}_6\text{F}_5)_2)$ (**12**) was characterized using X-ray diffraction. The solid state structure displays a single $-\text{NHBH}(\text{C}_6\text{F}_5)_2$ ligand coordinated to the hafnocene fragment through a Hf—N bond along with an additional β -B-agostic interaction with the hafnium center (**Figure 3.15**).

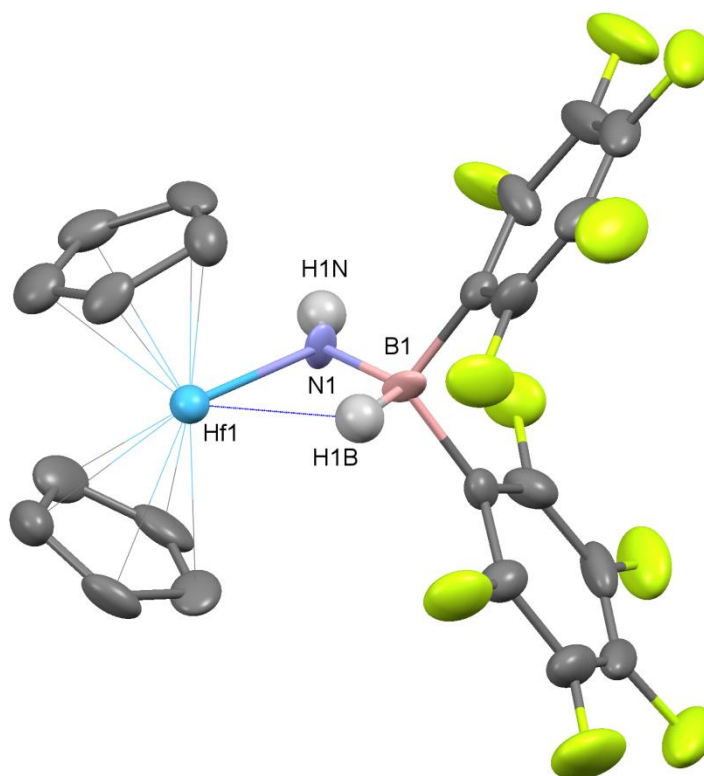


Figure 3.15: Crystal structure of $\text{Cp}_2\text{Hf}(\text{NHBH}(\text{C}_6\text{F}_5)_2)$ (**12**) with displacement ellipsoids displayed at the 50% probability level. Cyclopentadienyl hydrogen atoms and the toluene solvate molecule have been omitted for clarity. The β -B-agostic interaction is indicated in blue.

The Hf—N bond length of 2.282(5) Å is longer than reported hafnium—nitrogen double bonds^{239–241} and is therefore assigned as a Hf—N single bond. While the boron-bound hydrogen atom was located on the difference map, the diffraction data for compound **12** was unsuitable for location of the nitrogen-bound hydrogen atom. In order to balance the charge of the $[\text{Cp}_2\text{Hf}]^{2+}$ fragment, a single N—H bond was modelled for the dianionic $-\text{NHBH}(\text{C}_6\text{F}_5)_2$ ligand. This single N—H group is observed spectroscopically, where it appears as a broadened singlet at 7.59 ppm in the ^1H NMR spectrum. The crystallographic structure for compound **12** is therefore most accurately described as a zwitterion, although several resonance forms may contribute to its solution state structure (**Figure 3.16**).

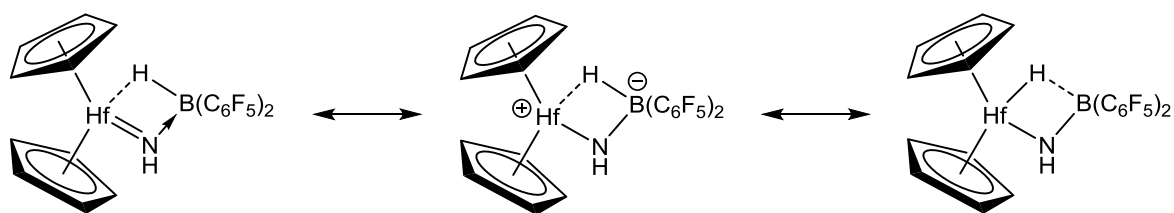


Figure 3.16: Resonance forms of compound **12**.

On one occasion, the reaction between Cp_2HfCl_2 and two equivalents of $\text{Li}[\text{NH}_2\text{BH}(\text{C}_6\text{F}_5)_2]$ produced a small amount of X-ray quality crystals which were identified as the double metathesis product $\text{Cp}_2\text{Hf}(\text{NH}_2\text{BH}(\text{C}_6\text{F}_5)_2)_2$. Consideration of the crude ^1H NMR spectrum and elimination of those resonances attributed to $\text{Cp}_2\text{Hf}(\text{NHBH}(\text{C}_6\text{F}_5)_2)_2$, the bis(amidoborane) species is responsible for the resonance at 5.29 ppm by integration against a broad resonance at 2.25 ppm (four protons) for the two NH_2 groups. This complex has been isolated on two instances, in the presence of excess thf and as a thf-free sample. The solid state structure of the thf solvate,¹⁰¹ $\text{Cp}_2\text{Hf}(\text{NH}_2\text{BH}(\text{C}_6\text{F}_5)_2)\cdot 4\text{thf}$ (**13-4thf**) (**Figure 3.17**), exhibits a hafnocene unit flanked by two amidoborane ligands, one of which participates in a β -B-agostic interaction with the metal center, similar to the zirconium analog $\text{Cp}_2\text{Zr}(\text{NH}_2\text{BH}(\text{C}_6\text{F}_5)_2)_2$.

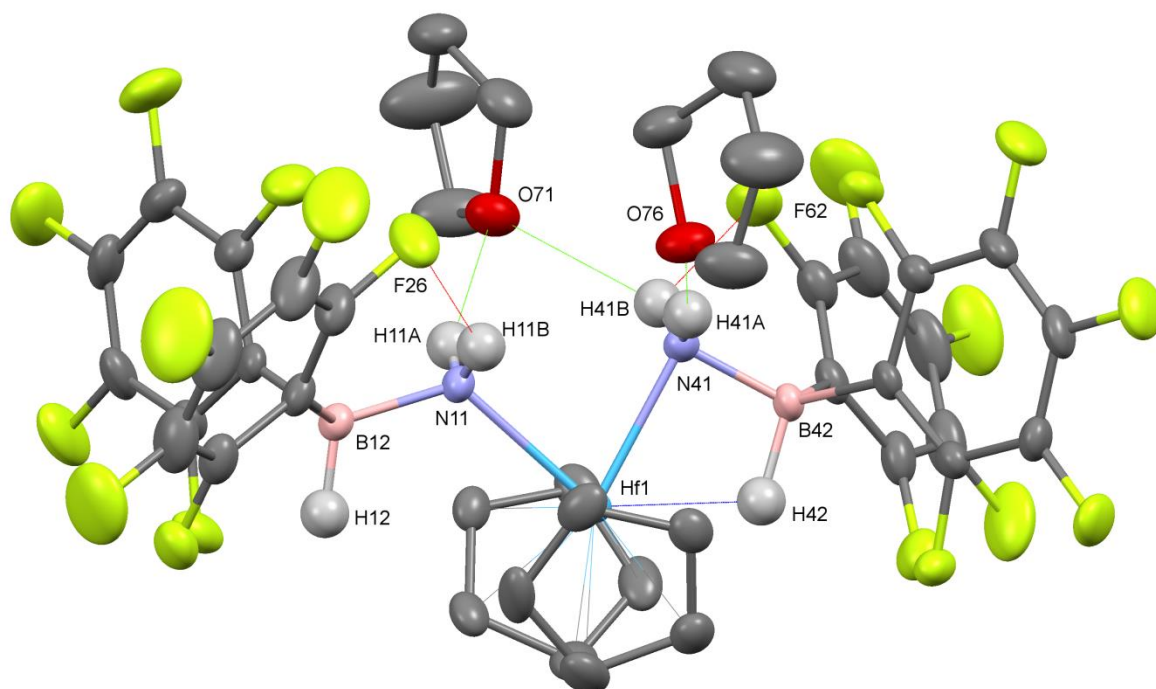


Figure 3.17: Crystal structure of $\text{Cp}_2\text{Hf}(\text{NH}_2\text{BH}(\text{C}_6\text{F}_5)_2)_2 \cdot 4\text{thf}$ (**13·4thf**) with displacement ellipsoids displayed at the 50% probability level. Two of the four thf solvate molecules, the hydrogen atoms of the remaining thf molecules and the cyclopentadienyl hydrogen atoms have been omitted for clarity. Intramolecular $\text{N—H}\cdots\text{F—C}$ interactions are indicated in red, hydrogen bonded $\text{thf}\cdots\text{H}_2\text{N}$ contacts are indicated in green and the β -B-agostic interaction is indicated in blue.

Two of the thf solvate molecules coordinate to the $-\text{NH}_2$ units through hydrogen bonding contacts, initially thought to facilitate crystallization by increasing the stability of the metallocene with two bulky ligands. However, the structure of $\text{Cp}_2\text{Hf}(\text{NH}_2\text{BH}(\text{C}_6\text{F}_5)_2)_2$ (**13**) without thf also consists of a hafnocene unit flanked by two amidoborane ligands. However, in the solid state, neither of the amidoborane ligands of **13** participate in a distinct β -B-agostic interaction with the metal center (**Figure 3.18**). In fact, both Hf—N—B angles adopt values intermediate to those previously discussed for agostically-bound (ca. 90°) and free (ca. 120°) $\text{B—H}\cdots\text{M}$ interactions, with the $\text{Hf}(1)\text{—N}(1)\text{—B}(1)$ and $\text{Hf}(1)\text{—N}(2)\text{—B}(2)$ bonds measuring $102.7(5)^\circ$ and $109.7(5)^\circ$, respectively. Three of the four N—H groups participate in intramolecular $\text{N—H}\cdots\text{F—C}$ interactions with *ortho*-fluorine atoms of the pentafluorophenyl rings.

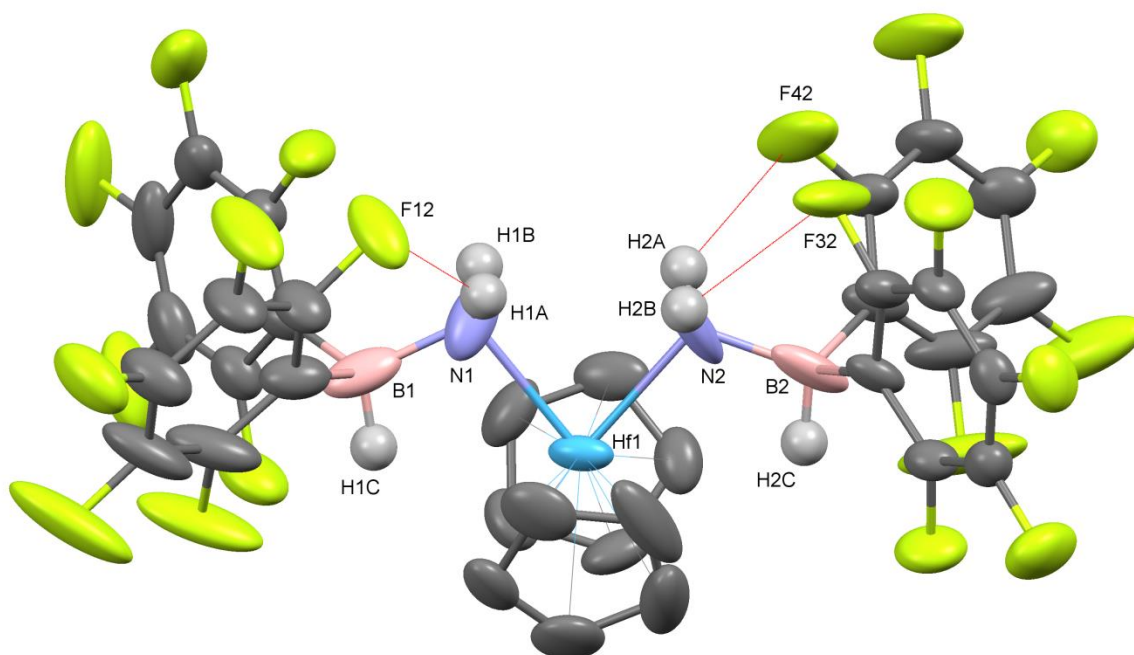
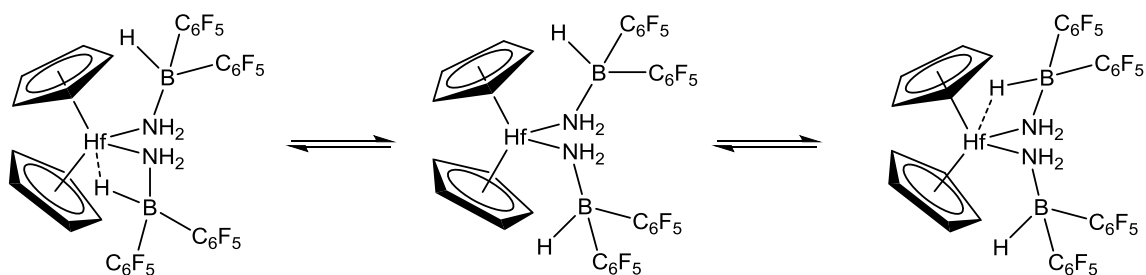


Figure 3.18: Crystal structure of $\text{Cp}_2\text{Hf}(\text{NH}_2\text{BH}(\text{C}_6\text{F}_5)_2)_2$ (**13**) with displacement ellipsoids displayed at the 50% probability level. The toluene solvate molecule and cyclopentadienyl hydrogen atoms have been omitted for clarity. Intramolecular $\text{N}-\text{H}\cdots\text{F}-\text{C}$ interactions are indicated in red.

This is the only example in the collection of complexes reported herein in which a β -B-agostic interaction is not distinctly present, despite the presence of a β -hydrogen and a similar structure with a chelate ligand.ⁱ Isolation and crystallization of both examples of $\text{Cp}_2\text{Hf}(\text{NH}_2\text{BH}(\text{C}_6\text{F}_5)_2)_2$ (thf-solvated and thf-free) provides some clues into the possible dynamic exchange between bound and free B—H groups in solution (**Scheme 3.9**).

ⁱ This is not the result of crystallographic disorder, an explanation which has been considered and dismissed.

Scheme 3.9: Possible dynamic exchange of **13** in solution.

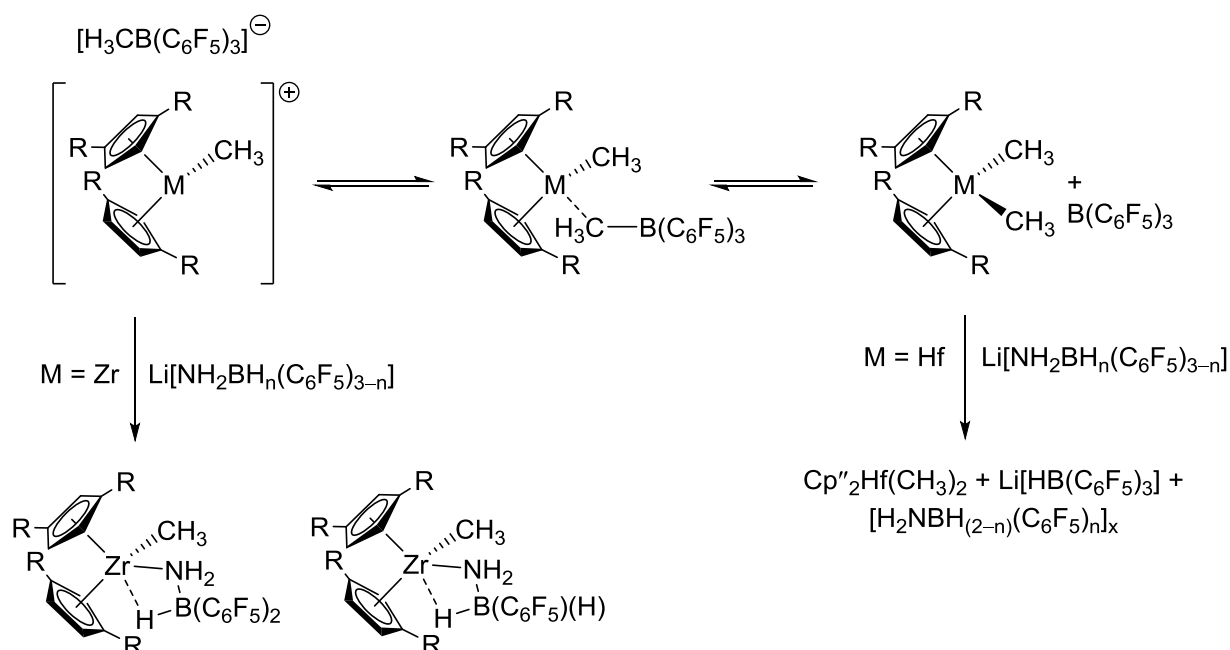


Gentle warming (60 °C) of a crude reaction mixture containing both $\text{Cp}_2\text{Hf}(\text{NHBH}(\text{C}_6\text{F}_5)_2)$ and $\text{Cp}_2\text{Hf}(\text{NH}_2\text{BH}(\text{C}_6\text{F}_5)_2)_2$ did not result in conversion of the latter to the former through thermal N—H bond activation, suggesting the two species are formed from separate mechanistic processes (**Scheme 3.12**). In all repeated cases of the reaction, the crude ^1H NMR spectrum indicated the presence of both species in varying ratios, and despite numerous attempts, no obvious control over the ratio could be obtained.

Treatment of $\text{Cp}''_2\text{Hf}(\text{CH}_3)_2$ with $\text{B}(\text{C}_6\text{F}_5)_3$ followed by $\text{Li}[\text{NH}_2\text{BH}_n(\text{C}_6\text{F}_5)_{3-n}]$ ($n = 1, 2$) in toluene solution resulted in very clean ^1H NMR spectra. Integration of the cyclopentadienyl resonance and the methyl region, in addition to spectral comparison with an authentic sample, resulted in the identification of regenerated $\text{Cp}''_2\text{Hf}(\text{CH}_3)_2$ as the major cyclopentadienyl containing product. The ^{19}F and ^{11}B spectra of the same reaction mixture indicated several reaction products, with the predominant resonances being attributed to $\text{Li}[\text{HB}(\text{C}_6\text{F}_5)_3]$, formed through hydride abstraction from $\text{Li}[\text{NH}_2\text{BH}_n(\text{C}_6\text{F}_5)_{3-n}]$ by $\text{B}(\text{C}_6\text{F}_5)_3$. Fractional crystallization of the lithium salt confirmed this result, with the diffraction data only being of sufficient quality to establish connectivity. This result is strikingly different from the analogous zirconium chemistry, and has been ascribed to incomplete methyl abstraction to form $\text{Cp}''_2\text{Hf}(\text{CH}_3)_2$.^{2,242} This observed difference in reactivity between zirconium and hafnium has been related to the relative M—CH₃ bond strengths, where the Zr—CH₃ bond is found to be 10 kcal mol⁻¹ weaker than the

analogous Hf—CH₃ bond.² Therefore, in the presence of a methyl abstraction reagent, the zirconocene species reacts through complete Zr—CH₃ bond cleavage while hafnocene reagent reacts through more favourable cleavage of the bridging H₃C···B(C₆F₅)₃ bond of Cp₂Hf(CH₃)(μ-CH₃B(C₆F₅)₃) followed by regeneration of the starting components (**Scheme 3.10**).

Scheme 3.10: Observed difference of the reactivity of zirconocenes and hafnocenes in the presence of the methyl abstraction reagent, B(C₆F₅)₃.



Hafnocene complexes of the $-NH_2BH_2(C_6F_5)$ and $-NH_2BH(C_6F_5)_2$ ligands were later prepared through reaction of the lithium salts with the related electrophilic metal center $Cp_2Hf(CH_3)(\mu-H_3CB(C_6F_5)_3)$ generated in an analogous fashion to the procedure described for the zirconocene complexes $Cp_2Zr(CH_3)(NH_2BH_n(C_6F_5)_{3-n})$ ($n = 1, 2$). Confirmation of product formation was acquired solely through multinuclear NMR spectroscopy in the absence of X-ray quality crystals for both species. The 1H NMR

spectrum for $\text{Cp}_2\text{Hf}(\text{CH}_3)(\text{NH}_2\text{BH}_2(\text{C}_6\text{F}_5))$ (**14**) shows resonances of correct integration at 5.29, 0.99 and -0.29 ppm for the cyclopentadienyl, NH_2 and CH_3 groups, respectively. In addition, the ^{19}F NMR spectrum contains a set of $-\text{C}_6\text{F}_5$ resonances consistent with those for the analogous zirconocene complex, $\text{Cp}_2\text{Zr}(\text{CH}_3)(\text{NH}_2\text{BH}_2(\text{C}_6\text{F}_5))$. The presence of an agostic interaction is confirmed in the ^{11}B spectrum, with a sharp triplet at -25 ppm with a $^1J_{\text{B,H}}$ coupling constant of 86 Hz.

Formation of $\text{Cp}_2\text{Hf}(\text{CH}_3)(\text{NH}_2\text{BH}(\text{C}_6\text{F}_5)_2)$ (**15**) from reaction between the electrophilic metallocene and $\text{Li}[\text{NH}_2\text{BH}(\text{C}_6\text{F}_5)_2]$ was also confirmed through the NMR spectra. Integration of the ^1H spectrum resonances for the cyclopentadienyl, $-\text{NH}_2$ and $-\text{CH}_3$ groups (5.25, 1.75 and -0.19 ppm, respectively) present in the molecule confirmed the presence of one amidoborane ligand and one methyl group bound to the hafnium center. The absence of an appreciable amount of any side products has resulted in a sufficiently clean NMR spectrum to observe the B—H resonance as a quartet at -0.48 ppm in the ^1H NMR spectrum. A single set of ^{19}F resonances reflecting the $-\text{C}_6\text{F}_5$ group on the borane fragment in addition to a sharp doublet at -24 ppm in the ^{11}B NMR spectrum with a $^1J_{\text{B,H}}$ coupling constant of 68 Hz confirms the presence of an agostically bound amidoborane ligand.

3.2.3 *[Cp₂Ti] complexes bearing $-\text{C}_6\text{F}_5$ substituted amidoborane ligands*

As the most catalytically active of the group 4 metals, titanium complexes bearing ligands which feature either a protic N—H and / or hydridic B—H groups would likely be unstable towards further bond activation. Indeed, only a few examples of titanocene amidoborane complexes have been reported, all of which feature a Ti(III) center. However, with respect to proposed catalytic mechanisms which feature a Ti(II) / Ti(IV) redox cycle, the formation of stable Ti(III) amidoboranes suggest the existence of a more complex reaction pathway during dehydrocoupling. For these reasons, isolation of pentafluorophenyl stabilized

titanocene amidoborane complexes allows for a significant glimpse into the underlying catalytic cycle(s).

Treatment of a thf solution of Cp_2TiCl_2 with two equivalents of $\text{Li}[\text{NH}_2\text{BH}_2(\text{C}_6\text{F}_5)]$ at ambient temperature resulted in rapid evolution of a gaseous product (assumed to be dihydrogen)¹¹² along with an observed sequence of color changes from red to green and finally a vibrant royal blue. The ^1H and ^{11}B NMR spectra of the crude reaction mixture contain only those resonances associated with residual solvent, while the ^{19}F spectrum reveals a set of slightly broadened and unresolved $-\text{C}_6\text{F}_5$ resonances. The crude product material was extracted into light petroleum and dissolved in toluene. Cooling to $-25\text{ }^\circ\text{C}$ overnight afforded X-ray quality blue crystals of $\text{Cp}_2\text{Ti}(\text{NH}_2\text{BH}_2(\text{C}_6\text{F}_5))$ (**16**) (**Figure 3.19**).

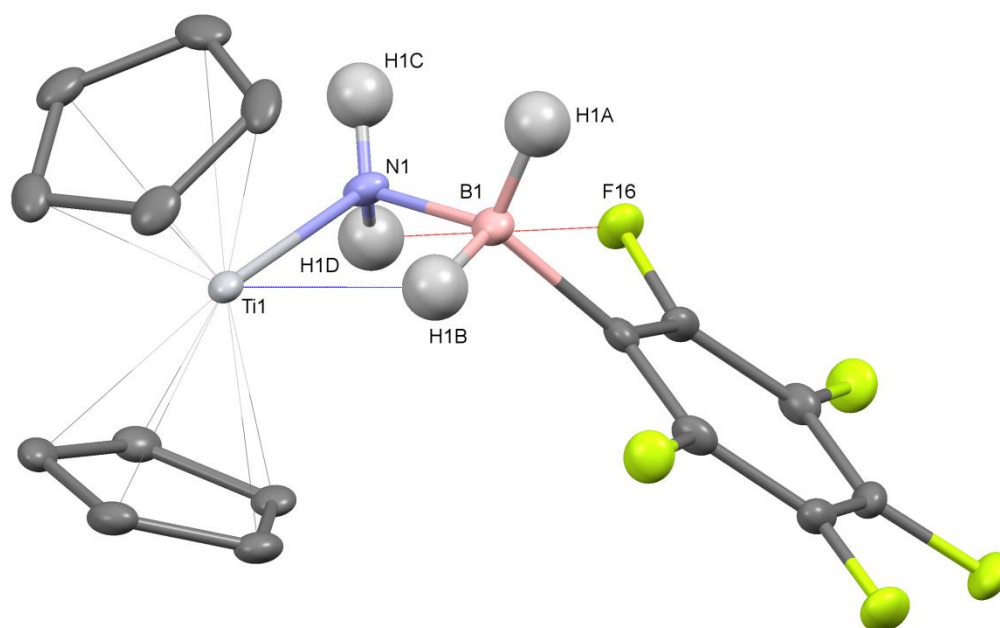


Figure 3.19: Crystal structure of $\text{Cp}_2\text{Ti}(\text{NH}_2\text{BH}_2(\text{C}_6\text{F}_5))$ (**16**) with displacement ellipsoids displayed at the 50% probability level. The cyclopentadienyl hydrogen atoms have been omitted for clarity. The intramolecular $\text{N}-\text{H}\cdots\text{F}-\text{C}$ interaction is indicated in red and the β -B-agostic interaction is indicated in blue.

The structure contains a Ti(III) center, with the titanocene fragment ligated by a single amidoborane ligand. The Ti—N single bond measures 2.165(2) Å, and the coordination at titanium includes a β -B-agostic interaction producing a Ti(1)—N(1)—B(1) bond angle of 84.5(1)°. The weak N—H...F—C interaction between one of the protic N—H groups and an *ortho*-fluorine atom of the $-\text{C}_6\text{F}_5$ ring is 2.471 Å in length. This paramagnetic Ti(III) metallocene amidoborane results from reduction of Ti(IV) to Ti(III) with one equivalent of the lithium amidoborane salt and metathesis between the remaining Ti—Cl functionality and the second equivalent of lithium salt in solution. This type of reactivity has been reported for the treatment of Cp_2TiCl_2 with $\text{Li}[\text{NH}_2\text{BH}_3]$ to produce the unsubstituted Ti(III) amidoborane, $\text{Cp}_2\text{Ti}(\text{NH}_2\text{BH}_3)$.¹¹¹ In the absence of full NMR spectral characterization, $\text{Cp}_2\text{Ti}(\text{NH}_2\text{BH}_2(\text{C}_6\text{F}_5))$ was characterized by IR spectroscopy, where the N—H, terminal B—H and agostic B—H peaks were identified at 3444 (NH), 3365 (NH), 2391 (BH_{term}) and 1841 ($\text{BH}_{\text{agostic}}$) cm^{-1} . To confirm that production of $\text{Cp}_2\text{Ti}(\text{NH}_2\text{BH}_2(\text{C}_6\text{F}_5))$ occurred through reduction followed by metathesis, compound **16** was also prepared through reaction between Cp_2TiCl and one equivalent of $\text{Li}[\text{NH}_2\text{BH}_2(\text{C}_6\text{F}_5)]$. Comparison of the IR spectra between reactions starting with Cp_2TiCl_2 and Cp_2TiCl indicate the same final product, $\text{Cp}_2\text{Ti}(\text{NH}_2\text{BH}_2(\text{C}_6\text{F}_5))$.

In a similar fashion to the preparation of compound **16**, Cp_2TiCl_2 was treated with two equivalents of $\text{Li}[\text{NH}_2\text{BH}(\text{C}_6\text{F}_5)_2]$ in toluene or thf solution at -78 °C. The crude reaction mixture immediately after warming to ambient temperature appeared brown / red in color, which changed to brown / green over the course of 30 minutes at ambient temperature. The multinuclear NMR spectra of an aliquot of this solution reveal at least five cyclopentadienyl-containing products and numerous sets of ^{19}F $-\text{C}_6\text{F}_5$ resonances. After considerable reaction time (12 hours), the reaction mixture was green in color, changing to yellow upon exposure to trace amounts of atmosphere. These observations may be attributed to slow or possibly competing reaction pathways, with titanium reduction based

on the highly sensitive nature of the resulting material towards the atmosphere. Despite numerous attempts, X-ray quality crystals could not be isolated from this reaction mixture.

Use of the Ti(III) precursor Cp_2TiCl with $\text{Li}[\text{NH}_2\text{BH}(\text{C}_6\text{F}_5)_2]$ facilitated rapid reaction. Treatment of a thf solution of Cp_2TiCl with $\text{Li}[\text{NH}_2\text{BH}(\text{C}_6\text{F}_5)_2]$ at ambient temperature produced an immediate color change from red to brown and ultimately blue / purple. Extraction into light petroleum and cooling of a 1,2-difluorobenzene / light petroleum solution of the crude material to $-25\text{ }^\circ\text{C}$ produced X-ray quality crystals of $\text{Cp}_2\text{Ti}(\text{NH}_2\text{BH}(\text{C}_6\text{F}_5)_2)$ (**17**) (**Figure 3.20**). Two crystallographically independent molecules of $\text{Cp}_2\text{Ti}(\text{NH}_2\text{BH}(\text{C}_6\text{F}_5)_2)$ are found in the crystal structure, and one has been selected for the following description.

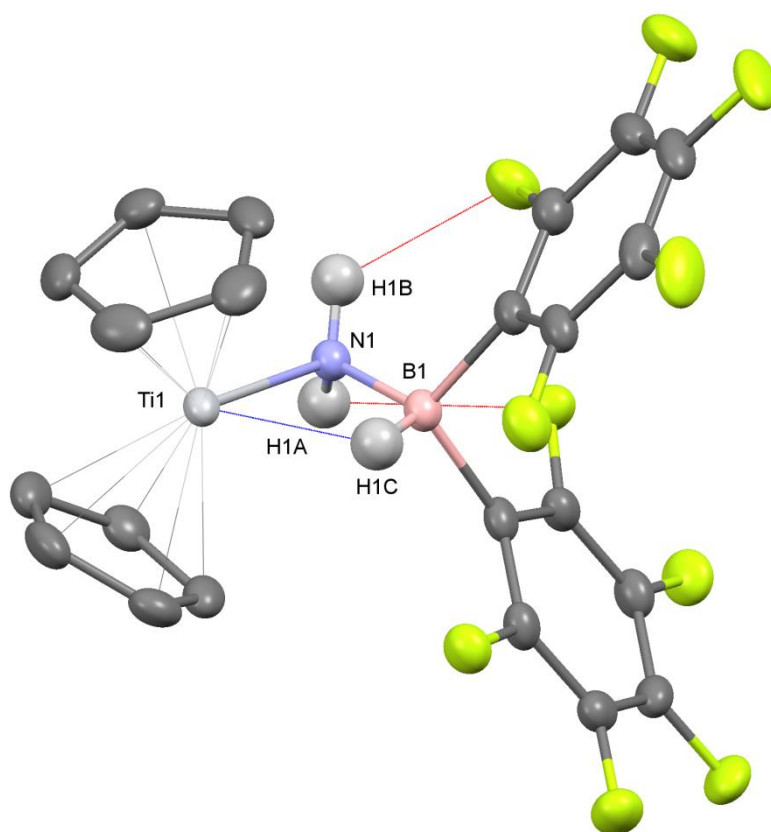


Figure 3.20: One of two crystallographically independent molecules in the unit cell of $\text{Cp}_2\text{Ti}(\text{NH}_2\text{BH}(\text{C}_6\text{F}_5)_2)$ (**17**) with displacement ellipsoids displayed at the 50% probability level. The cyclopentadienyl hydrogen atoms have been omitted for clarity. The intramolecular $\text{N}-\text{H}\cdots\text{F}-\text{C}$ interaction is indicated in red and the β -B-agostic interaction is indicated in blue.

The titanocene is coordinated to the amidoborane ligand bearing two electron withdrawing pentafluorophenyl rings through a Ti(1)—N(1) single bond (2.166(3) Å) and a β -B-agostic interaction, with a Ti(1)—N(1)—B(1) bond angle of 85.7(2)°. The ^1H and ^{11}B NMR spectra for $\text{Cp}_2\text{Ti}(\text{NH}_2\text{BH}(\text{C}_6\text{F}_5)_2)$ contain no discernible resonances due to the paramagnetic nature of the titanium center. A set of broadened ^{19}F resonances have been attributed to the pentafluorophenyl rings. The *ortho*- and *meta*-fluorine signals are very broad and almost indistinguishable from the baseline while the *para*-fluorine signal appears as an unresolved singlet, a result of its distance from the paramagnetic titanium center. The solution phase IR spectrum of **17** (3436 (NH), 3325 (NH) and 1861 ($\text{BH}_{\text{agostic}}$) cm^{-1}) is nearly identical to that of **16** with the exception of the absence of a BH_{term} peak. This suggests that the agostic interaction in **17** is strong and does not participate in a solution equilibrium such as that presented in **Scheme 3.9**, which shows the presence of a complex with no, or only low concentrations of, an agostic interaction.

The predominance of the +3 oxidation state in titanocene complexes with the amidoborane ligands $-\text{NH}_2\text{BH}_n(\text{C}_6\text{F}_5)_{3-n}$ ($n = 1, 2$) may be attributed to the reducing power of amidoborane salts. The parent lithium amidoborane, $\text{Li}[\text{NH}_2\text{BH}_3]$ was first prepared in 1994²⁴³ and is commonly used as a reducing agent for tertiary amides,²⁴⁴ ketones and imines.²⁴⁵ This, in combination with the relatively facile reduction of Ti(IV) to Ti(III),²⁴⁶ results in titanium amidoborane complexes being most stable in the +3 oxidation state.^{111,112} Therefore, attempted isolation of a Ti(IV) amidoborane complex was pursued with the tri-substituted amidoborane ligand $-\text{NH}_2\text{B}(\text{C}_6\text{F}_5)_3$. Treatment of Cp_2TiCl_2 with two equivalents of $\text{Li}[\text{NH}_2\text{B}(\text{C}_6\text{F}_5)_3]$ resulted in slow solution color change from red to brown over the course of 12 hours at ambient temperature. No metallocene species were isolated from the reaction mixture. However, generation of a more electrophilic metal center followed by treatment with the lithium salt proceeded rapidly at ambient temperature. Halide abstraction from Cp_2TiCl_2 with AgOTf generates the electrophilic metallocene $[\text{Cp}_2\text{TiCl}]^+$,²⁴⁷ which exhibits rapid reaction with $\text{Li}[\text{NH}_2\text{B}(\text{C}_6\text{F}_5)_3]$. However,

rather than the expected metallocene amidoborane chloride or metallocene amidoborane triflate, isolated small red / orange crystals were examined by X-ray diffraction methods and found to be $[\text{Li}(\text{thf})_4][\text{Cp}_2\text{Ti}(\text{NHB}(\text{C}_6\text{F}_5)_3)(\text{NH}_2\text{B}(\text{C}_6\text{F}_5)_3)]$ (**18**) (Figure 3.21).

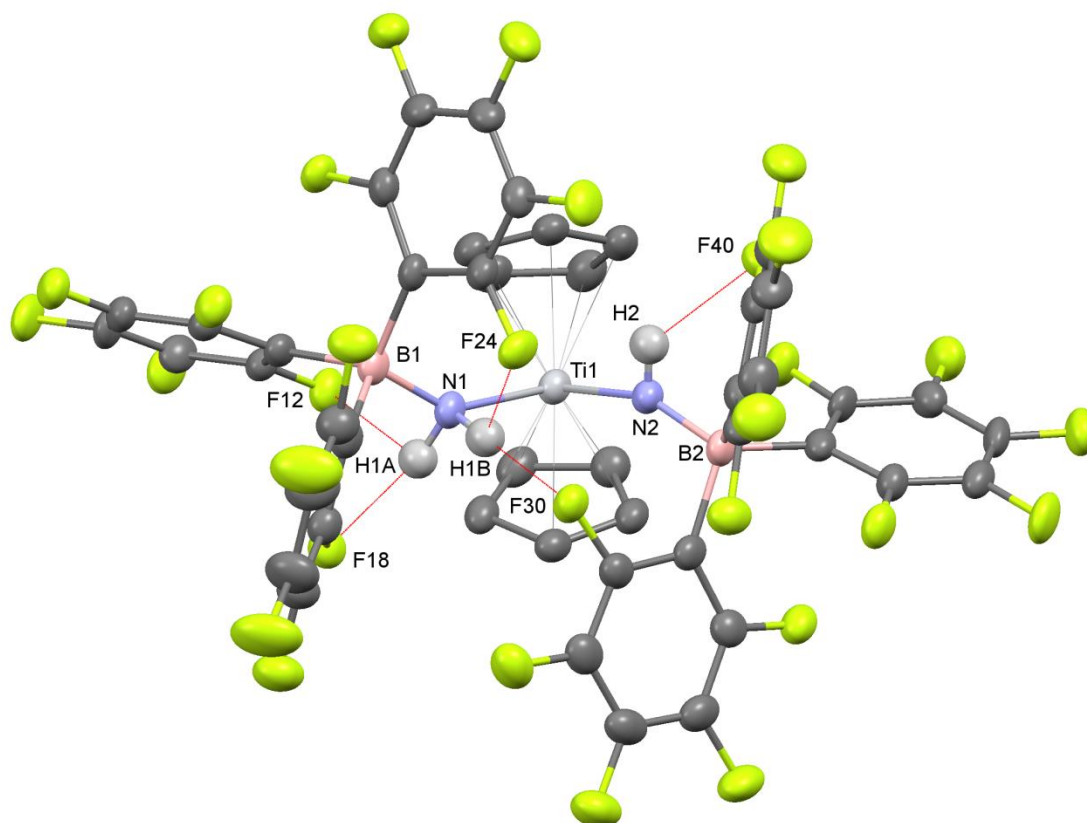


Figure 3.21: Crystal structure of $[\text{Cp}_2\text{Ti}(\text{NHB}(\text{C}_6\text{F}_5)_3)(\text{NH}_2\text{B}(\text{C}_6\text{F}_5)_3)]^-$ ion (**18**) with displacement ellipsoids displayed at the 50% probability level. The $[\text{Li}(\text{thf})_4]^+$ cation, toluene solvate molecule and cyclopentadienyl hydrogen atoms have been omitted for clarity. The intramolecular $\text{N}-\text{H}\cdots\text{F}-\text{C}$ interactions are indicated in red.

The solid state structure of compound **18** consists of solvent separated $[\text{Cp}_2\text{Ti}(\text{NHB}(\text{C}_6\text{F}_5)_3)(\text{NH}_2\text{B}(\text{C}_6\text{F}_5)_3)]^-$ and $[\text{Li}(\text{thf})_4]^+$ ions. The anionic titanocene fragment is coordinated by one amidoborane ligand and one imidoborane ligand, a new and unexpected bonding pattern for titanocene complexes. While the $\text{Ti}(1)-\text{N}(1)$ amido-bond is consistent in length with typical $\text{Ti}-\text{N}$ single bonds ($\text{Ti}(1)-\text{N}(1)$ 2.244(3) Å), the $\text{Ti}-\text{N}$

imido-bond length is considerably shorter, measuring 1.932(3) Å. The Ti—N—B bond angles measure 145.6(3)° for the amidoborane ligand and 153.5(3)° for the imidoborane ligand. The crude ¹H NMR spectrum displays a major Cp resonance at 5.5 ppm in addition to a broad resonance at 0.83 which may be attributed to the NH₂ group. Two sets of ¹⁹F resonances and two major ¹¹B resonances appear in the corresponding NMR spectra, which is to be expected for the –B(C₆F₅)₃ fragments on the different ligands (see Appendix). An additional set of resonances was identified in each spectrum which is consistent with the hydrolysis product, H₃N·B(C₆F₅)₃. Despite the unique and interesting outcome, the crystal structure does not reflect the reaction stoichiometry and must therefore be a minor product. However, it is tempting to speculate on the mode of formation (see **Section 3.3**).

3.2.4 Group 4 metallocene complexes bearing the –NHP_hBH₂(C₆F₅) ligand

Despite the divergent reactivity pathways observed for reactions between group 4 metallocenes and the salts Li[NH₂BH_n(C₆F₅)_{3-n}], reproducible methods were established for isolation of metallocene complexes bearing at least one amidoborane ligand. For zirconium and hafnium, the most reliable and high yielding method involved the generation of the highly electrophilic metallocene species [Cp₂M(CH₃)]⁺ and reaction with one equivalent of the lithium salt. The chemistry of titanocene with these ligands is dominated by the tendency for the amidoborane to act as a reducing agent, and all titanium complexes of the hydridic amidoborane ligands contained titanium in the +3 oxidation state.

These synthetic procedures have been extended to include amidoborane ligands with substitution at the nitrogen atom in addition to the presence of at least one –C₆F₅ group on boron. The aniline adduct of tris(pentafluorophenyl)borane, PhH₂N·B(C₆F₅)₃, and its lithium salt Li[NHP_hB(C₆F₅)₃] were reported in 2009.¹⁵⁹ This Lewis adduct is prepared

through analogous methods to those reported for $\text{PhH}_2\text{N}\cdot\text{BH}_n(\text{C}_6\text{F}_5)_{3-n}$ ($n = 1, 2$) discussed in **Chapter 2**. Facile deprotonation of $\text{PhH}_2\text{N}\cdot\text{B}(\text{C}_6\text{F}_5)_3$ with ${}^n\text{BuLi}$ produces the lithium salt in quantitative yield, resulting in ligand precursors similar to $-\text{NH}_2\text{BH}_n(\text{C}_6\text{F}_5)_{3-n}$ ($n = 1, 2, 3$) with potential reactivity with group 4 metallocene complexes.

Treatment of the adducts $\text{PhH}_2\text{N}\cdot\text{BH}_n(\text{C}_6\text{F}_5)_{3-n}$ ($n = 1, 2$) with ${}^n\text{BuLi}$ in thf at $-78\text{ }^\circ\text{C}$ quantitatively produces the corresponding lithium salts. In the case of $n = 1$, the addition of two equivalents of 12-crown-4 to the solution of $[\text{Li}(\text{thf})_x][\text{NHPhBH}(\text{C}_6\text{F}_5)_2]$ (**19**) and cooling of a dichloromethane / light petroleum solution afforded X-ray quality crystals of $[\text{Li}\{12\text{-crown-4}\}_2][\text{NHPhBH}(\text{C}_6\text{F}_5)_2]$ (**19a**) (**Figure 3.22**).

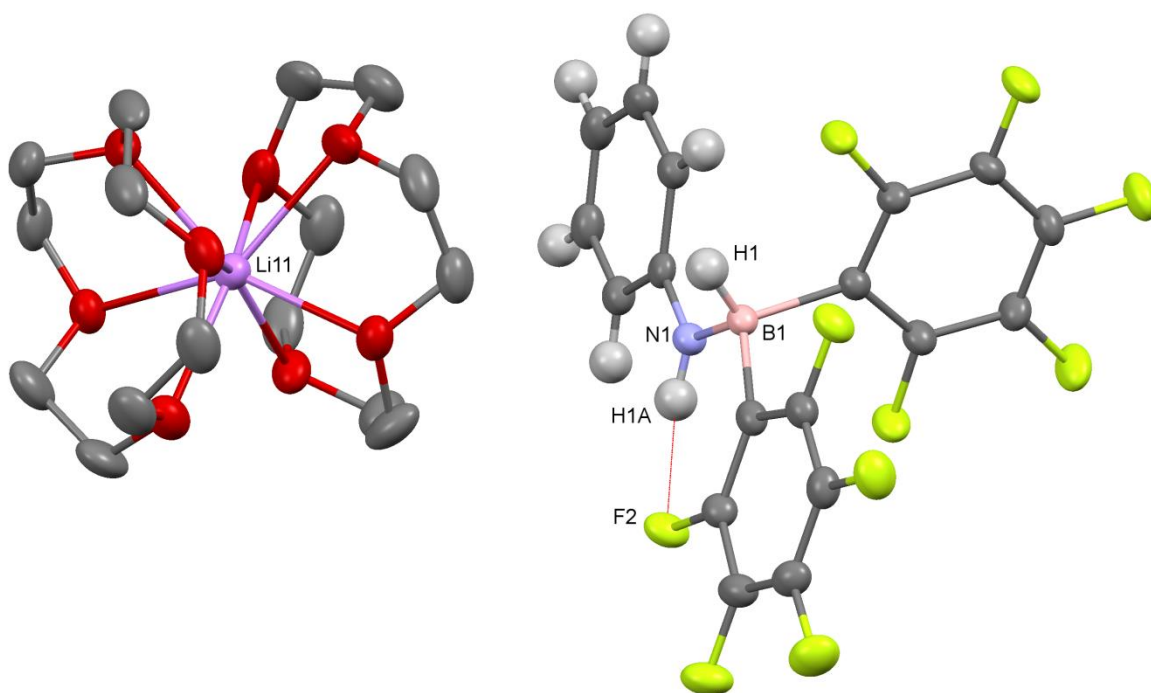


Figure 3.22: Crystal structure of $[\text{Li}\{12\text{-crown-4}\}_2][\text{NHPhBH}(\text{C}_6\text{F}_5)_2]$ (**19a**) with displacement ellipsoids displayed at the 50% probability level. The crown ether hydrogen atoms have been omitted for clarity. The intramolecular $\text{N}-\text{H}\cdots\text{F}-\text{C}$ interaction is indicated in red.

The B—N bond length of **19a** measures 1.530(5) Å, significantly shorter than that of the adduct (1.632(2) Å). The observed B—N bond shortening after deprotonation of the adduct is consistent with that observed for the deprotonation of the analogous ammonia adduct, $\text{H}_3\text{N}\cdot\text{BH}(\text{C}_6\text{F}_5)_2$ to prepare $\text{Li}[\text{NH}_2\text{BH}(\text{C}_6\text{F}_5)_2]$.^{101,102} Deprotonation of $\text{PhH}_2\text{N}\cdot\text{BH}_2(\text{C}_6\text{F}_5)$ with ${}^n\text{BuLi}$ at $-78\text{ }^\circ\text{C}$ in thf produces the lithium salt $[\text{Li}\{\text{thf}\}_x][\text{NHPPhBH}_2(\text{C}_6\text{F}_5)]$ (**20**) in quantitative yield. Addition of 12-crown-4 affords the crown ether adduct $[\text{Li}\{12\text{-crown-4}\}][\text{NHPPhBH}_2(\text{C}_6\text{F}_5)]$ (**20a**), which was characterized by multinuclear NMR spectroscopy. Despite numerous attempts, no X-ray quality crystals of **20** or **20a** could be isolated.

Treatment of a toluene solution of $\text{Cp}_2\text{M}(\text{CH}_3)_2$ ($\text{M} = \text{Zr}, \text{Hf}$) with $\text{Li}[\text{NHPPhBH}_2(\text{C}_6\text{F}_5)]$ results in clean and quantitative conversion to $\text{Cp}_2\text{M}(\text{CH}_3)(\text{NHPPhBH}_2(\text{C}_6\text{F}_5))$. In the case of $\text{M} = \text{Zr}$, the crude ${}^1\text{H}$ NMR spectrum displayed resonances between 6.83 and 7.10 ppm assigned to the amido-bound phenyl group. In addition, the cyclopentadienyl resonance at 5.37 ppm along with a broad NH resonance at 3.72 ppm and a sharp singlet for the metal-bound methyl group at -0.18 ppm confirmed the formation of $\text{Cp}_2\text{Zr}(\text{CH}_3)(\text{NHPPhBH}_2(\text{C}_6\text{F}_5))$ (**21**) as the major product. The BH_2 resonance in the ${}^1\text{H}$ NMR spectrum is sufficiently broadened that it is indistinguishable from the background, therefore the ${}^{11}\text{B}$ NMR spectrum confirms the BH_2 moiety as a sharp triplet at -23 ppm (${}^1J_{\text{B,H}} = 80$ Hz). In contrast to the zirconium analog, for which crystals suitable for X-ray diffraction could not be isolated, the crystalline hafnium complex $\text{Cp}_2\text{Hf}(\text{CH}_3)(\text{NHPPhBH}_2(\text{C}_6\text{F}_5))$ (**22**) was isolated from a concentrated toluene solution at $-25\text{ }^\circ\text{C}$. The solid state structure features the amidoborane ligand $-\text{NHPPhBH}_2(\text{C}_6\text{F}_5)$ bound to the hafnium through a Hf—N single bond and a β -B-agostic interaction (**Figure 3.23**). The single N—H group engages in an intramolecular N—H \cdots F—C interaction with an *ortho*-fluorine of the pentafluorophenyl ring (H(1)—H(1C) \cdots F(19)—C(19), 2.228 Å).

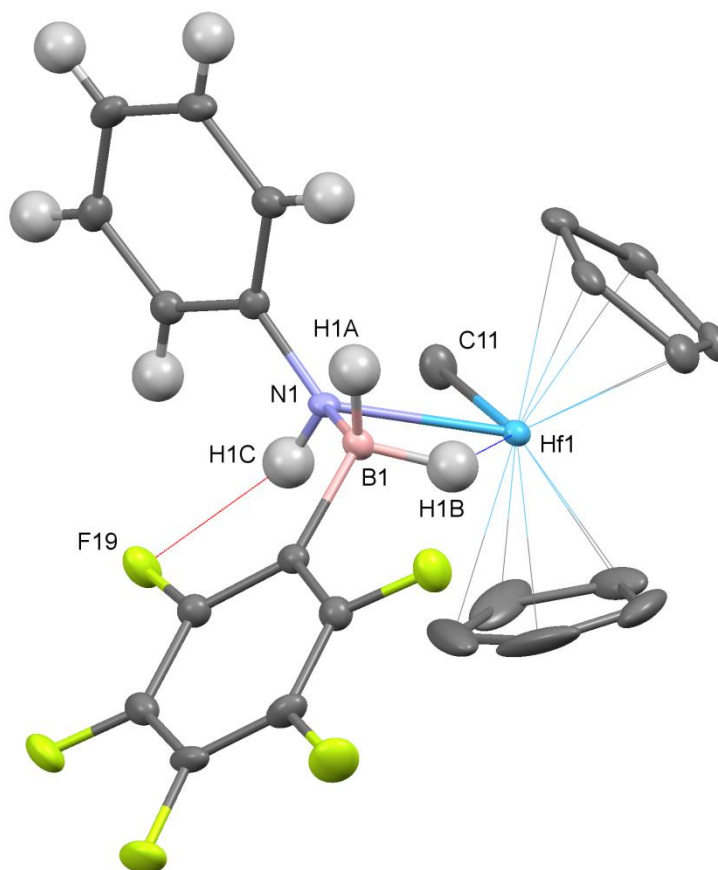


Figure 3.23: Crystal structure of $\text{Cp}_2\text{Hf}(\text{CH}_3)(\text{NHPPhBH}_2(\text{C}_6\text{F}_5))$ (**22**) with displacement ellipsoids displayed at the 50% probability level. Cyclopentadienyl and methyl hydrogen atoms have been omitted for clarity. The intramolecular $\text{N—H}\cdots\text{F—C}$ interaction is indicated in red and the $\beta\text{-B-agostic}$ interaction is indicated in blue.

The $\text{—NHPPhBH}_2(\text{C}_6\text{F}_5)$ lithium reagent acts in an analogous fashion to the unsubstituted $\text{—NH}_2\text{BH}_2(\text{C}_6\text{F}_5)$ ligand towards Cp_2TiCl_2 through facile reduction of the titanium center from Ti(IV) to Ti(III). In addition, salt metathesis between the *in situ* generated Cp_2TiCl and $\text{Li}[\text{NHPPhBH}_2(\text{C}_6\text{F}_5)]$ resulted in the Ti(III) amidoborane $\text{Cp}_2\text{Ti}(\text{NHPPhBH}_2(\text{C}_6\text{F}_5))$. Deep blue X-ray quality crystals are obtained by cooling a concentrated toluene solution to $-2\text{ }^\circ\text{C}$. The solid state structure shows the amidoborane ligand bound to the titanium center in an agostic fashion. Unlike most of the previously described structures, the protic N—H group does not engage in any intramolecular $\text{N—H}\cdots\text{F—C}$ interactions (**Figure 3.24**).

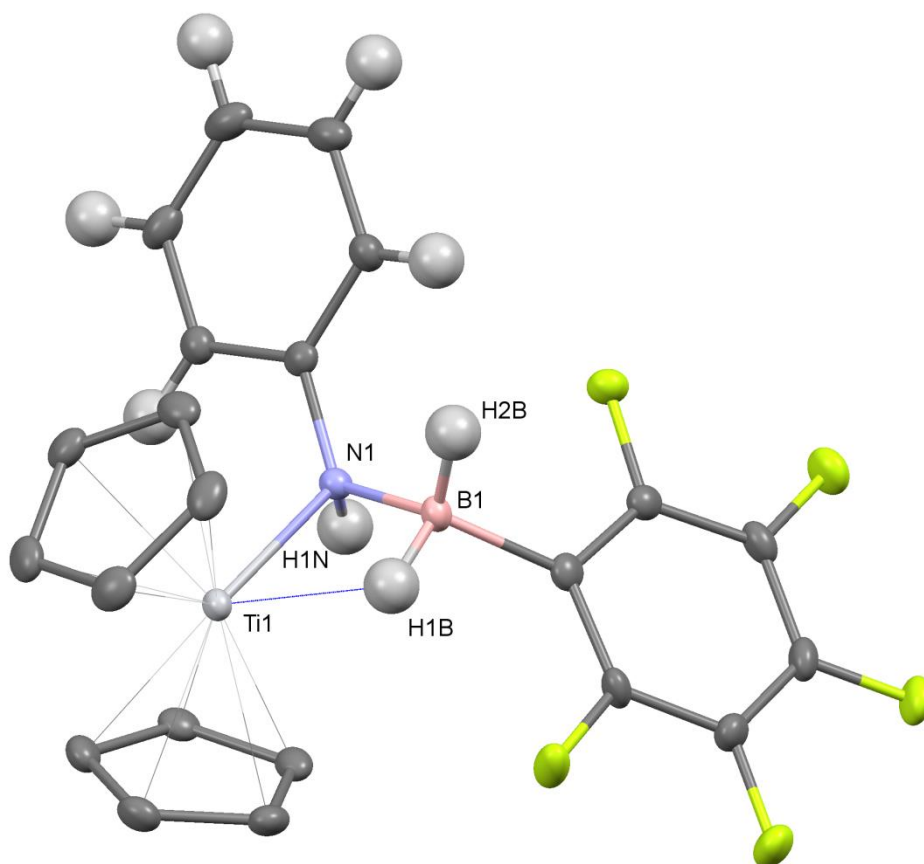


Figure 3.24: Crystal structure of $\text{Cp}_2\text{Ti}(\text{NHPhBH}_2(\text{C}_6\text{F}_5))$ (**23**) with displacement ellipsoids displayed at the 50% probability level. The cyclopentadienyl hydrogen atoms have been omitted for clarity. The β -B-agostic interaction is indicated in blue.

The addition of a phenyl group at the nitrogen center causes a lengthening of the Ti—N bond from 2.165(2) Å in $\text{Cp}_2\text{Ti}(\text{NH}_2\text{BH}_2(\text{C}_6\text{F}_5))$ to 2.217(2) Å in $\text{Cp}_2\text{Ti}(\text{NHPhBH}_2(\text{C}_6\text{F}_5))$. The observed bond lengthening has also been reported for alkyl and aryl substitution of the Ti(III) amide $\text{Cp}^*_2\text{Ti}(\text{NH}_2)$. The Ti—N bond length in the parent $\text{Cp}^*_2\text{Ti}(\text{NH}_2)$ measures 1.933(3) Å,²⁴⁸ indicating additional lone pair donation from the nitrogen to the titanium center and partial double bond character. For the substituted Ti(III) amides, $\text{Cp}^*_2\text{Ti}(\text{NMeH})$ and $\text{Cp}^*_2\text{Ti}(\text{NMePh})$, the analogous Ti—N bond lengths are 1.955(5) Å²⁴⁹ and 2.045(2) Å,²⁵⁰ respectively, consistent in nature with the observed Ti—N bond lengthening pattern for the pentafluorophenyl substituted Ti(III) amidoboranes **16** and **23**.

3.3 Discussion

Despite the isoelectronic relationship between amine boranes and alkanes, their structural organization about a transition metal center is considerably different. This is due to the protic N—H and hydridic B—H groups in amine boranes, a combination which facilitates molecular polarity and a usual end-on bonding mode in transition metal complexes (**Figure 3.1**). In contrast, the coordination of alkanes to transition metal centers occurs through the formation of a highly reactive σ -complex formed from side-on coordination of a C—H bond (**Scheme 3.4**). However, the bonding of the related amidoborane ($-\text{NR}_2\text{BX}_3$; R = H, alkyl / aryl; X = H, C_6F_5) and ethyl ligands to transition metal centers display many similarities. In addition to the propensity for the formation of agostic interactions in structures bearing amidoborane or ethyl ligands, the nature of the B—N or C—C bond in response to ligation is the same for both types of ligand. Upon bonding to a metal, the B—N bonds of amidoborane ligands and the C—C bonds of ethyl ligands shorten with respect to those of the amine borane adduct or free alkane, as can be compared in **Table 3.3**.

Table 3.3: Comparison between the B—N / C—C bond lengths between the neutral free small molecule and bound anionic ligand ($-\text{NH}_2\text{BH}_3$ / $-\text{CH}_2\text{CH}_3$).

Complex	B—N (Å)	Ref.	Complex	C—C (Å)	Ref
$\text{H}_3\text{N}\cdot\text{BH}_3$	1.58(2)	115	$\text{H}_3\text{C—CH}_3$	1.532	133
$\text{Cp}_2\text{Ti}(\text{NH}_2\text{BH}_3)$	1.534(5)	111	$\text{Ti}(\text{Me}_2\text{PCH}_2\text{CH}_2\text{PMe}_2)\text{EtCl}_3$	1.463(13)	235
$\text{Cp}_2\text{Zr}(\text{H})(\text{NH}_2\text{BH}_3)^{\text{a}}$	1.531(4)	110	$\text{ClEtRh}(\text{C}_2\text{H}_6\text{NO})(\text{C}_5\text{H}_5\text{N})_2$	1.462(9)	251
$\text{Cp}_2\text{Zr}(\text{Cl})(\text{NH}_2\text{BH}_3)$	1.523(5)	110	EtZnCl	1.533(4)	41

^a Two polymorphs have been reported for $\text{Cp}_2\text{Zr}(\text{H})(\text{NH}_2\text{BH}_3)$ and the B—N bond length for one has been used for this comparison.

The observed B—N and C—C bond shortening of amidoborane and ethyl ligands is reported to be, in part, a result of the additional agostic bonding between the ligand to the metal center. This agostic interaction facilitates charge redistribution on the ligand, in which some of the agostically bound B—H or C—H groups donate electron density into an available metal d-orbital.¹¹¹ Due to the B—H group of the amidoborane ligand already exhibiting high polarity, the agostic interaction serves to minimize this polarity, creating a less hydridic B—H group and a resulting M...H interaction which has significant metal—hydride character. This tendency towards strong metal—hydride interaction has been attributed, in part, to redistribution of the M—N electron density over the entire amidoborane ligand.¹¹¹ The opposite effect is observed for ethyl ligands, in which the relatively nonpolar C—H bond develops polarity through donation of electron density from the ligand back into the metal d-orbital. Analogous charge redistribution is slight in comparison with the amidoborane ligand. As a result, examples of agostically bound amidoborane ligands have been more forthcoming than those of the relatively non-polar alkyl derivatives.

Transition metal complexes featuring an agostic interaction have been known since the 1980s with the report of $\text{Ti}(\text{Me}_2\text{PCH}_2\text{CH}_2\text{PMe}_2)\text{EtCl}_3$.²³⁵ In contrast, the chemistry of the amidoborane ligand on transition metals was first reported in 2009 with the characterization of Zr(IV) amidoborane hydrides and chlorides (**Figure 3.25**).¹¹⁰

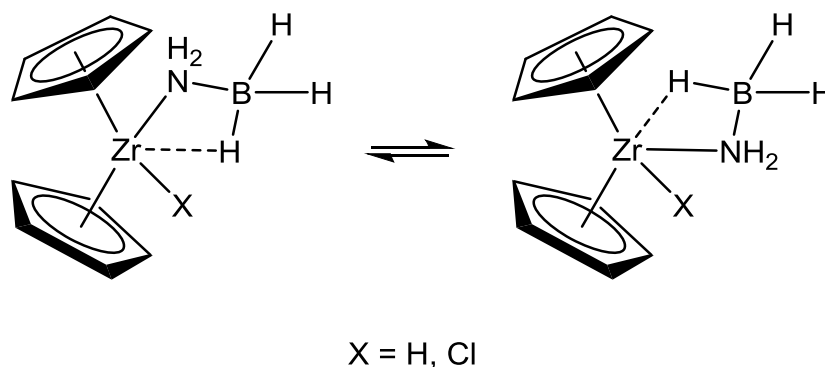


Figure 3.25: The first structurally characterized transition metal amidoborane complexes.¹¹⁰

Both sets of zirconocene amidoborane complexes exist in a solution equilibrium between a *cis* and *trans* configuration with respect to the Zr—H and Zr...H moieties. The two stereoisomers are observed in the ¹H NMR spectrum, but crystallographic characterization is limited to the *cis* isomer for the zirconocene amidoborane hydride and the *trans* isomer for the zirconocene amidoborane chloride.¹¹⁰ These complexes are prepared through treatment of the metallocene dichlorides with one or two equivalents of Li[NH₂BH₃]. The mechanism of formation of the zirconocene amidoborane hydrides is thought to occur through formation of Cp₂Zr(NH₂BH₃)₂ and β-hydrogen activation to produce the metallocene amidoborane hydride and oligomeric or polymeric polyaminoborane. The use of the substituted amidoborane ligand —NH₂BH(C₆F₅)₂ has provided evidence for the presence of a metallocene bis(amidoborane) species under similar conditions. The electron withdrawing nature of the pentafluorophenyl substituents render the B—H group less hydridic in character. This, in addition to the steric bulk of the amidoborane ligand contribute to the increased stability of Cp₂Zr(NH₂BH(C₆F₅)₂)₂ towards rapid β-hydrogen activation and elimination over the postulated Cp₂Zr(NH₂BH₃)₂ species. Recently, Manners isolated the zirconocene(IV) amidoborane hydride Cp₂Zr(H)(NMe₂BH₃) from reaction between zirconocene dichloride and two equivalents of Li[NMe₂BH₃].¹¹² This complex exhibits a *trans* configuration analogous to Roesler's Cp₂Zr(Cl)(NH₂BH₃).

In a similar fashion to the solid state structure of Roesler's $\text{Cp}_2\text{Zr}(\text{H})(\text{NH}_2\text{BH}_3)$, the solid state structure of $\text{Cp}_2\text{Zr}(\text{CH}_3)(\text{NH}_2\text{BH}(\text{C}_6\text{F}_5)_2)$ is characterized by the *cis* arrangement with respect to the $\text{Zr}-\text{CH}_3$ and $\text{Zr}\cdots\text{H}$ moieties. It is the only example of a pentafluorophenyl stabilized metallocene amidoborane in which this ligand arrangement is favourable in the solid state. Although a solution equilibrium likely exists between a *cis* and *trans* isomer of $\text{Cp}_2\text{Zr}(\text{CH}_3)(\text{NH}_2\text{BH}(\text{C}_6\text{F}_5)_2)$ and the closely related $\text{Cp}''_2\text{Zr}(\text{CH}_3)(\text{NH}_2\text{BH}_n(\text{C}_6\text{F}_5)_{3-n})$ ($n = 1, 2$), a single cyclopentadienyl, NH and CH_3 resonance is observed for each compound in the ^1H NMR spectrum. The structural parameters of the zirconocene methyl amidoborane complexes described in **Section 3.2.1**, the hydride and chloride analogs reported by Roesler and the N-methylated analogs reported by Manners are similar (**Table 3.4**).

Table 3.4: Structural parameters of group 4 metallocene amidoborane complexes.

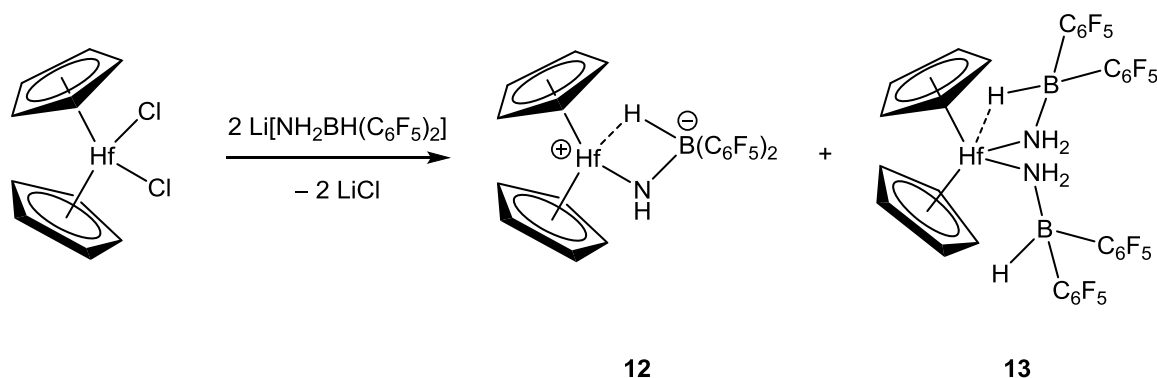
Zirconocene amidoborane	Zr—N—B	Zr—N	N—B	Zr...H	Ref.
	87.9(2)	2.268(2)	1.523(5)	2.02(3)	110
	92.0(1)	2.295(2)	1.531(4)	2.18(2)	102
	85.9(1) ^a	2.284(2)	1.531(4)	2.284(2)	110
	87.54(8)	2.309(1)	1.547(2)	2.1979(3)	102
	84.5(1)	2.337(2)	1.540(3)	1.97(3)	112

^a Two polymorphs have been reported for Cp₂Zr(H)(NH₂BH₃) and the structural data for one has been used for this comparison.

In contrast to the B—H bond activation reaction observed in addition to the formation of Cp₂Zr(NH₂BH(C₆F₅)₂), to produce the pentafluorophenyl substituted polyaminoborane {H₂NB(C₆F₅)₂}₃, the analogous treatment for hafnocene results in activation of the N—H bond, rather than the B—H bond. Treatment of Cp₂HfCl₂ with two equivalents of Li[NH₂BH(C₆F₅)₂] produces two major cyclopentadienyl containing products,

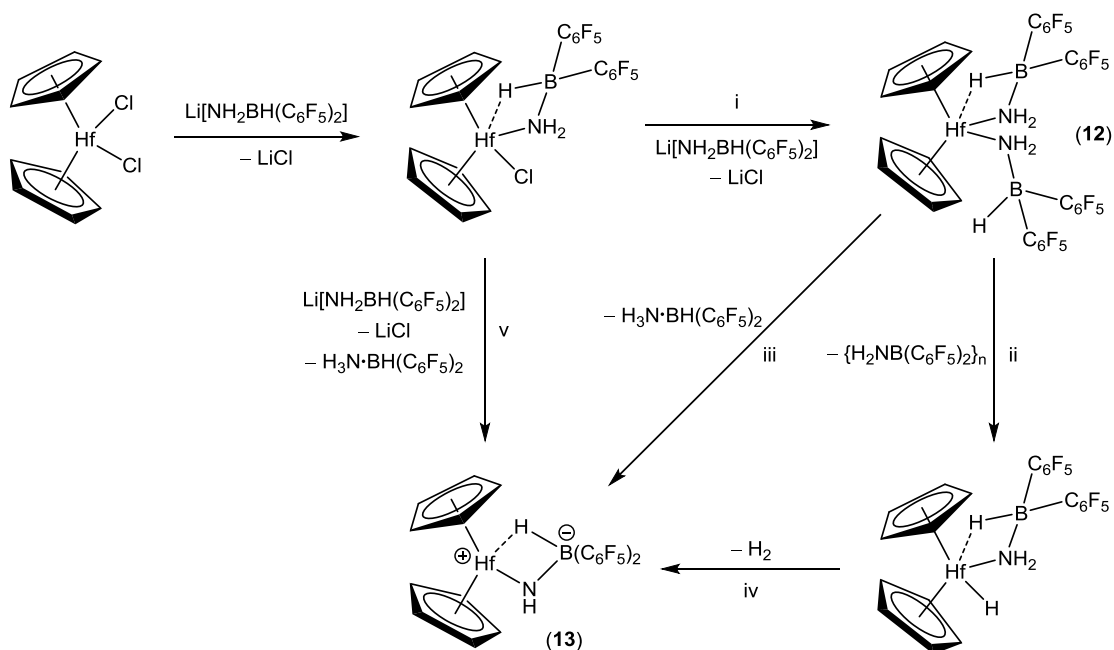
$\text{Cp}_2\text{Hf}(\text{NH}_2\text{BH}(\text{C}_6\text{F}_5)_2)_2$ and $\text{Cp}_2\text{Hf}(\text{NHBH}(\text{C}_6\text{F}_5)_2)$ (**Scheme 3.11**). Despite numerous attempts, reaction conditions could not be adjusted to favour formation of one or the other as the sole product, and the intensity ratio of the cyclopentadienyl resonances in the ^1H NMR spectra of the crude reaction mixtures could not be related to any experimental consideration.

Scheme 3.11: Preparation of pentafluorophenyl stabilized hafnocene complexes.



Three possible mechanisms have been postulated for the formation of the hafnocene imidoborane complex $\text{Cp}_2\text{Hf}(\text{NHBH}(\text{C}_6\text{F}_5)_2)$ (**Scheme 3.12**). The common entry point in the proposed reaction pathways is salt metathesis to produce $\text{Cp}_2\text{Hf}(\text{Cl})(\text{NH}_2\text{BH}(\text{C}_6\text{F}_5)_2)$ along with the precipitation of LiCl .

Scheme 3.12: Proposed routes to compound **12**.



From here, three reaction pathways can be considered for the preparation of $\text{Cp}_2\text{Hf}(\text{NHBH}(\text{C}_6\text{F}_5)_2)$. In the first, a second metathesis reaction occurs (i) to produce the crystallographically characterized hafnocene bis(amidoborane) complex, $\text{Cp}_2\text{Hf}(\text{NH}_2\text{BH}(\text{C}_6\text{F}_5)_2)_2$. An analogous mechanism has been proposed to occur in the case of reaction of zirconocene dichloride with two equivalents of $\text{Li}[\text{NH}_2\text{BH}_3]$.¹¹⁰ The hafnocene bis(amidoborane) may further react through either B—H bond activation to produce $\{\text{H}_2\text{NB}(\text{C}_6\text{F}_5)_2\}_n$ and the hafnocene amidoborane hydride $\text{Cp}_2\text{Hf}(\text{H})(\text{NH}_2\text{BH}(\text{C}_6\text{F}_5)_2)$ (ii) or intramolecular N—H bond activation to release one equivalent of $\text{H}_3\text{N}\cdot\text{BH}(\text{C}_6\text{F}_5)_2$ and produce $\text{Cp}_2\text{Hf}(\text{NHBH}(\text{C}_6\text{F}_5)_2)$ (iii). In the former pathway, further loss of dihydrogen (iv) would result in the production of the hafnocene imidoborane as well. Alternatively, rather than a second instance of salt metathesis from $\text{Cp}_2\text{Hf}(\text{Cl})(\text{NH}_2\text{BH}(\text{C}_6\text{F}_5)_2)$ and $\text{Li}[\text{NH}_2\text{BH}(\text{C}_6\text{F}_5)_2]$, the lithium salt may act as a base (v), deprotonating the amidoborane ligand to produce the parent amine borane, $\text{H}_3\text{N}\cdot\text{BH}(\text{C}_6\text{F}_5)_2$, lithium chloride precipitate and $\text{Cp}_2\text{Hf}(\text{NHBH}(\text{C}_6\text{F}_5)_2)$.

Interpreting NMR spectra of crude reaction mixtures with reference to the described mechanisms is not straightforward. In all reaction attempts, at least two cyclopentadienyl resonances were identified, with relative integrations apparently independent of the reaction conditions. Repeated isolation of crystalline samples of $\text{Cp}_2\text{Hf}(\text{NHBH}(\text{C}_6\text{F}_5)_2)$ has resulted in those resonances attributed to this compound to be confidently assigned, allowing for a tentative assignment of the second major cyclopentadienyl resonance to be attributed to the presence of $\text{Cp}_2\text{Hf}(\text{NH}_2\text{BH}(\text{C}_6\text{F}_5)_2)_2$. Gentle warming of the reaction mixture (60 °C) did not result in a noticeable change in the resonance intensities, suggesting that $\text{Cp}_2\text{Hf}(\text{NHBH}(\text{C}_6\text{F}_5)_2)$ is not formed from N—H bond activation of $\text{Cp}_2\text{Hf}(\text{NH}_2\text{BH}(\text{C}_6\text{F}_5)_2)_2$. No direct NMR spectroscopic evidence of the formation of $\text{Cp}_2\text{Hf}(\text{H})(\text{NH}_2\text{BH}(\text{C}_6\text{F}_5)_2)$ in solution was identified. Consideration of the observed stability of the zirconium analog $\text{Cp}_2\text{Zr}(\text{H})(\text{NH}_2\text{BH}(\text{C}_6\text{F}_5)_2)$ and the distinctive Zr—H resonance in the ^1H NMR spectrum suggests that if formed in solution, the stability of $\text{Cp}_2\text{Hf}(\text{H})(\text{NH}_2\text{BH}(\text{C}_6\text{F}_5)_2)$ should be sufficient for identification by NMR. However, by comparison with hafnium alkyls, the hafnocene bis(amidoborane) complex $\text{Cp}_2\text{Hf}(\text{NH}_2\text{BH}(\text{C}_6\text{F}_5)_2)_2$ should demonstrate increased stability towards β -hydride elimination than the corresponding zirconocene complex.^{252–254} Identification of $\text{H}_3\text{N}\cdot\text{BH}(\text{C}_6\text{F}_5)_2$ in the ^{19}F and ^{11}B NMR spectra of crude reaction mixtures may be indicative of reaction pathways iii and / or v. However, $\text{H}_3\text{N}\cdot\text{BH}(\text{C}_6\text{F}_5)_2$ is also the product of hydrolysis and therefore its presence in crude NMR spectra is unavoidable and its origin cannot be confidently determined. The proposed reaction pathway for the formation of $\text{Cp}_2\text{Hf}(\text{NHBH}(\text{C}_6\text{F}_5)_2)$ is undeniably complex and the consideration of simultaneous multiple reaction pathways must not be dismissed.

Dehydrocoupling of amine boranes by titanocene was first reported by Manners in 2006.¹⁴⁸ Until this time, most of the studied dehydrocoupling catalysts were based on late transition metals, such as rhodium and iridium. However, the potential for commercial application of dehydrocoupling resulted in increased use of catalysts based on the

cheaper and more abundant early transition metals. Amine borane dehydrocoupling by titanocene was proposed to occur through a Ti(II) / Ti(IV) redox cycle, with initial N—H bond activation at titanocene followed by coupling and cyclization reactions to produce polyaminoboranes.¹⁵⁰ However, a recent follow up report¹¹² describes the identification of Ti(III) amidoborane complexes from similar reaction conditions, indicating the likely participation of a Ti(III) species within the catalytic cycle. Results presented in **Section 3.2.3** are consistent with the suggestion of an intricate catalytic cycle which includes a Ti(III) species.

The pentafluorophenyl substituted Ti(III) amidoborane complexes are structurally similar to the pentafluorophenyl-free derivatives $\text{Cp}_2\text{Ti}(\text{NH}_2\text{BH}_3)$ and $\text{Cp}_2\text{Ti}(\text{NMe}_2\text{BH}_3)$. These Ti(III) amidoborane complexes were prepared through metathesis reactions between Cp_2TiCl_2 and the lithium salts. In most cases, *in situ* reduction of the titanium from Ti(IV) to Ti(III) by the lithium salt generates stoichiometric amounts of Cp_2TiCl . The second lithium salt reacts through a metathesis reaction to generate the amidoborane ligand. In the case of $-\text{NH}_2\text{BH}(\text{C}_6\text{F}_5)_2$, pre-reduction of the titanium is required for the reaction to reach completion. All reduction reactions are accompanied by the loss of a gaseous by-product (assumed to be dihydrogen), but the fate of the B/N containing species has only been formulated for the purposes of equation balancing. While Manners' Ti(III) amidoborane $\text{Cp}_2\text{Ti}(\text{NMe}_2\text{BH}_3)$ and phosphinoborane $\text{Cp}_2\text{Ti}(\text{PPh}_2\text{BH}_3)$ were found to be active towards amine borane dehydrocoupling, $\text{Cp}_2\text{Ti}(\text{NH}_2\text{BH}_2(\text{C}_6\text{F}_5))$ did not react further with $\text{H}_3\text{N}\cdot\text{BH}_n(\text{C}_6\text{F}_5)_{3-n}$ ($n = 1, 2, 3$) even after extended periods in toluene solution at ambient temperature.

Numerous synthetic approaches were attempted to isolate a Ti(IV) amidoborane complex of either the $-\text{NH}_2\text{BH}_2(\text{C}_6\text{F}_5)$ or $-\text{NH}_2\text{BH}(\text{C}_6\text{F}_5)_2$ ligands starting from titanium precursors with various oxidation states. $\text{Cp}_2\text{Ti}(\text{PMe}_3)_2$ was prepared by reduction of Cp_2TiCl_2 with magnesium in the presence of excess trimethylphosphine. Treatment of a toluene solution of $\text{Cp}_2\text{Ti}(\text{PMe}_3)_2$ with $\text{H}_3\text{N}\cdot\text{BH}_2(\text{C}_6\text{F}_5)$ resulted the isolation of an air sensitive

slate-blue colored solid. This was identified as $\text{Cp}_2\text{Ti}(\text{NH}_2\text{BH}_2(\text{C}_6\text{F}_5))$, a result which has been observed with the formation of $\text{Cp}_2\text{Ti}(\text{NMe}_2\text{BH}_3)$ from the reaction between $\text{Cp}_2\text{Ti}(\text{PMe}_3)_2$ with $\text{Me}_2\text{HN}\cdot\text{BH}_3$ reported by Manners.¹¹² Analogous reaction with the $-\text{NH}_2\text{BH}(\text{C}_6\text{F}_5)_2$ ligand did not result in an identifiable product. Therefore, treatment of a Ti(II), Ti(III) or Ti(IV) precursor with $\text{H}_3\text{N}\cdot\text{BH}_2(\text{C}_6\text{F}_5)$ or its lithium salt results in the Ti(III) amidoborane $\text{Cp}_2\text{Ti}(\text{NH}_2\text{BH}_2(\text{C}_6\text{F}_5))$. Use of the tri-substituted amidoborane ligand $-\text{NH}_2\text{B}(\text{C}_6\text{F}_5)_3$ facilitated the formation of a stable Ti(IV) center with an amidoborane ligand. The salt $[\text{Li}\{\text{thf}\}_4][\text{Cp}_2\text{Ti}(\text{NH}_2\text{B}(\text{C}_6\text{F}_5)_3)(\text{NHB}(\text{C}_6\text{F}_5)_3)]$ is a novel example of a mixed amido- / imido-borane ligand system on titanium. The imidoborane functionality displays slight double bond character, with a Ti—N bond length of 1.932(3) Å. Previous titanocene amide complexes such as $\text{Cp}^*_2\text{TiNRR}'$ have Ti—N bond lengths ranging from 1.933(3) Å to 2.045(2) Å, with increasing bond length associated with the presence of an alkyl or aryl R group (**Table 3.5**). The length of the M—N bond length increases upon substitution due to the decrease in π -donor strength of the nitrogen lone pair.

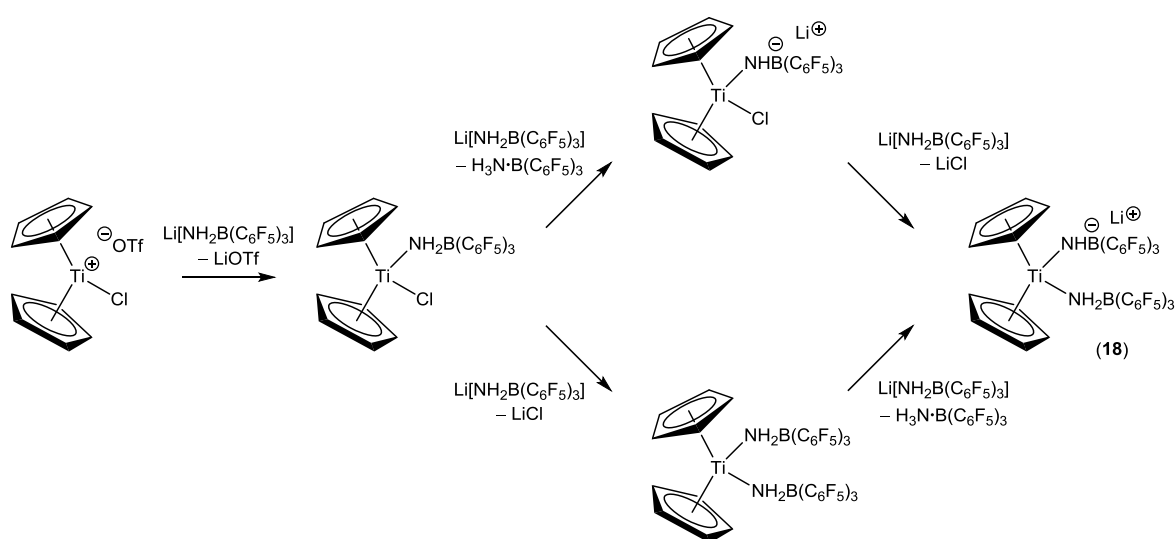
Table 3.5: Ti—N bond lengths for selected titanocene amides.

Compound	Ti—N bond length (Å)	Ref.
$\text{Cp}''_2\text{Ti}(\text{NH}_2)$	1.933(3)	248
$\text{Cp}^*_2\text{Ti}(\text{NH}_2)$	1.944(2)	255
$\text{Cp}^*_2\text{Ti}(\text{N}(\text{Me})(\text{H}))$	1.955(5)	249
$\text{Cp}^*_2\text{Ti}(\text{N}(\text{Me})(\text{Ph}))$	2.045(2)	250

In the case where R is the electron withdrawing Lewis acid $\text{B}(\text{C}_6\text{F}_5)_3$, observed in $[\text{Li}\{\text{thf}\}_4][\text{Cp}_2\text{Ti}(\text{NH}_2\text{B}(\text{C}_6\text{F}_5)_3)(\text{NHB}(\text{C}_6\text{F}_5)_3)]$, the Ti—N bond remains comparable in length to the sterically less hindered parent titanocene amide $\text{Cp}''_2\text{Ti}(\text{NH}_2)$. In a similar fashion to

the described double bond character for $\text{Cp}^*_2\text{Ti}(\text{NH}_2)$, the imidoborane ligand of $[\text{Li}\{\text{thf}\}_4][\text{Cp}_2\text{Ti}(\text{NH}_2\text{B}(\text{C}_6\text{F}_5)_3)(\text{NHB}(\text{C}_6\text{F}_5)_3)]$ may also be described as displaying partial double bond character. The isolation of $[\text{Li}\{\text{thf}\}_4][\text{Cp}_2\text{Ti}(\text{NH}_2\text{B}(\text{C}_6\text{F}_5)_3)(\text{NHB}(\text{C}_6\text{F}_5)_3)]$ from reaction between the electrophilic titanium center $[\text{Cp}_2\text{TiCl}]^+$ with $\text{Li}[\text{NH}_2\text{B}(\text{C}_6\text{F}_5)_3]$ was highly surprising as this product does not reflect the reaction stoichiometry. It is therefore evident that the underlying chemistry is quite complex, and may be proposed to occur through a combination of salt metathesis and deprotonation reactions (**Scheme 3.13**).

Scheme 3.13: Possible routes to compound **18**.



Reaction between the more electrophilic titanocene species $[\text{Cp}_2\text{TiCl}][\text{OTf}]$ and the lithium salt $\text{Li}[\text{NH}_2\text{B}(\text{C}_6\text{F}_5)_3]$ is likely to proceed through elimination of $\text{Li}[\text{OTf}]$ and the production of the titanocene amidoborane chloride, $\text{Cp}_2\text{Ti}(\text{Cl})(\text{NH}_2\text{B}(\text{C}_6\text{F}_5)_3)$. This is consistent with the observation of slow or unclear reaction between Cp_2TiCl_2 and $\text{Li}[\text{NH}_2\text{B}(\text{C}_6\text{F}_5)_3]$ (discussed in **Section 3.2.3**), suggesting unfavorable reaction with the $\text{Ti}-\text{Cl}$ bond using this salt. Two more equivalents of the lithium salt are required for the production of $[\text{Li}\{\text{thf}\}_4][\text{Cp}_2\text{Ti}(\text{NH}_2\text{B}(\text{C}_6\text{F}_5)_3)(\text{NHB}(\text{C}_6\text{F}_5)_3)]$, with one participating in an additional

metathesis reaction and the other acting as a base to deprotonate one $-\text{NH}_2\text{B}(\text{C}_6\text{F}_5)_3$ ligand. The distinguishing feature between the two reaction pathways is the formation of either the titanocene bis(amidoborane) $\text{Cp}_2\text{Ti}(\text{NH}_2\text{B}(\text{C}_6\text{F}_5)_3)_2$ or the titanocene amidoborane chloride $\text{Cp}_2\text{Ti}(\text{Cl})(\text{NH}_2\text{B}(\text{C}_6\text{F}_5)_3)$. However, in comparison with the observed chemistry between the group 4 metals and the $-\text{NH}_2\text{BH}_n(\text{C}_6\text{F}_5)_{3-n}$ ($n = 1, 2$) ligands, the participation of two simultaneous reaction pathways is a valuable consideration.

3.4 Conclusions

The use of the pentafluorophenyl substituted amidoborane ligands $-\text{NH}_2\text{BH}_n(\text{C}_6\text{F}_5)_{3-n}$ ($n = 0, 1, 2$) has allowed for stabilization of organometallic complexes which provide insight into the bonding interactions between the amidoborane ligand and transition metal center. The complexes $\text{Cp}_2\text{M}(\text{CH}_3)(\text{NHPPhBH}_2(\text{C}_6\text{F}_5))$ ($\text{M} = \text{Zr}, \text{Hf}$) and $\text{Cp}_2\text{Ti}(\text{NHPPhBH}_2(\text{C}_6\text{F}_5))$ are the first examples of N-substituted group 4 metallocene complexes bearing a pentafluorophenyl stabilized borane moiety. In all but one of the described group 4 metallocene amidoborane complexes, the amidoborane ligand participates in a β -B-agostic interaction, a structural motif that exists in the pentafluorophenyl-free analogs and is likely to participate during catalysis.^{110,111}

The reactivity observed with the amidoborane ligands $-\text{NH}_2\text{BH}(\text{C}_6\text{F}_5)_2$ and $-\text{NH}_2\text{BH}_2(\text{C}_6\text{F}_5)$ with group 4 metallocene precursors follows the general trend of decreasing catalytic activity / reactivity going down the group, in this case as applied to the understood catalytic dehydrocoupling of amine boranes. Stabilization of either the $-\text{NH}_2\text{BH}(\text{C}_6\text{F}_5)_2$ or $-\text{NH}_2\text{BH}_2(\text{C}_6\text{F}_5)$ ligands on a Ti(IV) center was unsuccessful due to facile reduction of any generated Ti(IV) amidoborane complexes. In the case of both ligands, reduction of the Ti(IV) to Ti(III) is observed, although this reaction is much more facile in the case of $-\text{NH}_2\text{BH}_2(\text{C}_6\text{F}_5)$. Consistent isolation of Ti(III) complexes agrees with reports in the literature and supports the consideration of Ti(III) playing an active role in catalysis.¹¹²

However, in the case of the tri-substituted amidoborane ligand, $-\text{NH}_2\text{B}(\text{C}_6\text{F}_5)_3$, formation of a unique mixed metallocene amido- / imido-borane complex was observed and structurally characterized.

The related zirconium chemistry allowed for the observation of both the metallocene amidoborane complexes and the isolation and characterization of several of the dehydrocoupling products. Isolation of $\text{Cp}_2\text{Zr}(\text{NH}_2\text{BH}(\text{C}_6\text{F}_5)_2)_2$ supports the reaction pathway proposed by Roesler for dehydrocoupling of $\text{H}_3\text{N}\cdot\text{BH}_3$ and related amine boranes by zirconocene catalyst precursors, which includes initial formation of a zirconocene bis(amidoborane) complex prior to β -hydrogen activation.¹¹⁰ The isolated bis(amidoborane) complex is observed to be in equilibrium with the zirconocene amidoborane hydride $\text{Cp}_2\text{Zr}(\text{H})(\text{NH}_2\text{BH}(\text{C}_6\text{F}_5)_2)$ and the product of dehydrocoupling. While the zirconocene amidoborane hydride was characterized solely by multinuclear NMR spectroscopy, spectral characteristics agree with those reported for the crystallographically characterized pentafluorophenyl-free analogs $\text{Cp}_2\text{Zr}(\text{H})(\text{NH}_2\text{BH}_3)$ ¹¹⁰ and $\text{Cp}_2\text{Zr}(\text{H})(\text{NMe}_2\text{BH}_3)$.¹¹² Further support for the formation of the amidoborane hydride comes from the isolation and crystallographic characterization of $\{\text{H}_2\text{NB}(\text{C}_6\text{F}_5)_2\}_3$ and the formation of $\text{Cp}_2\text{Zr}(\text{Cl})(\text{NH}_2\text{BH}(\text{C}_6\text{F}_5)_2)$ after treatment with dichloromethane. The spectral characteristics of $\text{Cp}_2\text{Zr}(\text{Cl})(\text{NH}_2\text{BH}(\text{C}_6\text{F}_5)_2)$ agree well with those of the structurally characterized pentafluorophenyl-free analog $\text{Cp}_2\text{Zr}(\text{Cl})(\text{NH}_2\text{BH}_3)$.¹¹⁰

The isolation of $\text{Cp}_2\text{Hf}(\text{NH}_2\text{BH}(\text{C}_6\text{F}_5)_2)_2$ provides further support for the formation of a group 4 metallocene bis(amidoborane) complex as a possible reaction intermediate during catalytic dehydrocoupling. Due in part to the decreased catalytic activity of hafnium in comparison to that of titanium and zirconium, further activation of the agostic B—H bond to facilitate dehydrocoupling is not observed. Rather, unexpected N—H bond activation to produce a hafnocene imidoborane species was observed. This is the first example of a hafnium imidoborane complex bearing no stabilizing R group on the nitrogen atom. The unexpected reactivity is of significant value to research involving the description of

dehydrocoupling by the group 4 metals, specifically by providing an example of direct N—H activation at the metal center, which has been suggested as the initial step in the catalytic cycle.¹⁵⁰

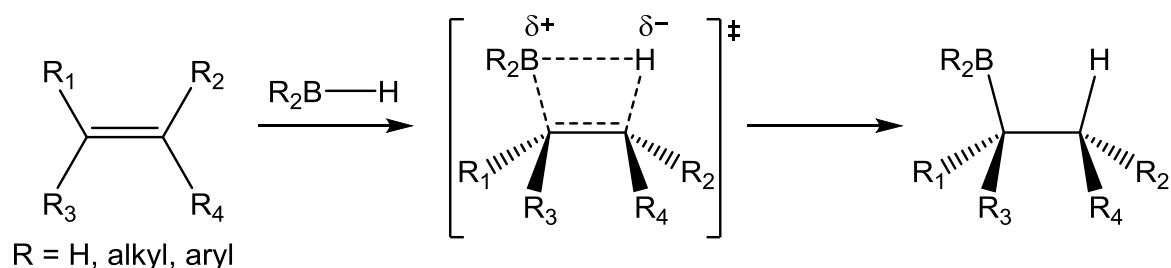
Despite the divergence in chemistry observed for the group 4 metallocene amidoborane complexes of $-\text{NH}_2\text{BH}_2(\text{C}_6\text{F}_5)$ and $-\text{NH}_2\text{BH}(\text{C}_6\text{F}_5)_2$, the use of pentafluorophenyl stabilized amidoborane ligands has allowed for the isolation of structural models for suggested short lived intermediates in amine borane dehydrocoupling. The presence of a β -B-agostic interaction supports those present in proposed catalytic cycles for $[\text{Cp}_2\text{Ti}]^{150}$ and agrees with already reported amidoborane structures of group 4 metallocenes.^{110–112} In addition, isolation of the dehydrocoupling products $\{\text{HNB}(\text{C}_6\text{F}_5)\}_3$ and $\{\text{H}_2\text{NB}(\text{C}_6\text{F}_5)_2\}_3$ is consistent with the formation of cyclic, rather than oligomeric or polymeric, polyaminoboranes in the presence of early transition metal catalysts. Identification of the major products of dehydrocoupling allows for increased insight into the mechanism through which they are formed, necessary for further applications of dehydrocoupling.

Chapter 4 Hydroboration using $\text{Me}_2\text{S}\cdot\text{BH}_n(\text{C}_6\text{F}_5)_{3-n}$ ($n = 1, 2$)

4.1 Introduction

The reactivity of diborane towards alkenic substrates has been a flourishing area of research as far back as the 1940s. Since initial reports of the reaction between diborane and unsaturated carbon—carbon²⁵⁶ and carbon—heteroatom bonds,²⁵⁷ the hydroboration reaction has become one of the most common and efficient methods for functionalizing multiple bonds, either in small organic molecules or as a method of ligand modification.^{98,258–264} Much of the early reported hydroboration chemistry was developed by Prof. Herbert Brown, who shared the 1979 Nobel Prize for his work towards the development of borane reagents for organic synthesis. Brown proposed that the hydroboration reaction occurred through a four-centered transition state, in which a monomeric borane with at least one polarized B—H bond will align with the unsaturated bond of the substrate to ultimately produce a new organoborane species (**Scheme 4.1**).^{265–268} The proposed mechanistic pathway was later supported by computational methods.²⁶⁹

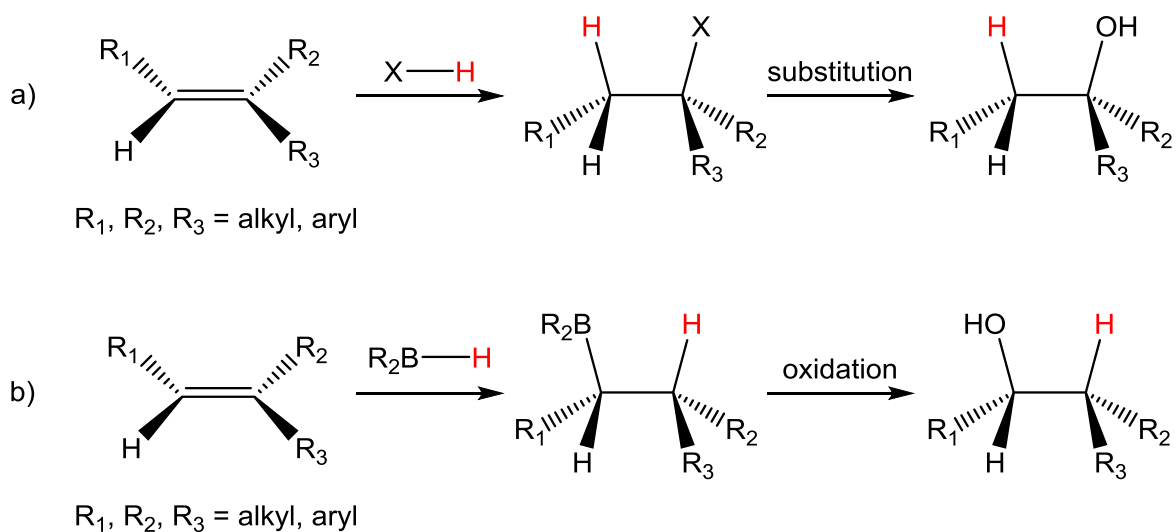
Scheme 4.1: Generic description of the hydroboration reaction.



Due to the synthetic versatility of the hydroboration reaction, various hydroboration reagents have been identified and developed which offer a selection of reaction protocols from which to prepare new organoborane complexes.^{270–272} In addition, transition metal catalysts have been employed to facilitate hydroboration at lower temperatures and with greater control over reaction selectivity than with the hydroboration reagent alone.^{273–275}

One synthetically desirable feature of the hydroboration reaction is the high favorability for anti-Markovnikov addition (**Scheme 4.2**). Due to the stereospecific nature of the transition state, in addition to the steric bulk of the borane, this functionality most often adds to the least sterically hindered atom of the substrate, placing the hydrogen atom at the most sterically hindered position. This addition pattern is the opposite to that observed from the addition H—X species (X = halide) across an unsaturated bond, in which the sterically bulky halide preferentially bonds to the most highly substituted carbon, known as the Markovnikov addition product. Therefore, the coupling of the hydroboration reaction with further oxidation provides a synthetic route to anti-Markovnikov alcohols and ketones.^{276,277}

Scheme 4.2: Markovnikov (a) and anti-Markovnikov (b) addition products using $H-X / H_3O^+$ and $B-H / H_2O_2$ to produce primary alcohols.



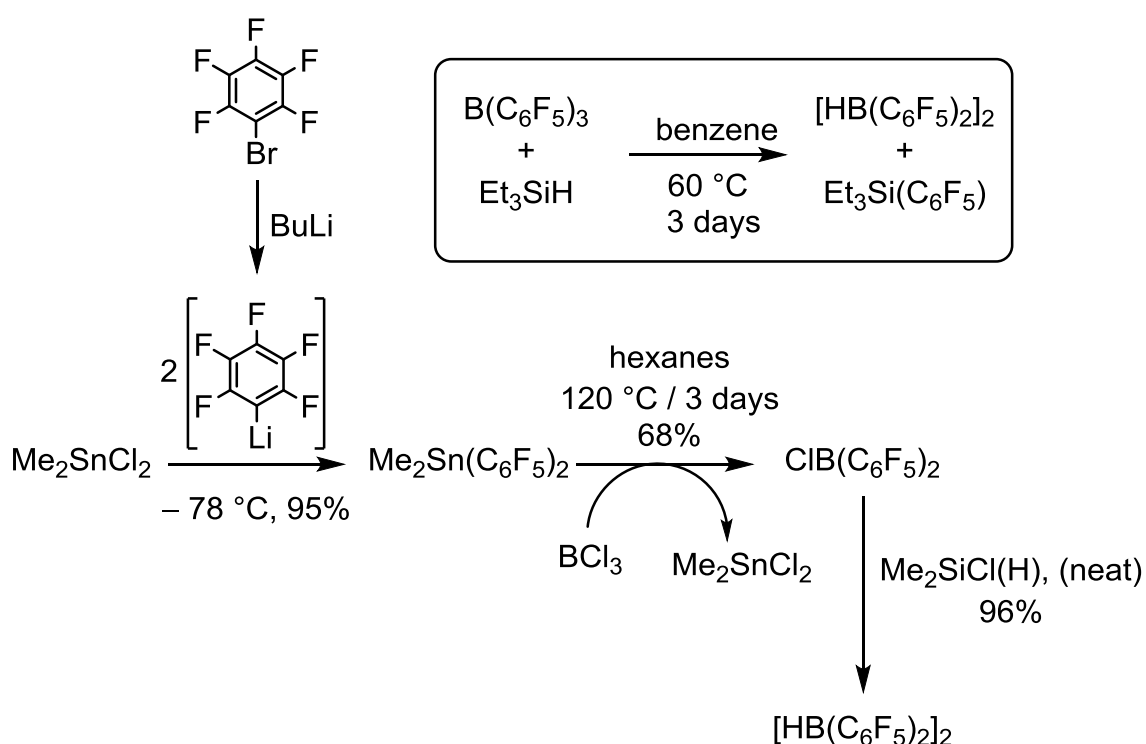
Borane, BH_3 , and its halide substituted derivatives, $H_{3-n}BX_n$ ($X = Cl, Br, I; n = 1, 2$), are still widely used as hydroboration agents, despite handling difficulties, typically as either thf or SMe_2 Lewis adducts. These Lewis adducts are commercially available, eliminating the requirement for diborane gas as a synthetic precursor. In addition to the use of borane Lewis adducts as hydroboration reagents themselves, they are also often employed as synthetic precursors for a variety of novel hydroboration reagents which offer increased selectivity. An example of this is the hydroboration reagent 9-borabicyclo[3.3.1]nonane (9-BBN), prepared from the double hydroboration of 1,5-cyclooctadiene with BH_3 (see **Section 4.3.3**).²⁷⁸

4.1.1 Use of perfluoroaryl boranes as hydroboration reagents

Since the first synthetic report of tris(pentafluorophenyl)borane by Stone and co-workers in 1963,²⁵ the chemical stability and resistance to hydrolysis of perfluoroaryl boranes and

borates has made these compounds attractive reagents, with a wide range of uses in organic synthesis and organometallic catalysis.²⁻⁴ While the synthesis of $B(C_6F_5)_3$ is facile, derivatives with one or two hydride groups, which would find use as hydroboration reagents, present considerable synthetic challenges. Prior to our work, two preparation methods for $[HB(C_6F_5)_2]_2$ (Piers' borane), had been reported,^{45,46} both of which present synthetically demanding aspects (**Scheme 4.3**).

Scheme 4.3: Synthetic methods reported for the preparation of Piers' borane.



The first method proceeds through initial $-C_6F_5$ transfer from LiC_6F_5 to Me_2SnCl_2 , to generate $Me_2Sn(C_6F_5)_2$. Whilst the tin reagent has undesirable toxicity, the more synthetically challenging aspect of this step is the isolation and successful use of LiC_6F_5 , which has been reported to decompose in a very exothermic and rapid fashion above $0\text{ }^\circ\text{C}$.³² Further issues include the use of volatile BCl_3 and regeneration of the toxic tin

starting material, as well as an extended reaction time at 120 °C to form $\text{ClB}(\text{C}_6\text{F}_5)_2$. Final reaction of $\text{ClB}(\text{C}_6\text{F}_5)_2$ with neat $\text{Me}_2\text{SiCl}(\text{H})$ produces the desired product, $[\text{HB}(\text{C}_6\text{F}_5)_2]_2$. An alternate preparation method proceeds via slow exchange between tris(pentafluorophenyl)borane and triethylsilane, from which the borane is isolated as a crystalline solid in 69% yield.⁴⁶ Piers' borane is dimeric in the solid state, similar to the structures of other common hydroboration agents such as diborane and 9-BBN, which all exhibit bridging hydrides (**Figure 4.1**).

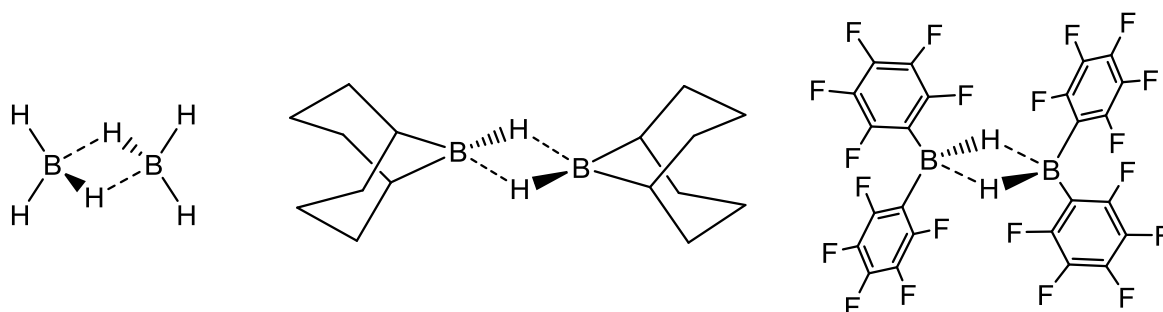
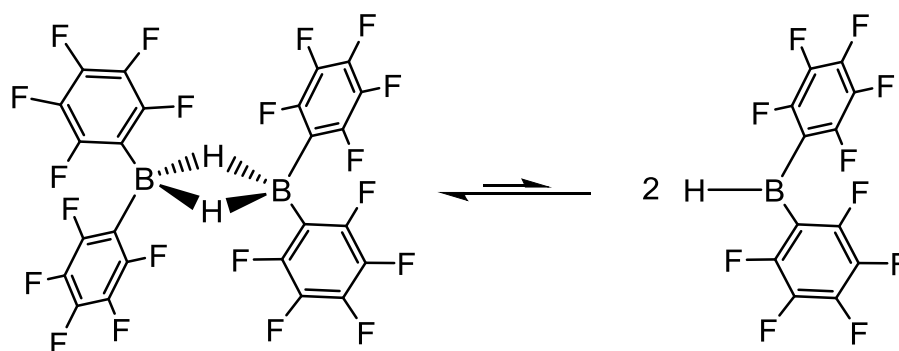


Figure 4.1: Molecular structure of diborane (left), 9-BBN (middle) and Piers' borane, $[\text{HB}(\text{C}_6\text{F}_5)_2]_2$ (right).

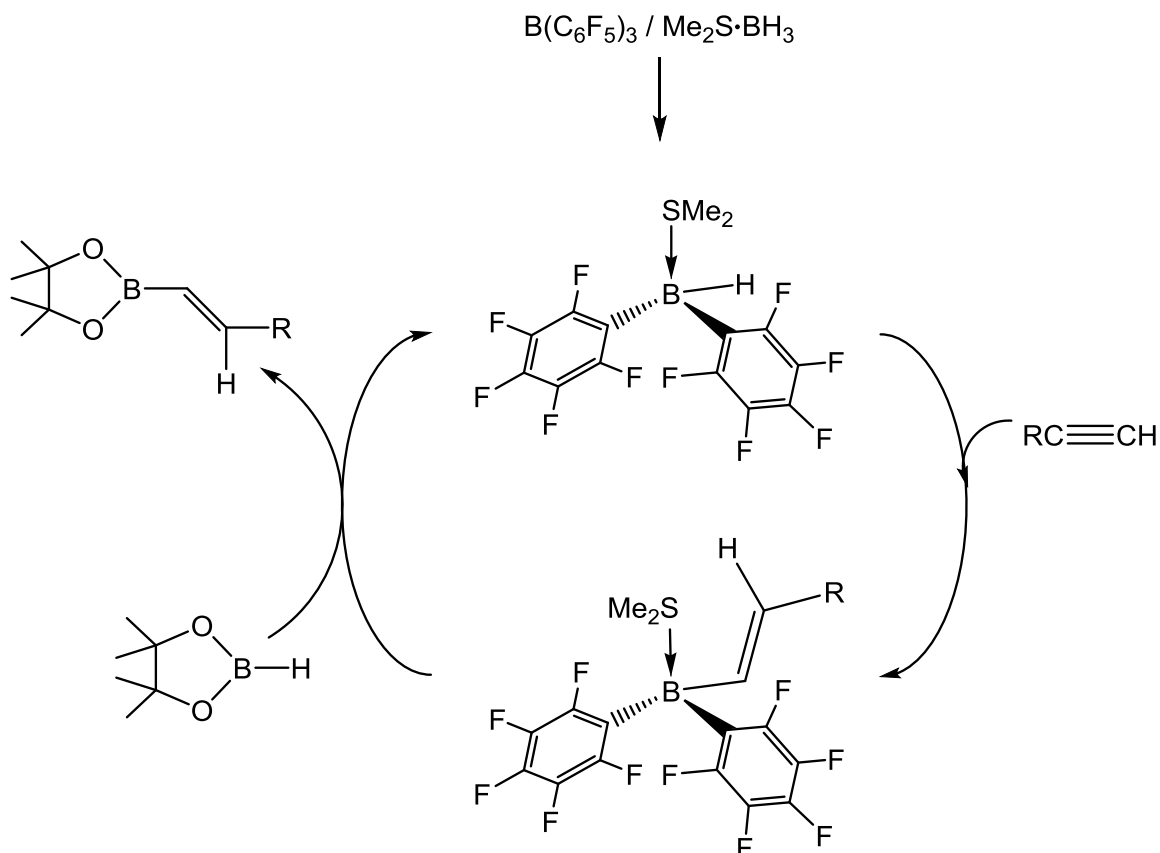
Piers and coworkers reported that $[\text{HB}(\text{C}_6\text{F}_5)_2]_2$ affects the rapid hydroboration of alkenes and alkynes under mild conditions in near quantitative yield, with good regio- and stereo-selectivity.⁴⁶ Piers' borane participates in the equilibrium shown in **Scheme 4.4**, in which its crystalline dimeric form undergoes partial dissociation to produce the highly active monomer in solution. The superior hydroboration performance of $[\text{HB}(\text{C}_6\text{F}_5)_2]_2$ in comparison with that of other common hydroboration reagents, such as BH_3 and 9-BBN, has been attributed to the increased favorability of monomer formation in solution. This is reflected in the energy barrier for dimer dissociation, found to be 5 kcal mol⁻¹ for $[\text{HB}(\text{C}_6\text{F}_5)_2]_2$ ⁴⁶ and 22 kcal mol⁻¹ for 9-BBN.^{267,268}

Scheme 4.4: *Equilibrium between the monomeric and dimeric forms of Piers' borane in solution.*



A useful synthetic strategy to promote dimer dissociation is treatment of the dimeric borane with a Lewis base, usually thf or dimethylsulfide, to produce the Lewis adduct. The reaction of Piers' borane with thf is reported to form thf·BH(C₆F₅)₂, but the adduct is unreactive with alkenic substrates at ambient temperature.⁴⁶ At elevated temperatures, thf ring opening competes with hydroboration, diminishing the functionality of the adduct as a hydroboration reagent.⁴⁶ However, mixtures of B(C₆F₅)₃ and Me₂S·BH₃ in hexane, thought to give the monomeric dimethylsulfide Lewis adduct, Me₂S·BH(C₆F₅)₂, have been used in catalytic hydroboration of alkynes with pinacolborane at ambient temperature (**Scheme 4.5**).²⁷⁹

Scheme 4.5: Catalytic hydroboration of alkynes using $\text{Me}_2\text{S}\cdot\text{BH}(\text{C}_6\text{F}_5)$ generated in situ.



While in some instances catalytic amounts of pentafluorophenylboranes may suffice to affect hydroboration, many synthetic applications require a convenient synthetic alternative to bis(pentafluorophenyl)borane. The facile synthesis of $\text{Me}_2\text{S}\cdot\text{BH}(\text{C}_6\text{F}_5)_2$ and $\text{Me}_2\text{S}\cdot\text{BH}_2(\text{C}_6\text{F}_5)$ as crystalline solids has recently been reported.⁴⁷ Both adducts are synthetically easier to prepare and are more soluble in hydrocarbon solvents than Piers' borane. The adducts have been used to prepare amine and nitrogen-donor adducts of mono- and bis-(pentafluorophenyl)borane which display a variety of supramolecular architectures in the solid state (see **Chapter 2**). In addition, the dimethylsulfide adducts are active hydroboration reagents towards carbon—carbon double and triple bonds.²⁸⁰ Herein the hydroboration activities of the monomeric perfluoroaryl boranes are reported and compared to that observed for Piers' borane. In addition, the structural

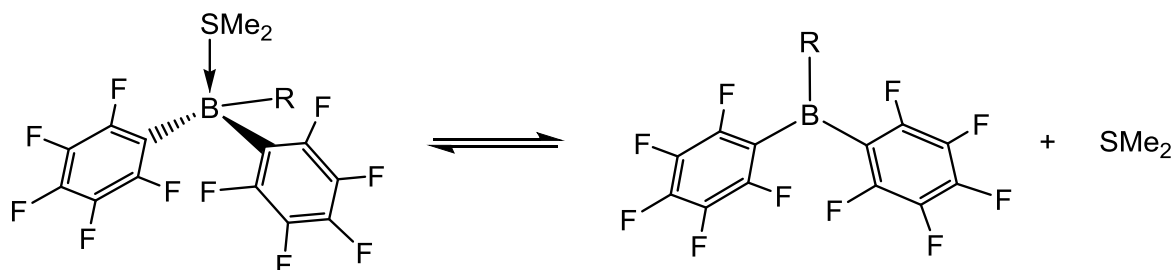
characterization of pentafluorophenyl substituted 9-BBN, formed from the double hydroboration reaction of 1,5-cyclooctadiene with $\text{Me}_2\text{S}\cdot\text{BH}_2(\text{C}_6\text{F}_5)$, is presented.

4.2 Results and discussion

The hydroboration activities of $\text{Me}_2\text{S}\cdot\text{BH}(\text{C}_6\text{F}_5)_2$ and $\text{Me}_2\text{S}\cdot\text{BH}_2(\text{C}_6\text{F}_5)$ with styrene, 1-hexene, 1,1-diphenylethylene and trimethylsilylacetylene have been investigated. Ambient temperature hydroboration of the substrates was found to be essentially instantaneous and quantitative, with the exception of the more sterically hindered 1,1-diphenylethylene which required 12 hours for complete reaction. All compounds have been characterized by multinuclear NMR spectroscopy (^1H , ^{11}B , ^{13}C , ^{19}F). In addition, the double hydroboration reaction of 1,5-cyclooctadiene with $\text{Me}_2\text{S}\cdot\text{BH}_2(\text{C}_6\text{F}_5)$ has been monitored by multinuclear NMR spectroscopy and the final thermodynamic product characterized by elemental analysis, multinuclear NMR spectroscopy and single crystal X-ray diffraction methods.

The ^{11}B NMR spectra of some of the hydroboration products contain, in addition to the resonance of the major product, a small amount of a minor product as a broad singlet resonance shifted to higher frequency to that of the major product, which has been attributed to slow ligand redistribution in solution.²⁸⁰ The position of the resonance associated with the major product is highly dependent on the concentration ratio of donor-free and donor-bound hydroboration product in solution. Due to the labile nature of the bound dimethylsulfide donor, the solution equilibrium between the bound and free states (**Scheme 4.6**) is affected by the addition or removal of small amounts of dimethylsulfide, causing the resonance frequency to change.

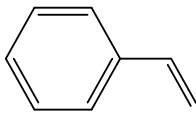
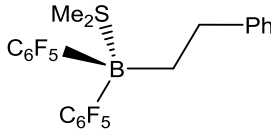
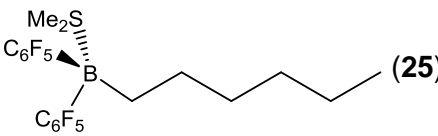
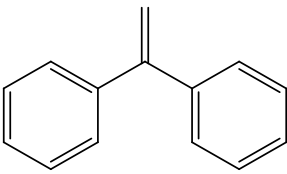
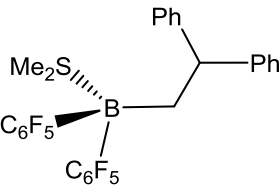
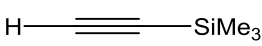
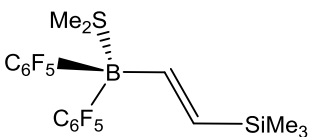
Scheme 4.6: Solution equilibrium of the hydroboration product from the reaction between $\text{Me}_2\text{S}\cdot\text{BH}(\text{C}_6\text{F}_5)_2$ and an alkenic substrate. The same equilibrium is observed for the analogous reactions with $\text{Me}_2\text{S}\cdot\text{BH}_2(\text{C}_6\text{F}_5)$.



4.2.1 Hydroboration using $\text{Me}_2\text{S}\cdot\text{BH}(\text{C}_6\text{F}_5)_2$

With the exception of the sterically hindered 1,1-diphenylethylene, hydroboration of the examined substrates using the dimethylsulfide adduct of monomeric bis(pentafluorophenyl)borane occurred rapidly and quantitatively, in a similar fashion to the hydroboration chemistry reported for Piers' borane. Each initial screening reaction was performed in an NMR tube, at ambient temperature, which was placed into the spectrometer immediately after reactant addition. An excess of dimethylsulfide was added to drive the dissociation equilibrium to the adducted form allowing for meaningful comparisons between the spectra (**Table 4.1**).

Table 4.1: Hydroboration of selected alkene and alkyne substrates with $\text{Me}_2\text{S}\cdot\text{BH}(\text{C}_6\text{F}_5)_2$.

Substrate	Hydroboration product	^{11}B NMR chemical shift	Reaction time
	 (24)	-1.2 ppm	< 1 min.
	 (25)	-0.5 ppm	< 1 min.
	 (26)	-0.9 ppm	< 12 hr.
	 (27)	-3.2 ppm	< 1 min.

Loss of the B—H resonance due to hydroboration provides a convenient means to assess reaction progress. The ^{11}B NMR spectrum of the starting material, $\text{Me}_2\text{S}\cdot\text{BH}(\text{C}_6\text{F}_5)_2$, consists of a sharp doublet at -12 ppm ($^1J_{\text{B,H}} = 81$ Hz) which is lost upon product formation. All of the hydroboration products, as the dimethylsulfide adducts, give ^{11}B NMR signals shifted downfield relative to that of the starting material, and as broad singlets rather than sharp doublets.

By ^1H NMR spectroscopy, reaction progress is assessed by loss of the alkenic C—H resonances and formation of new upfield resonances consistent with those of saturated carbon—carbon bonds. The regiochemistry of the final products (24 – 27) has been

assessed by ^1H NMR spectroscopy, which indicates a high selectivity for the anti-Markovnikov addition product. For example, spectral evidence for the hydroboration of styrene using $\text{Me}_2\text{S}\cdot\text{BH}(\text{C}_6\text{F}_5)_2$ suggests an overall reaction selectivity of 97:3, in agreement with results reported using Piers' borane.⁴⁶ However, while hydroboration of styrene using Piers' borane results in the Lewis base free product $(\text{PhCH}_2\text{CH}_2)\text{B}(\text{C}_6\text{F}_5)_2$, facile thermodynamic rearrangement of the product to form $(\text{PhCH}_2\text{CH}_2)_2\text{B}(\text{C}_6\text{F}_5)$ and $\text{B}(\text{C}_6\text{F}_5)_3$ occurs over several days in solution.⁴⁶ In contrast, no further reactivity was observed after hydroboration of styrene with $\text{Me}_2\text{S}\cdot\text{BH}(\text{C}_6\text{F}_5)_2$, even after extended periods of time. Coordination of the dimethylsulfide molecule at the boron center, through use of $\text{Me}_2\text{S}\cdot\text{BH}(\text{C}_6\text{F}_5)_2$, appears to inhibit or severely delay formation of this thermodynamic product, either as a result of steric constraints or reduced reactivity at the boron through occupation of its empty p-orbital.

Additional information on stereochemistry about the carbon—carbon double bond of the product is obtained by analysis of the vicinal coupling constants^{281,282} of the C—H resonances. For the case of the single hydroboration of trimethylsilylacetylene with $\text{Me}_2\text{S}\cdot\text{BH}(\text{C}_6\text{F}_5)_2$, the ^1H NMR spectrum displays two sets of doublets centered at 7.05 and 5.92 ppm which confirm the anti-Markovnikov addition product. In addition, the $^3J_{\text{H,H}}$ coupling constant of 21 Hz for both of the CH signals confirms a *trans* arrangement of the hydrogen atoms, and thus the borane and silyl groups, about the C=C bond. Due to the stereospecific nature of the reaction transition state, a *trans* arrangement is to be expected for all hydroboration products using this borane. This is consistent with the results reported using Piers' borane as the hydroboration reagent.⁴⁶

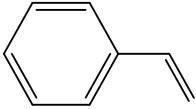
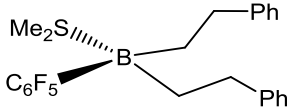
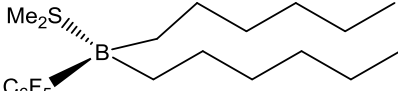
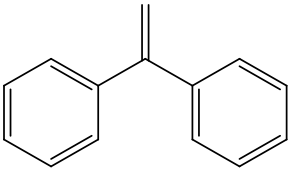
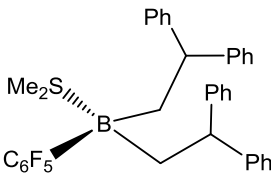
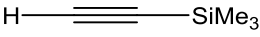
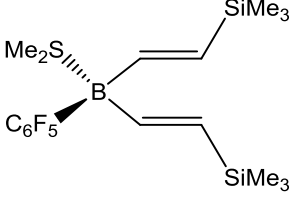
Extended drying of the hydroboration products $\text{Me}_2\text{S}\cdot\text{BR}(\text{C}_6\text{F}_5)_2$ under vacuum yields a final product retaining a single equivalent of dimethylsulfide. This was quantitatively confirmed by integration of the ^1H NMR spectra and the presence of a dimethylsulfide resonance in the ^{13}C NMR spectra. Retention of the dimethylsulfide may be attributed to

the high Lewis acidity at the boron center, a result of the presence of two electron withdrawing pentafluorophenyl groups.

4.2.2 Hydroboration using $\text{Me}_2\text{S}\cdot\text{BH}_2(\text{C}_6\text{F}_5)$

The dimethylsulfide adduct of mono(pentafluorophenyl)borane presents a rather unique $-\text{C}_6\text{F}_5$ substituted hydroboration reagent, as currently no base-free alternative for ' $\text{H}_2\text{B}(\text{C}_6\text{F}_5)$ ' has been isolated. Because of the presence of two B—H groups, the possibility exists for two hydroboration reactions, which results in a borane containing two R groups in addition to the $-\text{C}_6\text{F}_5$ ring. In a similar fashion to hydroboration using $\text{Me}_2\text{S}\cdot\text{BH}(\text{C}_6\text{F}_5)_2$, toluene solutions of $\text{Me}_2\text{S}\cdot\text{BH}_2(\text{C}_6\text{F}_5)$ were treated with a variety of alkenic substrates, followed by an excess of dimethylsulfide, at ambient temperature. The hydroboration reaction between $\text{Me}_2\text{S}\cdot\text{BH}_2(\text{C}_6\text{F}_5)$ with two equivalents of the substrates styrene, 1-hexene and trimethylsilylacetylene proceeded at ambient temperature instantaneously and quantitatively to give a major borane species with composition $\text{Me}_2\text{S}\cdot\text{B}(\text{R})_2(\text{C}_6\text{F}_5)$. Hydroboration of two equivalents of the more sterically hindered 1,1-diphenylethylene required 12 hours at ambient temperature for complete reaction to occur. A comparison between the ^{11}B signals in the presence of excess dimethylsulfide is presented in **Table 4.2**.

Table 4.2: Hydroboration of selected alkene and alkyne substrates with $\text{Me}_2\text{S}\cdot\text{BH}_2(\text{C}_6\text{F}_5)$.

Substrate	Hydroboration product	^{11}B NMR chemical shift	Reaction time
	 (28)	7.1 ppm	< 1 min.
	 (29)	16 ppm	< 1 min.
	 (30)	-6.9 ppm	< 12 hr.
	 (31)	6.8 ppm	< 1 min.

^{11}B NMR spectroscopy confirms that upon reaction the signal for the starting material $\text{Me}_2\text{S}\cdot\text{BH}_2(\text{C}_6\text{F}_5)$, which appears as a sharp triplet at -17 ppm ($^1J_{\text{B,H}} = 105$ Hz), is replaced by a broad higher frequency singlet. In the absence of excess dimethylsulfide, the resonance for the product organoborane shifts in the ^{11}B NMR spectrum, indicating the presence of the equilibrium between bound and free dimethylsulfide in solution (**Scheme 4.6**). In contrast to the hydroboration products of bis(pentafluorophenyl)borane, the ^1H and ^{13}C NMR spectra indicate that the hydroboration products of mono(pentafluorophenyl)borane readily lose the dimethylsulfide ligand under vacuum to give the Lewis base-free boranes. The slightly decreased Lewis acidity of the

hydroboration products with one $-\text{C}_6\text{F}_5$ ring in comparison with those containing two $-\text{C}_6\text{F}_5$ rings weakens the dative interaction, resulting in facile donor loss under vacuum.

The use of $\text{Me}_2\text{S}\cdot\text{BH}_2(\text{C}_6\text{F}_5)$ as a hydroboration reagent towards two equivalents of substrate resulted in ^1H NMR spectra indicating anti-Markovnikov addition as the predominant reaction pathway. However, in contrast to results observed using $\text{Me}_2\text{S}\cdot\text{BH}(\text{C}_6\text{F}_5)_2$, spectral resonances and splitting patterns attributed to Markovnikov addition are in greater relative proportion. This indicates that the selectivity observed when using $\text{Me}_2\text{S}\cdot\text{BH}_2(\text{C}_6\text{F}_5)$, a singly substituted borane, as a hydroboration reagent is diminished in comparison with that of the disubstituted borane $\text{Me}_2\text{S}\cdot\text{BH}(\text{C}_6\text{F}_5)_2$. This result is not surprising, specifically in consideration of the relatively low selectivity observed for hydroboration reactions using fully unsubstituted BH_3 .⁴⁶ In the case of the hydroboration of the triple bond in trimethylsilylacetylene, the ^1H NMR spectrum of the final product, $\text{Me}_2\text{S}\cdot\text{B}(\text{CHCH}(\text{SiMe}_3))_2(\text{C}_6\text{F}_5)$, displays two sets of doublets of doublets at 7.34 and 6.16 ppm with $^3J_{\text{H,H}}$ values of 28 and 20 Hz, respectively. Based on the value for the vicinal coupling constant,^{281,282} the geometry about the carbon—carbon double bonds of $\text{Me}_2\text{S}\cdot\text{B}(\text{CHCH}(\text{SiMe}_3))_2(\text{C}_6\text{F}_5)$ is therefore *trans* for both alkyl groups, the same result observed with the use of $\text{Me}_2\text{S}\cdot\text{BH}(\text{C}_6\text{F}_5)_2$ as the hydroboration reagent.

Hydroboration of 1,1-diphenylethylene was slow for both $\text{Me}_2\text{S}\cdot\text{BH}(\text{C}_6\text{F}_5)_2$ and $\text{Me}_2\text{S}\cdot\text{BH}_2(\text{C}_6\text{F}_5)$, with the reaction being complete only after 12 hours. However, the lengthy reaction time proved to be rather insightful with respect to examining the nature of reaction pathways for the hydroboration reactions using $\text{Me}_2\text{S}\cdot\text{BH}_2(\text{C}_6\text{F}_5)$. The double hydroboration reaction of 1,1-diphenylethylene with $\text{Me}_2\text{S}\cdot\text{BH}_2(\text{C}_6\text{F}_5)$ was monitored by ^{19}F NMR spectroscopy over the course of 12 hours. Within one hour at ambient temperature, the crude reaction mixture contained three distinct sets of $-\text{C}_6\text{F}_5$ ^{19}F resonances, including those of the starting material $\text{Me}_2\text{S}\cdot\text{BH}_2(\text{C}_6\text{F}_5)$ (**Figure 4.2 – Figure 4.4**).

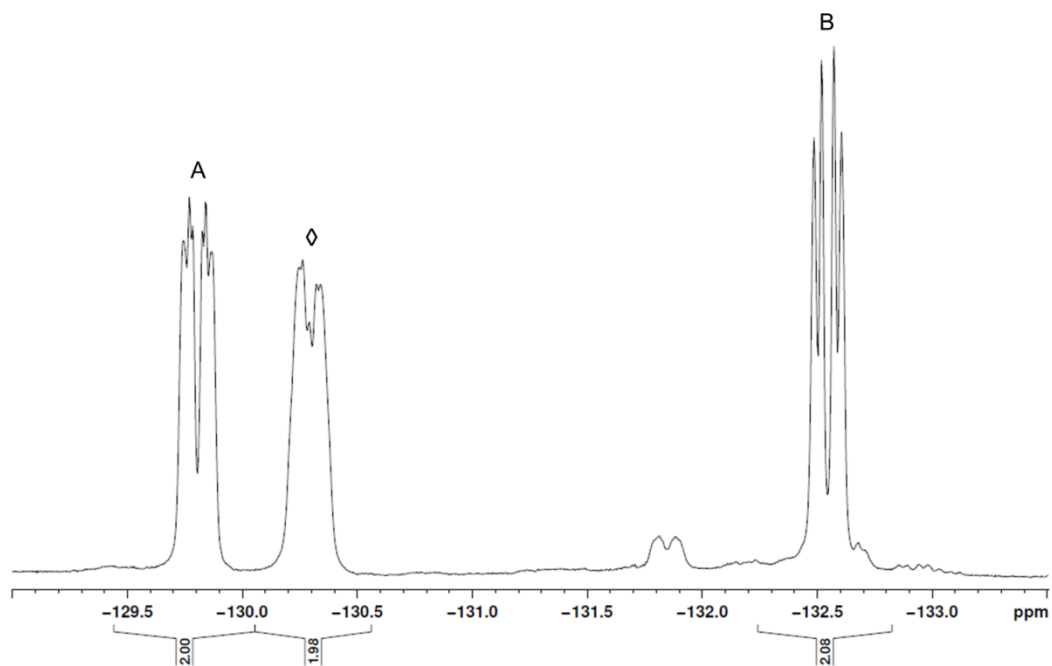


Figure 4.2: ^{19}F NMR spectrum showing three sets of ortho-fluorine resonances. The symbol \diamond indicates resonances associated with the starting material, $\text{Me}_2\text{S}\cdot\text{BH}_2(\text{C}_6\text{F}_5)$.

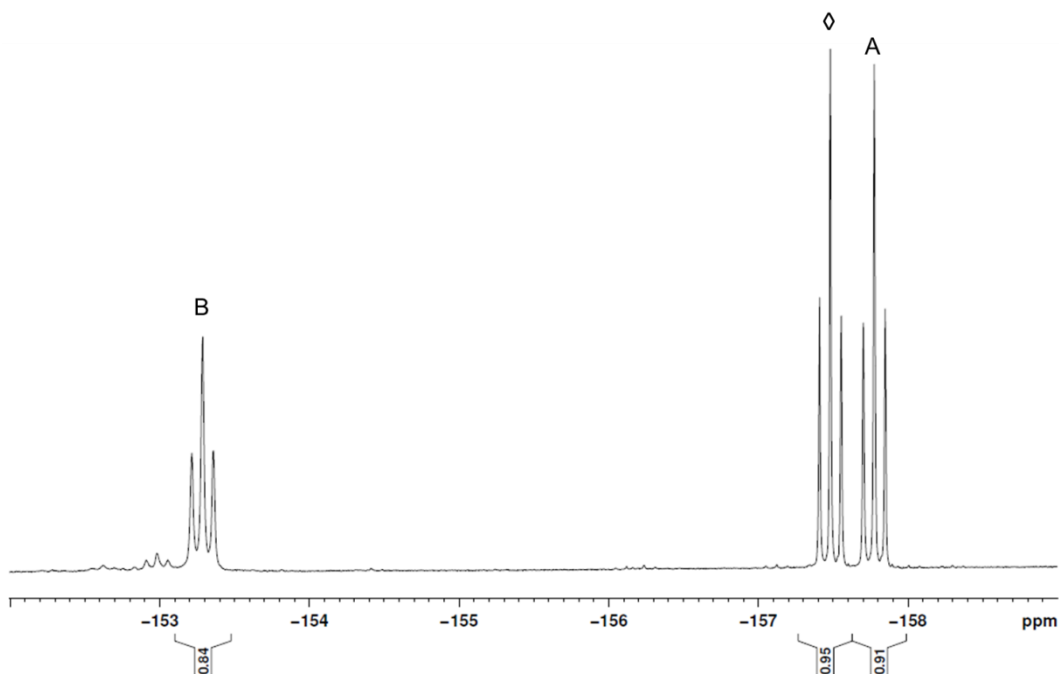


Figure 4.3: ^{19}F NMR spectrum showing three sets of para-fluorine resonances. The symbol \diamond indicates resonances associated with the starting material, $\text{Me}_2\text{S}\cdot\text{BH}_2(\text{C}_6\text{F}_5)$.

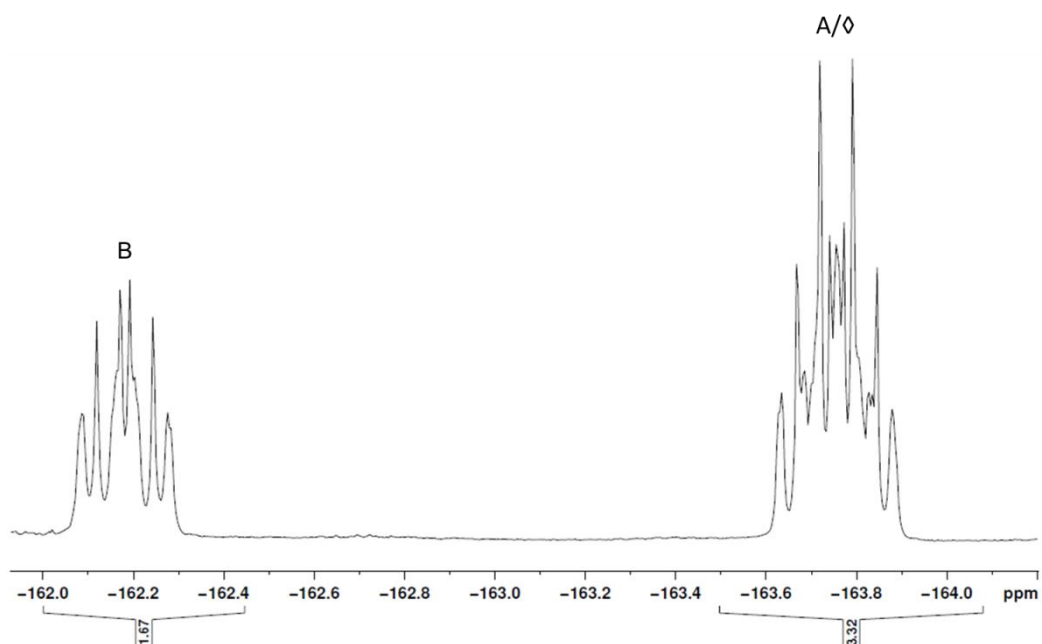


Figure 4.4: ^{19}F NMR spectrum showing three sets of meta-fluorine resonances (two overlapping). The symbol \diamond indicates resonances associated with the starting material, $\text{Me}_2\text{S}\cdot\text{BH}_2(\text{C}_6\text{F}_5)$.

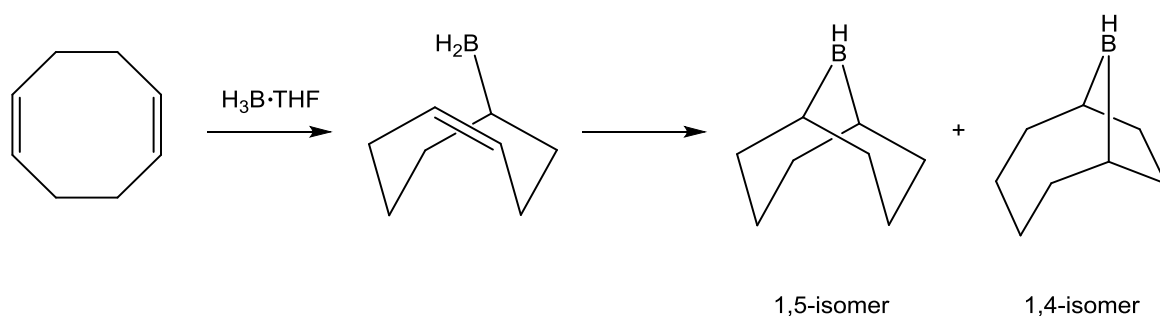
The remaining two sets of resonances have been attributed to the fully functionalized borane, $\text{Me}_2\text{S}\cdot\text{B}(\text{CH}_2\text{CHPh}_2)_2(\text{C}_6\text{F}_5)$ (**A**) and the singly hydroborated intermediate compound $\text{Me}_2\text{S}\cdot\text{B}(\text{CH}_2\text{CHPh}_2)(\text{H})(\text{C}_6\text{F}_5)$ (**B**). Identification of these three signals supports a proposed stepwise reaction pathway for double hydroboration reactions using $\text{Me}_2\text{S}\cdot\text{BH}_2(\text{C}_6\text{F}_5)$, and that the rate of the first and second hydroborations are similar at the beginning of the reaction. After 12 hours at room temperature, the ^{19}F NMR spectrum shows only those resonances assigned to the final product, $\text{Me}_2\text{S}\cdot\text{B}(\text{CH}_2\text{CHPh}_2)_2(\text{C}_6\text{F}_5)$. The intermediate species is not observed in the ^{11}B NMR spectrum, likely due to the corresponding ^{11}B resonance overlapping with that of the final product.

4.2.3 Double hydroboration of 1,5-cyclooctadiene with $\text{Me}_2\text{S}\cdot\text{BH}_2(\text{C}_6\text{F}_5)$

As previously noted, the earliest examples of hydroboration were reported using diborane, typically handled as the adduct $\text{thf}\cdot\text{BH}_3$ prepared *in situ*. The double hydroboration of 1,5-cyclooctadiene with $\text{thf}\cdot\text{BH}_3$ or $\text{Me}_2\text{S}\cdot\text{BH}_3$ produces 9-borabicyclo[3.3.1]nonane (9-BBN), itself a common hydroboration reagent, as a crystalline solid.^{278,283,284} The chloride, bromide, and iodide substituted derivatives of 9-BBN may be prepared through the starting boranes $\text{Me}_2\text{S}\cdot\text{BH}_2\text{X}$ where $\text{X} = \text{Cl}, \text{Br}$ and I .²⁸⁵ Although used frequently as a hydroboration reagent, 9-BBN exists as a dimer which requires dissolution prior to reactivity (**Section 4.1.1**).

The ambient temperature hydroboration of 1,5-cyclooctadiene by $\text{thf}\cdot\text{BH}_3$ proceeds to form both the 1,4- and 1,5-hydroborated products (**Scheme 4.8**).

Scheme 4.7: Room temperature double hydroboration of 1,5-cyclooctadiene.

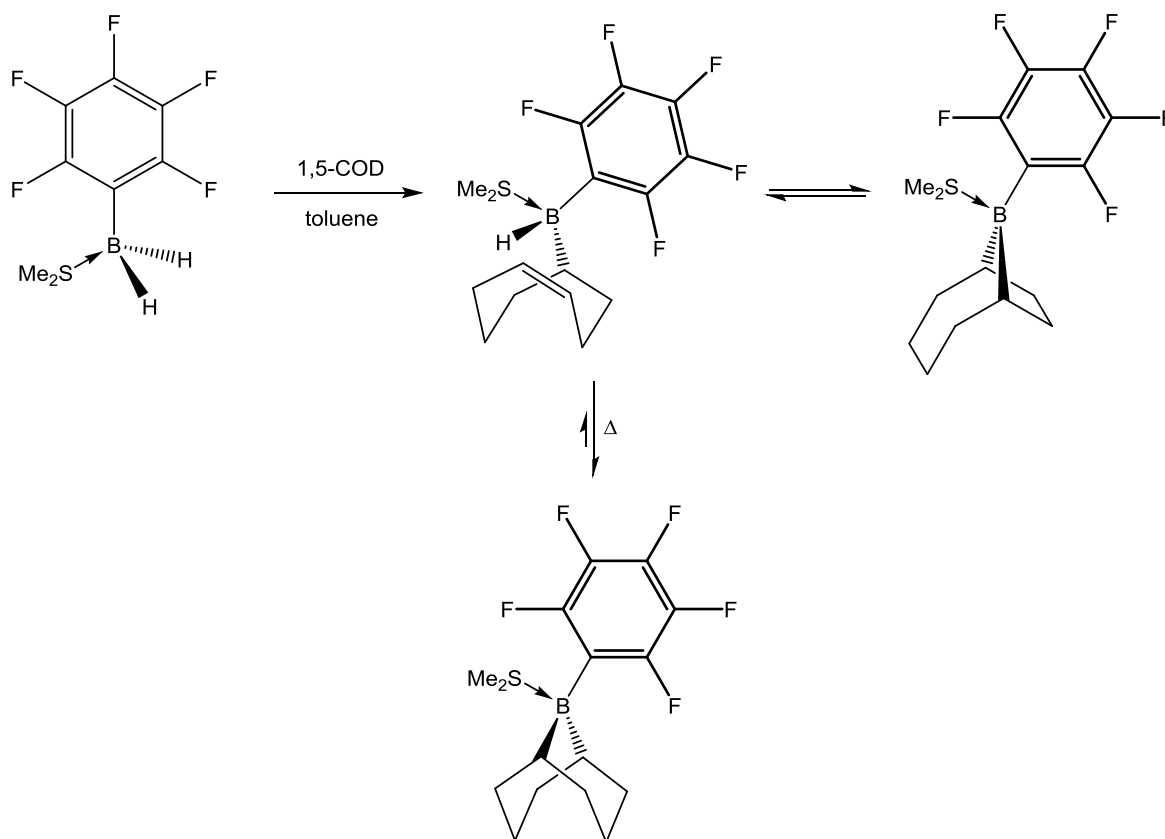


A thermodynamic consideration would conclude that the 1,5-isomer, containing two six membered rings, would be of lower energy than one five and one seven membered ring, as seen in the 1,4-isomer.²⁸⁶ Thermal isomerization of the reaction mixture facilitates the isolation of solely the 1,5-isomer. This process occurs through a retrohydroboration reaction to regenerate the intermediate singly hydroborated borane species which may

then undergo further hydroboration to generate the more stable 1,5-isomer. Once the 1,5-isomer is formed, the retrohydroboration becomes unfavorable and this enhances the solution stability of the 1,5-isomer to facilitate isolation.

Treatment of a toluene solution of 1,5-cyclooctadiene with one equivalent of $\text{Me}_2\text{S}\cdot\text{BH}_2(\text{C}_6\text{F}_5)$ at ambient temperature generates a reaction mixture with two major signals in the ^{11}B NMR spectrum. These have been assigned to the 1,4- and 1,5- isomers of the final product, consistent with the hydroboration chemistry of 1,5-cyclooctadiene with $\text{thf}\cdot\text{BH}_3$. Warming the crude reaction mixture to reflux for one hour produces the 1,5-isomer as the single reaction product in quantitative yield (**Scheme 4.9**).

Scheme 4.8: Double hydroboration of 1,5-cyclooctadiene using $\text{Me}_2\text{S}\cdot\text{BH}_2(\text{C}_6\text{F}_5)$.



Removal of the toluene and addition of a small amount of dimethylsulfide, followed by cooling to $-25\text{ }^{\circ}\text{C}$ affords colorless crystals of the pentafluorophenyl-9-borobicyclo[3.3.1]nonane dimethylsulfide adduct in 79% yield. Pentafluorophenyl-9-borobicyclo[3.3.1]nonane crystallizes as the dimethylsulfide Lewis adduct and features a near tetrahedral geometry about the boron atom (**Figure 4.5**). The C(11)—B(1)—C(7) bond angle measures $105.6(3)^{\circ}$, significantly smaller than the analogous C—B—C bond angle in dimeric 9-BBN ($111.6(2)^{\circ}$),²⁸⁷ but only slightly longer than the BBN-cycloalkane borate anions reported by Braunschweig and coworkers, ranging between $100.4(16)^{\circ}$ and $103.3(2)^{\circ}$.²⁸⁸

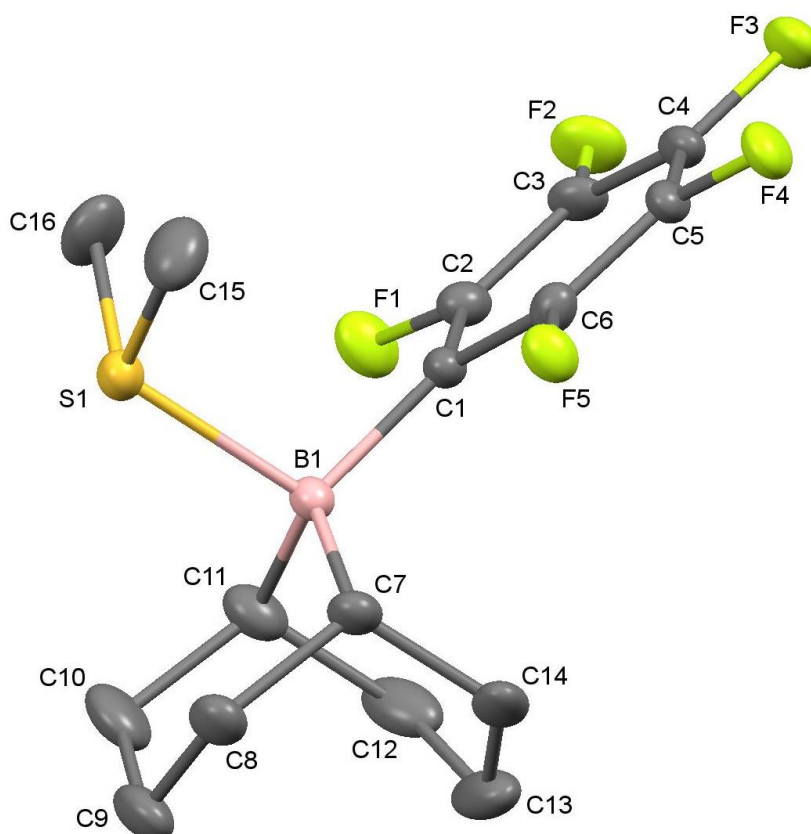


Figure 4.5: Crystal structure of pentafluorophenyl-9-borobicyclo[3.3.1]nonane dimethylsulfide adduct (**32**) with displacement ellipsoids displayed at the 50% probability level. Hydrogen atoms have been omitted for clarity.

4.3 Conclusions

Rapid and quantitative hydroboration of unhindered alkenes and alkynes is observed with the boranes $\text{Me}_2\text{S}\cdot\text{BH}(\text{C}_6\text{F}_5)_2$ and $\text{Me}_2\text{S}\cdot\text{BH}_2(\text{C}_6\text{F}_5)$ under mild reaction conditions. Use of these boranes allows for significantly less demanding reaction conditions in comparison with traditional hydroboration reagents such as BH_3 and 9-BBN. The high reaction selectivity with use of $\text{Me}_2\text{S}\cdot\text{BH}(\text{C}_6\text{F}_5)_2$ as a hydroboration reagent may be attributed to the high electrophilicity of the borane as a result of the electron withdrawing $-\text{C}_6\text{F}_5$ rings, a similar conclusion discussed for $[\text{HB}(\text{C}_6\text{F}_5)_2]_2$.⁴⁶ However, when used as a double hydroboration reagent, $\text{Me}_2\text{S}\cdot\text{BH}_2(\text{C}_6\text{F}_5)$ offers reduced overall reaction selectivity, as evidenced by the presence of a minor species in the resulting ^1H NMR spectra. Hydroboration of the sterically hindered 1,1-diphenylethylene with $\text{Me}_2\text{S}\cdot\text{BH}_2(\text{C}_6\text{F}_5)$ and $\text{Me}_2\text{S}\cdot\text{BH}(\text{C}_6\text{F}_5)_2$ requires a ambient temperature reaction time of 12 hours as a result of steric crowding from the large phenyl groups. In the case of the dihydroboration reaction, the intermediate species $(\text{Me}_2\text{S}\cdot\text{B}(\text{R})(\text{H})(\text{C}_6\text{F}_5))$ is observed in the ^{19}F NMR spectrum. Spectral analysis of the crude reaction mixture indicates that hydroboration occurs through a stepwise process, and that the lengthy reaction time is attributed to the sterically hindered substrate. In addition, the first and second hydroboration reactions appear to occur at a similar rate during the initial reaction stages. The alkyne trimethylsilylacetylene undergoes hydroboration in the presence of each reagent to produce *trans* organoborane products, confirmed through assessment of the vicinal coupling constants in the ^1H NMR spectra.

All of the hydroboration products were isolated as colorless solids or oils and are stable at ambient temperature either dried or in toluene solution. Of specific interest is the stability of the compound $\text{Me}_2\text{S}\cdot\text{B}(\text{CH}_2\text{CH}_2\text{Ph})(\text{C}_6\text{F}_5)_2$, formed from the hydroboration of styrene with $\text{Me}_2\text{S}\cdot\text{BH}(\text{C}_6\text{F}_5)_2$, which is inconsistent with results observed for the dimethylsulfide-free analog isolated from hydroboration using Piers' borane. While the unadducted borane $(\text{PhCH}_2\text{CH}_2)\text{B}(\text{C}_6\text{F}_5)_2$ undergoes further rearrangement to form the

thermodynamic product $(\text{PhCH}_2\text{CH}_2)_2\text{B}(\text{C}_6\text{F}_5)$, no such chemistry is observed for the dimethylsulfide adduct. This suggests that steric bulk provided by the dimethylsulfide ligand and occupation of the empty p-orbital on boron hinders further reactivity of the product. The double hydroboration of 1,5-cyclooctadiene using $\text{Me}_2\text{S}\cdot\text{BH}_2(\text{C}_6\text{F}_5)$ produces a mixture of the 1,4- and 1,5-isomer of the hydroboration product, similar to the result observed with the use of $\text{LB}\cdot\text{BH}_3$ ($\text{LB} = \text{thf}, \text{SMe}_2$). Thermal isomerization has led to the isolation and characterization of the pentafluorophenyl-9-borobicyclo[3.3.1]nonane dimethylsulfide adduct as a crystalline solid. In view of the facile preparation of $\text{Me}_2\text{S}\cdot\text{BH}(\text{C}_6\text{F}_5)_2$ and $\text{Me}_2\text{S}\cdot\text{BH}_2(\text{C}_6\text{F}_5)$ and the stability of the resulting hydroboration products, the dimethylsulfide adducts of mono- and bis-(pentafluorophenyl)borane should be useful additions to the myriad hydroboration reagents for organic synthesis and ligand modification.

Chapter 5 Experimental

All reactions were performed under a dry nitrogen or argon atmosphere using standard Schlenk techniques in flame-dried glassware. Solvents were dried using an appropriate drying agent and distilled under nitrogen prior to use; dichloromethane (CaH_2), light petroleum (sodium / dyglyme / benzophenone), tetrahydrofuran (sodium / benzophenone), diethyl ether (sodium / benzophenone) and toluene (sodium). NMR samples were prepared using degassed deuterated solvents dried over activated 4Å molecular sieves. NMR spectra were obtained using a Bruker Avance DPX300 spectrometer at 25 °C; J values are reported in Hz. Chemical shifts are reported in ppm and referenced to residual solvent resonances (^1H , ^{13}C); ^{19}F is relative to CFCl_3 ; ^{11}B is relative to $\text{Et}_2\text{O}\cdot\text{BF}_3$. IR spectra were recorded on a Bruker Vertex 80 in dried and degassed toluene. Elemental analyses were carried out at the Department of Health and Human Sciences, London Metropolitan University. Cp_2MCl_2 (M = Hf, Zr),²⁸⁹ $\text{Cp}_2\text{M}(\text{CH}_3)_2$ (M = Hf, Zr),²⁹⁰ Cp_2TiCl_2 ,²⁹¹ $\text{Cp}_2\text{Ti}(\text{PMe}_3)_2$,²⁹² $\text{Et}_2\text{O}\cdot\text{B}(\text{C}_6\text{F}_5)_3$,^{33,34} $\text{H}_3\text{N}\cdot\text{B}(\text{C}_6\text{F}_5)_3$,¹⁹² $\text{Me}_2\text{S}\cdot\text{BH}(\text{C}_6\text{F}_5)_2$, $\text{Me}_2\text{S}\cdot\text{BH}_2(\text{C}_6\text{F}_5)$,⁴⁷ $\text{H}_3\text{N}\cdot\text{BH}(\text{C}_6\text{F}_5)_2$, $\text{H}_3\text{N}\cdot\text{BH}_2(\text{C}_6\text{F}_5)$, $\text{Li}[\text{NH}_2\text{BH}_2(\text{C}_6\text{F}_5)]$ and $\text{Li}[\text{NH}_2\text{BH}(\text{C}_6\text{F}_5)_2]$ ¹⁰² were prepared according to literature procedures. Cp_2TiCl_2 and Me_2NH were purchased from Sigma-Aldrich and used without further purification. AgOTf was purchased from Sigma-Aldrich and recrystallized from dry toluene prior to use. Dimethylsulfide, cyclooctadiene and 12-crown-4 were purchased from Sigma-Aldrich and dried over 4Å molecular sieves and degassed prior to use. Pyridine and the amines PhNH_2 , $^t\text{BuNH}_2$, NEt_3 , BnNH_2 were purchased from Sigma-Aldrich and were distilled and dried over 4Å molecular sieves prior to use. Styrene was purchased from Sigma-Aldrich and passed through dry alumina prior to use. Trimethylsilylacetylene, 1,1-diphenylethylene and 1-hexene were purchased from Sigma-Aldrich and used without further purification.

Me₂HN·BH₂(C₆F₅) (1a)

Dimethylamine (1.1 mmol) was condensed and dissolved in light petroleum (10 mL) at $-78\text{ }^{\circ}\text{C}$. The dimethylamine solution was added to a solution of Me₂S·BH₂(C₆F₅) (0.27 g, 1.1 mmol) in toluene (40 mL). The reaction mixture was allowed to warm slowly to ambient temperature. All volatiles were removed and X-ray quality crystals of **1a** were grown from a toluene / light petroleum mixture at $-25\text{ }^{\circ}\text{C}$ (0.07 g, 0.28 mmol, 25%). Elemental analysis, calculated (found) for C₈H₉BF₅N: C, 42.71 (42.79); H, 4.03 (3.98); N, 6.23 (6.27). ¹H NMR (300.1 MHz, C₆D₆, 25 °C): δ 2.66 (br, 2H, BH₂), 2.47 (s, 1H, NH), 1.46 (m, 6H, CH₃). ¹³C NMR (75.5 MHz {¹H}, C₆D₆, 25 °C): δ 41.9 (CH₃). ¹¹B NMR (96.3 MHz, C₆D₆, 25 °C): δ -12.7 (t, ¹J_{B,H} = 102 Hz, BH₂). ¹⁹F NMR (282.4 MHz, C₆D₆, 25 °C): δ -132.21 (d, ³J_{F,F} = 23 Hz, 2F, *o*-F), -158.77 (t, ³J_{F,F} = 20 Hz, 1F, *p*-F), -163.98 (m, 2F, *m*-F).

^tBuH₂N·BH₂(C₆F₅) (1b)

Tert-butylamine (0.08 mL, 0.76 mmol) was added to a solution of Me₂S·BH₂(C₆F₅) (0.18 g, 0.74 mmol) in toluene (40 mL) at ambient temperature. The reaction mixture was stirred for 1 hour after which time all volatiles were removed to give a colorless powder. X-ray quality crystals of **1b** were grown at $-25\text{ }^{\circ}\text{C}$ from a toluene / light petroleum mixture (0.08 g, 0.32 mmol, 42%). Despite clean multinuclear NMR spectra (see Appendix), satisfactory elemental analysis data could not be obtained for **1b** despite several attempts. ¹H NMR (300.1 MHz, C₆D₆, 25 °C): δ 2.74 (br, 2H, BH₂), 2.46 (s, 2H, NH₂), 0.56 (s, 9H, CH₃). ¹³C NMR (75.5 MHz {¹H}, C₆D₆, 25 °C): δ 53.5 (C(CH₃)₃), 27.5 (C(CH₃)₃). ¹¹B NMR (96.3 MHz, C₆D₆, 25 °C): δ -19.6 (t, ¹J_{B,H} = 107 Hz, BH₂). ¹⁹F NMR (282.4 MHz, C₆D₆, 25 °C): δ -133.25 (d, ³J_{F,F} = 20 Hz, 2F, *o*-F), -159.33 (t, ³J_{F,F} = 21 Hz, 1F, *p*-F), -163.98 (m, 2F, *m*-F).

PhH₂N·BH₂(C₆F₅) (1c)

Aniline (0.18 mL, 1.97 mmol) was added to a solution of Me₂S·BH₂(C₆F₅) (0.48 g, 1.98 mmol) in toluene (40 mL) at ambient temperature. The reaction mixture was stirred for 1 hour after which time all volatiles were removed to give a colorless powder. X-ray quality crystals of **1c** were grown at 2 °C from a toluene / light petroleum mixture (0.23 g, 0.84 mmol, 43%). Elemental analysis, calculated (found) for C₁₂H₉BF₅N: C, 52.79 (52.68); H, 3.32 (3.47); N, 5.13 (5.19). ¹H NMR (300.1 MHz, C₆D₆, 25 °C): δ 6.74 (m, 3H, *m*-CH and *p*-CH), 6.42(m, 2H, *o*-H), 3.94 (s, 2H, NH₂), 2.98 (br, 2H, BH₂). ¹³C NMR (75.5 MHz {¹H}, C₆D₆, 25 °C): δ 137.9 (C_{ipso}), 129.3 (CH), 127.4 (CH), 121.7 (CH). ¹¹B NMR (96.3 MHz, C₆D₆, 25 °C): δ -14.0 (t, ¹J_{B,H} = 89 Hz, BH₂). ¹⁹F NMR (282.4 MHz, C₆D₆, 25 °C): δ -133.13 (d, ³J_{F,F} = 23 Hz, 2F, *o*-F), -158.63 (t, ³J_{F,F} = 21 Hz, 1F, *p*-F), -164.05 (m, 2F, *m*-F).

BnH₂N·BH₂(C₆F₅) (1d)

Benzylamine (0.12 mL, 1.1 mmol) was added to a solution of Me₂S·BH₂(C₆F₅) (0.26 g, 1.1 mmol) in toluene (40 mL) at ambient temperature and the reaction mixture was stirred for 1 hour. All volatiles were removed to give a colorless powder. X-ray quality crystals of **1d** were grown from a dichloromethane / light petroleum mixture at -25 °C (0.19 g, 0.66 mmol, 60%). Elemental analysis, calculated (found) for C₁₃H₁₁BF₅N: C, 54.40 (54.20); H, 3.86 (3.75); N, 4.88 (4.90). ¹H NMR (300.1 MHz, C₆D₆, 25 °C): δ 6.85 – 6.97 (m, 3H, *m*-CH and *p*-CH), 6.34 (d, ³J_{H,H} = 7.5 Hz, 2H, *o*-CH), 3.08 (m, 2H, CH₂), 2.75 (br, 2H, BH₂), 2.65 (s, 2H, NH₂). ¹³C NMR (75.5 MHz {¹H}, C₆D₆, 25 °C): δ 135.2 (C_{ipso}), 129.1 (CH), 128.8 (CH), remaining CH resonance obscured by C₆D₆ resonance, 50.9 (CH₂). ¹¹B NMR (96.3 MHz, C₆D₆, 25 °C): δ -16.1 (t, ¹J_{B,H} = 86 Hz, BH₂). ¹⁹F NMR (282.4 MHz, C₆D₆, 25 °C): δ -133.68 (d, ³J_{F,F} = 23 Hz, 2F, *o*-F), -159.25 (t, ³J_{F,F} = 20 Hz, 1F, *p*-F), -163.97 (m, 2F, *m*-F).

Et₃N·BH₂(C₆F₅) (1e)

Triethylamine (0.1 mL, 0.72 mmol) was added to a solution of Me₂S·BH₂(C₆F₅) (0.18 g, 0.74 mmol) in toluene (40 mL) at ambient temperature. The reaction mixture was stirred for 1 hour after which time all volatiles were removed to give a colorless oil. Despite clean multinuclear NMR spectra (see Appendix), isolation of **1e** as an oil prevented characterization by elemental analysis and X-ray diffraction. ¹H NMR (300.1 MHz, C₆D₆, 25 °C): δ 2.61 (br, 2H, BH₂), 2.14 (q, ³J_{H,H} = 7.2 Hz, 6H, CH₂), 0.72 (t, ³J_{H,H} = 7.2 Hz, 9H, CH₃). ¹³C NMR (75.5 MHz {¹H}, C₆D₆, 25 °C): δ 60.30 (CH₂), 8.11 (CH₃). ¹¹B NMR (96.3 MHz, C₆D₆, 25 °C): δ -13.89 (t, ¹J_{B,H} = 92 Hz, BH₂). ¹⁹F NMR (282.4 MHz, C₆D₆, 25 °C): δ -128.30 (d, ³J_{F,F} = 23 Hz, 2F, *o*-F), -158.08 (t, ³J_{F,F} = 21 Hz, 1F, *p*-F), -164.12 (m, 2F, *m*-F).

Py·BH₂(C₆F₅) (1f)

Pyridine (0.15 mL, 1.86 mmol) was added to a solution of Me₂S·BH₂(C₆F₅) (0.33 g, 1.36 mmol) in toluene (50 mL) at ambient temperature. The reaction mixture was stirred for 1 hour after which time all volatiles were removed to give a colorless powder. X-ray quality crystals of **1f** were grown at -25 °C from a dichloromethane / light petroleum mixture (0.14 g, 0.54 mmol, 40%). Elemental analysis, calculated (found) for C₁₁H₇BF₅N: C, 51.01 (50.94); H, 2.72 (2.58); N, 5.41 (5.50). ¹H NMR (300.1 MHz, C₆D₆, 25 °C): δ 7.98 (d, ³J_{H,H} = 5.0 Hz, 2H, *o*-CH), 6.49 (t, ³J_{H,H} = 7.6 Hz, 1H, *p*-CH), 6.13 (t, ³J_{H,H} = 7.9 Hz, 2H, *m*-CH), 3.91 (br, 2H, BH₂). ¹³C NMR (75.5 MHz {¹H}, C₆D₆, 25 °C): δ 147.3 (CH), 139.5 (CH), 125.3 (CH). ¹¹B NMR (96.3 MHz, C₆D₆, 25 °C): δ -10.3 (t, ¹J_{B,H} = 101 Hz, BH₂). ¹⁹F NMR (282.4 MHz, C₆D₆, 25 °C): δ -132.79 (d, ³J_{F,F} = 23 Hz, 2F, *o*-F), -159.20 (t, ³J_{F,F} = 20 Hz, 1F, *p*-F), -164.25 (m, 2F, *m*-F).

Me₂HN·BH(C₆F₅)₂ (2a)

Dimethylamine (1.4 mmol) was condensed and dissolved in light petroleum (10 mL) at -78 °C. The dimethylamine solution was added to a solution of Me₂S·BH(C₆F₅)₂ (0.57 g, 1.4 mmol) in toluene (40 mL). The reaction mixture was allowed to warm slowly to ambient temperature. All volatiles were removed and X-ray quality crystals of **2a** were grown from a toluene / light petroleum mixture by slowly cooling a concentrated solution from 50 °C to ambient temperature (0.17 g, 0.43 mmol, 31%). Elemental analysis, calculated (found) for C₈H₉BF₅N: C, 43.00 (42.96); H, 2.06 (1.91); N, 3.58 (3.64). ¹H NMR (300.1 MHz, C₆D₆, 25 °C): δ 3.79 (s, 1H, NH), 3.20 (br, 1H, BH₂), 1.36 (d, ³J_{H,H} = 5.5 Hz, 6H, CH₃). ¹³C NMR (75.5 MHz {¹H}, C₆D₆, 25 °C): δ 41.3 (CH₃). ¹¹B NMR (96.3 MHz, C₆D₆, 25 °C): δ -9.6 (d, ¹J_{B,H} = 87 Hz, BH). ¹⁹F NMR (282.4 MHz, C₆D₆, 25 °C): δ -134.15 (br, 4F, *o*-F), -157.24 (t, ³J_{F,F} = 20 Hz, 2F, *p*-F), -162.89 (m, 4F, *m*-F).

^tBuH₂N·BH(C₆F₅)₂ (2b)

Tert-butylamine (0.15 mL, 1.4 mmol) was added to a solution of Me₂S·BH(C₆F₅)₂ (0.57 g, 1.4 mmol) in toluene (20 mL) at ambient temperature. The reaction mixture was stirred for 1 hour and then light petroleum (10 mL) was added. X-ray quality crystals of **2b** were grown from this solution at 2 °C (0.11 g, 0.26 mmol, 19%). Elemental analysis, calculated (found) for C₁₆H₁₂BF₁₀N: C, 45.86 (45.98); H, 2.89 (3.00); N, 3.34 (3.38). ¹H NMR (300.1 MHz, C₆D₆, 25 °C): δ 3.68 (br, 1H, BH), 3.48 (s, 2H, NH₂), 0.53 (s, 9H, CH₃). ¹³C NMR (75.5 MHz {¹H}, C₆D₆, 25 °C): δ 55.2 (C(CH₃)₃), 27.4 (C(CH₃)₃). ¹¹B NMR (96.3 MHz, C₆D₆, 25 °C): δ -15.6 (d, ¹J_{B,H} = 96 Hz, BH). ¹⁹F NMR (282.4 MHz, C₆D₆, 25 °C): δ -134.17 (d, ³J_{F,F} = 20 Hz, 4F, *o*-F), -157.26 (t, ³J_{F,F} = 23 Hz, 2F, *p*-F), -162.96 (m, 2F, *m*-F).

PhH₂N·BH(C₆F₅)₂ (2c)

Aniline (0.13 mL, 1.4 mmol) was added to a solution of Me₂S·BH(C₆F₅)₂ (0.56 g, 1.4 mmol) in toluene (30 mL) at ambient temperature. The reaction mixture was stirred for 1 hour and then light petroleum (10 mL) was added. X-ray quality crystals of **2c** were grown from this solution at -25 °C (0.21 g, 0.48 mmol, 34%). Elemental analysis, calculated (found) for C₁₈H₈BF₁₀N: C, 49.24 (49.31); H, 1.84 (1.75); N, 3.19 (3.23). ¹H NMR (300.1 MHz, C₆D₆, 25 °C): δ 6.71 (m, 3H, *m*-CH and *p*-CH), 6.47 (m, 2H, *o*-H), 4.69 (s, 2H, NH₂), 3.84 (br, 2H, BH). ¹³C NMR (75.5 MHz {¹H}, C₆D₆, 25 °C): δ 135.9 (C_{ipso}), 129.5 (CH), 128.2 (CH), 122.1 (CH). ¹¹B NMR (96.3 MHz, C₆D₆, 25 °C): δ -11.2 (br, BH). ¹⁹F NMR (282.4 MHz, C₆D₆, 25 °C): δ -133.91 (d, ³J_{F,F} = 20 Hz, 4F, *o*-F), -156.79 (t, ³J_{F,F} = 20 Hz, 2F, *p*-F), -163.11 (m, 4F, *m*-F).

BnH₂N·BH(C₆F₅)₂ (2d)

Benzylamine (0.12 mL, 1.1 mmol) was added to a solution of Me₂S·BH(C₆F₅)₂ (0.44 g, 1.1 mmol) in toluene (20 mL). The reaction mixture was stirred for 1 hour at ambient temperature. All volatiles were removed to give a colorless solid. X-ray quality crystals of **2d** were grown from a toluene / light petroleum mixture at -25 °C (0.14 g, 0.3 mmol, 29%). Elemental analysis, calculated (found) for C₁₉H₁₀BF₁₀N: C, 50.37 (50.40); H, 2.22 (2.22); N, 3.09 (3.23). ¹H NMR (300.1 MHz, C₆D₆, 25 °C): δ 6.95 – 6.99 (m, 3H, *m*-CH and *p*-CH), 6.61 (m, 2H, *o*-CH), 3.63 (s, 2H, NH₂), 3.12 (m, 2H, CH₂), BH₂ resonance obscured by NH₂ and CH₂ resonances. ¹³C NMR (75.5 MHz {¹H}, C₆D₆, 25 °C): δ 134.3 (C_{ipso}), 129.4 (CH), 129.4 (CH), 128.5 (CH), 50.4 (CH₂). ¹¹B NMR (96.3 MHz, C₆D₆, 25 °C): δ -12.8 (br, BH). ¹⁹F NMR (282.4 MHz, C₆D₆, 25 °C): δ -134.51 (d, ³J_{F,F} = 23 Hz, 4F, *o*-F), -157.32 (t, ³J_{F,F} = 20 Hz, 2F, *p*-F), -163.07 (m, 4F, *m*-F).

Et₃N·BH(C₆F₅)₂ (2e)

Triethylamine (0.15 mL, 1.1 mmol) was added to a solution of Me₂S·BH(C₆F₅)₂ (0.44 g, 1.1 mmol) in toluene (20 mL) at ambient temperature. The reaction mixture was stirred for 1 hour and then light petroleum (10 mL) was added. X-ray quality crystals of **2e** were grown from this solution at -25 °C (0.34 g, 0.76 mmol, 68%). Elemental analysis, calculated (found) for C₁₉H₁₈BF₁₀N: C, 49.49 (49.38); H, 3.93 (3.81); N, 3.04 (3.12). ¹H NMR (300.1 MHz, C₆D₆, 25 °C): δ 3.67 (br, 1H, BH), 2.61 (q, ³J_{H,H} = 7.3 Hz, 6H, CH₂), 0.47 (t, ³J_{H,H} = 7.3 Hz, 9H, CH₃). ¹³C NMR (75.5 MHz {¹H}, C₆D₆, 25 °C): δ 51.3 (CH₂), 9.1(CH₃). ¹¹B NMR (96.3 MHz, C₆D₆, 25 °C): δ -8.4 (br, BH). ¹⁹F NMR (282.4 MHz, C₆D₆, 25 °C): δ -127.87 (d, ³J_{F,F} = 23 Hz, 4F, *o*-F), -157.42 (t, ³J_{F,F} = 21 Hz, 2F, *p*-F), -163.50 (m, 4F, *m*-F).

Py·BH(C₆F₅)₂ (2f)

Pyridine (0.13 mL, 1.6 mmol) was added to a solution of Me₂S·BH(C₆F₅)₂ (0.66 g, 1.6 mmol) in toluene (20 mL) at ambient temperature. The reaction mixture was stirred for 1 hour and then light petroleum (10 mL) was added. X-ray quality crystals of **2f** were grown from this solution at -25 °C (0.18 g, 0.37 mmol, 27%). Elemental analysis, calculated (found) for C₁₇H₆BF₁₀N: C, 48.04 (47.88); H, 1.42 (1.36); N, 3.30 (3.30). ¹H NMR (300.1 MHz, C₆D₆, 25 °C): δ 7.74 (d, ³J_{H,H} = 5.5 Hz, 2H, *o*-CH), 6.57 (t, ³J_{H,H} = 7.5 Hz, 1H, *p*-CH), 6.19 (t, ³J_{H,H} = 7.2 Hz, 2H, *m*-CH), 4.68 (br, 1H, BH). ¹³C NMR (75.5 MHz {¹H}, C₆D₆, 25 °C): δ 146.5 (CH), 140.6 (CH), 125.4 (CH). ¹¹B NMR(96.3 MHz, C₆D₆, 25 °C): δ -8.0 (d, ¹J_{B,H} = 90 Hz, BH). ¹⁹F NMR (282.4 MHz, C₆D₆, 25 °C): δ -133.36 (d, ³J_{F,F} = 25 Hz, 4F, *o*-F), -157.15 (t, ³J_{F,F} = 20 Hz, 2F, *p*-F), -163.52 (m, 4F, *m*-F).

Cp₂Zr(NH₂BH(C₆F₅)₂)₂ (3) and Cp₂Zr(H)(NH₂BH(C₆F₅)₂) (4)

A solution of Cp₂ZrCl₂ (0.14 g, 0.47 mmol) in toluene (20 mL) was cooled to -78 °C. To this a solution of Li[NH₂BH(C₆F₅)₂] (0.36 g, 0.99 mmol) prepared in toluene (5 mL) was added. The reaction mixture was allowed to stir for 20 min. at -78 °C and then for 1 hour at ambient temperature. The resulting solution was filtered and cooled to -25 °C, yielding Cp₂Zr(H)(NH₂BH(C₆F₅)₂) (4) (0.05 g, 0.08 mmol, 17%) and the dehydrocoupling product, {H₂NB(C₆F₅)₂}₃ (6). (Note: On one occasion Cp₂Zr(NH₂BH(C₆F₅)₂)₂ (3) was isolated as the major crystalline product.)

Elemental analysis, calculated (found) for Cp₂Zr(NH₂BH(C₆F₅)₂)₂ (3), C₃₄H₁₆B₂F₂₀N₂Zr: C, 43.20 (42.93); H, 1.71 (1.87); N, 2.96 (2.82).

Elemental analysis, calculated (found) for Cp₂Zr(H)(NH₂BH(C₆F₅)₂) (4), C₂₂H₁₄BF₁₀NZr: C, 45.22 (45.19); H, 2.41 (2.36); N, 2.40 (2.59). ¹H NMR (300.1 MHz, CD₂Cl₂, 25 °C): δ 5.7 (s, 10H, C₅H₅), 3.8 (d, ²J_{H,H} = 4.5 Hz, 1H, ZrH), 1.9 (s, 2H, NH₂), -0.71 (q, ¹J_{H,B} = 60 Hz, 1H, BH). ¹³C NMR (75.5 MHz {¹H}, CD₂Cl₂, 25 °C): δ 104.6 (C₅H₅). ¹¹B NMR (96.3 MHz, CD₂Cl₂, 25 °C): δ -25.6 (d, ¹J_{B,H} = 60 Hz, BH). ¹⁹F NMR (282.4 MHz, CD₂Cl₂, 25 °C): δ -134.40 (br, 4F, *o*-F), -158.10 (br, 2F, *p*-F), -163.69 (br, 4F, *m*-F). IR (ATR): ν 3366 (NH), 1884 (BH_{agostic}), 1559 (ZrH).

Cp₂Zr(Cl)(NH₂BH(C₆F₅)₂) (5)

Treatment of Cp₂Zr(H)(NH₂BH(C₆F₅)₂) (4) with dichloromethane over the course of 16 hours resulted in near quantitative conversion to Cp₂Zr(Cl)(NH₂BH(C₆F₅)₂) (5). Elemental analysis, calculated (found) for C₂₂H₁₃BClF₁₀NZr: C, 42.70 (42.60); H, 2.12 (1.98); N, 2.26 (2.35). ¹H NMR (300.1 MHz, CD₂Cl₂, 25 °C): δ 6.16 (s, 10H, C₅H₅), 2.9 (s, 2H, NH₂), -0.14 (q, ¹J_{H,B} = 60 Hz, 1H, BH). ¹³C NMR (75.5 MHz {¹H}, CD₂Cl₂, 25 °C): δ 113.8 (C₅H₅). ¹¹B NMR (96.3 MHz, CD₂Cl₂, 25 °C): δ -17.8 (d, ¹J_{B,H} = 64 Hz, BH).

^{19}F NMR (282.4 MHz, CD_2Cl_2 , 25 °C): δ -134.0 (br, 4F, *o*-F), -156.9 (t, $^3J_{\text{F,F}} = 20$ Hz, 2F, *p*-F), -162.7 (m, 4F, *m*-F).

$\{\text{H}_2\text{NB}(\text{C}_6\text{F}_5)_2\}_3$ (6**)**

A sample of $\{\text{H}_2\text{NB}(\text{C}_6\text{F}_5)_2\}_3$ was isolated following treatment of the crude reaction mixture from the preparation of **3** and **4** with dichloromethane and fractional crystallization at -25 °C. Elemental analysis, calculated (found) for $\text{C}_{36}\text{H}_6\text{BF}_{30}\text{N}$: C, 39.93 (39.93); H, 0.56 (0.58); N, 3.88 (3.75). ^1H NMR (300.1 MHz, CD_2Cl_2 , 25 °C): δ 4.9 (s, NH_2). ^{11}B NMR (96.3 MHz, CD_2Cl_2 , 25 °C): δ -5.2 (s). ^{19}F NMR (282.4 MHz, CD_2Cl_2 , 25 °C): δ -137.54 (m, 12F, *o*-F), -152.47 (t, $^3J_{\text{F,F}} = 20$ Hz, 6F, *p*-F), -160.57 (m, 12F, *m*-F).

$\text{Cp}''_2\text{Zr}(\text{CH}_3)(\text{NH}_2\text{BH}_2(\text{C}_6\text{F}_5))$ (8**)**

A toluene (5 mL) solution of $\text{B}(\text{C}_6\text{F}_5)_3$ (0.50 g, 1.0 mmol) was added to a solution of $\text{Cp}''_2\text{Zr}(\text{CH}_3)_2$ (0.53 g, 1.0 mmol) in toluene (4 mL) at -78 °C. To this a freshly prepared solution of $[\text{Li}(\text{thf})_x][\text{NH}_2\text{BH}_2(\text{C}_6\text{F}_5)]$ (1.0 mmol) in toluene (4 mL) was added at -78 °C. The reaction mixture was allowed to stir for 20 min. at -78 °C and then for 1 hour at ambient temperature. All volatiles were removed to yield a pasty yellow solid. The product was extracted with light petroleum (10 mL) and filtered through celite. X-ray quality crystals of **8** were obtained from a toluene solution cooled to -25 °C overnight (0.21 g, 0.29 mmol, 29%). Elemental analysis, calculated (found) for $\text{C}_{29}\text{H}_{49}\text{BF}_5\text{Si}_4\text{ZrN}$: C 48.30 (48.2), H 6.85 (6.9), N 1.94 (1.9). ^1H NMR (300.1 MHz, C_6D_6 , 25 °C): δ 6.4 (m, 4H, $\text{C}_5\text{H}_3(\text{Si}(\text{CH}_3)_3)_2$), 6.0 (m, 2H, $\text{C}_5\text{H}_3(\text{Si}(\text{CH}_3)_3)_2$), 1.7 (br, 2H, NH_2), 0.3 (s, 3H, CH_3), 0.184 (s, 18H, $\text{Si}(\text{CH}_3)_3$), 0.181 (s, 18H, $\text{Si}(\text{CH}_3)_3$). ^{13}C NMR (75.5 MHz $\{^1\text{H}\}$, C_6D_6 , 25 °C): δ 135.6 (CH), 119.0(CH), 115.5(CH), 21.2 (CH_3), 0.82 ($\text{Si}(\text{CH}_3)_3$), 0.68 ($\text{Si}(\text{CH}_3)_3$).

^{11}B NMR (96.3 MHz, C_6D_6 , 25 °C): δ -25.1 ppm (br, BH_2). ^{19}F NMR (282.4 MHz, C_6D_6 , 25 °C): δ -133.7 (m, 2F, *o*-F), -158.9 (t, $^3J_{\text{F,F}} = 21$ Hz, 1F, *p*-F), -163.8 (m, 2F, *m*-F).

$\text{Cp}^*\text{Zr}(\text{CH}_3)(\text{NH}_2\text{BH}(\text{C}_6\text{F}_5)_2)$ (9)

A solution of $\text{B}(\text{C}_6\text{F}_5)_3$ (0.50 g, 1.0 mmol) in toluene (5 mL) was added to a solution of $\text{Cp}^*\text{Zr}(\text{CH}_3)_2$ (0.53 g, 1.0 mmol) in toluene (4 mL) at -78 °C. To this a solution of $[\text{Li}(\text{thf})_x][\text{NH}_2\text{BH}(\text{C}_6\text{F}_5)_2]$ (1.0 mmol) in toluene (4 mL) was added at -78 °C. The reaction mixture was allowed to stir for 20 min. at -78 °C and then for 1 hour at ambient temperature. All volatiles were removed to yield a pasty yellow solid. The product was extracted with light petroleum (10 mL) and filtered through celite. X-ray quality crystals of **9** were obtained from a toluene solution cooled to -25 °C overnight (0.14 g, 0.16 mmol, 16%). Elemental analysis, calculated (found) for $\text{C}_{35}\text{H}_{48}\text{BF}_{10}\text{Si}_4\text{ZrN}$: C 47.39 (47.25), H 5.45 (5.37), N 1.58 (1.63). ^1H NMR (300.1 MHz, C_6D_6 , 25 °C): δ 6.4 (m, 2H, $\text{C}_5\text{H}_3(\text{Si}(\text{CH}_3)_3)_2$), 6.3 (m, 2H, $\text{C}_5\text{H}_3(\text{Si}(\text{CH}_3)_3)_2$), 6.0 (m, 2H, $\text{C}_5\text{H}_3(\text{Si}(\text{CH}_3)_3)_2$), 2.4 (br, 2H, NH_2), 0.4 (s, 3H, CH_3), 0.10 (s, 18H, $\text{Si}(\text{CH}_3)_3$), 0.09 (s, 18H, $\text{Si}(\text{CH}_3)_3$). ^{13}C NMR (75.5 MHz $\{^1\text{H}\}$, C_6D_6 , 25 °C): δ 134.9 (CH), 127.5 ($\underline{\text{C}}(\text{Si}(\text{CH}_3)_3)$), 122.0 (CH), 120.2 ($\underline{\text{C}}(\text{Si}(\text{CH}_3)_3)$), 116.9 (CH), 26.9 (CH_3), 0.6 ($\text{Si}(\text{CH}_3)_3$). ^{11}B NMR (96.3 MHz, C_6D_6 , 25 °C): δ -22.1 (d, $^1J_{\text{B,H}} = 74$ Hz, BH). ^{19}F NMR (282.4 MHz, C_6D_6 , 25 °C): δ -130.9 (br, 4F, *o*-F), -157.0 (t, $^3J_{\text{F,F}} = 20$ Hz, 2F, *p*-F), -162.3 ppm (m, 4F, *m*-F).

$\text{Cp}_2\text{Zr}(\text{CH}_3)(\text{NH}_2\text{BH}(\text{C}_6\text{F}_5)_2)$ (10)

A toluene (5 mL) solution of $\text{B}(\text{C}_6\text{F}_5)_3$ (0.24 g, 0.5 mmol) was added to a solution of $\text{Cp}_2\text{Zr}(\text{CH}_3)_2$ (0.1 g, 0.5 mmol) in toluene (4 mL) at -78 °C. A solution of $[\text{Li}(\text{thf})_x][\text{NH}_2\text{BH}(\text{C}_6\text{F}_5)_2]$ (0.5 mmol) in toluene (4 mL) was added at -78 °C. The reaction mixture was allowed to stir for 20 min. at -78 °C and then for 1 hour at ambient

temperature. All volatiles were removed to yield a clear yellow oil. The zirconocene product was extracted with light petroleum (10 mL) and filtered through celite. Compound **10** was crystallised from toluene at $-25\text{ }^{\circ}\text{C}$ overnight (0.04 g, mmol, 12%). Elemental analysis, calculated (found) for $\text{Cp}_2\text{Zr}(\text{CH}_3)(\text{NH}_2\text{BH}(\text{C}_6\text{F}_5)_2)\cdot\text{tol}$, $\text{C}_{30}\text{H}_{24}\text{BF}_{10}\text{ZrN}$: C, 52.18 (52.7), H 3.50 (2.3), N 2.03 (1.9). ^1H NMR (300.1 MHz, C_6D_6 , $25\text{ }^{\circ}\text{C}$): δ 5.2 (s, 10H, C_5H_5), 1.5 (br, 2H, NH_2), 0.03 (s, 3H, CH_3), 0.32 (q, $^1J_{\text{H,B}} = 66\text{ Hz}$, 1H, BH). ^{13}C NMR (75.5 MHz $\{^1\text{H}\}$, C_6D_6 , $25\text{ }^{\circ}\text{C}$): δ 110.1 (C_5H_5), 22.9 (CH_3). ^{11}B NMR (96.3 MHz, C_6D_6 , $25\text{ }^{\circ}\text{C}$): δ -22.8 (d, $^1J_{\text{B,H}} = 64\text{ Hz}$, BH). ^{19}F NMR (282.4 MHz, C_6D_6 , $25\text{ }^{\circ}\text{C}$): δ -133.96 (br, 4F, $o\text{-F}$), -156.07 (t, $^3J_{\text{F,F}} = 21\text{ Hz}$, 2F, $p\text{-F}$), -162.13 (m, 4F, $m\text{-F}$).

$\text{Cp}_2\text{Zr}(\text{CH}_3)(\text{NH}_2\text{BH}_2(\text{C}_6\text{F}_5))$ (11**)**

A toluene (5 mL) solution of $\text{B}(\text{C}_6\text{F}_5)_3$ (0.51 g, 1.0 mmol) was added to a solution of $\text{Cp}_2\text{Zr}(\text{CH}_3)_2$ (0.25 g, 1.0 mmol) in toluene (5 mL) at $-78\text{ }^{\circ}\text{C}$. A solution of $[\text{Li}(\text{thf})_x][\text{NH}_2\text{BH}_2(\text{C}_6\text{F}_5)]$ (1.0 mmol) in toluene (4 mL) was added at $-78\text{ }^{\circ}\text{C}$. The reaction mixture was allowed to stir for 20 min. at $-78\text{ }^{\circ}\text{C}$ and then for 1 hour at ambient temperature. All volatiles were removed to yield a pasty yellow solid. The zirconocene product was extracted with diethyl ether (10 mL) and filtered through celite. Despite multinuclear NMR spectra indicating product formation (see Appendix), X-ray quality crystals of **11** could not be isolated. *The following NMR assignments are based on the crude reaction spectra.* ^1H NMR (300.1 MHz, C_6D_6 , $25\text{ }^{\circ}\text{C}$): δ 5.3 (s, 10H, C_5H_5), 0.9 (br, 2H, NH_2), -0.12 (s, 3H, CH_3). The BH_2 resonance was not observed in the crude ^1H NMR spectrum. ^{11}B NMR (96.3 MHz, C_6D_6 , $25\text{ }^{\circ}\text{C}$): δ -25.3 (t, $^1J_{\text{B,H}} = 83\text{ Hz}$, BH_2). ^{19}F NMR (282.4 MHz, C_6D_6 , $25\text{ }^{\circ}\text{C}$): δ -135.62 (m, 2F, $o\text{-F}$), -158.85 (t, $^3J_{\text{F,F}} = 21\text{ Hz}$, 1F, $p\text{-F}$), -163.71 (m, 2F, $m\text{-F}$).

Cp₂Hf{NHBH(C₆F₅)₂} (12) and Cp₂Hf(NH₂BH(C₆F₅)₂)₂ (13)

A thf-free solution of Li[NH₂BH(C₆F₅)₂] (0.71 g, 1.92 mmol) in toluene (10 mL) was cooled to -78 °C and treated with a solution of Cp₂HfCl₂ (0.36 g, 0.96 mmol) in toluene (10 mL). The reaction was left to stir at -78 °C for two hours before warming to ambient temperature. The solvent was removed under reduced pressure and the crude product extracted with toluene (20 mL). Colorless crystals of **12** were obtained by concentrating the toluene solution, layering with light petroleum and cooling to -25 °C for 3 days (0.07 g, 0.10 mmol, 11%). (Note: On one occasion Cp₂Hf(NH₂BH(C₆F₅)₂)₂ (**13**) was isolated as the major crystalline product.) Elemental analysis, calculated (found) for Cp₂Hf{NHBH(C₆F₅)₂} (**12**), C₂₂H₁₂BF₁₀HfN: C, 39.46 (39.37); H, 1.81(1.69); N, 2.09 (1.97). ¹H NMR (300.1 MHz, C₇D₈, 25 °C): δ 7.59 (s, 1H, NH), 5.17 (s, 10H, C₅H₅), -0.83 (q, ¹J_{H,B} = 60 Hz, 1H, HB); ¹³C NMR (75.5 MHz {¹H}, C₆D₆, 25 °C): δ 103.6 (C₅H₅); ¹¹B NMR (96.3 MHz, C₇D₈, 25 °C): δ -27.5 (d, ¹J_{B,H} = 63 Hz, BH); ¹⁹F NMR (282.4 MHz, C₇D₈, 25 °C): δ -133.70 (br, 4F, *o*-F), -156.32 (t, ³J_{F,F} = 21 Hz, 2F, *p*-F), -162.45 (br, 4F, *m*-F).

Cp₂Hf(CH₃)(NH₂BH₂(C₆F₅)) (14)

A toluene (5 mL) solution of B(C₆F₅)₃ (0.51 g, 1.0 mmol) was added to a solution of Cp₂Hf(CH₃)₂ (0.34 g, 1.0 mmol) in toluene (5 mL) at -78 °C. A solution of [Li(thf)_x][NH₂BH₂(C₆F₅)] (1.0 mmol) in toluene (4 mL) was added at -78 °C. The reaction mixture was allowed to stir for 20 min. at -78 °C and then for 1 hour at ambient temperature. All volatiles were removed to yield a sticky white solid. The product was extracted with light petroleum (10 mL) and filtered through celite. Despite multinuclear NMR spectra indicating product formation (see Appendix), X-ray quality crystals of **14** could not be isolated. *The following tentative NMR assignments are based on the crude reaction spectra.* ¹H NMR (300.1 MHz, C₆D₆, 25 °C): δ 5.3 (s, 10H, C₅H₅), 1.0 (br, 2H, NH₂), -0.3 (s, 3H, CH₃). The BH₂ resonance was not observed in the crude ¹H NMR

spectrum. ^{11}B NMR (96.3 MHz, C_6D_6 , 25 °C): δ -25.8 (t, $^1J_{\text{B,H}} = 86$ Hz, BH_2).ⁱⁱ ^{19}F NMR (282.4 MHz, C_6D_6 , 25 °C): δ -137.01 (m, 2F, *o*-F), -158.60 (t, $^3J_{\text{F,F}} = 20$ Hz, 1F, *p*-F), -163.51 (m, 2F, *m*-F).

$\text{Cp}_2\text{Hf}(\text{CH}_3)(\text{NH}_2\text{BH}(\text{C}_6\text{F}_5)_2)$ (15)

A toluene (5 mL) solution of $\text{B}(\text{C}_6\text{F}_5)_3$ (0.72 g, 1.4 mmol) was added to a solution of $\text{Cp}_2\text{Zr}(\text{CH}_3)_2$ (0.47 g, 1.4 mmol) in toluene (4 mL) at -78 °C. A solution of $[\text{Li}(\text{thf})_x][\text{NH}_2\text{BH}(\text{C}_6\text{F}_5)_2]$ (1.4 mmol) in toluene (4 mL) was added at -78 °C. The reaction mixture was allowed to stir for 20 min. at -78 °C and then for 1 hour at ambient temperature. All volatiles were removed to yield a clear yellow oil. The product was extracted with light petroleum (10 mL), filtered through celite and was crystallised from toluene at -25 °C overnight (0.085 g, 0.12 mmol, 9%). Elemental analysis, calculated (found) for $\text{Cp}_2\text{Hf}(\text{CH}_3)(\text{NH}_2\text{BH}(\text{C}_6\text{F}_5)_2) \cdot \frac{1}{2} \text{tol}$, $\text{C}_{26.5}\text{H}_{20}\text{BF}_{10}\text{HfN}$: C 43.50 (43.35), H 2.75 (2.07), N 1.91 (1.67). ^1H NMR (300.1 MHz, C_6D_6 , 25 °C): δ 5.3 (s, 10H, C_5H_5), 1.7 (br, 2H, NH_2), -0.2 (s, 3H, CH_3), -0.36 (q, $^1J_{\text{H,B}} = 66$ Hz, 1H, HB). ^{13}C NMR (75.5 MHz $\{^1\text{H}\}$, C_6D_6 , 25 °C): δ 109.5 (C_5H_5), 26.4 (CH_3). ^{11}B NMR (96.3 MHz, C_6D_6 , 25 °C): δ -23.6 (d, $^1J_{\text{B,H}} = 67$ Hz, BH). ^{19}F NMR (282.4 MHz, C_6D_6 , 25 °C): δ -134.10 (br, 4F, *o*-F), -156.01 (t, $^3J_{\text{F,F}} = 21$ Hz, 2F, *p*-F), -162.03 (m, 4F, *m*-F).

$\text{Cp}_2\text{Ti}(\text{NH}_2\text{BH}_2(\text{C}_6\text{F}_5))$ (16)

A solution of Cp_2TiCl_2 (0.25 g, 1 mmol) in thf (5 mL) was treated with a thf solution of $\text{Li}[\text{NH}_2\text{BH}_2(\text{C}_6\text{F}_5)]$ (2.0 mmol) at ambient temperature. The reaction mixture immediately turned green and then blue, concomitant with the formation of a gaseous by-product (assumed to be dihydrogen). Removal of all solvents, extraction with toluene (15 mL)

ⁱⁱ A minor (1:3) ^{11}B resonance occurs at -24.3 ppm (t, $^1J_{\text{B,H}} = 67$ Hz).

and subsequent cooling to $-25\text{ }^{\circ}\text{C}$ yielded blue X-ray quality crystals of $\text{Cp}_2\text{Ti}(\text{NH}_2\text{BH}_2(\text{C}_6\text{F}_5))$ (**16**) (0.16 g, 0.44 mmol, 45%). Elemental analysis, calculated (found) for $\text{C}_{16}\text{H}_{14}\text{BF}_5\text{NTi}$: C, 51.39 (51.27); H, 3.77 (3.87); N, 3.75 (3.82). ^1H NMR (300.1 MHz, C_6D_6 , $25\text{ }^{\circ}\text{C}$): silent. ^{13}C NMR (75.5 MHz $\{^1\text{H}\}$, C_6D_6 , $25\text{ }^{\circ}\text{C}$): silent. ^{11}B NMR (96.3 MHz, C_6D_6 , $25\text{ }^{\circ}\text{C}$): silent. ^{19}F NMR (282.4 MHz, C_6D_6 , $25\text{ }^{\circ}\text{C}$): δ -135.40 (br, 2F, *o*-F), -159.42 (br, 1F, *p*-F), -163.55 (br, 2F, *m*-F). IR (toluene): ν 3444 (NH), 3365 (NH), 2391 (BH_{term}), 1841 ($\text{BH}_{\text{agostic}}$).

Compound **16** is also easily prepared from and one equivalent of $\text{Li}[\text{NH}_2\text{BH}_2(\text{C}_6\text{F}_5)]$ in thf at room temperature followed by extraction into toluene. No gaseous product is formed using the latter preparation method.

$\text{Cp}_2\text{Ti}(\text{NH}_2\text{BH}(\text{C}_6\text{F}_5)_2)$ (17**)**

A solution of Cp_2TiCl (0.21 g, 1 mmol) in thf (5 mL) was treated with a thf solution of $\text{Li}[\text{NH}_2\text{BH}(\text{C}_6\text{F}_5)_2]$ (1 mmol) at ambient temperature. The reaction mixture immediately turned a blue/purple color. Removal of all solvents, extraction with toluene and crystallization from a 1,2-difluorobenzene / light petroleum mixture yielded X-ray quality crystals of $\text{Cp}_2\text{Ti}(\text{NH}_2\text{BH}(\text{C}_6\text{F}_5)_2)$ (0.05 g, 0.1 mmol, 10%). Elemental analysis, calculated (found) for $\text{C}_{22}\text{H}_{13}\text{BF}_{10}\text{NTi}$: C, 48.93 (48.84); H, 2.43 (2.51); N, 2.59 (2.47). ^1H NMR (300.1 MHz, C_6D_6 , $25\text{ }^{\circ}\text{C}$): silent. ^{13}C NMR (75.5 MHz $\{^1\text{H}\}$, C_6D_6 , $25\text{ }^{\circ}\text{C}$): silent. ^{11}B NMR (96.3 MHz, C_6D_6 , $25\text{ }^{\circ}\text{C}$): silent. ^{19}F NMR (282.4 MHz, C_6D_6 , $25\text{ }^{\circ}\text{C}$): *o*-F and *m*-F are silent, -155.68 (br, 2F, *p*-F). IR (toluene): ν 3436 (NH), 3325 (NH), 1861 ($\text{BH}_{\text{agostic}}$).

[Li{thf}_x][NHPbBH(C₆F₅)₂] (19) and [Li{12-crown-4}₂][NHPbBH(C₆F₅)₂] (19a)

A solution of PhH₂N·BH(C₆F₅)₂ (0.60 g, 1.3 mmol) in thf (10 mL) was cooled to -78 °C and ⁿBuLi (1.6M, 0.81 mL, 1.3 mmol) was added dropwise to form **19** in quantitative yield. The crude reaction mixture was warmed to ambient temperature and 12-crown-4 (0.42 mL, 2.6 mmol) was added. Slow cooling of the thf solution to -25 °C yielding colorless crystals of **19a**.

Elemental analysis, calculated (found) for C₃₄H₃₉BF₁₀LiNO₈ (**19a**): C, 51.21 (50.88); H, 4.93 (4.83); N, 1.76 (1.66). ¹H NMR (300.1 MHz, CDCl₃, 25 °C): δ 6.93 (t, ³J_{H,H} = 7.5 Hz, 2H, *m*-CH), 6.73 (d, ³J_{H,H} = 7.6 Hz, 2H, *o*-CH), 6.35 (t, ³J_{H,H} = 6.9 Hz, 1H, *p*-CH), 4.49 (s, 1H, NH), 4.02 (br, 1H BH), 3.58 (s, 32H, CH₂). ¹¹B NMR (96.3 MHz, CDCl₃, 25 °C): δ -16.3 (d, ¹J_{B,H} = 92 Hz, BH). ¹⁹F NMR (282.4 MHz, CDCl₃, 25 °C): δ -134.87 (d, ³J_{F,F} = 23 Hz, 4F, *o*-F), -163.18 (t, ³J_{F,F} = 20 Hz, 2F, *p*-F), -166.04 (m, 4F, *m*-F).

[Li{thf}_x][NHPbBH₂(C₆F₅)] (20)

A solution of H₂PhN·BH₂(C₆F₅) (0.27 g, 1.0 mmol) in thf (5 mL) was cooled to -78 °C and ⁿBuLi (1.6M, 0.63 mL, 1.0 mmol) was added dropwise before warming the reaction mixture to ambient temperature. Removal of all solvents yielded a colorless pasty solid in quantitative yield. Despite clean multinuclear NMR spectra (see Appendix), satisfactory elemental analysis data could not be obtained despite several attempts. ¹H NMR (300.1 MHz, C₆D₆, 25 °C): δ 7.11 (t, ³J_{H,H} = 7.6 Hz, 2H, *m*-CH), 6.98 (d, ³J_{H,H} = 8.0 Hz, 2H, *o*-CH), 6.64 (t, ³J_{H,H} = 7.1 Hz, 1H, *p*-CH), NH and BH resonances are obscured by those of residual thf (3.42 ppm and 1.33 ppm). ¹¹B NMR (96.3 MHz, C₆D₆, 25 °C): δ -20.0 (t, ¹J_{B,H} = 84 Hz, BH₂). ¹⁹F NMR (282.4 MHz, C₆D₆, 25 °C): δ -134.82 (d, ³J_{F,F} = 20 Hz, 2F, *o*-F), -162.97 (t, ³J_{F,F} = 20 Hz, 1F, *p*-F), -165.81 (m, 2F, *m*-F).

[Li{12-crown-4}_x][NHPPhBH₂(C₆F₅)] (**20a**)

A solution of H₂PhN·BH₂(C₆F₅) (0.38 g, 1.4 mmol) in thf (10 mL) was cooled to -78 °C and ⁿBuLi (1.6M, 0.88 mL, 1.4 mmol) was added dropwise before warming the reaction mixture to ambient temperature. 12-crown-4 (0.22 mL, 1.4 mmol) was added before removal of all solvents to produce a colorless pasty solid. Despite clean multinuclear NMR spectra (see Appendix) X-ray quality crystals of **20a** could not be isolated. Elemental analysis, calculated (found) for C₂₀H₂₄BF₅LiNO₄: C, 52.78 (52.72); H, 5.32 (5.32); N, 3.08 (3.14). ¹H NMR (300.1 MHz, CDCl₃, 25 °C): δ 6.96 (t, ³J_{H,H} = 7.7 Hz, 2H, *m*-CH), 6.73 (d, ³J_{H,H} = 8.3 Hz, 2H, *o*-CH), 6.42 (t, ³J_{H,H} = 7.1 Hz, 1H, *p*-CH), 3.66 (s, 42H, CH₂), 3.40 (s, 1H, NH), 2.64 (br, 2H, BH₂). ¹¹B NMR (96.3 MHz, CDCl₃, 25 °C): δ -20.4 (t, ¹J_{B,H} = 88 Hz, BH₂). ¹⁹F NMR (282.4 MHz, CDCl₃, 25 °C): δ -134.32 (d, ³J_{F,F} = 23 Hz, 2F, *o*-F), -163.81 (t, ³J_{F,F} = 20 Hz, 1F, *p*-F), -166.34 (m, 2F, *m*-F).

Cp₂Zr(CH₃)(NHPPhBH₂(C₆F₅)) (**21**)

A toluene (5 mL) solution of B(C₆F₅)₃ (0.53 g, 1.0 mmol) was added to a solution of Cp₂Zr(CH₃)₂ (0.26 g, 1.0 mmol) in toluene (4 mL) at -78 °C. A solution of [Li(thf)_x][NHPPhBH(C₆F₅)₂] (1.0 mmol) dissolved in toluene (4 mL) was added at -78 °C. The reaction mixture was allowed to stir for 20 min. at -78 °C and then for 1 hour at ambient temperature. All volatiles were removed to yield a dark pink oil. The product was extracted with light petroleum (10 mL), filtered through celite, and reduced to dryness to give (**21**) as a pink sticky powder. Despite clean multinuclear NMR spectra (see Appendix), X-ray quality crystals of **21** could not be isolated. Elemental analysis, calculated (found) for C₂₃H₂₁BF₅NZr: C, 54.33 (54.12); H, 4.16 (3.95); N, 2.75 (2.82). ¹H NMR (300.1 MHz, C₆D₆, 25 °C): δ 7.10 (t, ³J_{H,H} = 7.8 Hz, 2H, *m*-CH), 6.83 – 6.88 (m, 3H, *o*-CH and *p*-CH), 3.72 (s, 1H, NH), 0.55 (br, 2H, BH₂), -0.18 (s, 3H, CH₃). ¹³C NMR (75.5 MHz {¹H}, C₆D₆, 25 °C): δ 148.2 (C_{ipso}), 128.7 (CH), 122.8 (CH), 120.7 (CH), 109.5

(C₅H₅), 24.4 (CH₃). ¹¹B NMR (96.3 MHz, C₆D₆, 25 °C): δ -22.65 (t, ¹J_{B,H} = 80 Hz, BH₂).
¹⁹F NMR (282.4 MHz, C₆D₆, 25 °C): δ -136.31 (d, ³J_{F,F} = 17 Hz, 2F, o-F), -158.17 (t, ³J_{F,F} = 21 Hz, 1F, p-F), -163.21 (m, 2F, m-F).

Cp₂Hf(CH₃)(NHPPhBH₂(C₆F₅)) (22)

A toluene (5 mL) solution of B(C₆F₅)₃ (0.53 g, 1.0 mmol) was added to a solution of Cp₂Hf(CH₃)₂ (0.35 g, 1.0 mmol) in toluene (4 mL) at -78 °C. A solution of [Li(thf)_x][NHPPhBH(C₆F₅)₂] (1.0 mmol) dissolved in toluene (4 mL) was added at -78 °C. The reaction mixture was allowed to stir for 20 min. at -78 °C and then for 1 hour at ambient temperature. All volatiles were removed to yield an orange oil. The product was extracted with light petroleum (10 mL), filtered through celite, and reduced to dryness to give a colorless free flowing powder (0.15 g, 0.025 mmol, 25%). X-ray quality crystals of **22** were isolated from a concentrated toluene solution at -25 °C. Elemental analysis, calculated (found) for C₂₃H₂₁BF₅NHf: C, 46.37 (46.27); H, 3.55 (3.51); N, 2.35 (2.46). ¹H NMR (300.1 MHz, C₆D₆, 25 °C): δ 7.10 (t, ³J_{H,H} = 7.7 Hz, 2H, *m*-CH), 6.86 (m, 3H, *o*-CH and *p*-CH), 3.82 (s, 1H, NH), 0.81 (br, 2H, BH₂), -0.29 (s, 3H, CH₃). ¹³C NMR (75.5 MHz {¹H}, C₆D₆, 25 °C): δ 147.8 (C_{ipso}), 128.6 (CH), 123.1 (CH), 121.1 (CH), 108.6 (C₅H₅), 25.9 (CH₃). ¹¹B NMR (96.3 MHz, C₆D₆, 25 °C): δ -23.2 (t, ¹J_{B,H} = 77 Hz, BH₂). ¹⁹F NMR (282.4 MHz, C₆D₆, 25 °C): δ -136.51 (m, 2F, *o*-F), -158.04 (t, ³J_{F,F} = 21 Hz, 1F, *p*-F), -163.14 (m, 2F, *m*-F).

Cp₂Ti(NHPPhBH₂(C₆F₅)) (23)

A solution of Cp₂TiCl₂ (0.25 g, 1 mmol) in thf (5 mL) was treated with a thf solution of Li[NHPPhBH₂(C₆F₅)] (2.0 mmol) at ambient temperature. The reaction mixture immediately turned green and then blue, concomitant with the formation of a gaseous by-product

(assumed to be dihydrogen). Removal of all solvents, extraction with toluene (15 mL) and subsequent cooling to $-25\text{ }^{\circ}\text{C}$ yielded blue X-ray quality crystals of $\text{Cp}_2\text{Ti}(\text{NHPPhBH}_2(\text{C}_6\text{F}_5))$ (**23**) (0.1 g, 0.22 mmol, 22%). Elemental analysis, calculated (found) for $\text{C}_{22}\text{H}_{18}\text{BF}_5\text{NTi}$: C, 58.71 (58.64); H, 4.03 (4.12); N, 3.11 (3.12). ^1H NMR (300.1 MHz, C_6D_6 , $25\text{ }^{\circ}\text{C}$): silent. ^{13}C NMR (75.5 MHz $\{^1\text{H}\}$, C_6D_6 , $25\text{ }^{\circ}\text{C}$): silent. ^{11}B NMR (96.3 MHz, C_6D_6 , $25\text{ }^{\circ}\text{C}$): silent. ^{19}F NMR (282.4 MHz, C_6D_6 , $25\text{ }^{\circ}\text{C}$): *o*-F is silent, -157.22 (br, 1F, *p*-F), -164.09 (br, 2F, *m*-F). IR (toluene): ν 3386 (NH), 2963 (CH), 2431 (BH_{term}), 2076 ($\text{BH}_{\text{agostic}}$), 2033 ($\text{BH}_{\text{agostic}}$).

Compound **23** is also easily prepared from the pre-reduced Cp_2TiCl and one molar equivalent of $\text{Li}[\text{NHPPhBH}_2(\text{C}_6\text{F}_5)]$ in thf at room temperature and extraction with toluene. No gaseous product is formed using the latter preparation method.

The following general procedure was used for compounds 24 – 31:

The substrate was added dropwise with stirring to a toluene solution of the borane dimethylsulfide adduct at ambient temperature. The reaction mixture was allowed to stir for 5 minutes, after which time the volatiles were removed under reduced pressure to give the product as a pale yellow oil in quantitative yield.

$\text{Me}_2\text{S}\cdot\text{B}(\text{CH}_2\text{CH}_2\text{Ph})(\text{C}_6\text{F}_5)_2$ (24**)**

^1H NMR (300.1 MHz, C_6D_6 , $25\text{ }^{\circ}\text{C}$): δ 6.97 – 7.21 (m, 5H, C_6H_5), 2.44 (m, 2H, BCH_2), 1.50 (t, $^3\text{J}_{\text{H,H}} = 8.3$ Hz, 2H, CH_2), 1.06 (s, 6H, $\text{S}(\text{CH}_3)_2$). ^{13}C NMR (75.5 MHz $\{^1\text{H}\}$, C_6D_6 , $25\text{ }^{\circ}\text{C}$): δ 145.9 (C_{ipso}), 129.9 (CH), 129.2 (CH), 128.4 (CH), 33.8 (CH_2), 24.5 (BCH_2), 19.6 ($\text{S}(\text{CH}_3)_2$). ^{11}B NMR (96.3 MHz, C_6D_6 , $25\text{ }^{\circ}\text{C}$): δ 1.0 (br). ^{19}F NMR (282.4 MHz, C_6D_6 , $25\text{ }^{\circ}\text{C}$): δ -130.65 (m, 4F, *o*-F), -155.98 (t, $^3\text{J}_{\text{F,F}} = 21$ Hz, 2F, *p*-F), -162.69 (m, 4F, *m*-F).

Me₂S·B((CH₂)₅CH₃)(C₆F₅)₂ (25)

¹H NMR (300.1 MHz, C₆D₆, 25 °C): δ 1.18–1.38 (m, 10H, CH₂), 1.08 (s, 6H, S(CH₃)₂), 0.86 (t, ³J_{H,H} = 6.7 Hz, 3H, CH₃). ¹³C NMR (75.5 MHz {¹H}, C₆D₆, 25 °C): δ 33.9 (CH₂), 32.7 (CH₂), 27.4 (CH₂), 23.8 (CH₂), 23.1 (BCH₂), 19.6 (S(CH₃)₂), 14.9 (CH₃). ¹¹B NMR (96.3 MHz, C₆D₆, 25 °C): δ 6.2 (br). ¹⁹F NMR (282.4 MHz, C₆D₆, 25 °C): δ -130.78 (m, 4F, *o*-F), -155.69 (t, ³J_{F,F} = 21 Hz, 2F, *p*-F), -162.75 (m, 4F, *m*-F).

Me₂S·B(CH₂CH(Ph))₂(C₆F₅)₂ (26)

¹H NMR (300.1 MHz, C₆D₆, 25 °C): δ 6.87–7.29 (m, 10H, C₆H₅), 3.87 (t, ³J_{H,H} = 6.7 Hz, 1H, CH), 2.15 (d, ³J_{H,H} = 6.7 Hz, 2H, CH₂), 0.95 (s, 6H, S(CH₃)₂). ¹³C NMR (75.5 MHz {¹H}, C₆D₆, 25 °C): δ 147.4 (C_{ipso}), 128.3 (CH), 127.3 (CH), 125.8 (CH), 49.9 (CH), 27.4 (BCH₂), 18.8 (S(CH₃)₂). ¹¹B NMR (96.3 MHz, C₆D₆, 25 °C): δ 1.6 (br). ¹⁹F NMR (282.4 MHz, C₆D₆, 25 °C): δ -130.04 (d, ³J_{F,F} = 20 Hz, 4F, *o*-F), -156.14 (t, ³J_{F,F} = 21 Hz, 2F, *p*-F), -162.85 (m, 4F, *m*-F).

Me₂S·B(CHCH(SiMe₃))(C₆F₅)₂ (27)

Elemental analysis, calculated (found) for C₁₉H₁₇BF₁₀SSi: C, 45.07 (44.98); H, 3.38 (3.30).

¹H NMR (300.1 MHz, CD₂Cl₂, 25 °C): δ 7.05 (dm, ³J_{H,H} = 21 Hz, 1H, CH), 5.92 (d, ³J_{H,H} = 21 Hz, 1H, CH), 2.12 (s, 6H, S(CH₃)₂), 0.07 (s, 9H, Si(CH₃)₃). ¹³C NMR (75.5 MHz {¹H}, CD₂Cl₂, 25 °C): δ 145.8 (CH), 117.4 (BCH), 20.6 (S(CH₃)₂), -1.2 (Si(CH₃)₃). ¹¹B NMR (96.3 MHz, CD₂Cl₂, 25 °C): δ -0.5 (br). ¹⁹F NMR (282.4 MHz, CD₂Cl₂, 25 °C): δ -130.91 (m, 4F, *o*-F), -157.20 (t, ³J_{F,F} = 20 Hz, 2F, *p*-F), -163.78 (m, 4F, *m*-F).

(C₆F₅)B(CH₂CH₂Ph)₂ (28)

¹H NMR (300.1 MHz, C₆D₆, 25 °C): δ 6.83 – 7.15 (m, 10H, C₆H₅), 2.60 (t, ³J_{H,H} = 7.7 Hz, 4H, BCH₂), 1.74 (t, ³J_{H,H} = 7.8 Hz, 4H, CH₂). ¹³C NMR (75.5 MHz {¹H}, C₆D₆, 25 °C): δ 144.2 (C_{ipso}), 129.3 (CH), 129.2 (CH), 126.8 (CH), 32.5 (BCH₂), 31.5 (CH₂). ¹¹B NMR (96.3 MHz, C₆D₆, 25 °C): δ 81.2 (br). ¹⁹F NMR (282.4 MHz, C₆D₆, 25 °C): δ -133.15 (m, 2F, *o*-F), -152.83 (t, ³J_{F,F} = 20 Hz, 1F, *p*-F), -161.55 (m, 2F, *m*-F).

(C₆F₅)B((CH₂)₅CH₃)₂ (29)

¹H NMR (300.1 MHz, C₆D₆, 25 °C): δ 1.16–1.52 (m, 20H, CH₂), 0.9 (t, ³J_{H,H} = 6.0 Hz, 6H, CH₃). ¹³C NMR (75.5 MHz {¹H}, C₆D₆, 25 °C): δ 33.3 (CH₂), 32.6 (CH₂), 31.8 (BCH₂), 25.4 (CH₂), 23.6 (CH₂), 14.8 (CH₃). ¹¹B NMR (96.3 MHz, C₆D₆, 25 °C): δ 84.9 (br). ¹⁹F NMR (282.4 MHz, C₆D₆, 25 °C): -133.80 (m, 2F, *o*-F), -153.51 (t, ³J_{F,F} = 20 Hz, 1F, *p*-F), -161.67 (m, 2F, *m*-F).

(C₆F₅)B(CH₂CH(Ph))₂ (30)

¹H NMR (300.1 MHz, C₆D₆, 25 °C): δ 6.93–7.31 (m, 20H, C₆H₅), 4.21 (t, ³J_{H,H} = 8.1 Hz, 2H, CH), 2.32 (d, ³J_{H,H} = 8.1 Hz, 4H, CH₂). ¹³C NMR (75.5 MHz {¹H}, C₆D₆, 25 °C): δ 145.9 (C_{ipso}), 128.5 (CH), 127.5 (CH), 126.2 (CH), 47.7 (CH), 38.5 (BCH₂). ¹¹B NMR (96.3 MHz, C₆D₆, 25 °C): δ 83.4 (br). ¹⁹F NMR (282.4 MHz, C₆D₆, 25 °C): δ -132.68 (m, 2F, *o*-F), -153.02 (t, ³J_{F,F} = 21 Hz, 1F, *p*-F), -162.07 (m, 2F, *m*-F).

(C₆F₅)B(CHCH(SiMe₃))₂ (31)

¹H NMR (300.1 MHz, C₆D₆, 25 °C): δ 7.34 (dd, ³J_{H,H} = 28 Hz, 2H, CH), 6.16 (dd, ³J_{H,H} = 20 Hz, 2H, CH), 0.08 (s, 9H, Si(CH₃)₃), 0.05 (s, 9H, Si(CH₃)₃). ¹³C NMR (75.5 MHz {¹H},

C₆D₆, 25 °C): δ 168.6 (CH), 141.7 (BCH), 0.13 (Si(CH₃)₃), -1.4 (Si(CH₃)₃). ¹¹B NMR (96.3 MHz, C₆D₆, 25 °C): δ 63.5 (br). ¹⁹F NMR (282.4 MHz, C₆D₆, 25 °C): δ -130.00 (m, 2F, *o*-F), -152.20 (t, ³J_{F,F} = 20 Hz, 1F, *p*-F), -161.95 (m, 2F, *m*-F).

Pentafluorophenyl-9-borobicyclo[3.3.1]nonane-SMe₂ (32)

A sample of Me₂S·BH₂(C₆F₅) (1.04 g, 4.3 mmol) was dissolved in toluene (75 mL). To this was added dropwise 1,5-cyclooctadiene (0.53 mL, 4.3 mmol) at ambient temperature. The mixture was heated to reflux for 1 hour. Once cooled, the toluene was removed to give a colorless oil. X-ray quality crystals were obtained by dissolution in 1 mL of neat dimethylsulfide and cooling to -25 °C. The conversion was quantitative by ¹¹B NMR spectroscopic analysis and the product was isolated as a colorless solid (1.18 g, 3.3 mmol, 79%). Elemental analysis, calculated (found) for C₁₆H₂₀BF₅S: C, 54.88 (54.81); H, 5.76 (5.67). ¹H NMR (300.1 MHz, C₆D₆, 25 °C): δ 1.58 – 2.17 (mm, 14H, CH and CH₂), 1.11 (s, 6H, S(CH₃)₂). ¹³C NMR (75.5 MHz {¹H}, C₆D₆, 25 °C): δ 33.3 (CH₂), 25.1 (CH₂), 24.3 (CH), 17.3 (S(CH₃)₂). ¹¹B NMR (96.3 MHz, C₆D₆, 25 °C): δ 19 (br). ¹⁹F NMR (282.4 MHz, C₆D₆, 25 °C): δ -130.40 (m, 2F, *o*-F), -155.25 (m, 1F, *p*-F), -162.87 (m, 2F, *m*-F).

Chapter 6 Crystallography

Suitable crystals were suspended in oil and mounted on a glass fiber prior to being put in the nitrogen stream of the diffractometer. With the exception of compound **2f**, all crystals were analyzed using Mo-K α radiation. Structural data for **1f**, **2a**, **9**, **12** and **32** was collected, solved and refined by Dr David Hughes (**1f** and **2a**), Dr Dan Smith (**32**) and Dr Joseph Wright (**9** and **12**) at the University of East Anglia using an Oxford Diffraction X-Calibur-3 CCD diffractometer equipped with a graphite monochromator. The data were processed using CrysAlisPro²⁹³ (**1f**, **2a**, **12**, **32**) or CrystalClear-SM²⁹⁴ (**9**) and the structures were refined in SHELXL.²⁹⁵ Structural data for the remaining compounds was collected by Dr Graham Tizzard at the National Crystallography Service,²⁹⁶ University of Southampton either on a Bruker-Nonis Apex II diffractometer equipped with confocal mirrors (**3**, **7**, **13**) or a Rigaku Saturn 724+ diffractometer equipped with a confocal micrometer (**1a-d**, **2b-e**, **6**, **8**, **10**, **16**, **17**, **18**, **19a**, **22** and **23**). The data were processed using DENZO and COLLECT²⁹⁷ (**3**, **7** and **13**) or CrystalClear-SM²⁹⁴ (**1a-d**, **2b-e**, **6**, **8**, **10**, **16**, **17**, **18**, **19a**, **22** and **23**) and refined using SHELXL.²⁹⁵ Data for compound **2f** was collected, refined and solved by Dr Graham Tizzard at the Diamond Light Source, Beamline I19 using Zr-K α radiation. The collected diffraction data was processed using CrystalClear-SM²⁹⁴ and refined using SHELXL.²⁹⁵ A consideration for crystallographic disorder observed for compound **13** was assessed and dismissed by Dr Simon Coles at the National Crystallography Service, University of Southampton.

Chapter 7 References

- (1) Frankland, E. *J. Chem. Soc.* **1862**, 363–381.
- (2) Piers, W. E.; Chivers, T. *Chem. Soc. Rev.* **1997**, 26, 345–354.
- (3) Piers, W. E. In *Advances in Organometallic Chemistry*; 2005; Vol. 52.
- (4) Erker, G. *Dalton Trans.* **2005**, 1883–1890.
- (5) Greenwood, N. N. *Coord. Chem. Rev.* **2002**, 226, 61–69.
- (6) Jones, D. S.; Lipscomb, W. N. *Acta Crystallogr. A* **1970**, 26, 196–207.
- (7) Dulmage, W. J.; Lipscomb, W. N. *Acta Crystallogr.* **1952**, 5, 260–264.
- (8) Kasper, J. S.; Lucht, C. M.; Harker, D. *J. Am. Chem. Soc.* **1948**, 70, 881.
- (9) Wade, K. *J. Chem. Soc. D Chem. Commun.* **1971**, 792–793.
- (10) Hirao, H.; Omoto, K.; Fujimoto, H. *J. Phys. Chem. A* **1999**, 103, 5807–5811.
- (11) Brown, H. C.; Holmes, R. R. *J. Am. Chem. Soc.* **1956**, 78, 2173–2176.
- (12) Shriver, D. F.; Swanson, B. *Inorg. Chem.* **1971**, 10, 1354–1365.
- (13) Pearson, R. G. *Inorg. Chem.* **1988**, 27, 734–740.
- (14) Yabroff, L.; Branch, G. E. K.; Almquist, H. J. *J. Am. Chem. Soc.* **1933**, 55, 2935–2941.
- (15) Wamser, C. A. *J. Am. Chem. Soc.* **1951**, 73, 409–416.
- (16) Johnson, A. R. *J. Phys. Chem.* **1912**, 16, 1–28.
- (17) Bowlus, H.; Nieuwland, J. A. *J. Am. Chem. Soc.* **1931**, 53, 3835–3840.
- (18) Kraus, C. A.; Brown, E. H. *J. Am. Chem. Soc.* **1929**, 51, 2690–2696.
- (19) Staubitz, A.; Robertson, A. P. M.; Sloan, M. E.; Manners, I. *Chem. Rev.* **2010**, 110, 4023–4078.
- (20) Sugden, S.; Waloff, M. *J. Chem. Soc.* **1932**, 1492–1497.
- (21) Zaidlewicz, M.; Kanth, J. V. B.; Brown, H. C. *J. Org. Chem.* **2000**, 65, 6697–6702.
- (22) Smith, K. *Chem. Soc. Rev.* **1974**, 3, 443–465.
- (23) Parsons, T. D.; Baker, E. D.; Burg, A. B.; Juvinal, G. L. *J. Am. Chem. Soc.* **1961**, 83, 250–251.

- (24) Stafford, S. L.; Stone, F. G. A. *J. Am. Chem. Soc.* **1960**, *82*, 6238–6240.
- (25) Massey, A. G.; Park, A. J.; Stone, F. G. A. *Proc. Chem. Soc.* **1963**, 212.
- (26) Danopoulos, A. A.; Galsworthy, J. R.; Green, M. L. H.; Cafferkey, S.; Doerrer, L. H.; Hursthouse, M. B. *Chem. Commun.* **1998**, 2529–2530.
- (27) Janiak, C.; Braun, L.; Scharmann, T. G.; Girgsdies, F. *Acta Crystallogr. C Commun.* **1998**, *54*, 1722–1724.
- (28) Doerrer, L. H.; Green, M. L. H. *J. Chem. Soc. Dalton Trans.* **1999**, 4325–4329.
- (29) Döring, S.; Erker, G.; Fröhlich, R.; Meyer, O.; Bergander, K. *Organometallics* **1998**, *17*, 2183–2187.
- (30) Jacobsen, H.; Berke, H.; Döring, S.; Kehr, G.; Erker, G.; Fröhlich, R.; Meyer, O. *Organometallics* **1999**, *18*, 1724–1735.
- (31) Beckett, M. A.; Brassington, D. S.; Coles, S. J.; Hursthouse, M. B. *Inorg. Chem. Commun.* **2000**, *3*, 530–533.
- (32) Chen, E. Y.-X.; Metz, M. V.; Li, L.; Stern, C. L.; Marks, T. J. *J. Am. Chem. Soc.* **1998**, *120*, 6287–6305.
- (33) Pohlmann, J. L. W.; Brinckmann, F. E. *Zeitschrift für Naturforsch.* **1965**, 5–11.
- (34) Lancaster, S. J. <http://cssp.chemspider.com/Article.aspx?id=215>.
- (35) Childs, R. F.; Mulholland, D. L.; Nixon, A. *Can. J. Chem.* **1982**, *60*, 801–808.
- (36) Mayer, U.; Gutmann, V.; Gerger, W. *Monatshefte für Chemie* **1975**, *106*, 1235–1257.
- (37) Yang, X.; Stern, C. L.; Marks, T. J. *J. Am. Chem. Soc.* **1991**, *113*, 3623–3625.
- (38) Yang, X.; Stern, C. L.; Marks, T. J. *J. Am. Chem. Soc.* **1994**, *116*, 10015–10031.
- (39) Bochmann, M. *J. Chem. Soc. Dalton Trans.* **1996**, 255–270.
- (40) Chen, E. Y.-X.; Marks, T. J. *Chem. Rev.* **2000**, *100*, 1391–1434.
- (41) Guerrero, A.; Hughes, D. L.; Bochmann, M. *Organometallics* **2006**, *25*, 1525–1527.
- (42) Ishihara, K.; Yamamoto, H. *European J. Org. Chem.* **1999**, 527–538.
- (43) Krossing, I.; Raabe, I. *Angew. Chem. Int. Ed.* **2004**, *43*, 2066–2090.
- (44) Chen, E.-X.; Lancaster, S. J. In *Comprehensive Inorganic Chemistry II*; Elsevier Ltd., 2013; Vol. 1, pp. 707–754.
- (45) Parks, D. J.; von H Spence, R. E.; Piers, W. E. *Angew. Chem. Int. Ed. Engl.* **1995**, *34*, 809–811.

- (46) Parks, D. J.; Piers, W. E.; Yap, G. P. A. *Organometallics* **1998**, *17*, 5492–5503.
- (47) Fuller, A.-M.; Hughes, D. L.; Lancaster, S. J.; White, C. M. *Organometallics* **2010**, *29*, 2194–2197.
- (48) Naumann, D.; Tyrre, W. *J. Chem. Soc. Chem. Commun.* **1989**, 47–50.
- (49) Frohn, H. J.; Jakobs, S. *J. Chem. Soc. Chem. Commun.* **1989**, 625–627.
- (50) Metzler, N.; Denkb, M. *Chem. Commun.* **1996**, 2657–2658.
- (51) Kalamarides, H. A.; Iyer, S.; Lipian, J.; Rhodes, L. F.; Day, C. *Organometallics* **2000**, *19*, 3983–3990.
- (52) Klosin, J.; Roof, G. R.; Chen, E. Y.-X.; Abboud, K. A. *Organometallics* **2000**, *19*, 4684–4686.
- (53) Walker, D. A.; Woodman, T. J.; Hughes, D. L.; Bochmann, M. *Organometallics* **2001**, *20*, 3772–3776.
- (54) Woodman, T. J.; Thornton-Pett, M.; Hughes, D. L.; Bochmann, M. *Organometallics* **2001**, *20*, 4080–4091.
- (55) Massey, A. G.; Park, A. J. *J. Organomet. Chem.* **1964**, *2*, 245–250.
- (56) Focante, F.; Mercandelli, P.; Sironi, A.; Resconi, L. *Coord. Chem. Rev.* **2006**, *250*, 170–188.
- (57) Blackwell, J. M.; Piers, W. E.; Parvez, M.; McDonald, R. *Organometallics* **2002**, *21*, 1400–1407.
- (58) Mountford, A. J.; Lancaster, S. J.; Coles, S. J.; Horton, P. N.; Hughes, D. L.; Hursthouse, M. B.; Light, M. E. *Inorg. Chem.* **2005**, *44*, 5921–5933.
- (59) Bradley, D. C.; Hursthouse, M. B.; Motevalli, M.; Dao-hong, Z. *J. Chem. Soc. Chem. Commun.* **1991**, 7–8.
- (60) Chase, P. A.; Parvez, M.; Piers, W. E. *Acta Crystallogr. E* **2006**, *62*, o5181–o5183.
- (61) Welch, G. C.; Cabrera, L.; Chase, P. A.; Hollink, E.; Masuda, J. D.; Wei, P.; Stephan, D. W. *Dalton Trans.* **2007**, 3407–3414.
- (62) Welch, G. C.; Stephan, D. W. *J. Am. Chem. Soc.* **2007**, *129*, 1880–1881.
- (63) Brown, H. C.; Schlesinger, H. I.; Cardon, S. Z. *J. Am. Chem. Soc.* **1942**, *64*, 325–329.
- (64) Stephan, D. W. *Org. Biomol. Chem.* **2008**, *6*, 1535–1539.
- (65) Welch, G. C.; San Juan, R. R.; Masuda, J. D.; Stephan, D. W. *Science* **2006**, *314*, 1124–1126.

- (66) Chase, P. A.; Welch, G. C.; Jurca, T.; Stephan, D. W. *Angew. Chem. Int. Ed.* **2007**, *46*, 8050–8053.
- (67) Stephan, D. W. *Dalton Trans.* **2009**, 3129–36.
- (68) Stephan, D. W.; Erker, G. *Angew. Chem. Int. Ed.* **2010**, *49*, 46–76.
- (69) Erker, G. *Dalton Trans.* **2011**, *40*, 7475–83.
- (70) Mömming, C. M.; Otten, E.; Kehr, G.; Fröhlich, R.; Grimme, S.; Stephan, D. W.; Erker, G. *Angew. Chem. Int. Ed.* **2009**, *48*, 6643–6646.
- (71) Otten, E.; Neu, R. C.; Stephan, D. W. *J. Am. Chem. Soc.* **2009**, *131*, 9918–9919.
- (72) Zhao, X.; Stephan, D. W. *Chem. Sci.* **2012**, *3*, 2123–2132.
- (73) Dobrovetsky, R.; Stephan, D. W. *J. Am. Chem. Soc.* **2013**, *135*, 4974–4977.
- (74) Miller, A. J. M.; Bercaw, J. E. *Chem. Commun.* **2010**, *46*, 1709–1711.
- (75) Chapman, A. M.; Haddow, M. F.; Wass, D. F. *J. Am. Chem. Soc.* **2011**, *133*, 8826–8829.
- (76) Chapman, A. M.; Wass, D. F. *Dalton Trans.* **2012**, *41*, 9067–9072.
- (77) Appelt, C.; Sloatweg, J. C.; Lammertsma, K.; Uhl, W. *Angew. Chem. Int. Ed.* **2013**, *52*, 4256–4259.
- (78) Satyapal, S.; Petrovic, J.; Read, C.; Thomas, G.; Ordaz, G. *Catal. Today* **2007**, *120*, 246–256.
- (79) Schlapbach, L.; Züttel, A. *Nature* **2001**, *414*, 353–358.
- (80) Schüth, F.; Bogdanović, B.; Felderhoff, M. *Chem. Commun.* **2004**, 2249–2258.
- (81) Sakintuna, B.; Lamari-Darkrim, F.; Hirscher, M. *Int. J. Hydrogen Energy* **2007**, *32*, 1121–1140.
- (82) Dillon, A. C.; Jones, K. M.; Bekkedahl, T. A.; Kiang, C. H.; Bethune, D. S.; Heben, M. J. *Nature* **1997**, *386*, 377–379.
- (83) Rowsell, J. L. C.; Yaghi, O. M. *Angew. Chem. Int. Ed.* **2005**, *44*, 4670–4769.
- (84) Collins, D. J.; Zhou, H.-C. *J. Mater. Chem.* **2007**, *17*, 3154–3160.
- (85) Chua, Y. S.; Chen, P.; Wu, G.; Xiong, Z. *Chem. Commun.* **2011**, *47*, 5116–5129.
- (86) Xiong, Z.; Yong, C. K.; Wu, G.; Chen, P.; Shaw, W.; Karkamkar, A.; Autrey, T.; Jones, M. O.; Johnson, S. R.; Edwards, P. P.; David, W. I. F. *Nat. Mater.* **2008**, *7*, 138–41.

- (87) Diyabalanage, H. V. K.; Nakagawa, T.; Shrestha, R. P.; Semelsberger, T. A.; Davis, B. L.; Scott, B. L.; Burrell, A. K.; David, W. I. F.; Ryan, K. R.; Jones, M. O.; Edwards, P. P. *J. Am. Chem. Soc.* **2010**, *132*, 11836–11837.
- (88) Diyabalanage, H. V. K.; Shrestha, R. P.; Semelsberger, T. A.; Scott, B. L.; Bowden, M. E.; Davis, B. L.; Burrell, A. K. *Angew. Chem. Int. Ed.* **2007**, *46*, 8995–8997.
- (89) Stephens, F. H.; Pons, V.; Baker, R. T. *Dalton Trans.* **2007**, 2613–2626.
- (90) Staubitz, A.; Robertson, A. P. M.; Manners, I. *Chem. Rev.* **2010**, *110*, 4079–4124.
- (91) Denney, M. C.; Pons, V.; Hebden, T. J.; Heinekey, D. M.; Goldberg, K. I. *J. Am. Chem. Soc.* **2006**, *128*, 12048–12049.
- (92) Waterman, R. *Chem. Soc. Rev.* **2013**, *42*, 5629–5641.
- (93) Aldridge, S.; Downs, A. J.; Tang, C. Y.; Parsons, S.; Clarke, M. C.; Johnstone, R. D. L.; Robertson, H. E.; Rankin, D. W. H.; Wann, D. A. *J. Am. Chem. Soc.* **2009**, *131*, 2231–2243.
- (94) Paine, R. T.; Narula, C. K. *Chem. Rev.* **1990**, *90*, 73–91.
- (95) Whittell, G. R.; Manners, I. *Angew. Chem. Int. Ed.* **2011**, *50*, 10288–10289.
- (96) Stubbs, N. E.; Jurca, T.; Leitao, E. M.; Woodall, C. H.; Manners, I. *Chem. Commun.* **2013**, *49*, 9098–9100.
- (97) Fazen, P. J.; Remsen, E. E.; Beck, J. S.; Carroll, P. J.; McGhie, A. R.; Sneddon, L. G. *Chem. Mater.* **1995**, *7*, 1942–1956.
- (98) Jiang, C.; Blacque, O.; Berke, H. *Organometallics* **2009**, *28*, 5233–5239.
- (99) Wang, Y.; Chen, W.; Lu, Z.; Li, Z. H.; Wang, H. *Angew. Chem. Int. Ed.* **2013**, *52*, 7496–7499.
- (100) Mountford, A. J.; Hughes, D. L.; Lancaster, S. J. *Chem. Commun.* **2003**, 2148–2149.
- (101) Jacobs, E. A.; Fuller, A.-M.; Lancaster, S. J.; Wright, J. A. *Chem. Commun.* **2011**, *47*, 5870–5872.
- (102) Jacobs, E. A.; Fuller, A.; Coles, S. J.; Jones, G. A.; Tizzard, G. J.; Wright, J. A.; Lancaster, S. J. *Chem. Eur. J.* **2012**, *18*, 8647–8658.
- (103) Wu, H.; Zhou, W.; Yildirim, T. *J. Am. Chem. Soc.* **2008**, *130*, 14834–14839.
- (104) Zhang, Q.; Tang, C.; Fang, C.; Fang, F.; Sun, D.; Ouyang, L.; Zhu, M. *J. Phys. Chem. C* **2010**, *114*, 1709–1714.
- (105) Fijalkowski, K. J.; Genova, R. V.; Filinchuk, Y.; Budzianowski, A.; Derzsi, M.; Jaroń, T.; Leszczyński, P. J.; Grochala, W. *Dalton Trans.* **2011**, *40*, 4407–4413.

- (106) Wu, H.; Zhou, W.; Pinkerton, F. E.; Meyer, M. S.; Yao, Q.; Gadipelli, S.; Udovic, T. J.; Yildirim, T.; Rush, J. J. *Chem. Commun.* **2011**, *47*, 4102–4104.
- (107) Tang, Z.; Tan, Y.; Chen, X.; Yu, X. *Chem. Commun.* **2012**, *48*, 9296–7298.
- (108) Kim, D. Y.; Singh, N. J.; Lee, H. M.; Kim, K. S. *Chem. Eur. J.* **2009**, *15*, 5598–5604.
- (109) Wolstenholme, D. J.; Titah, J. T.; Che, F. N.; Trabousee, K. T.; Flogeras, J.; McGrady, G. S. *J. Am. Chem. Soc.* **2011**, *133*, 16598–16604.
- (110) Forster, T. D.; Tuononen, H. M.; Parvez, M.; Roesler, R. *J. Am. Chem. Soc.* **2009**, *131*, 6689–6691.
- (111) Wolstenholme, D. J.; Trabousee, K. T.; Decken, A.; McGrady, G. S. *Organometallics* **2010**, *29*, 5769–5772.
- (112) Helten, H.; Dutta, B.; Vance, J. R.; Sloan, M. E.; Haddow, M. F.; Sproules, S.; Collison, D.; Whittell, G. R.; Lloyd-Jones, G. C.; Manners, I. *Angew. Chem. Int. Ed.* **2013**, *52*, 437–440.
- (113) Mountford, A. J.; Clegg, W.; Coles, S. J.; Harrington, R. W.; Horton, P. N.; Humphrey, S. M.; Hursthouse, M. B.; Wright, J. A.; Lancaster, S. J. *Chem. Eur. J.* **2007**, *13*, 4535–4547.
- (114) Paetzold, P. In *Advances in Inorganic Chemistry*; Emeléus, H. J.; Sharpe, A. G., Eds.; Elsevier Ltd., 1987; Vol. 31, pp. 123–170.
- (115) Klooster, W. T.; Koetzle, T. F.; Siegbahn, P. E. M.; Richardson, T. B.; Crabtree, R. H. *J. Am. Chem. Soc.* **1999**, *121*, 6337–6343.
- (116) Malcolm, A. C.; Sabourin, K. J.; McDonald, R.; Ferguson, M. J.; Rivard, E. *Inorg. Chem.* **2012**, *51*, 12905–12916.
- (117) Hamilton, C. W.; Baker, R. T.; Staubitz, A.; Manners, I. *Chem. Soc. Rev.* **2009**, *38*, 279–293.
- (118) Bøddeker, K. W.; Shore, S. G.; Bunting, R. K. *J. Am. Chem. Soc.* **1966**, *88*, 4396–4401.
- (119) Paetzold, P. *Pure Appl. Chem.* **1991**, *63*, 345–350.
- (120) Ma, K.; Scheibitz, M.; Scholz, S.; Wagner, M. *J. Organomet. Chem.* **2002**, *652*, 11–19.
- (121) Schlesinger, H. I.; Burg, A. B. *J. Am. Chem. Soc.* **1938**, *60*, 290–299.
- (122) Schultz, D. R.; Parry, R. W. *J. Am. Chem. Soc.* **1958**, *80*, 4–8.
- (123) Shore, S. G.; Parry, R. W. *J. Am. Chem. Soc.* **1958**, *80*, 8–12.
- (124) Chen, X.; Zhao, J.-C.; Shore, S. G. *Acc. Chem. Res.* **2013**, *46*, 2666–75.

- (125) Davis, B. L.; Dixon, D. A.; Garner, E. B.; Gordon, J. C.; Matus, M. H.; Scott, B.; Stephens, F. H. *Angew. Chem. Int. Ed.* **2009**, *48*, 6812–6186.
- (126) Sutton, A. D.; Burrell, A. K.; Dixon, D. A.; Garner, E. B.; Gordon, J. C.; Nakagawa, T.; Ott, K. C.; Robinson, J. P.; Vasiliu, M. *Science* **2011**, *331*, 1426–1429.
- (127) Summerscales, O. T.; Gordon, J. C. *Dalton Trans.* **2013**, *42*, 10075–10084.
- (128) Li, H.; Yang, Q.; Chen, X.; Shore, S. G. *J. Organomet. Chem.* **2013**, 1–7.
- (129) Shore, S. G.; Parry, R. W. *J. Am. Chem. Soc.* **1955**, *77*, 6084–6085.
- (130) Chen, X.; Bao, X.; Billet, B.; Shore, S. G.; Zhao, J.-C. *Chem. Eur. J.* **2012**, *18*, 11994–11999.
- (131) Hughes, E. W. *J. Am. Chem. Soc.* **1956**, *78*, 502–503.
- (132) Lippert, E. L.; Libscomb, W. N. *J. Am. Chem. Soc.* **1956**, *78*, 503–504.
- (133) Van Nes, G. J. H.; Vos, A. *Acta Crystallogr. B* **1978**, *34*, 1947–1956.
- (134) Frueh, S.; Kellett, R.; Mallery, C.; Molter, T.; Willis, W. S.; King'onde, C.; Suib, S. L. *Inorg. Chem.* **2011**, *50*, 783–792.
- (135) Sewell, L. J.; Lloyd-Jones, G. C.; Weller, A. S. *J. Am. Chem. Soc.* **2012**, *134*, 3598–3610.
- (136) Pons, V.; Baker, R. T.; Szymczak, N. K.; Heldebrant, D. J.; Linehan, J. C.; Matus, M. H.; Grant, D. J.; Dixon, D. A. *Chem. Commun.* **2008**, 6597–6599.
- (137) Friedrich, A.; Drees, M.; Schneider, S. *Chem. Eur. J.* **2009**, *15*, 10339–10342.
- (138) Stevens, C. J.; Dallanegra, R.; Chaplin, A. B.; Weller, A. S.; Macgregor, S. A.; Ward, B.; McKay, D.; Alcaraz, G.; Sabo-Etienne, S. *Chem. Eur. J.* **2011**, *17*, 3011–3020.
- (139) Johnson, H. C.; Robertson, A. P. M.; Chaplin, A. B.; Sewell, L. J.; Thompson, A. L.; Haddow, M. F.; Manners, I.; Weller, A. S. *J. Am. Chem. Soc.* **2011**, *133*, 11076–11079.
- (140) Vance, J. R.; Robertson, A. P. M.; Lee, K.; Manners, I. *Chem. Eur. J.* **2011**, *17*, 4099–4103.
- (141) Jaska, C. A.; Temple, K.; Lough, A. J.; Manners, I. *J. Am. Chem. Soc.* **2003**, *125*, 9424–9434.
- (142) Staubitz, A.; Sloan, M. E.; Robertson, A. P. M.; Friedrich, A.; Schneider, S.; auf der Günne, J. S.; Manners, I. *J. Am. Chem. Soc.* **2010**, *132*, 13332–13345.
- (143) Tang, C. Y.; Thompson, A. L.; Aldridge, S. *Angew. Chem. Int. Ed.* **2010**, *49*, 921–925.

- (144) Tang, C. Y.; Thompson, A. L.; Aldridge, S. *J. Am. Chem. Soc.* **2010**, *132*, 10578–10591.
- (145) Vidovic, D.; Addy, D. A.; Krämer, T.; McGrady, J.; Aldridge, S. *J. Am. Chem. Soc.* **2011**, *133*, 8494–8497.
- (146) Euzenat, L.; Horhant, D.; Ribourdouille, Y.; Duriez, C.; Alcaraz, G.; Vaultier, M. *Chem. Commun.* **2003**, 2280–2281.
- (147) Keaton, R. J.; Blacquiere, J. M.; Baker, R. T. *J. Am. Chem. Soc.* **2007**, *129*, 1844–1845.
- (148) Clark, T. J.; Russell, C. a; Manners, I. *J. Am. Chem. Soc.* **2006**, *128*, 9582–9583.
- (149) Pun, D.; Lobkovsky, E.; Chirik, P. J. *Chem. Commun.* **2007**, 3297–3299.
- (150) Sloan, M. E.; Staubitz, A.; Clark, T. J.; Russell, C. a; Lloyd-Jones, G. C.; Manners, I. *J. Am. Chem. Soc.* **2010**, *132*, 3831–3841.
- (151) Blaquiere, N.; Diallo-Garcia, S.; Gorelsky, S. I.; Black, D. A.; Fagnou, K. *J. Am. Chem. Soc.* **2008**, *130*, 14034–14035.
- (152) Käß, M.; Friedrich, A.; Drees, M.; Schneider, S. *Angew. Chem. Int. Ed.* **2009**, *48*, 905–907.
- (153) Sewell, L. J.; Huertos, M. A.; Dickinson, M. E.; Weller, A. S.; Lloyd-Jones, G. C. *Inorg. Chem.* **2013**, *52*, 4509–4516.
- (154) Bochmann, M. *J. Organomet. Chem.* **2004**, *689*, 3982–3998.
- (155) Brookhart, M.; Grant, B.; Volpe, Jr., A. F. *Organometallics* **1992**, *11*, 3920–3922.
- (156) Dunitz, J. D.; Taylor, R. *Chem. Eur. J.* **1997**, *3*, 89–98.
- (157) Lancaster, S. J.; Rodriguez, A.; Lara-Sanchez, A.; Hannant, M. D.; Walker, D. A.; Hughes, D. H.; Bochmann, M. *Organometallics* **2002**, *21*, 451–453.
- (158) Etter, M. C. *J. Phys. Chem.* **1991**, *95*, 4601–4610.
- (159) Fuller, A.-M.; Mountford, A. J.; Scott, M. L.; Coles, S. J.; Horton, P. N.; Hughes, D. L.; Hursthouse, M. B.; Lancaster, S. J. *Inorg. Chem.* **2009**, *48*, 11474–11482.
- (160) Dagonne, S.; Janowska, I.; Welter, R.; Zakrzewski, J.; Jaouen, G. *Organometallics* **2004**, *23*, 4706–4710.
- (161) Chase, P. A.; Stephan, D. W. *Angew. Chem. Int. Ed.* **2008**, *47*, 7433–7437.
- (162) Chase, P. A.; Jurca, T.; Stephan, D. W. *Chem. Commun.* **2008**, 1701–1703.
- (163) O'Hagan, D.; Rzepa, H. S. *Chem. Commun.* **1997**, 645–652.
- (164) Barbarich, T. J.; Rithner, C. D.; Miller, S. M.; Anderson, O. P.; Strauss, S. H. *J. Am. Chem. Soc.* **1999**, *121*, 4280–4281.

- (165) Reichenbächer, K.; Süß, H. I.; Hulliger, J. *Chem. Soc. Rev.* **2005**, *34*, 22–30.
- (166) Chopra, D.; Row, T. N. G. *Cryst. Eng. Commun.* **2011**, *13*, 2175–2186.
- (167) Berger, R.; Resnati, G.; Metrangolo, P.; Weber, E.; Hulliger, J. *Chem. Soc. Rev.* **2011**, *40*, 3496–3508.
- (168) Ewing, W. C.; Carroll, P. J.; Sneddon, L. G. *Inorg. Chem.* **2013**, *52*, 10690–7.
- (169) Ullrich, M.; Lough, A. J.; Stephan, D. W. *J. Am. Chem. Soc.* **2009**, *131*, 52–53.
- (170) Voss, T.; Mahdi, T.; Otten, E.; Fröhlich, R.; Kehr, G.; Stephan, D. W.; Erker, G. *Organometallics* **2012**, *31*, 2367–2378.
- (171) Bochmann, M. *Acc. Chem. Res.* **2010**, *43*, 1267–1278.
- (172) Millot, N.; Santini, C. C.; Fenet, B.; Basset, J. M. *Eur. J. Inorg. Chem.* **2002**, 3328–3335.
- (173) Parks, D. J.; Piers, W. E. *J. Am. Chem. Soc.* **1996**, *7863*, 9440–9441.
- (174) Blackwell, J. M.; Foster, K. L.; Beck, V. H.; Piers, W. E. *J. Org. Chem.* **1999**, *64*, 4887–4892.
- (175) Blackwell, J. M.; Sonmor, E. R.; Scoccitti, T.; Piers, W. E. *Org. Lett.* **2000**, *2*, 3921–3923.
- (176) Röttger, D.; Schmuck, S.; Erker, G. *J. Organomet. Chem.* **1996**, *508*, 263–265.
- (177) Plečnik, C. E.; Liu, F.-C.; Liu, S.; Liu, J.; Meyers, E. A.; Shore, S. G. *Organometallics* **2001**, *20*, 3599–3606.
- (178) Ding, E.; Liu, F.-C.; Liu, S.; Meyers, E. A.; Shore, S. G. *Inorg. Chem.* **2002**, *41*, 5329–5335.
- (179) Yan, K.; Upton, B. M.; Ellern, A.; Sadow, A. D. *J. Am. Chem. Soc.* **2009**, *131*, 15110–15111.
- (180) Helten, H.; Robertson, A. P. M.; Staubitz, A.; Vance, J. R.; Haddow, M. F.; Manners, I. *Chem. Eur. J.* **2012**, *18*, 4665–4680.
- (181) Kelly, H. C.; Marchelli, F. R.; Giusto, M. B. *Inorg. Chem.* **1964**, *3*, 431–437.
- (182) Camacho, C.; Uribe, G.; Contreras, R. *Synthesis* **1982**, 1027–1030.
- (183) Brown, H. C.; Murray, L. T. *Inorg. Chem.* **1984**, *23*, 2746–2753.
- (184) Brown, H. C.; Zaidlewicz, M.; Dalvi, P. V. *Organometallics* **1998**, *17*, 4202–4205.
- (185) Crabtree, R. H. *Angew. Chem. Int. Ed. Engl.* **1993**, *32*, 789–805.
- (186) Labinger, J. A.; Bercaw, J. E. *Nature* **2002**, *417*, 507–514.

- (187) Clark, T. J.; Lee, K.; Manners, I. *Chem. Eur. J.* **2006**, *12*, 8634–8648.
- (188) Jaska, C. A.; Temple, K.; Lough, A. J.; Manners, I. *Chem. Commun.* **2001**, *2*, 962–963.
- (189) Kawano, Y.; Uruichi, M.; Shimoj, M.; Taki, S.; Kawaguchi, T.; Kakizawa, T.; Ogino, H. *J. Am. Chem. Soc.* **2009**, *131*, 14946–14957.
- (190) Hill, M. S.; Kociok-Köhn, G.; Robinson, T. P. *Chem. Commun.* **2010**, *46*, 7587–7589.
- (191) Miyazaki, T.; Tanabe, Y.; Yuki, M.; Miyake, Y.; Nishibayashi, Y. *Organometallics* **2011**, *30*, 2394–2404.
- (192) Mountford, A. J.; Clegg, W.; Harrington, R. W.; Humphrey, S. M.; Lancaster, S. J. *Chem. Commun.* **2005**, 2044–2046.
- (193) Fuller, A.-M.; Clegg, W.; Harrington, R. W.; Hughes, D. L.; Lancaster, S. J. *Chem. Commun.* **2008**, 5776–5778.
- (194) Fuller, A.-M.; Hughes, D. L.; Lancaster, S. J. *Dalton Trans.* **2011**, *40*, 7434–7441.
- (195) Fuller, A.-M.; Hughes, D. L.; Jones, G. A.; Lancaster, S. J. *Dalton Trans.* **2012**, *41*, 5599–5609.
- (196) Göttker-Schnetmann, I.; White, P.; Brookhart, M. *J. Am. Chem. Soc.* **2004**, *126*, 1804–1811.
- (197) Tang, C. Y.; Phillips, N.; Bates, J. I.; Thompson, A. L.; Gutmann, M. J.; Aldridge, S. *Chem. Commun.* **2012**, *48*, 8096–8098.
- (198) Kim, S.-K.; Han, W.-S.; Kim, T.-J.; Kim, T.-Y.; Nam, S. W.; Mitoraj, M.; Piekoś, Ł.; Michalak, A.; Hwang, S.-J.; Kang, S. O. *J. Am. Chem. Soc.* **2010**, *132*, 9954–9955.
- (199) Vogt, M.; de Bruin, B.; Berke, H.; Trincado, M.; Grützmacher, H. *Chem. Sci.* **2011**, *2*, 723–727.
- (200) O'Neill, M.; Addy, D. A.; Riddlestone, I.; Kelly, M.; Phillips, N.; Aldridge, S. *J. Am. Chem. Soc.* **2011**, *133*, 11500–11503.
- (201) Huang, J.; Schanz, H.-J.; Stevens, E. D.; Nolan, S. P. *Organometallics* **1999**, *18*, 2370–2375.
- (202) Cavallo, L.; Correa, A.; Costabile, C.; Jacobsen, H. *J. Organomet. Chem.* **2005**, *690*, 5407–5413.
- (203) Díez-González, S.; Nolan, S. P. *Coord. Chem. Rev.* **2007**, *251*, 874–883.
- (204) Ledger, A. E. W.; Ellul, C. E.; Mahon, M. F.; Williams, J. M. J.; Whittlesey, M. K. *Chem. Eur. J.* **2011**, 8704–8713.
- (205) Luo, Y.; Ohno, K. *Organometallics* **2007**, *26*, 3597–3600.

- (206) Rossin, A.; Caporali, M.; Gonsalvi, L.; Guerri, A.; Lledós, A.; Peruzzini, M.; Zanobini, F. *Eur. J. Inorg. Chem.* **2009**, 3055–3059.
- (207) Chaplin, A. B.; Weller, A. S. *Angew. Chem. Int. Ed.* **2010**, *49*, 581–584.
- (208) Kumar, R.; Jagirdar, B. R. *Inorg. Chem.* **2013**, *52*, 28–36.
- (209) Dallanegra, R.; Chaplin, A. B.; Weller, A. S. *Angew. Chem. Int. Ed.* **2009**, *48*, 6875–6878.
- (210) Douglas, T. M.; Chaplin, A. B.; Weller, A. S. *J. Am. Chem. Soc.* **2008**, *130*, 14432–14433.
- (211) Douglas, T. M.; Chaplin, A. B.; Weller, A. S.; Yang, X.; Hall, M. B. *J. Am. Chem. Soc.* **2009**, *131*, 15440–15456.
- (212) Chaplin, A. B.; Weller, A. S. *Acta Crystallogr. C* **2011**, *67*, m355–m358.
- (213) Alcaraz, G.; Sabo-Etienne, S. *Angew. Chem. Int. Ed.* **2010**, *49*, 7170–7179.
- (214) Chaplin, A. B.; Weller, A. S. *Inorg. Chem.* **2010**, *49*, 1111–1121.
- (215) Dallanegra, R.; Chaplin, A. B.; Tsim, J.; Weller, A. S. *Chem. Commun.* **2010**, *46*, 3092–3094.
- (216) Crabtree, R. H. *J. Organomet. Chem.* **2004**, *689*, 4083–4091.
- (217) Alcaraz, G.; Vendier, L.; Clot, E.; Sabo-Etienne, S. *Angew. Chem. Int. Ed.* **2010**, *49*, 918–920.
- (218) Frenking, G.; Fröhlich, N. *Chem. Rev.* **2000**, *100*, 717–774.
- (219) Zeise, W. C. *Ann. der Phys. und Chemie* **1831**, *97*, 497.
- (220) Wunderlich, J. A.; Mellor, D. P. *Acta Crystallogr.* **1954**, *7*, 130.
- (221) Love, R. A.; Koetzle, T. F.; Williams, G. J. B.; Andrews, L. C.; Bau, R. *Inorg. Chem.* **1975**, *14*, 2653–2657.
- (222) Forniés, J.; Martín, A.; Martín, L. F.; Menjón, B. *Organometallics* **2005**, *24*, 3539–3546.
- (223) Morse, P. M.; Shelby, Q. D.; Kim, D. Y.; Girolami, G. S. *Organometallics* **2008**, *4*, 984–993.
- (224) Schaefer, J.; Himmel, D.; Krossing, I. *Eur. J. Inorg. Chem.* **2013**, 2712–2717.
- (225) Bar-Haim, G.; Shach, R.; Kol, M. *Chem. Commun.* **1997**, 229–230.
- (226) Lancaster, S. J.; Al-benna, S.; Thornton-Pett, M.; Bochmann, M. *Organometallics* **2000**, *19*, 1599–1608.

- (227) Brookhart, M.; Green, M. L. H. *J. Organomet. Chem.* **1983**, *250*, 395–408.
- (228) Scherer, W.; McGrady, G. S. *Angew. Chem. Int. Ed.* **2004**, *43*, 1782–806.
- (229) Haaland, A.; Scherer, W.; Ruud, K.; McGrady, G. S.; Downs, A. J.; Swang, O. *J. Am. Chem. Soc.* **1998**, *120*, 3762–3772.
- (230) Brookhart, M.; Green, M. L. H.; Parkin, G. *Proc. Natl. Acad. Sci.* **2007**, *104*, 6908–6914.
- (231) Dawoodi, Z.; Green, M. L. H.; Mtetwa, V. S. B.; Prout, K. *J. Chem. Soc. Chem. Commun.* **1982**, 1410–1411.
- (232) Dunlop-Brière, A. F.; Budzelaar, P. H. M.; Baird, M. C. *Organometallics* **2012**, *31*, 1591–1594.
- (233) La Placa, S. J.; Ibers, J. A. *Inorg. Chem.* **1965**, *4*, 778–783.
- (234) Brown, R. K.; Williams, J. M.; Schultz, A. J.; Stucky, G. D.; Ittel, S. D.; Harlow, R. L. *J. Am. Chem. Soc.* **1980**, *102*, 981–987.
- (235) Dawoodi, Z.; Green, M. L. H.; Mtetwa, V. S. B.; Prout, K. *J. Chem. Soc. Chem. Commun.* **1982**, 802–803.
- (236) Bouwkamp, M. W.; de Wolf, J.; del Hierro Morales, I.; Gercama, J.; Meetsma, A.; Troyanov, S. I.; Hessen, B.; Teuben, J. H. *J. Am. Chem. Soc.* **2002**, *124*, 12956–12957.
- (237) Mountford, A. J.; Lancaster, S. J.; Coles, S. J. *Acta Crystallogr. C* **2007**, *63*, m401–m404.
- (238) Harshbarger, W.; Lee, G.; Porter, R. F.; Bauer, S. H. *Inorg. Chem.* **1969**, *8*, 1683–1689.
- (239) Hillhouse, G. L.; Bulls, A. R.; Santarsiero, B. D.; Bercaw, J. E. *Organometallics* **1988**, *7*, 1309–1312.
- (240) Thorman, J. L.; Guzei, I. A.; Young, V. G.; Woo, L. K. *Inorg. Chem.* **1999**, *38*, 3814–3824.
- (241) Hamaki, H.; Takeda, N.; Tokitoh, N. *Organometallics* **2006**, *25*, 2457–2464.
- (242) Deck, P. A.; Marks, T. J. *J. Am. Chem. Soc.* **1995**, *117*, 6128–6129.
- (243) Myers, A. G.; Yang, B. H.; Chen, H.; Gleason, J. L. *J. Am. Chem. Soc.* **1994**, *116*, 9361–9362.
- (244) Myers, A. G.; Yang, B. H.; David, K. J. *Tetrahedron Lett.* **1996**, *37*, 3623–3626.
- (245) Xu, W.; Wu, G.; Yao, W.; Fan, H.; Wu, J.; Chen, P. *Chem. Eur. J.* **2012**, *18*, 13885–13892.

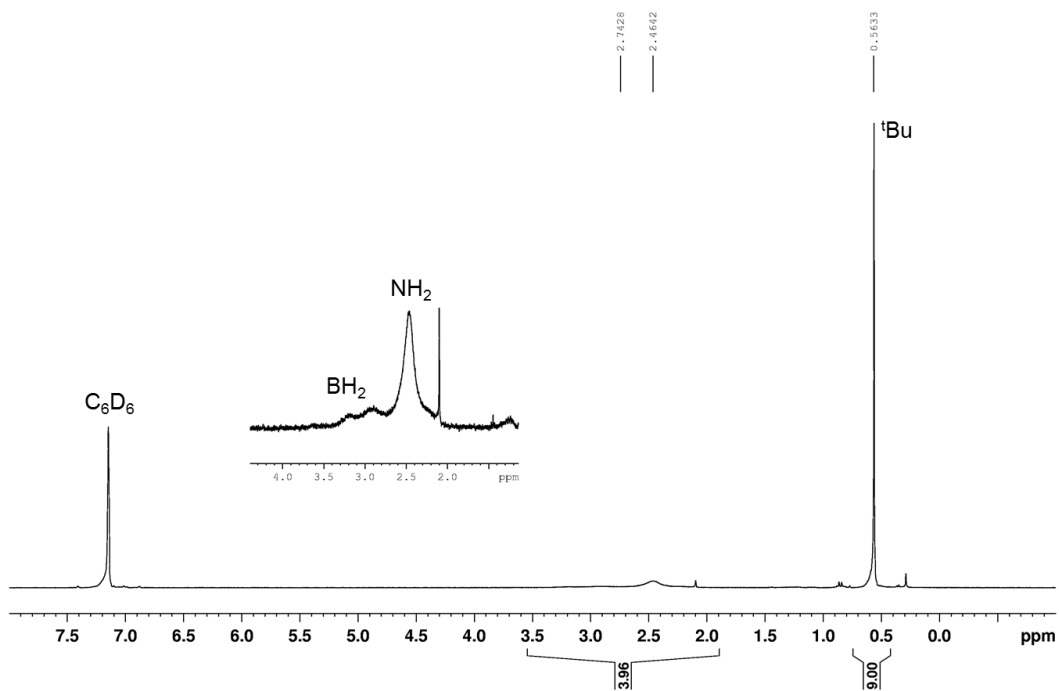
- (246) Enemærke, R. J.; Larsen, J.; Skrydstrup, T.; Daasbjerg, K. *J. Am. Chem. Soc.* **2004**, *126*, 7853–7864.
- (247) Cuenca, T.; Royo, P. *J. Organomet. Chem.* **1985**, *293*, 61–67.
- (248) Sofield, C. D.; Walter, M. D.; Andersen, R. A. *Acta Crystallogr. C* **2004**, *60*, m465–m466.
- (249) Lukens Jr., W. W.; Milton III, R. S.; Andersen, R. A. *J. Am. Chem. Soc.* **1996**, *118*, 1719–1728.
- (250) Feldman, J.; Calabrese, J. C. *J. Chem. Soc. Chem. Commun.* **1991**, 1042–1044.
- (251) Suggs, J. W.; Wovkulich, M.; Cox, S. D. *Organometallics* **1985**, *4*, 1101–1107.
- (252) Lancaster, S. J.; Robinson, O. B.; Bochmann, M.; Coles, S. J.; Hursthouse, M. B. *Organometallics* **1995**, *14*, 2456–2462.
- (253) Bochmann, M.; Lancaster, S. J. *J. Organomet. Chem.* **1995**, *497*, 55–59.
- (254) Mehrkhodavandi, P.; Schrock, R. R. *J. Am. Chem. Soc.* **2001**, *123*, 10746–10747.
- (255) Brady, E.; Telford, J. R.; Mitchell, G.; Lukens, W. *Acta Crystallogr. C Commun.* **1995**, *51*, 558–560.
- (256) Hurd, D. T. *J. Am. Chem. Soc.* **1948**, *70*, 2053–2055.
- (257) Stone, F. G. A.; Emeléus, H. J. *J. Chem. Soc.* **1950**, 2755–2759.
- (258) Spies, P.; Kehr, G.; Bergander, K.; Wibbeling, B.; Fröhlich, R.; Erker, G. *Dalton Trans.* **2009**, 1534–1541.
- (259) Theuergarten, E.; Schlüns, D.; Grunenberg, J.; Daniliuc, C. G.; Jones, P. G.; Tamm, M. *Chem. Commun.* **2010**, *46*, 8561–8563.
- (260) Chapman, A. M.; Haddow, M. F.; Orton, J. P. H.; Wass, D. F. *Dalton Trans.* **2010**, *39*, 6184–6186.
- (261) Rojas, R. S.; Peoples, B. C.; Cabrera, A. R.; Valderrama, M.; Fröhlich, R.; Kehr, G.; Erker, G.; Wiegand, T.; Eckert, H. *Organometallics* **2011**, *30*, 6372–6382.
- (262) Xu, B.-H.; Kehr, G.; Fröhlich, R.; Grimme, S.; Erker, G. *J. Am. Chem. Soc.* **2011**, *133*, 3480–3491.
- (263) Xu, B.; Kehr, G.; Fröhlich, R.; Erker, G. *Organometallics* **2011**, *30*, 5080–5083.
- (264) Schwendemann, S.; Fröhlich, R.; Kehr, G.; Erker, G. *Chem. Sci.* **2011**, *2*, 1842–1849.
- (265) Brown, H. C.; Zweifel, G. *J. Am. Chem. Soc.* **1960**, *82*, 4708–4712.
- (266) Brown, H. C.; Zweifel, G. *J. Am. Chem. Soc.* **1961**, *83*, 2544–2551.

- (267) Brown, H. C.; Chandrasekharan, J.; Wang, K. K. *Pure Appl. Chem.* **1983**, *55*, 1387–1414.
- (268) Chandrasekharan, J.; Brown, H. C. *J. Org. Chem.* **1985**, *50*, 518–520.
- (269) Want, X.; Li, Y.; Wu, Y.-D.; Padden-Row, M. N.; Rondan, N. G.; Houk, K. N. *J. Org. Chem.* **1990**, *55*, 2601–2609.
- (270) Brown, H. C. *Tetrahedron* **1961**, *12*, 117–138.
- (271) Brown, H. C.; Ramachandran, P. V. *Pure Appl. Chem.* **1991**, *63*, 307–316.
- (272) Burkhardt, E. R.; Matos, K. *Chem. Rev.* **2006**, *106*, 2617–2650.
- (273) Burgess, K.; Ohlmeyer, M. J. *Chem. Rev.* **1991**, *91*, 1179–1191.
- (274) Bijpost, E. A.; Duchateau, R.; Teuben, J. H. *J. Mol. Catal. A Chem.* **1995**, *95*, 121–128.
- (275) Beletskaya, I.; Pelter, A. *Tetrahedron* **1997**, *53*, 4957–5026.
- (276) Brown, H. C.; Rao, B. C. S. *J. Am. Chem. Soc.* **1956**, *78*, 5694–5695.
- (277) Brown, H. C.; Zweifel, G. *J. Am. Chem. Soc.* **1959**, *81*, 247.
- (278) Knights, E. F.; Brown, H. C. *J. Am. Chem. Soc.* **1968**, 5280–5281.
- (279) Hoshi, M.; Shirakawa, K.; Okimoto, M. *Tetrahedron Lett.* **2007**, *48*, 8475–8478.
- (280) Jacobs, E. A.; Chandrasekar, R.; Smith, D. A.; White, C. M.; Bochmann, M.; Lancaster, S. J. *J. Organomet. Chem.* **2013**, *730*, 44–48.
- (281) Karplus, M. *J. Chem. Phys.* **1959**, *30*, 11–15.
- (282) Minch, M. J. *Concepts Magn. Reson.* **1994**, 41–56.
- (283) Brown, H. C.; Knights, E. F.; Scoutenb, C. G. *J. Am. Chem. Soc.* **1974**, *96*, 7765–7770.
- (284) Soderquist, J. A.; Brown, H. C. *J. Org. Chem.* **1981**, *46*, 4599–4600.
- (285) Brown, H. C.; Kulkarni, S. U. *J. Org. Chem.* **1979**, *44*, 2422–2425.
- (286) Wiberg, K. B. *Angew. Chem. Int. Ed. Engl.* **1986**, *25*, 312–322.
- (287) Essalah, K.; Barthelat, J.-C.; Montiel, V.; Lachaize, S.; Donnadiou, B.; B, C.; Sabo-
Etienne, S. *J. Organomet. Chem.* **2003**, *680*, 182–187.
- (288) Braunschweig, H.; D'Andola, G.; Welton, T.; White, A. J. P. *Chem. Eur. J.* **2006**, *12*, 600–606.
- (289) Wilkinson, G.; Birmingham, J. M. *J. Am. Chem. Soc.* **1954**, *76*, 4281–4284.

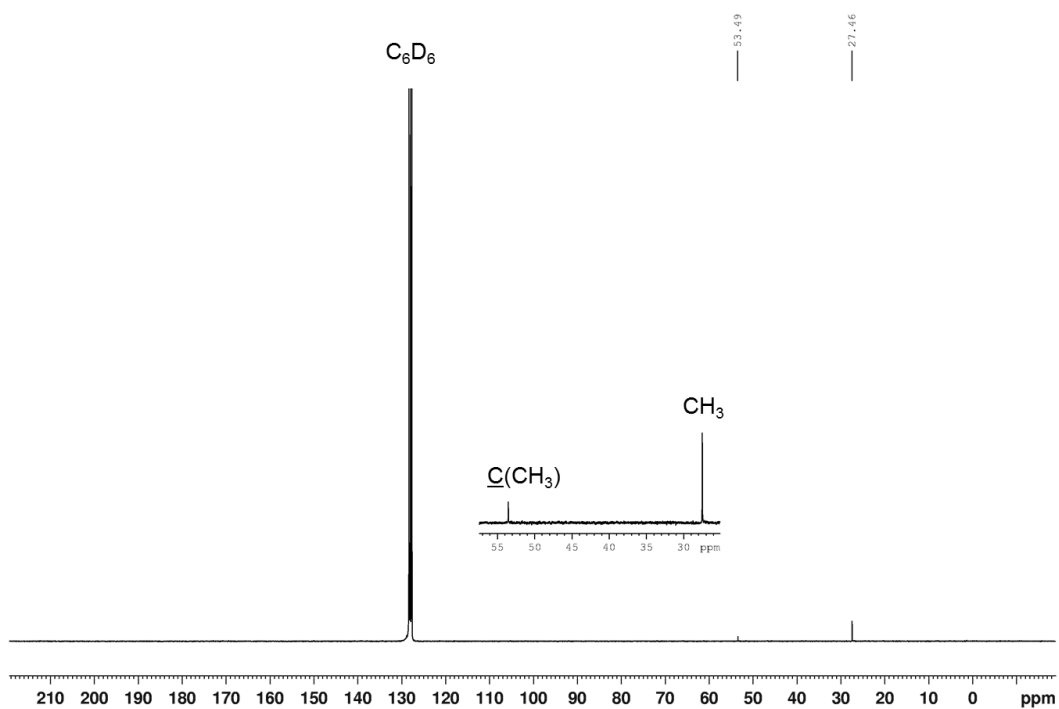
- (290) Samuel, E.; Rausch, M. D. *J. Am. Chem. Soc.* **1973**, 6263–6267.
- (291) Ziegler, F. E.; Sarpong, M. A. *Tetrahedron* **2003**, 59, 9013–9018.
- (292) Kool, L. B.; Rausch, M. D.; Alt, H. G.; Herberhold, M.; Thewalt, U.; Wolf, B. *Angew. Chem. Int. Ed.* **1985**, 24, 394–401.
- (293) Oxford Diffraction Ltd. *CrysAlisPro* **2010**, Albington, UK.
- (294) Rigaku Europe *CrystalClear-SM Expert* **2011**, Sevenoaks, UK.
- (295) Sheldrick, G. M. *Acta Crystallogr. A* **2008**, 64, 112–122.
- (296) Coles, S. J.; Gale, P. A. *Chem. Sci.* **2012**, 3, 683–689.
- (297) Otwinowski, Z.; Minor, W. *Methods in Enzymology Vol. 276*; Academic Press, 1997; pp. 307–326.

Chapter 8 Appendix

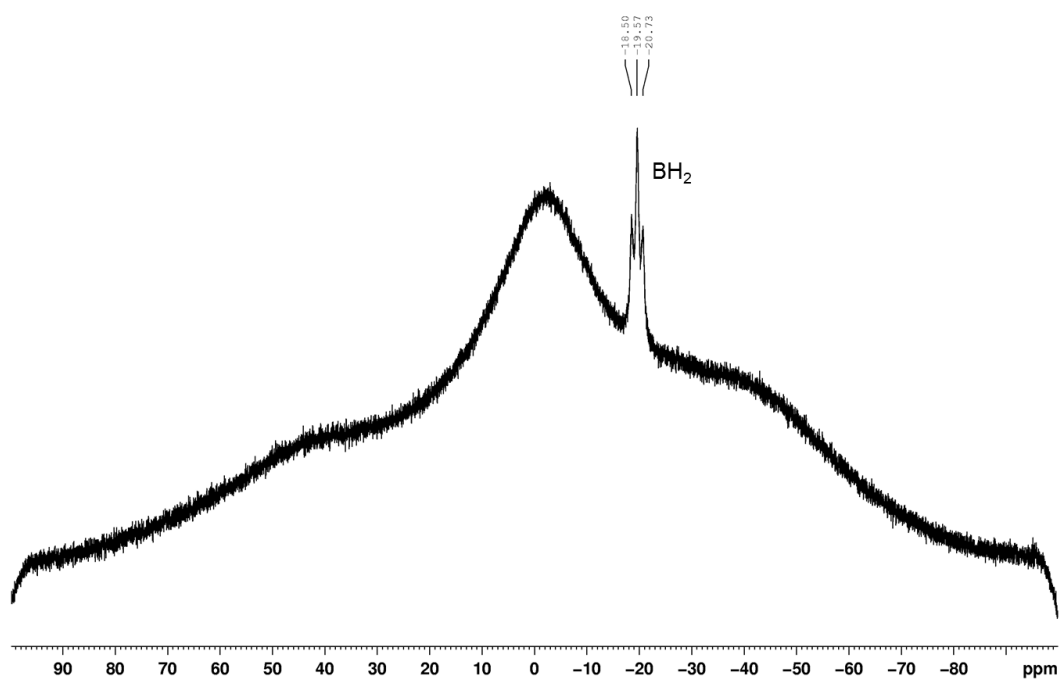
${}^1\text{BuH}_2\text{N}\cdot\text{BH}_2(\text{C}_6\text{F}_5)$ (**1b**)



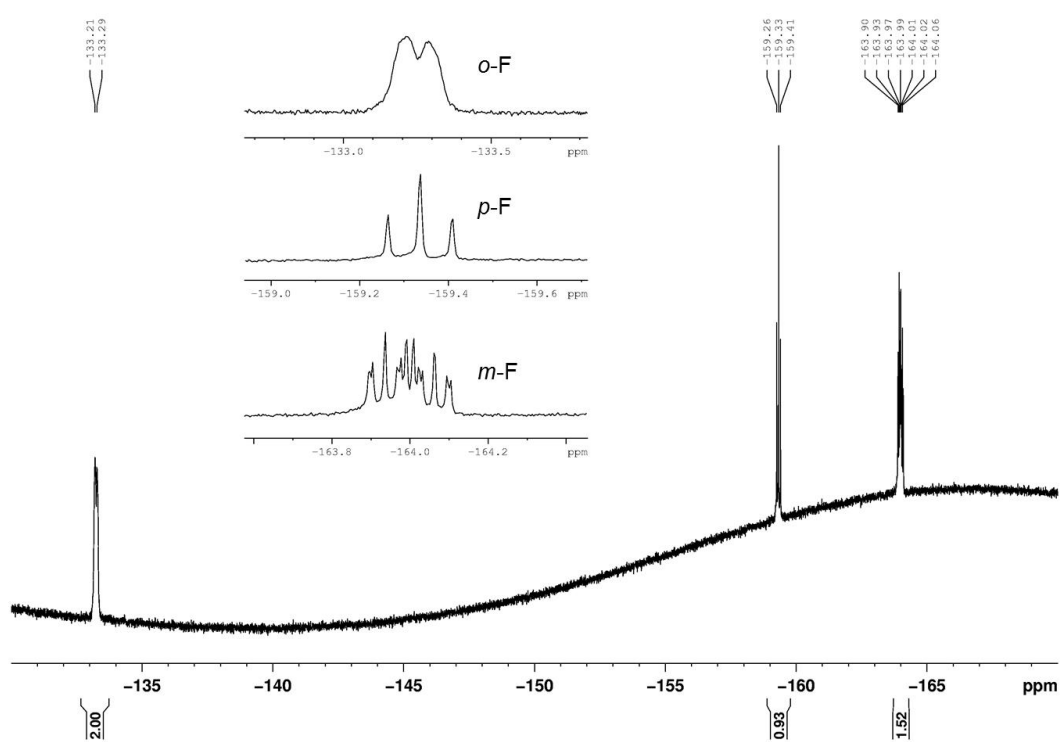
${}^1\text{BuH}_2\text{N}\cdot\text{BH}_2(\text{C}_6\text{F}_5)$ (**1b**)



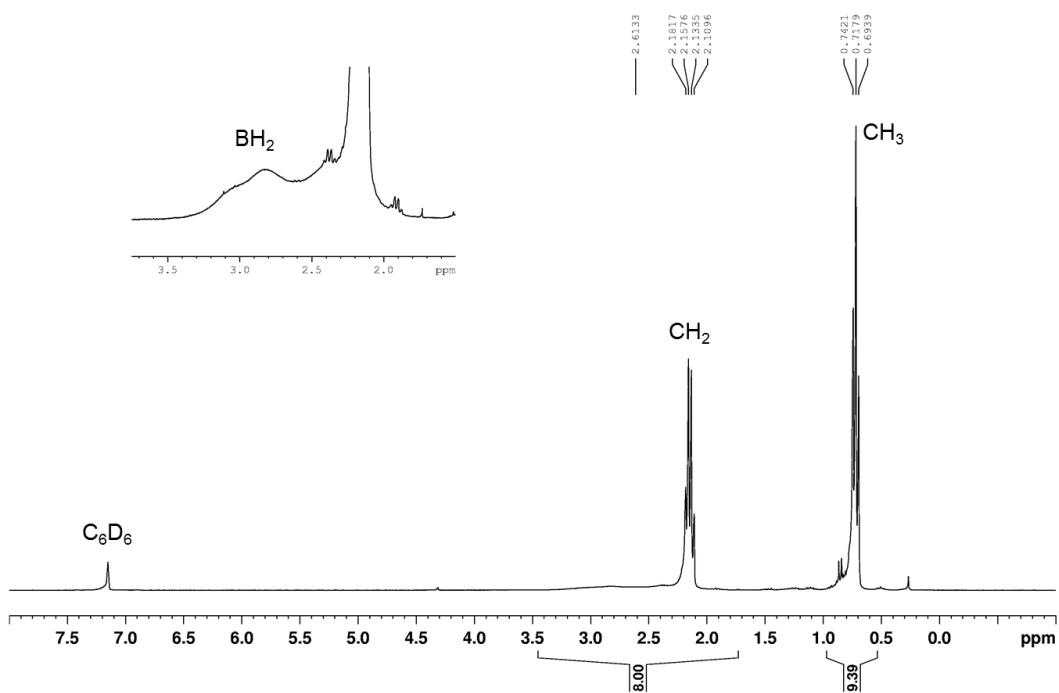
$t\text{BuH}_2\text{N}\cdot\text{BH}_2(\text{C}_6\text{F}_5)$ (**1b**)



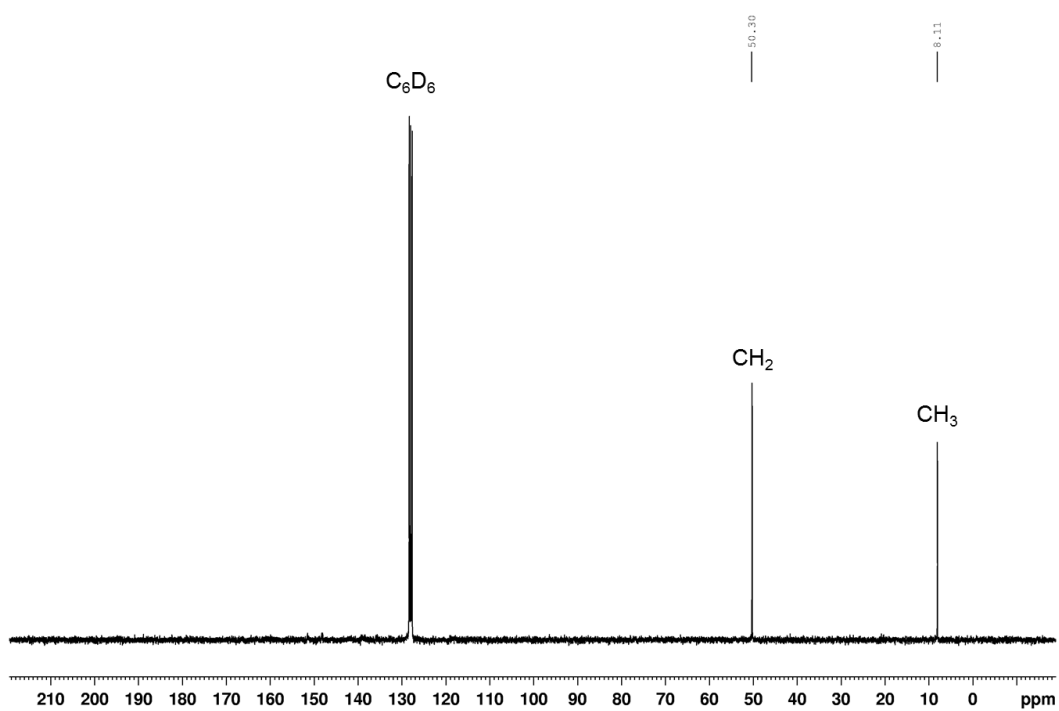
$t\text{BuH}_2\text{N}\cdot\text{BH}_2(\text{C}_6\text{F}_5)$ (**1b**)



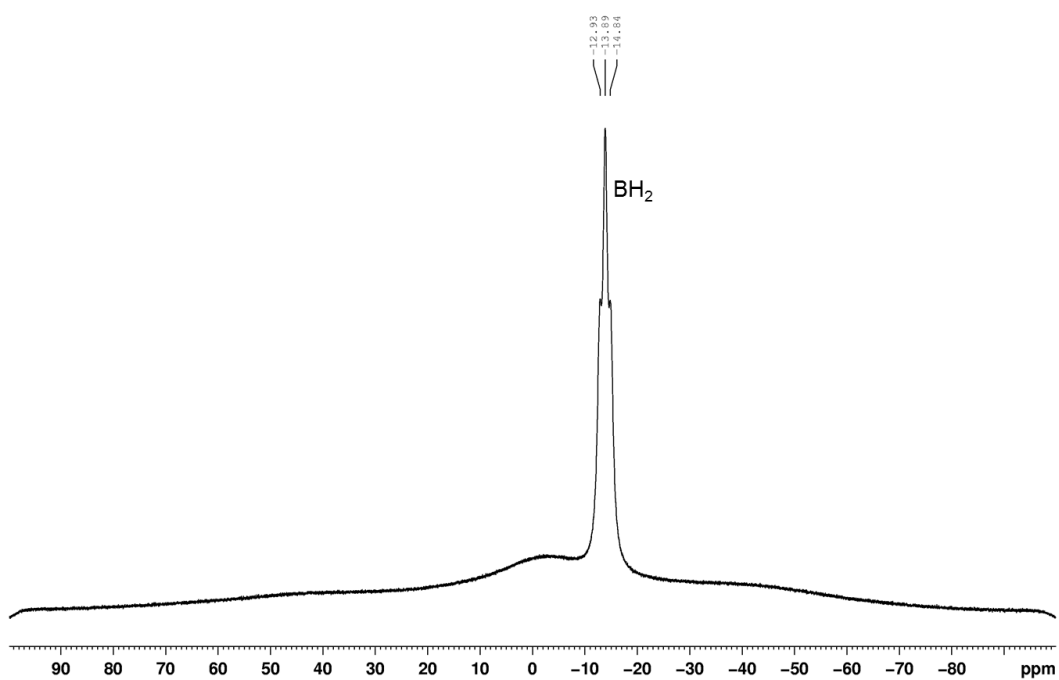
$\text{Et}_3\text{N}\cdot\text{BH}_2(\text{C}_6\text{F}_5)$ (**1e**)



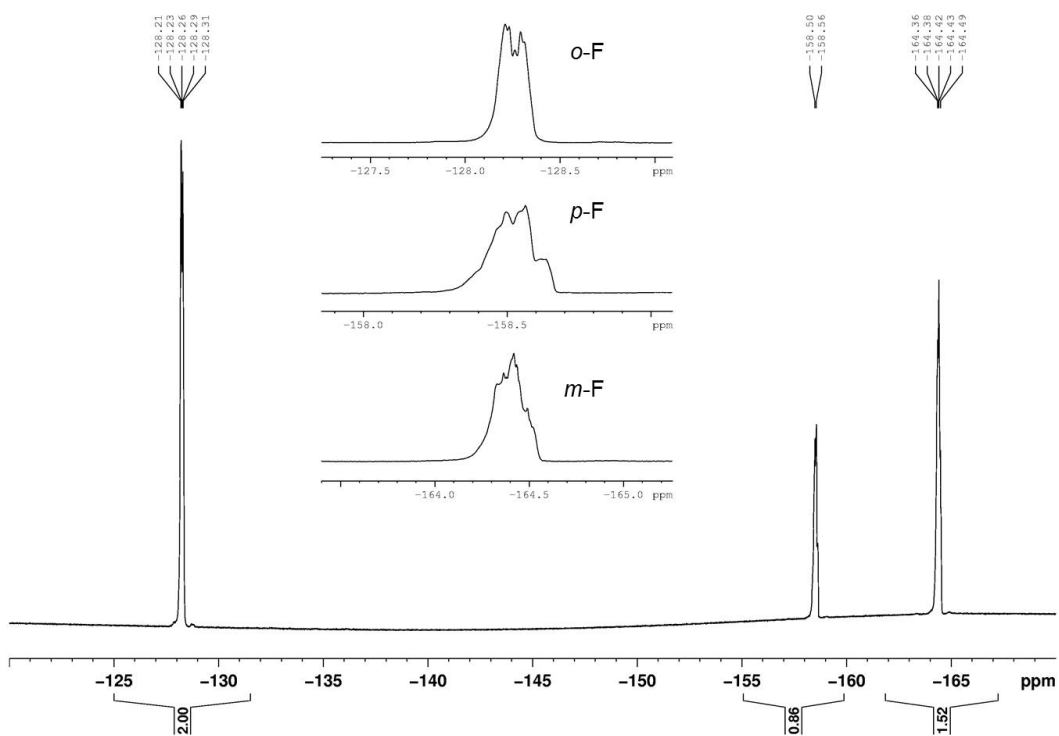
$\text{Et}_3\text{N}\cdot\text{BH}_2(\text{C}_6\text{F}_5)$ (**1e**)



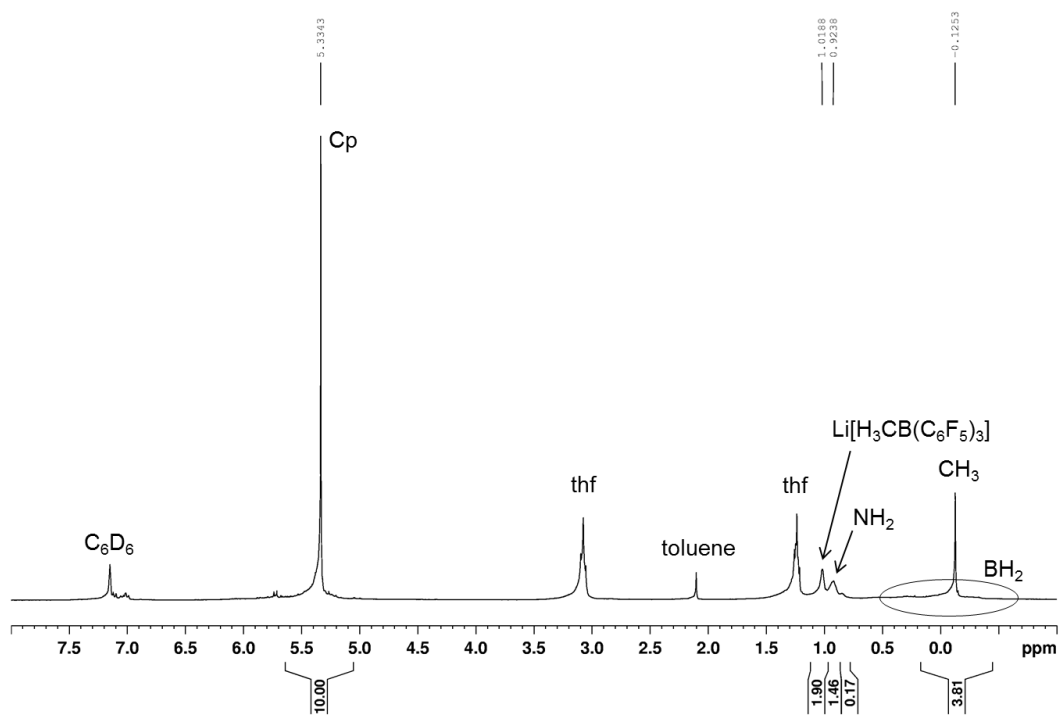
Et₃N·BH₂(C₆F₅) (1e)



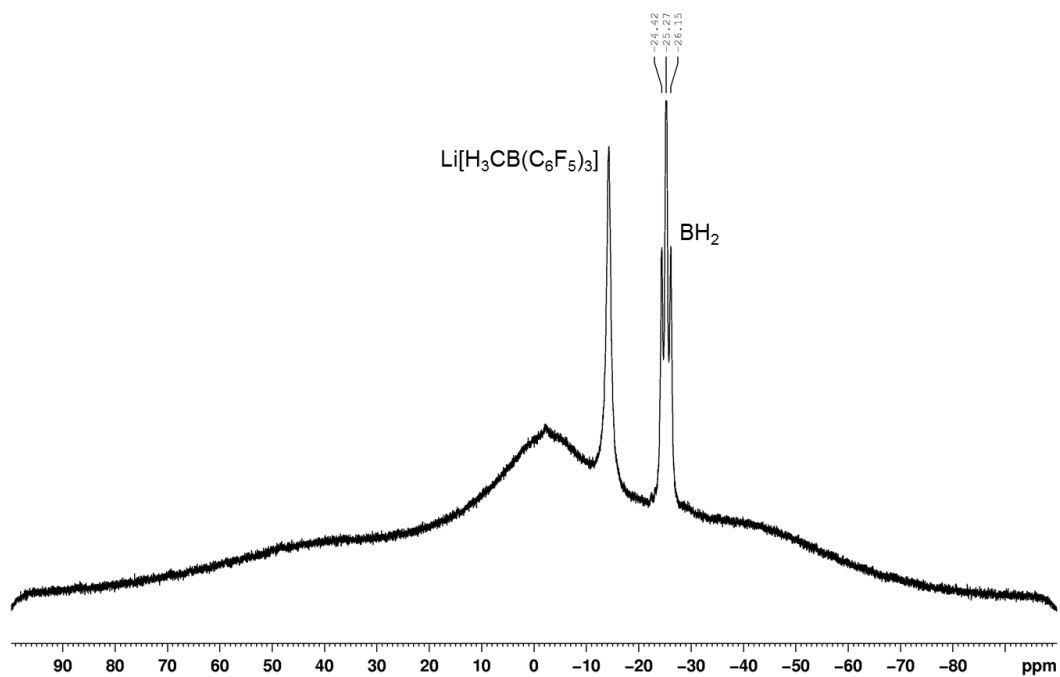
Et₃N·BH₂(C₆F₅) (1e)



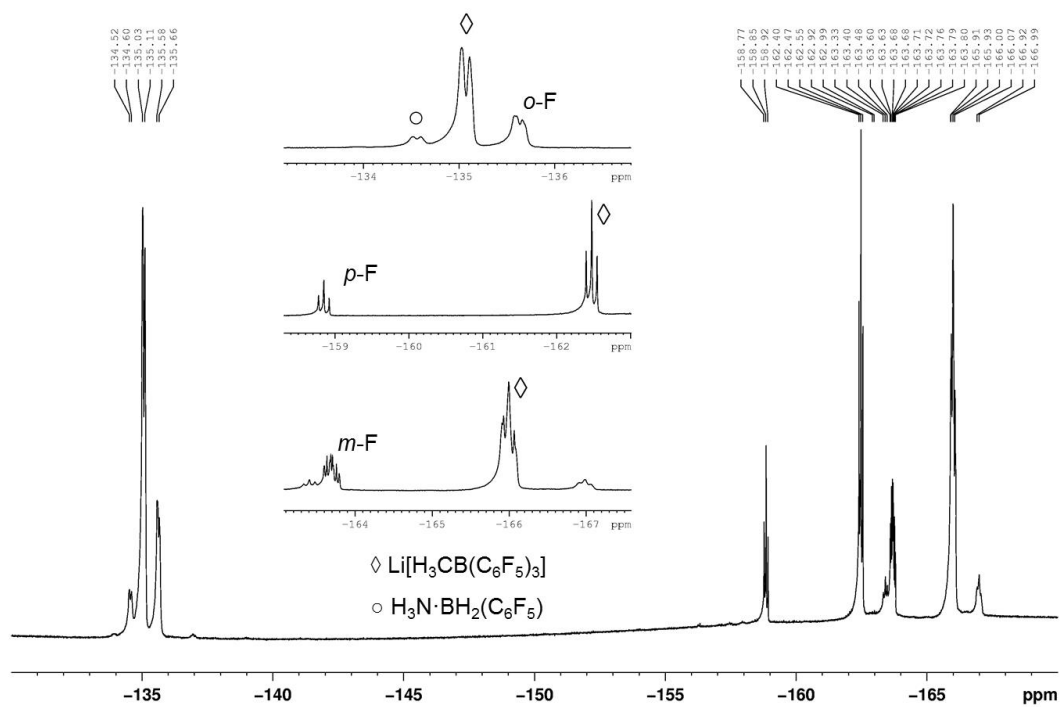
$\text{Cp}_2\text{Zr}(\text{CH}_3)(\text{NH}_2\text{BH}_2(\text{C}_6\text{F}_5))$ (**11**) – crude



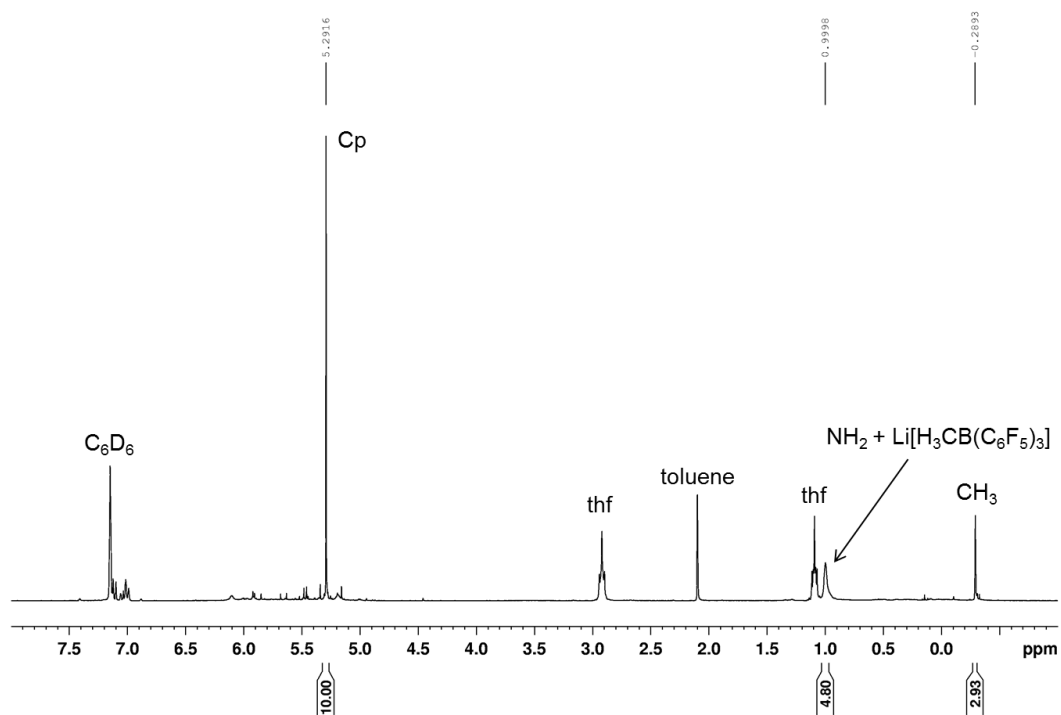
$\text{Cp}_2\text{Zr}(\text{CH}_3)(\text{NH}_2\text{BH}_2(\text{C}_6\text{F}_5))$ (**11**) – crude



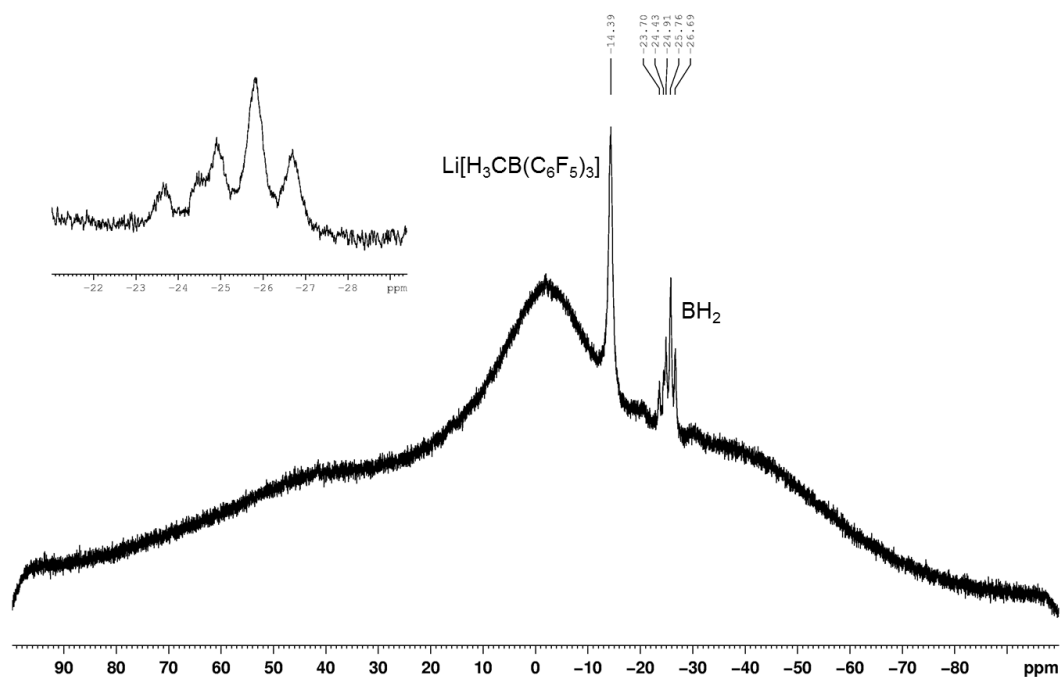
$\text{Cp}_2\text{Zr}(\text{CH}_3)(\text{NH}_2\text{BH}_2(\text{C}_6\text{F}_5))$ (**11**) – crude



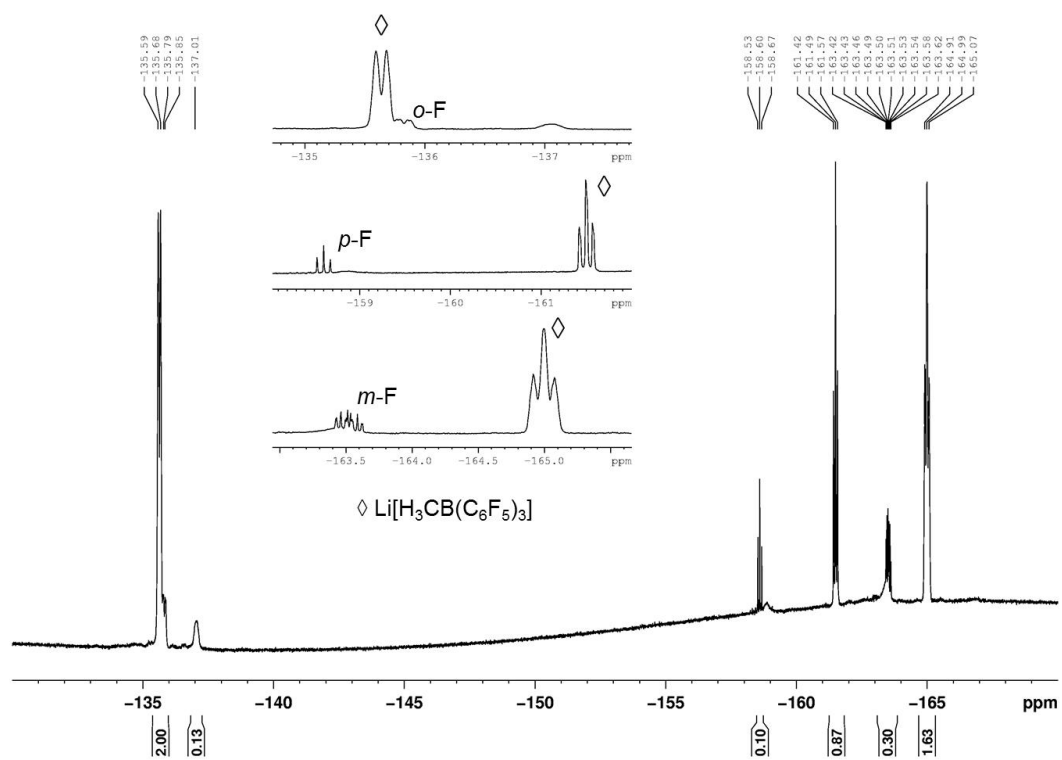
$\text{Cp}_2\text{Hf}(\text{CH}_3)(\text{NH}_2\text{BH}_2(\text{C}_6\text{F}_5))$ (**14**) – crude

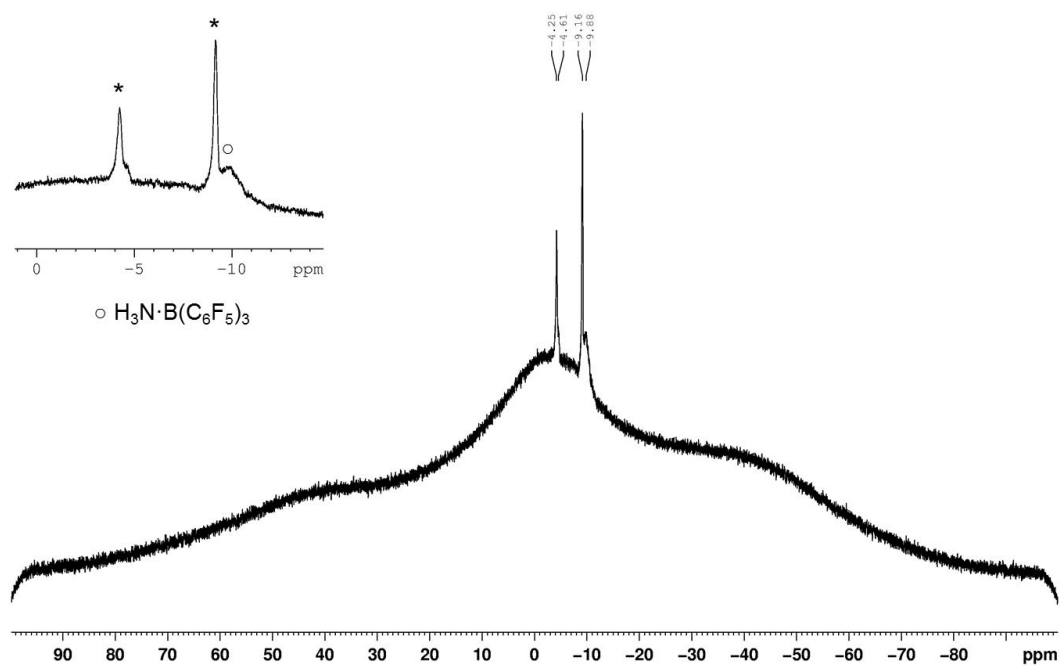
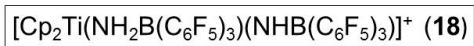
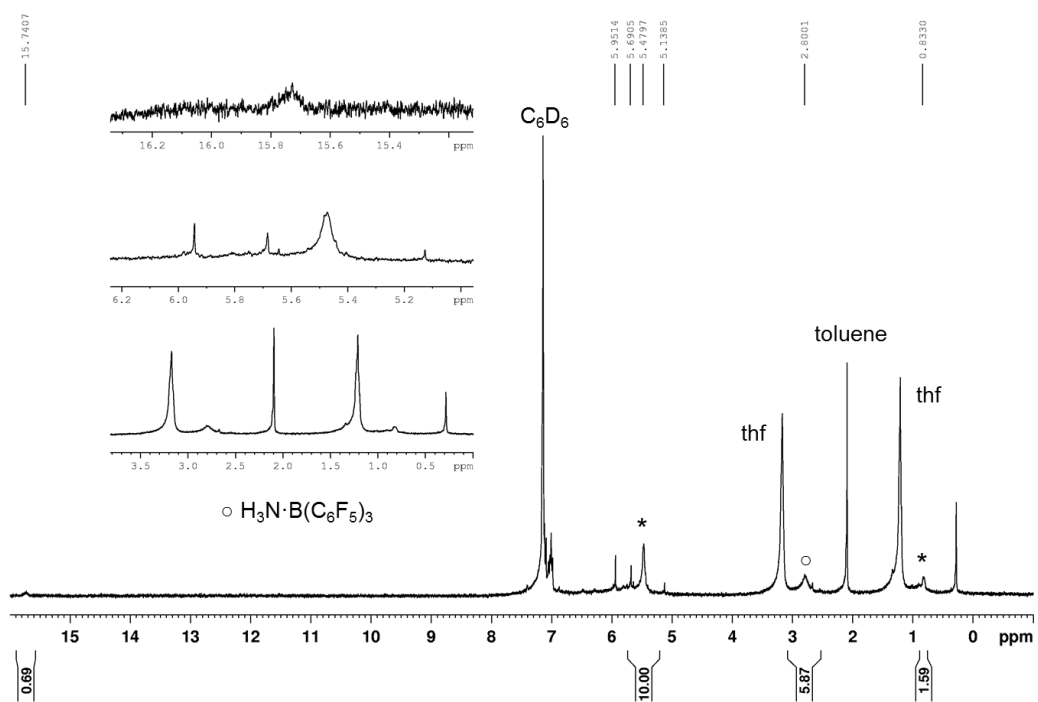
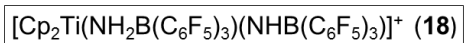


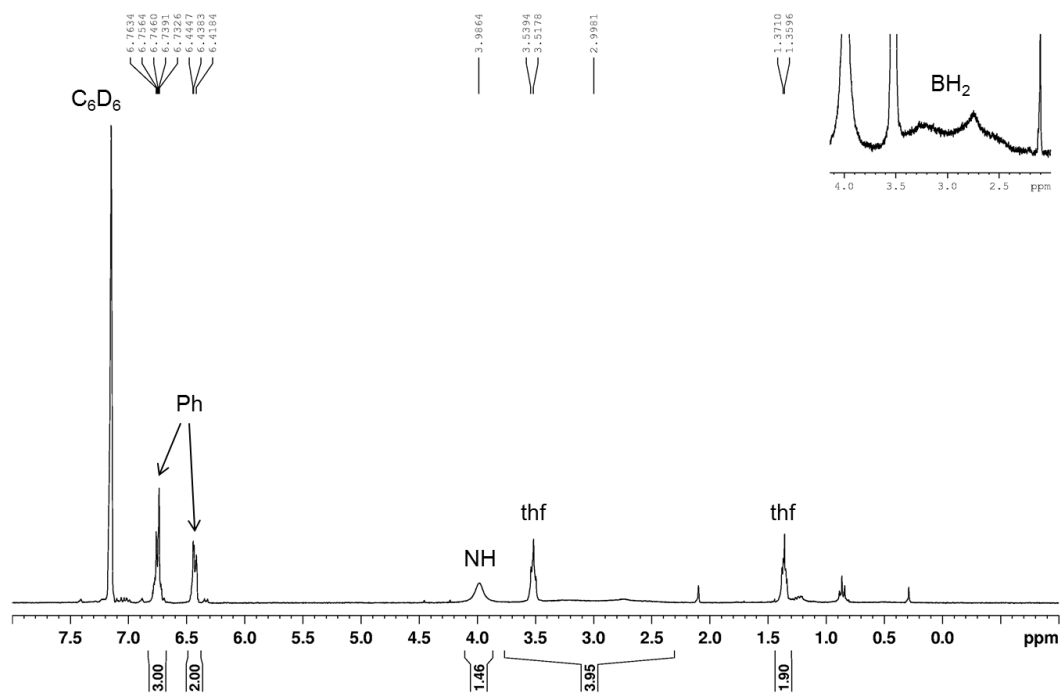
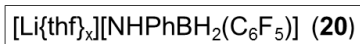
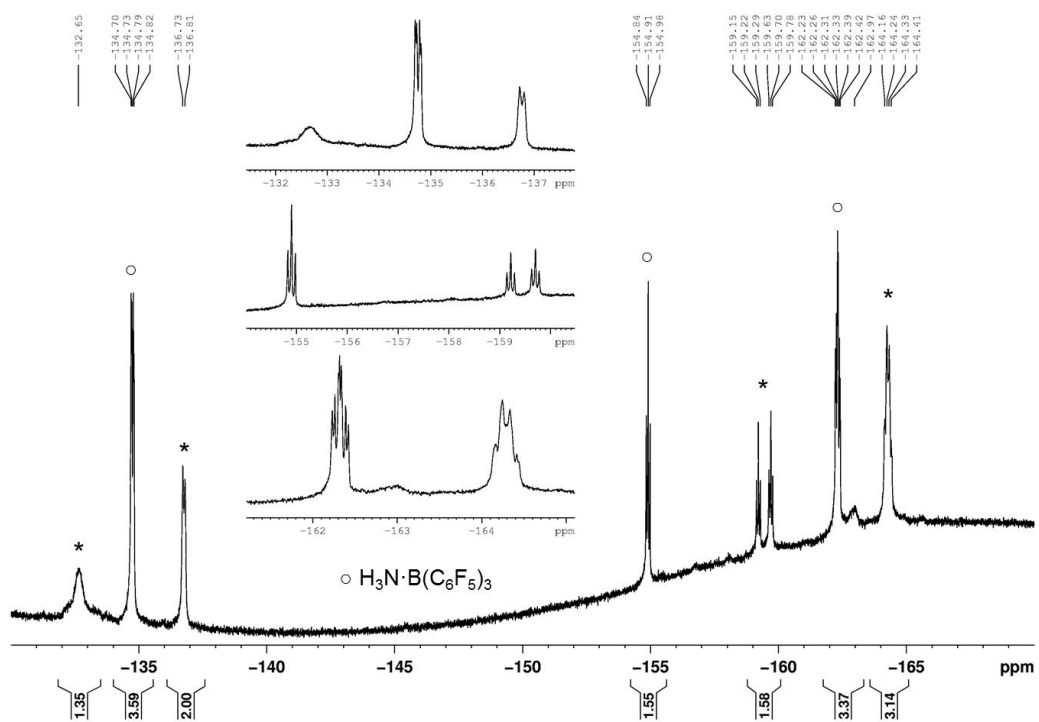
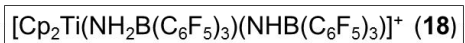
$\text{Cp}_2\text{Hf}(\text{CH}_3)(\text{NH}_2\text{BH}_2(\text{C}_6\text{F}_5))$ (**14**) – crude

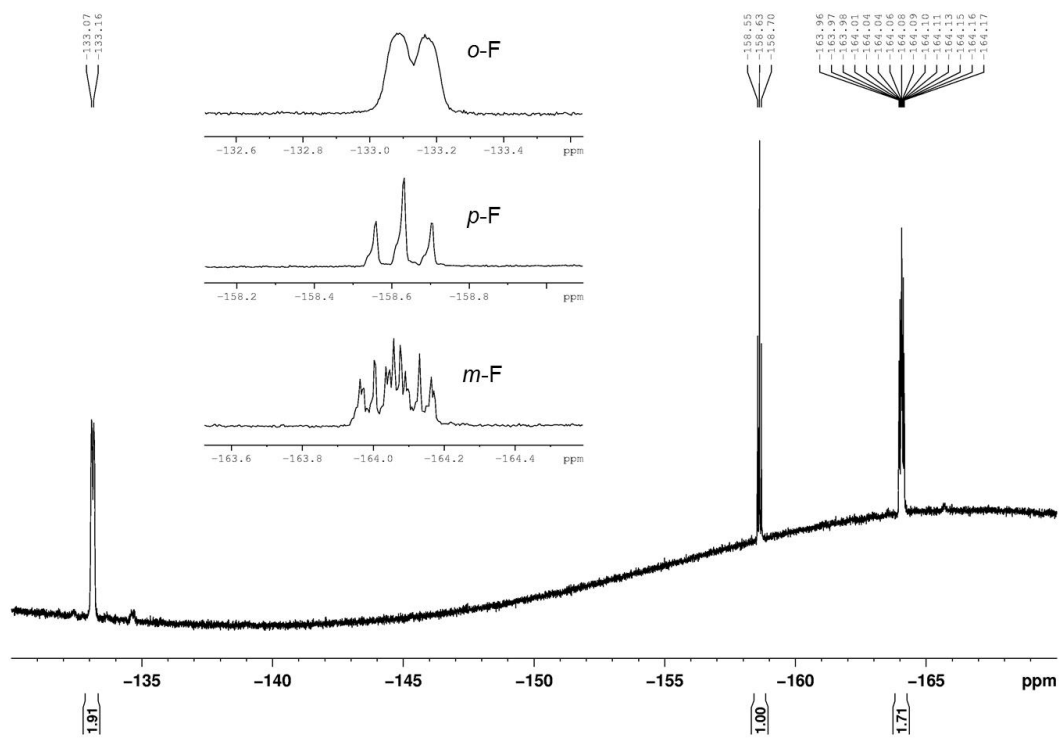
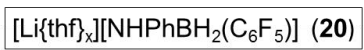
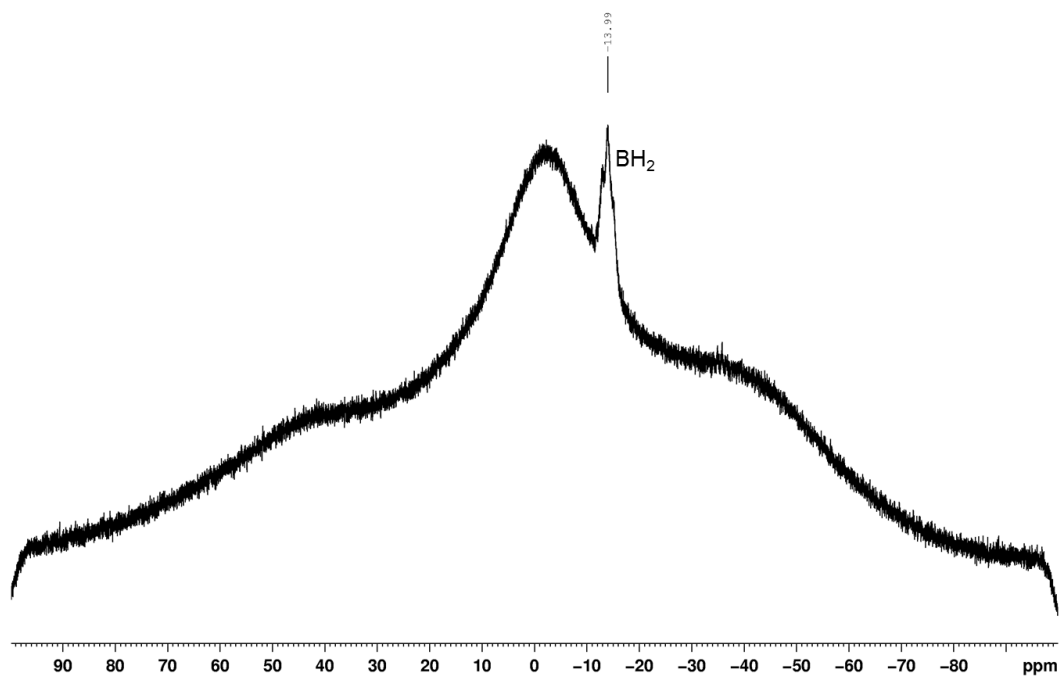


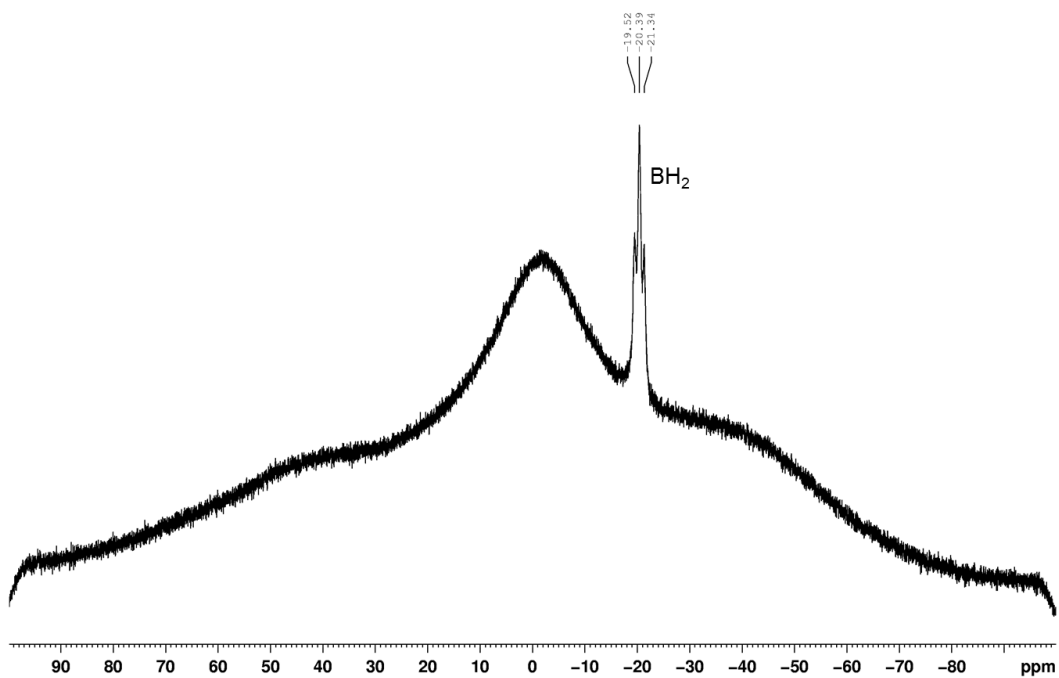
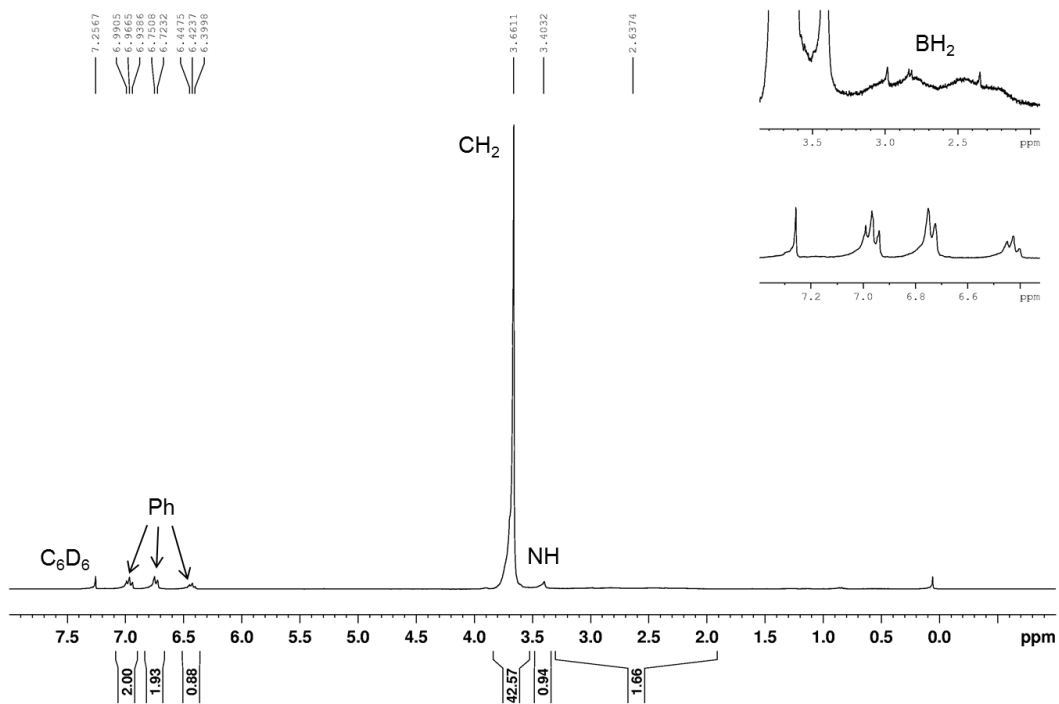
$\text{Cp}_2\text{Hf}(\text{CH}_3)(\text{NH}_2\text{BH}_2(\text{C}_6\text{F}_5))$ (**14**) – crude



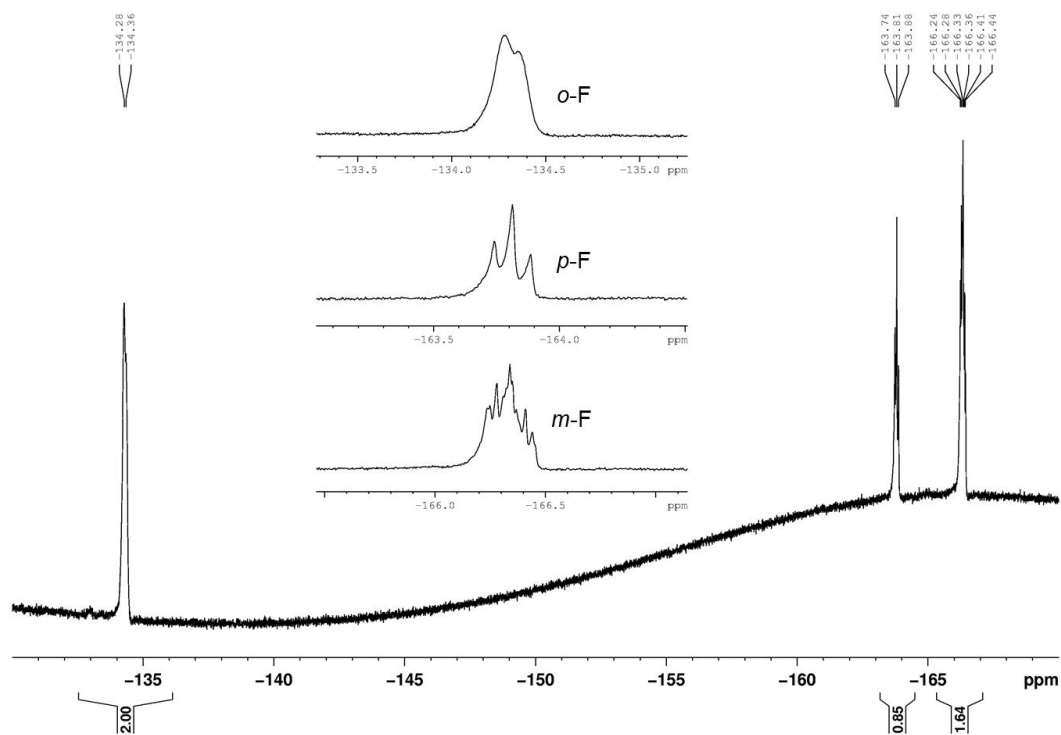








[Li{12-crown-4}_x][NHPPhBH₂(C₆F₅)] (20a)



Cp₂Zr(CH₃)(NHPPhBH₂(C₆F₅)) (21)

